VOLUME 77 AUGUST 30, 1973 NUMBER 18

JPCHAx

THE JOURNAL OF PHYSICAL CHEMISTRY

PUBLISHED BIWEEKLY BY THE AMERICAN CHEMICAL SOCIETY

THE JOURNAL OF

PHYSICAL CHEMISTRY

AMERICAN CHEMICAL SOCIETY, *1155 Sixteenth St., N.W., Washington, D. C. 20036*

Books and Journals Division

JOHN K CRUM *Director*
RUTH REYNARD *Assistant to the Director*

CHARLES R. BERTSCH *Head, Editorial Processing Department*
D. H. MICHAEL BOWEN *Head, Journals Department*
BACIL GUILEY *Head, Graphics and Production Department*
SELDON W. TERRANT *Head, Research and Development Department*

 Published biweekly by the American Chemical Society at 20th and Northampton Sts., Easton, Pa. 18042. Second-class postage paid at Washington, D. C., and at additional mailing offices.

All manuscripts should be sent to *The Journal of Physical Chemistry*, Department of Chemistry, University of Minnesota, Minneapolis, Minn. 55455.

Additions and Corrections are published once yearly in the final issue. See Volume 76, Number 26 for the proper form.

Extensive or unusual alterations in an article after it has been set in type are made at the author's expense, and it is understood that by requesting such alterations the author agrees to defray the cost thereof.

The American Chemical Society and the Editor of *The Journal of Physical Chemistry* assume no responsibility for the statements and opinions advanced by contributors.

Correspondence regarding accepted copy, proofs, and reprints should be directed to Editorial Processing Department, American Chemical Society, 20th and Northampton Sts., Easton, Pa. 18042. Head: CHARLES R. BERTSCH. Assistant Editor: EDWARD A. BORGER. Editorial Assistant: JOSEPH E. YURVATI.

Advertising Office: Centcom, Ltd., 142 East Avenue, Norwalk, Conn. 06851.

Business and Subscription Information

Send all new and renewal subscriptions *with payment* to: Office of the Controller, 1155 16th Street, N.W., Washington, D. C. 20036. Subscriptions should be renewed promptly to avoid a break in your series. All correspondence and telephone calls regarding changes of address, claims for missing issues, subscription service, the status of records, and accounts should be directed to Manager, Membership and Subscription Services, American Chemical Society, P.O. Box 3337, Columbus, Ohio 43210. Telephone (614) 421-7230.

On changes of address, include both old and new addresses with ZIP code numbers, accompanied by mailing label from a recent issue. Allow four weeks for change to become effective.

Claims for missing numbers will not be allowed (1) if loss was due to failure of notice of change in address to be received before the date specified, (2) if received more than sixty days from date of issue plus time normally required for postal delivery of journal and claim, or (3) if the reason for the claim is "issue missing from files."

Subscription rates (1973): members of the American Chemical Society, $20.00 for 1 year; to nonmembers, $60.00 for 1 year. Those interested in becoming members should write to the Admissions Department, American Chemical Society, 1155 Sixteenth St., N.W., Washington, D. C. 20036. Postage to Canada and countries in the Pan-American Union, $5.00; all other countries, $6.00. Single copies for current year: $3.00. Rates for back issues from Volume 56 to date are available from the Special Issues Sales Department, 1155 Sixteenth St., N.W., Washington, D. C. 20036.

Subscriptions to this and the other ACS periodical publications are available on microfilm. Supplementary material not printed in this journal is now available in microfiche form on a current subscription basis. For information on microfilm or microfiche subscriptions, write Special Issues Sales Department at the address above.

Notice to Authors last printed in the issue of June 21, 1973

THE JOURNAL OF
PHYSICAL CHEMISTRY

Volume 77, Number 18 August 30, 1973

JPCHAx 77(18) 2163-2256 (1973)
ISSN 0022-3654

■ Supplementary material for this paper is available separately, in photocopy or microfiche form. Ordering information is given in the paper.

* In papers with more than one author, the asterisk indicates the name of the author to whom inquiries about the paper should be addressed.

AUTHOR INDEX

THE JOURNAL OF
PHYSICAL CHEMISTRY

VOLUME 77, NUMBER 18 AUGUST 30, 1973

Rate of Electron Transfer between Tris(3,4,7,8-tetramethyl-1,10-phenanthroline)iron(II) and -(III) Ions from Nuclear Magnetic Resonance Studies[1]

Man-Sheung Chan, J. Barry DeRoos,[2] and Arthur C. Wahl*

Department of Chemistry Washington University, St. Louis, Missouri 63130 *(Received May 9, 1973)*

Publication costs assisted by the National Science Foundation

The rate of electron exchange between tris(3,4,7,8-tetramethyl-1,10-phenanthroline)iron(II) and -(III) ions in acetonitrile has been measured by the nmr line-broadening method in the temperature range from −5 to 35°. For a total reactant concentration of 0.035 M, the second-order rate constant at 25° is $(1.7 \pm 0.1) \times 10^7\ M^{-1}\ \text{sec}^{-1}$, and the experimental activation energy is 2 ± 1 kcal/mol.

Introduction

Earlier investigations of the rate of electron exchange between tris(1,10-phenanthroline)iron(II) and -(III) and also between their methyl derivatives by tracer, optical activity, and nmr methods resulted only in establishing lower limits for the rate.[3-6] Our more recent investigations of these exchange reactions with a high-frequency nmr spectrometer (100 MHz instead of the 60 MHz used previously) have shown that the rates can now be measured. The widths of the exchange-averaged resonance lines for the phenanthroline 2,9 protons in solutions containing both the diamagnetic and paramagnetic ions are considerably larger than those calculated for the fast-exchange limit, showing that exchange rates are in the measurable range. For most systems the spin-spin coupling between the 2, 3, and 4 (9, 8, and 7) protons, evidence for which both Miller and Prince[7] and we have observed, complicates interpretation of the data, and appropriate methods of analysis are currently being developed. However, this problem does not exist for 3,4,7,8-tetramethyl derivatives, and data for exchange between these reactants are reported in this article.

Results and Discussion

Since the electron spin-lattice relaxation time ($T_{1e} \simeq 10^{-10}$ sec)[8] is much less than the measured mean lifetime of the paramagnetic ion ($\tau_P \simeq 10^{-6}$ sec), the exchange conditions may be represented by a two-site system (paramagnetic (P) and diamagnetic sites (D)). The exact equation for absorption under steady-state conditions, achieved by slow passage, is a complex function,[11] but with suitable approximations, which seem justifiable for the system investigated, the equation may be simplified to give a simple relationship between line widths and reactant lifetimes.[6,15] If the rate law for electron transfer is first order with respect to each reactant concentration, as it is for most electron-transfer reactions,[16] the measured line width, $W_{DP} = (\pi T_2)_{DP}^{-1}$ (the full-width at half-maximum measured in Hz of a Lorenzian shaped absorption line), is related by eq 1 to the rate constant, k, the natural line widths of each reactant, $W_D = (\pi T_2)_D^{-1}$ and $W_P = (\pi T_2)_P^{-1}$, the total reactant concentration, c (in moles/liter), of which the fraction, f_P is in the paramagnetic form, and the contact shift, $\delta\nu$ (in Hz)

$$W_{DP} = f_P W_P + (1 - f_P) W_D + f_P(1 - f_P) 4\pi(\delta\nu)^2/kc \qquad (1$$

Equation 1 was programmed as a subroutine for use with the ORGLS least-squares computer program,[17] and for a series of measurements in which f_P was varied, k was calculated by the method of least squares from measured values of W_{DP}, W_D, W_P, f_P, c, and $\delta\nu$. Figure 1 shows a plot of data determined at various temperatures; the lines represent the least-squares fit of the data. The measured values of W_D, W_P, c, and $\delta\nu$ used and the values of k determined are listed in Table I. The excellent fit of the data by the curves indicates that eq 1 is indeed valid and that the rate of the exchange is proportional to the con-

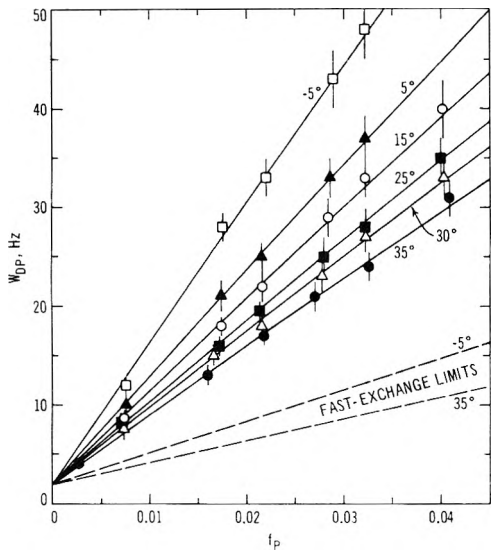

Figure 1. Variation of W_{DP}, the line width, with f_P, the fraction of reactant ions present as the paramagnetic species. The total reactant concentration, c, is 0.035 *M* in acetonitrile; the anion is PF_6^-. The lines are least-square fits of eq 1 to the data shown as points with estimated uncertainties. The dashed lines represent the fast-exchange limits, $f_P/T_{2P} + (1 - f_P)/T_{2D}$.

TABLE I: Temperature Dependence of the Exchange Rate[a]

Temp, °C	W_P, Hz	$\delta\nu$, Hz	k, 10^7 M^{-1} sec^{-1}
−5	300 ± 25	5880 ± 50	1.10 ± 0.09
5	290 ± 25	5630 ± 50	1.40 ± 0.10
15	260 ± 20	5460 ± 50	1.53 ± 0.11
25	250 ± 20	5270 ± 50	1.69 ± 0.12
30	240 ± 20	5190 ± 50	1.77 ± 0.10
35	220 ± 20	5100 ± 50	1.91 ± 0.11

[a] c = 0.035 *M*; CD_3CN is the solvent; PF_6^- is the anion; W_D = 2.0 ± 0.2 Hz at all temperatures.

centration of the paramagnetic species, as assumed. (The assumed first-order dependence of the rate on the concentration of the diamagnetic species has not been checked for this exchange system, but for the similar exchange system involving tris(4,4′-dimethyldipyridyl)iron(II) and -(III) ions, preliminary analysis of the data indicates that the rate is proportional to the concentration of diamagnetic species when the nature and concentration of the electrolyte are held constant by addition of the corresponding ruthenium(II) salt.)

To test further the validity of eq 1 for the exchange reaction investigated, the measured absorption line shapes were compared with those calculated from the line-shape equation for a two-site system.[11] Agreement was found within experimental uncertainties. (For other exchange systems in which coupling is involved, appreciable differences were observed between experimental and calculated line shapes.)

The uncertainties listed for the values of k in Table I are the square root of the sum of the squares of the standard deviations obtained from the least-squares fit of eq 1 and the average changes in k caused by changing the other parameters in eq 1 one at a time by plus or minus their uncertainties. The most important contributions to the uncertainties in k were the ~3, ~4, and ~1% uncertainties in c, W_P, and $\delta\nu$, respectively, which caused ~3, ~4, and ~2% uncertainties in k, respectively.

The activation energy derived from the k values is 2.0 ± 1.0 kcal/mol. This value and the rate constants determined in solutions with ionic strengths of ~0.1 *M* are about the same as those calculated from the Marcus theory[18] ($E_{act.}$ = 2.5 kcal/mol, $k(25°)$ = 4 × 10^6 M^{-1} sec^{-1}) for spherical reactants with radii of 7 Å in infinitely dilute solutions with continuous and unsaturated dielectric properties. It was assumed that rearrangement of the ligands was unnecessary and, as recommended by Marcus,[18] that the preexponential coefficients κ and ρ are unity. The agreement between theoretical and experimental values may be fortuitous because no account is taken of electrolyte effects on the rate, and studies in progress of the reaction between tris(4,4′-dimethyldipyridyl)osmium(II) and -iron(III) ions in acetonitrile indicate that the effect on the rate may be several orders of magnitude.[19]

Experimental Section

$Fe(3,4,7,8\text{-}Me_4\text{-}phen)_3(PF_6)_2$ was prepared by mixing aqueous solutions of $FeSO_4 \cdot 7H_2O$ (Fisher) and the ligand (G. F. Smith) in stoichiometric amounts[4] and then adding excess $NaPF_6$ (Alfa) to precipitate the compound, which was filtered, washed, and dried *in vacuo* over P_2O_5. $Fe(3,4,7,8\text{-}Me_4\text{-}phen)_3(PF_6)_3$ was prepared by treating an aqueous solution prepared as described above with PbO_2 and H_2SO_4[10] and, after removal of $PbSO_4$ and excess PbO_2, precipitating the compound by addition of excess $NaPF_6$. After being dried *in vacuo* over P_2O_5, the compound was dissolved in CH_3CN and reprecipitated by addition of CCl_4 and again dried *in vacuo*. Spectrophotometric analysis showed that both compounds were ≥99% pure, based on the extinction coefficient for $Fe(3,4,7,8\text{-}Me_4\text{-}phen)_3^{2+}$ reported by Brandt and Smith.[20]

The exchange reaction was studied in CD_3CN because the iron(III) complex was more stable in this solvent than in D_2O or in several other solvents investigated. Solutions for nmr measurements were prepared by mixing 0.035 *M* solutions of each reactant, a given solution being measured at the various temperatures before addition of more of the paramagnetic reactant and mixing to achieve the larger f_P values. Each f_P value was determined from the position of the resonance peak, assuming that the position was that for fast exchange[21] $f_P = (\nu_{DP} - \nu_D)/\delta\nu$. The f_P values calculated in this way were consistent with, but more accurate than, those determined from measurement of the very small volumes of solutions used, and account was taken automatically of any reduction of the paramagnetic reactant that might have occurred.

References and Notes

(1) Supported by the National Science Foundation under Grants No. GP-5939X and GP-28260X.
(2) Present address, Community College of Denver, Auraria Campus, Denver, Colo.
(3) E. Eichler and A. C. Wahl, *J. Amer. Chem. Soc.*, **80**, 4145 (1958).
(4) M. W. Dietrich and A. C. Wahl, *J. Chem. Phys.*, **38**, 1591 (1963).
(5) D. W. Larsen and A. C. Wahl, *J. Chem. Phys.*, **41**, 908 (1964).
(6) D. W. Larsen and A. C. Wahl, *J. Chem. Phys.*, **43**, 3765 (1965).
(7) J. D. Miller and R. H. Prince, *J. Chem. Soc.*, 4706 (1965).
(8) T_{1e} was estimated from the equation given by McGarvey[9] with our magnetic field value of H_0 = 23,500 G, DeSimone and Drago's g values of $g_\perp$ = −2.69 and $g_\parallel$ = 1.19 for $Fe(phen)_3(PF_6)_3$(s),[10] and a tumbling time of 1.3 × 10^{-10} sec. The resonance frequency of the electron (ν_0) was estimated using an average g value of $(g_\parallel + 2g_\perp)/3$. Hyperfine interactions between the electron and magnetic nuclei were neglected since no fine structure was observed in the esr spectrum.[10]
(9) B. R. McGarvey, *J. Phys. Chem.*, **61**, 1232 (1957).
(10) R. E. DeSimone and R. S. Drago, *J. Amer. Chem. Soc.*, **92**, 2343 (1970).

(11) The line-shape equation for a two-site system under steady-state conditions was derived from the Bloch equations[12,13] and is the same as that derived by Gutowsky and Holm,[14] except for the more general condition that $T_{2A} \neq T_{2B}$ their term T_2^{-1} is replaced by $(p_A T_{2A}^{-1} + p_B T_{2B}^{-1})$, and T_2^{-2} is replaced by $T_{2A}^{-1} T_{2B}^{-1}$.
(12) T. J. Swift and R. E. Connick, *J. Chem. Phys.*, **37**, 307 (1962).
(13) J. A. Pople, W. G. Schneider, and H. J. Bernstern, "High-Resolution Nuclear Magnetic Resonance," McGraw-Hill, New York, N. Y., 1959, p 219.
(14) H. S. Gutowsky and C. H. Holm, *J. Chem. Phys.*, **25**, 1228 (1956).
(15) A. Carrington and A. D. McLachlan, "Introduction to Magnetic Resonance," Harper and Row, New York, N. Y., 1967, p 208.
(16) *E.g.*, see F. Basolo and R. G. Pearson, "Mechanisms of Inorganic Reactions," Wiley, New York, N. Y., 1967, pp 455–489.
(17) L. A. Busing and H. A. Levy, Oak Ridge National Laboratory Report No. ORNLTM-271, 1962 (unpublished).
(18) R. A. Marcus, *J. Chem. Phys.*, **43**, 679 (1965).
(19) N. D. Stalnacher and A. C. Wahl, unpublished results.
(20) W. W. Brandt and G. F. Smith, *Anal. Chem.*, **21**, 1313 (1949).
(21) H. S. Gutowsky and A. Saika, *J. Chem. Phys.*, **21**, 1688 (1953).

Luminescence Induced by Crystallization of Organic Binary Mixtures

Keiji Takeda,* Takeshi Tomotsu, and Hisatake Ono

Research Laboratories, Tokyo, Fuji Photo Film Co. Ltd., Asaka, Saitama, Japan *(Received March 26, 1973)*

Publication costs assisted by Fuji Photo Film Co. Ltd.

A novel series of crystalloluminescent organic materials is discovered. The binary mixture of a nonconjugated ketone and acetonitrile or *N,N*-dimethylacetamide emits blue-white light pulses on crystallization at 77°K. The experimental conditions for effective emission are described. The experimental facts suggest the excitation mechanism that the emission phenomenon is essentially triboluminescence, brought about by strain energy in the mixed crystal. The crystalloluminescence spectra were recorded photographically with the use of a continuous interference filter. The emission spectra, with the maximum at about 460 nm, are able to be replaced by different spectra by the addition of a small amount of appropriate sensitizers. The mechanism of the emission process is elucidated by comparing the crystalloluminescence spectrum with photoluminescence spectra. In the absence of sensitizers, the crystalloluminescence emission comes from the lowest excited triplet state of the nonconjugated ketones, while with doped sensitizers, the triplet energy transfer takes place from the ketone to the sensitizers, the triplet states of which are responsible for the observed emission.

Introduction

The luminescence phenomenon which accompanies crystallization is known as "crystalloluminescence."[1,2] Luminescence has been observed when crystals precipitate from the saturated aqueous solution of a variety of inorganic salts such as alkali halides,[1-3] arsenic trioxide,[4] and barium chlorate.[4] On the other hand, only a few organic compounds such as benzanilide[5,6] have been found to luminesce on crystallization from the alcoholic solution.

There are several views on the mechanism of the crystalloluminescence; while Trautz[7] ascribed the crystalloluminescence to triboluminescence, caused by fracture of crystals formed, Garten and Head[2,8] deduced that the crystallization of each glassy nucleus causes one luminescence pulse. There had been no detailed study on the emission process of the crystalloluminescence.

We discovered a novel series of crystalloluminescent organic compounds. When a binary mixture of a nonconjugated ketone and another compound, *e.g.*, a mixture of acetone and acetonitrile, is frozen to crystallize in liquid nitrogen, a blue-white emission of light can be observed in a dark room or sometimes even in room light. The emission occurs as short discrete pulses from the whole crystal or a series of consecutive local flashes or sometimes a homogeneous faint glow, depending on particular compounds and on the pressure of dissolved gases in the crystal. The luminescence can be repeated by melting and refreezing the mixed compounds.

In this work, a search was first done for the crystalloluminescent combination among various organic compounds and also for experimental conditions for the effective emission. The emission spectra were recorded photographically with the use of a continuous interference filter. The mechanism of the emission process was studied in detail by comparing the emission spectra with phosphorescence and fluorescence spectra, obtained by photoexcitation. Discussion is also presented on the mechanism of the excitation process of the crystalloluminescence.

Experimental Section

Materials used in this work were from Wako Pure Chemical or Tokyo Kasei. Acetone and toluene were Wako Spectrosol. Biacetyl and 2,3-pentanedione were purified by distillation. Tetracyanoethylene (TCNE) and *N,N,N′,N′*-tetramethyl-*p*-phenylenediamine (TMPD), which was prepared by neutralization of the hydrochloride, were purified by sublimation. Other materials were used without further purification.

Samples for the crystalloluminescence were sealed in a Pyrex tube of 8–10 mm o.d. under a high vacuum. The crystalloluminescence was observed through a quartz window of a dewar vessel, in which the sample tube was im-

mersed in liquid nitrogen. The crystalloluminescence spectra were obtained with the use of the Continuous Interference Filter S-60 (Jenaer Glasswerk Schott & Gen.) and were recorded on photographic film (ASA 400), followed by densitometry. To ensure homogeneous exposure of the emitting light to the whole length of the filter, the filter with the attached film was moved in front of the luminescence source. The exposure was performed at a distance of about 3 cm between the film and the light source for about 5 min in one freezing batch. The batch was repeated by melting and refreezing the sample for the total exposure time of 1 hr. After the exposure, the optical density of the blackened film amounts 1 to 1.5 for most luminescent compounds. The filter is transparent for light of 380–730-nm wavelength with spectral resolution of 17 nm by half-width, while the photographic film has no sensitivity above 650 nm, so that the spectral distribution of the crystalloluminescence emission could be measured for the wavelength range from 380 to 650 nm. Corrections of emission spectra thus obtained were made allowing for the characteristic curve (*i.e.*, the density *vs.* exposure energy) of the film and the wavelength dependence of transmittance of the filter and of sensitivity of the film.

The photoluminescence spectra were measured using a Hitachi Fluorescence Spectrophotometer MPF-2A with a rotating sector for the phosphorescence measurement. The fluorescence was recorded in a dilute solution in acetonitrile at room temperature, while the phosphorescence was recorded in the crystalline state at 77°K. The spectra were obtained both in air and under vacuum, but no large difference was found between them. No correction was made on either of the photoluminescence spectra.

Results and Discussion

I. Combination of Compounds for Crystalloluminescence. Any pure compound examined does not luminesce on crystallization, while many compounds luminesce in a mixture with a suitable compound. For a binary mixture of organic compounds, A–B, with high solubility in each other, *e.g.*, acetone–acetonitrile, a large number of compounds (about 90 and 60 compounds for A and B, respectively) were examined as to occurrence of the luminescence on freezing at 77°K. The optimum composition of the A–B mixture for intense and frequent emission ranges widely about 50% for most cases so long as the sample freezes as a crystal but not as a glassy solid. The results of the luminescence are listed in Table I. In the mixture with acetonitrile or *N,N*-dimethylacetamide (DMA), most nonconjugated ketones examined luminesce, while all conjugated ketones examined do not luminesce at all or do so only slightly, without exception. Esters and amides luminesce in the mixture with acetonitrile but the emission of these carbonyl compounds is less intense than that of nonconjugated ketones. On the other hand, in the mixture with acetone (or some other nonconjugated ketones), acetonitrile and DMA are the most effective reagents for the crystalloluminescence. Most other nitriles (alkyl monocyanides, alkyl dicyanides, etc.) and amides (*N,N*-dimethylformamide, *N*-methylformamide, and formamide) fail to luminesce because of the glassification on freezing. A variety of compounds (alcohols and even benzene) are fairly luminescent. Mixtures of different ketones do not luminesce. Thus, one component for the binary systems must be a nonconjugated ketone for intense and frequent crystalloluminescence, while another component is not restricted to a particular kind of compound, *i.e.*, compounds with a particular functional group. The color of the emission is usually blue-white except the case of benzylacetone, which emits violet light.

II. Conditions for the Luminescence and Mechanism of the Excitation Process. The following possibilities are considered as the energy source of the crystalloluminescence: (a) energy of crystallization from liquid; (b) energy of crystallization from microglasses;[1] (c) energy of phase transition between polymorphic states;[9] (d) energy of strain in crystals;[7,10] (e) energy liberated by chemical interaction between two component molecules.

The experimental observations which should be taken into account in connection with the mechanism of excitation are as follows.

(1) Crystallization of the mixture is necessary for luminescence. No emission is observed when the mixture freezes as a transparent glass even if the mixture of the same components crystallizes to luminesce at a different composition ratio. The annealing of this glassy solid does not lead to the emission of light even though it crystallizes.

(2) The luminescent sample must be a mixture of different compounds. The pure constituent compounds do not luminesce on crystallization.

(3) In a narrower sample tube, the emission is less frequent than in a thicker tube, even though the crystal forms.

(4) The intense light pulses are usually accompanied by the occurrence of sound which can be caused by the destruction of crystals.

(5) The rate of crystallization has an effect on the luminescence. When the mixed sample is cooled to crystallize slowly in a space above liquid nitrogen in a dewar, followed by immersing the sample in liquid nitrogen, no emission is observed in the case of methyl ethyl ketone–acetonitrile and methyl *n*-butyl ketone–DMA or only slight emission is observed in the case of acetone–acetonitrile.

(6) The emission pulses occur mostly after the completion of the crystallization and last for more than 0.5 hr. The emission can be observed also on annealing the crystal at higher temperatures.

(7) There is an effect of dissolved gases on the luminescence. It is found that the presence of gases dissolved in the mixed sample affects the appearance of the luminescence, *i.e.*, the intensity, duration time, and luminescent area of each pulse and the frequency of pulses. The results are shown in Table II. The color of light emitted is not affected by the atmosphere.

(8) In general, the luminescent portion propagates in the crystal like a chain reaction, as observed in the crystalloluminescence of alkali halides.[2]

(9) One component of the luminescent mixture must be a nonconjugated ketone for effective emission, as stated before. On the other hand, there appears to be no selectivity of the chemical nature of the second component compound for the luminescence of the mixture; *i.e.*, not only highly polar molecules such as acetonitrile and DMA but also nonpolar molecules such as benzene are useful.

Experimental facts 5 and 6 rule out mechanism a for the excitation energy. No luminescence is observed when the phase transition between crystalline polymorphs occurs easily on slow cooling as in the case of the acetonitrile[11]–acetone mixture. This fact opposes mechanism c. Fact 9 excludes the mechanism e; *i.e.*, no selectivity in

TABLE I: The Crystalloluminescent Compounds

Luminescent	Not luminescent[b]
(a) In Mixture with Acetonitrile[a]	
Nonconjugated ketones	Nonconjugated ketones
CH_3COR (acetone, methyl ethyl ketone, methyl *n*-propyl ketone, methyl isopropyl ketone, methyl *n*-butyl ketone, methyl isobutyl ketone, methyl *n*-pentyl ketone, methyl *n*-hexyl ketone, methyl *n*-heptyl ketone, etc.)	Methyl *tert*-butyl ketone, diethyl ketone, and di-*n*-butyl ketone
$RCOR'$ (ethyl *n*-butyl ketone, diisobutyl ketone, etc.)	Conjugated ketones
Cyclic ketones (cyclopentanone, cyclohexanone, and its methyl derivatives)	Aromatic ketones (acetophenone, propiophenone, *n*-butyrophenone, phenyl isopropyl ketone, phenyl *n*-butyl ketone and α-naphthyl methyl ketone)
Polyketones other than α-diketones (acetylacetone, acetonylacetone, etc.)	Biacetyl, mesityl oxide, 1-acetyl-1-cyclohexene, 2,4-heptadiene-6-one, etc.
Benzylacetone	Other compounds
Other compounds (weakly luminescent)	Hydrocarbon (benzene)
Esters (methyl acetate, *tert*-butyl acetate, etc.)	Nitro compounds (nitromethane, 1-nitropropane, and 2-nitropropane)
Amides (*N,N*-dimethylacetamide and *N,N*-dimethylformamide)	Aldehydes (propionaldehyde, butyraldehyde, etc.)
	Amines (diethylamine and triethylamine)
	Alcohols (methanol, ethanol, 2-propanol, and water)
	Ethers (1,4-dioxane and diisopropyl ether)
(b) In Mixture with Acetone[c]	
Nitriles	Nitriles
Acetonitrile, isobutyronitrile, and methacrylonitrile	*tert*-Butyl cyanide
Amides	Ketones
N,N-Dimethylacetamide	Methyl ethyl ketone, acetophenone, etc.
Other compounds (weakly luminescent)	
Alcohols (isopropyl alcohol, *n*-butyl alcohol, isobutyl alcohol and *tert*-butyl alcohol).	
Hydrocarbon (benzene)	

[a] Most compounds which are luminescent in mixture with acetonitrile are also luminescent in mixture with *N,N*-dimethylacetamide. [b] A large number of compounds, the mixtures of which are not luminescent because of glassification on freezing, are not included in this table. [c] Most compounds which are luminescent in mixture with acetone are also luminescent in mixture with other nonconjugated ketones.

TABLE II. Effect of Dissolved Gases on Crystalloluminescence

	Intensity of pulses	Duration of a pulse	Luminescent area of a pulse	Frequency of pulses
1 atm pressure of air, N_2, and Ar	Intense	Very short	Whole crystal	One or few
After once evacuated	Weak	Short or longer	Local	Frequent
At about 10^{-3} mm	Intense	Very short	Whole crystal	Frequent

the chemical nature of the component used in the mixture with ketones rules out the chemical energy such as hydrogen bonding, charge-transfer interaction, or electrical dipolar interaction as a possible energy source for crystalloluminescence. Mechanism b could be the case. Microglassy particles could be metastabilized in the rapidly frozen solid mixture, although the opaque white solid appears as a crystal. In the case of alkali halides, Garten and Head[2] reported that a glassy particle crystallizes yielding a single pulse of light. However, this mechanism is not likely in the present luminescence of the organic binary mixture for two reasons. First, no luminescence is observed when the transparent bulk of the glassy mixture crystallizes by annealing, although the same compounds can crystallize and luminesce at a little different composition ratio of the two compounds (fact 1). Second, the energy of crystallization of nonionic crystals, like the present luminescent materials, is not sufficient to cause crystalloluminescence.[1]

The crystalloluminescence of the present systems is probably triboluminescence, as proposed for the luminescence of benzanilide;[1] *i.e.*, the energy source for the crystalloluminescence is probably the energy of strain built up in the rapidly frozen mixed crystals, the strain being released by fracturing of the crystal (mechanism d). This mechanism is implied by experimental facts 5 and 4; *i.e.*, the strain may not be built up sufficiently by slow crystallization and the sound as well as the photoemission may arise by fracture of crystals. Fact 3 coincides with the above mechanism such that, in a narrower sample tube, crystals formed are usually more oriented[12] and probably less strained than in a thicker tube as the result of effect of the wall.

As shown in Table II, the dissolved air as well as nitrogen and argon depress the frequency of the crystalloluminescence pulses remarkably. Therefore, the effect of air is not due to the chemical quenching of the excited state by moelcular oxygen but these gases may affect the mixed crystals physically by decreasing the strain of or friction between crystals.

Fact 2, together with the fact 9, suggests that nonconjugated ketones satisfy the chemical condition for excitation (*i.e.*, to the n,π^* state), while the second component of the mixture *e.g.*, acetonitrile, DMA, benzene, etc., physically affects the mixed crystal to be unstable and highly

strained. This is supported by the fact that the crystalloluminescence emission is actually from the lowest excited triplet state of the ketones, as will be shown later.

The failure to observe the crystalloluminescence of conjugated ketones seems significant in relation to the mechanism of molecular excitation by crystallization. It is obvious that the absence of crystalloluminescence of conjugated ketones comes from the lack of excitation process itself, because the photoemission from excited conjugated ketones is actually observed when a small amount of these molecules is dissolved in a nonconjugated ketone–acetonitrile (or DMA) mixture, as will be shown later. The conjugated ketones probably inhibit the excitation by stabilizing or capturing electrons, formed in the fractured surface of the crystal,[10] which otherwise discharge[13] to bombard molecules to excitation as for nonconjugated ketones. This explanation is coincident with the mechanism of triboluminescence.[7,10]

With the purpose of further proving the above mechanism, experiments were attempted to scavenge transient electrons by strong electron acceptors, TCNE and iodine. TCNE forms a yellow charge-transfer complex in acetone–acetonitrile solution, and TCNE radical anions were found by electron spin resonance (esr) in methyl *n*-butyl ketone (MBK)–DMA solution; 0.4% added TCNE and 0.07% iodine are found to be enough to quench the crystalloluminescence of MBK–DMA mixed crystals (2:3). However, the same amount of additives also quenches the photoexcited phosphorescence of MBK–DMA mixed crystals. Therefore, it is not clear from this experiment whether the crystalloluminescence is quenched at the excitation stage or at the emission stage.

The effect of other electron scavengers was also examined. Nitrous oxide, saturated in MBK–DMA solution, did not affect the crystalloluminescence intensity; 2.5% added carbon tetrachloride did not quench the crystalloluminescence of MBK–DMA mixture either. However, these facts are not necessarily contrary to the idea that crystalloluminescence is excited by electron bombardment, because the energy of electrons could be too high to be captured by these electron scavengers.

It could be a possible mechanism of excitation of the crystalloluminescence that free radicals may be formed by the fracture of crystals and that their recombination may excite molecules, as mentioned by Garten and Head.[1] In order to examine the possibility, 2,2′-diphenyl-1-picrylhydrazyl (DPPH) was used as a radical scavenger in the crystalloluminescent MBK–DMA mixture; 0.07% added DPPH quenches the crystalloluminescence but it also quenches the phosphorescence as TCNE and iodine did. The concentration of dissolved DPPH in the MBK–DMA system is followed by esr while repeating crystallization and melting of the mixture. However, after 15 repetitions of the cycle, no decay of DPPH was found. No esr signal was detected from the MBK–DMA crystal. Therefore, free radicals may not be responsible for excitation of the crystalloluminescence or the radical yield may be too low (if there is any) to be detected by the experiment.

III. Crystalloluminescence Spectra and Mechanism of the Emission Process. For elucidation of the mechanism of the emission process, *i.e.*, the process in which the state, first excited by crystallization, leads to the final emitting state of the crystalloluminescence, assignment of the crystalloluminescence spectra was done by comparing them with photoluminescence spectra, *i.e.*, phosphorescence and fluorescence or total emission spectra. The measurements of the phosphorescence and total emission spectra were carried out at the same experimental conditions used for the crystalloluminescence, *i.e.*, the same composition of the binary constituents, concentration of additives, purity, and the same state of the solid. In this way, the impurity emission, if any, should appear both in the phosphorescence and crystalloluminescence spectra as well if the emitting state of the crystalloluminescence is the lowest triplet state, and the discrepancy in the phosphorescence spectra between the crystalline and glassy states, which is actually observed in many cases, does not affect the assignment of crystalloluminescence spectra. The fluorescence spectra were obtained in a dilute solution in acetonitrile to avoid the inner filter effect on the spectral shape of the fluorescence, which is close to the absorption bands, so that any quantitative comparison between intensities of the phosphorescence and fluorescence cannot be made.

a. Nonconjugated Ketone–Acetonitrile or -N,N-Dimethylacetamide (DMA) Binary Mixtures. The binary mixtures of acetone, methyl ethyl ketone, or methyl *n*-butyl ketone (MBK) with DMA or acetonitrile and the mixture of ethyl *n*-butyl ketone with DMA show nearly identical broad, structureless crystalloluminescence spectra spreading from 400 to 600 nm, with its maximum at 460 ± 5 nm. The crystalloluminescence spectra of acetone–acetonitrile (1:1) and MBK–DMA (2:3) mixtures are shown in Figures 1 and 2, respectively, together with the phosphorescence spectra. In general, the crystalloluminescence and phosphorescence spectra coincide fairly well, although sometimes the crystalloluminescence spectra appear at somewhat higher wavelength than the phosphorescence spectra. The reported peak, λ_{max}, of the phosphorescence of acetone is at 455 nm,[14] which agrees well with the present observation. No emission peak corresponding to the fluorescence peak at 410 nm[14] is found in the crystalloluminescence spectrum of acetone–acetonitrile mixture. Therefore, the emitting species in these crystalloluminescent systems is thought to be the lowest excited triplet state of the ketones. This assignment is supported by the fact that the triplet quenchers, TCNE, iodine, and DPPH quench the crystalloluminescence, as stated before. It is appropriate to mention here that the triboluminescence emission is usually from nitrogen molecules which are excited by electron discharge.[10] The latter mechanism is not applicable to the present crystalloluminescence because the observed spectra do not fit to the emission of nitrogen molecule and the crystalloluminescence is observed even at a high vacuum.

The crystalloluminescence spectrum of benzylacetone–acetonitrile (1:1) mixture has a poorly resolved structure, which agrees with the vibronic fine structure of the phosphorescence of the same mixture, peaking at 390, 415, 442 nm, etc., although the crystalloluminescence peaks are red-shifted by about 10 nm from those of the phosphorescence. As a model for this system, the phosphorescence of toluene–acetone–acetonitrile (1:1:2) mixture was recorded in the crystalline state. The use of this model is verified by the fact that the absorption spectrum of the latter mixture in solution is identical with that of benzylacetone. The phosphorescence of toluene mixture, peaking at 400, 425, 445 nm, does not fit the phosphorescence of the benzylacetone–acetonitrile mixture. Therefore, the observed phosphorescence of the latter mixture is neither from the excited phenyl nor ketone parts of benzylacetone. The observed phosphorescence and crystallolumines-

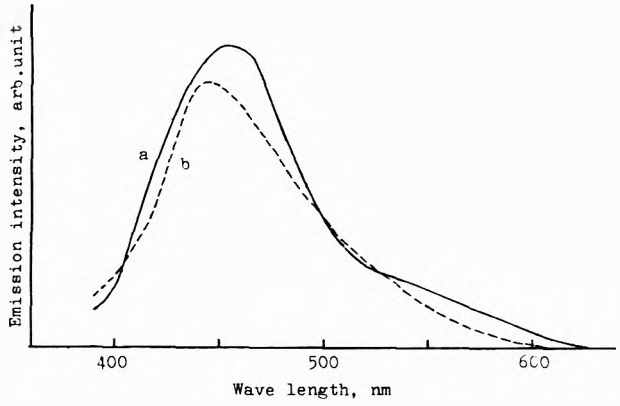

Figure 1. Emission spectra of acetone–acetonitrile 1:1 mixed crystals: (a) crystalloluminescence, recorded at 77°K photographically with use of a continuous interference filter (corrected); (b) phosphorescence, excited at 320 nm, recorded at 77°K by Hitachi Fluorescence Spectrophotometer MPF-2A (uncorrected). The same methods of measurement are used for all crystalloluminescence and phosphorescence spectra shown in following figures.

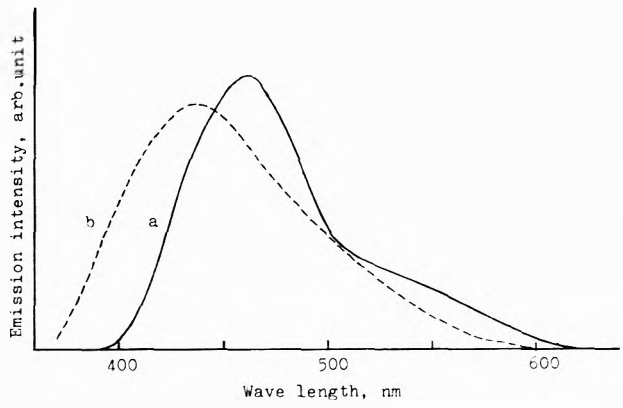

Figure 2. Emission spectra of methyl *n*-butyl ketone (MBK)–*N,N*-dimethylacetamide (DMA) 2:3 mixed crystals: (a) crystalloluminescence; (b) phosphorescence, excited at 320 nm.

cence spectra are found to be identical with those of the MBK–DMA mixture, doped with a small amount of acetophenone, as will be shown later. This fact leads us to the conclusion that the phosphorescence and crystalloluminescence of the benzylacetone system are due to the impurity acetophenone.

b. Effect of Additives on Crystalloluminescence Spectra. Spectral Sensitization. It is found that a small amount of additives is able to shift remarkably the crystalloluminescence spectra of acetone–acetonitrile or MBK–DMA systems.

Benzophenone. The crystalloluminescence of the MBK–DMA (2:3) mixture, doped with 6.7% benzophenone shows a structured spectrum and coincides with the phosphorescence spectrum of the same sample, as shown in Figure 3. The phosphorescence spectrum, peaking at 422, 454, 488, 524 nm, is assigned to that of benzophenone molecules.[15,16] Therefore it is clear that the emitting species of the crystalloluminescence of this system is the lowest excited triplet state of added benzophenone.

Acetophenone. The crystalloluminescence of MBK–DMA (2:3), doped with 6.7% acetophenone is red-shifted from the phosphorescence of the same mixture by 10 nm, but the crystalloluminescence spectrum agrees well in the structure and line shape with the phosphorescence which peaks at 388, 415, 442 nm and coincides with the phosphorescence of acetophenone molecules.[15,16]

Michler's Ketone. The addition of 3.3% Michler's ketone (*p,p'*-tetramethyldiaminobenzophenone) quenches completely the crystalloluminescence of the MBK–DMA (2:3) mixture, peaking at 460 nm (Figure 2) and a new emission peak appears at 490 nm (max), as shown in Figure 4. The crystalloluminescence peak coincides with the phosphorescence of the same system but not with the fluorescence. The emission with λ_{max} at 490 nm is obviously due to the phosphorescence of Michler's ketone molecules.[16]

Biacetyl. The addition of 3.3% biacetyl replaces the crystalloluminescence of MBK–DMA mixture to the emission, peaking at 475, 520 (max), and 560 nm, as shown in Figure 5. The latter two peaks coincide with the phosphorescence of the same system, which is assignable to the phosphorescence of biacetyl molecules.[15,16] The peak at

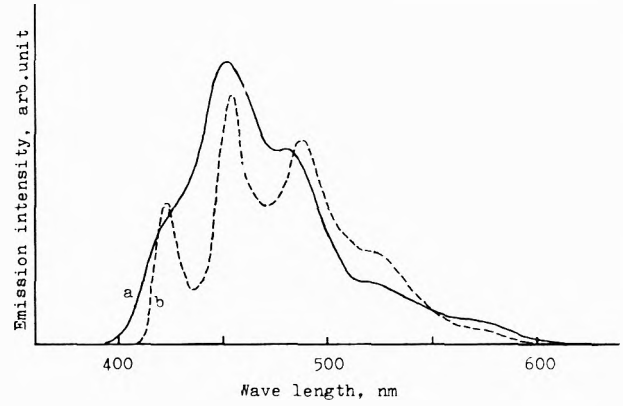

Figure 3. Emission spectra of MBK–DMA (2:3) mixed crystals, doped with 6.7% benzophenone: (a) crystalloluminescence; (b) phosphorescence, excited at 380 nm.

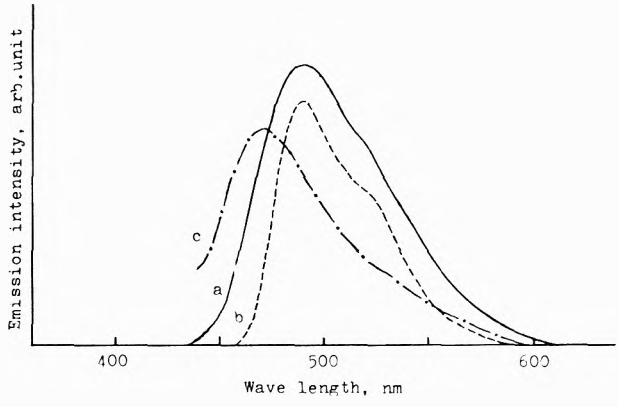

Figure 4. Emission spectra of MBK–DMA (2:3) mixture, doped with 3.3% Michler's ketone: (a) crystalloluminescence; (b) phosphorescence in crystal, excited at 400 nm; (c) fluorescence, excited at 420 nm, recorded with dilute solution (about 1%) in acetonitrile at room temperature by Hitachi Fluorescence Spectrophotometer MPF-2A (uncorrected). The same method of measurement is used for all fluorescence spectra, shown in following figures. Relative intensities among different spectra are arbitrary.

475 nm of the crystalloluminescence does not fit either phosphorescence or fluorescence. A similar spectral sensitization of the crystalloluminescence by biacetyl is observed also in the mixture of acetone and acetonitrile.

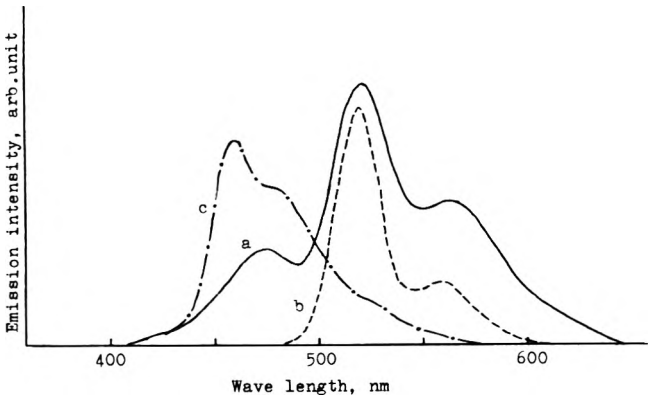

Figure 5. Emission spectra of MBK–DMA (2:3) mixture, doped with 3.3% biacetyl: (a) crystalloluminescence; (b) phosphorescence in crystal, exicted at 420 nm; (c) fluorescence in solution, excited at 400 nm. Relative intensities among different spectra are arbitrary.

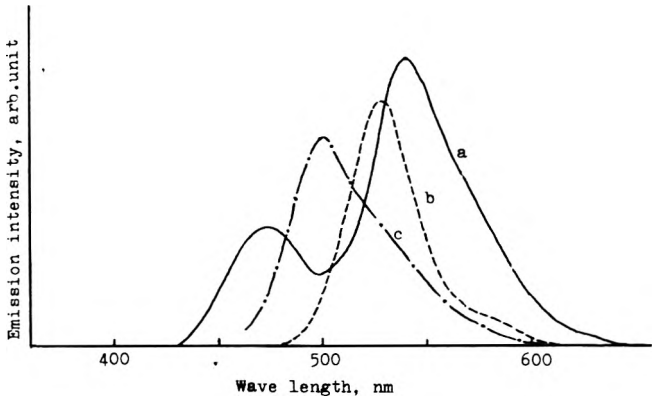

Figure 6. Emission spectra of MBK–DMA (2:3) mixture, doped with 3.3% benzil: (a) crystalloluminescence; (b) phosphorescence in crystal, excited at 400 nm; (c) fluorescence in solution, excited at 400 nm. Relative intensities among different spectra are arbitrary.

2,3-Pentanedione. The addition of 3.3% 2,3-pentanedione, doped in MBK–DMA, sensitizes spectrally the crystalloluminescence spectrum of the undoped mixture to longer wavelength, *i.e.*, to the peaks at 520 (max) and 560 nm, both of which coincide approximately with the phosphorescence of the mixture and is assigned to that of the additive.[16] A small emission peak appears also at 475 nm, which does not fit to the fluorescence, as in the case of biacetyl.

Benzil. The addition of 3.3% benzil replaces the crystalloluminescence of both MBK–DMA and acetone–acetonitrile mixtures, peaking at about 460 nm (max) to emission peaks at 475 and 540 nm (max), as shown in Figure 6. The latter peak is nearly identical with the phosphorescence of the system, which is assignable to the phosphorescence of benzil molecules.[16] However, the emission at 475 nm does not fit either fluorescence or phosphorescence.

Oxazoles. Oxazoles are known as fluorescent organic scintillators.[17] *p*-Di(5-phenyl-2-oxazolyl)benzene (POPOP) and 2-phenyl-5-biphenylyl-1,3,4-oxadiazole (PBO) show intense fluorescence in acetonitrile solution, with the emission maxima at 415 and 380 nm, respectively. The fluorescence, measured from the crystalline powder of these compounds, deviates largely from that in the solution, the maxima being at 443 and 400 nm, respectively. On the other hand, the crystalloluminescence spectrum of MBK–DMA, doped with 0.2% POPOP or 2.6% PBO, remains the same as that of undoped sample, and none of fluorescence and phosphorescence peaks appears in the crystalloluminescence spectra.

Other Additives. Added naphthalene and biphenyl do not alter the crystalloluminescence of the MBK–DMA mixture; no emission corresponding to the phosphorescence of these additives is observed. When diphenyloxazole, *trans*-stilbene, fluorenone, acridine, and some other compounds are added to the crystalloluminescent mixture, the frequency of luminescence pulses is reduced too much for the emission spectra to be recorded.

As shown above, a small amount of various conjugated ketones generally sensitizes spectrally the crystalloluminescence emission of nonconjugated ketone–acetonitrile or –DMA mixture to the wavelength of phosphorescence of the additives. The emission peak at 475 nm, observed in the case of α-diketone sensitizers, is not due to the phosphorescence or fluorescence of the sensitizer. The peak does not appear even in the photoexcited total emission spectrum, recorded at 77°K in the crystalline state, so that it could not be the emission of an exciplex or phosphorescence of very short lifetime. It could not be due to an impurity in the additives because any impurity emission is expected to be observed in the phosphorescence or in the fluorescence as well as in the crystalloluminescence spectra.

The emission of the α-diketone system at 475 nm could be due to an intermediate species which may be formed in the excitation process of crystalloluminescence but not by photoexcitation. It is well known that α-diketones like biacetyl and benzil are electron acceptors and their radical anions were actually observed by esr.[18] In this work, radical anions of biacetyl and benzil are prepared by ultraviolet photolysis of 2-methyltetrahydrofuran solution of the α-diketone and TMPD. The esr measurement confirmed the formation of trapped anions of biacetyl (5 or 7 lines with the hyperfine splitting of 6.4 G) and of benzil (unresolved line of 5-G width between the maximum slopes) which were formed by attachment of electrons liberated by photoionization of TMPD.[19] This sample does not show any phosphorescence emission other than that of α-diketones themselves. This fact, together with the observation that no esr signal is detected from the crystalloluminescent system of acetone–acetonitrile, doped with α-diketones, rules out the possibility of 475-nm emission in the crystalloluminescence spectra as due to the radical anions of α-diketone. At present, the emission peak cannot be assigned.

In some cases of additives, the crystalloluminescence spectra do not fit the phosphorescence exactly but are shifted to the longer wavelength by 10 nm or less from the latter spectrum. This may be the result of some errors, especially in the uncorrected spectra of the photoluminescence.

c. *Mechanism of the Emission Process.* The mechanism of the emission process is discussed below on the basis of the preceding observations. Nonconjugated ketones and sensitizing additives are abbreviated as K and S, respectively, and isc and P represent the intersystem crossing and the emission which corresponds to the phosphorescence, respectively.

In the absence of the sensitizing additives, processes 1 or 2 are consistent with the experimental observations. Process 1 is more general than process 2, but the direct excitation to the triplet state in process 2 should not be

neglected in the case of the excitation by electron bombardment or generally by high-energy radiation.[20] Fluorescence from $^1K^*$ was not observed in the crystalloluminescence spectra.

$$K \xrightarrow{\text{crystallization}} {}^1K^* \xrightarrow{\text{isc}} {}^3K^* \longrightarrow h\nu\,(P) \quad (1)$$

$$K \xrightarrow{\text{crystallization}} {}^3K^* \longrightarrow h\nu\,(P) \quad (2)$$

In the presence of the sensitizing additives, the original emission from $^3K^*$ is placed by the emission from $^3S^*$, the intensity of which remains about the same as that of $^3K^*$. Therefore, at least, the most emission comes from $^3S^*$ which is formed by energy transfer from $^3K^*$ and the following direct excitation of S may be neglected

$$S \xrightarrow{\text{crystallization}} {}^1S^* \xrightarrow{\text{isc}} {}^3S^* \longrightarrow h\nu\,(P) \quad (3)$$

$$S \xrightarrow{\text{crystallization}} {}^3S^* \longrightarrow h\nu\,(P) \quad (4)$$

Fluorescence from $^1S^*$ is not observed even for oxazoles. Therefore, the possible mechanism is

$$K \xrightarrow{\text{crystallization}} {}^1K^* \quad (5)$$

$${}^1K^* \xrightarrow{S} {}^1S^* \xrightarrow{\text{isc}} {}^3S^* \longrightarrow h\nu\,(P) \quad (6)$$

$${}^1K^* \xrightarrow{\text{isc}} {}^3K^* \xrightarrow{S} {}^3S^* \longrightarrow h\nu\,(P) \quad (7)$$

$$K \xrightarrow{\text{crystallization}} {}^3K^* \quad (8)$$

$${}^3K^* \xrightarrow{S} {}^3S^* \longrightarrow h\nu\,(P) \quad (9)$$

Process 6 involves singlet energy transfer from K to S, while processes 7 and 9 involve triplet energy transfer. In general, triplet energy transfer is more important.[21] Actually in the case of strongly fluorescent oxazoles, no fluorescence emission is observed in the crystalloluminescence spectra, so that the process involving the singlet energy transfer (6) is not the case. However, for ketones, the quantum yield of the intersystem crossing is near unity,[15,16] so process 6 cannot be excluded simply from the fact that no fluorescence emission is found in the crystalloluminescence spectra.

References and Notes

(1) V. A. Garten and R. B. Head, *Nature* (London), **209**, 705 (1966)
(2) V. A. Garten and R. B. Head, *Phil. Mag.*, **8**, 1793 (1963).
(3) C. Racz, *C. R. Acad. Sci.* **212**, 900 (1941).
(4) S. Tsuda, T. Takeda, and E. Shibata, *J. Chem. Soc. Jap.*, **60**, 157 (1939).
(5) G. P. Safonov, V. Ya. Shlyapintokh, and S. G. Entelis, *Nature (London)*, **205**, 1203 (1965).
(6) G. P. Safonov, V. Ya. Shlyapintokh, and S. G. Entelis, *Izv. Akad. Nauk SSSR, Ser. Khim.*, 1432, (1967).
(7) M. Trautz, *Z. Phys. Chem.*, **53**, 1 (1905).
(8) V. A. Garten and R. B. Head, *Phil. Mag.*, **14**, 1243 (1966); *J. Cryst. Growth*, **6**, 349 (1970).
(9) N. M. Johnson and F. Daniels, *J. Chem. Phys.*, **34**, 1434 (1961)
(10) H. Longchambon, *Bull. Soc. Fr. Mineral.*, **48**, 130 (1925).
(11) K. Takeda and F. Williams, *Mol. Phys.*, **17**, 677 (1969).
(12) M. A. Bonin, K. Takeda, and F. Williams, *J. Chem. Phys.*, **50**, 5423 (1969).
(13) H. Garcia-Fernandez, *Bull. Soc. Chim. Fr.*, 1599 (1969).
(14) R. Borkman and D. Kearns, *J. Chem. Phys.*, **44**, 945 (1966).
(15) R. S. Becker, "Theory and Interpretation of Fluorescence and Phosphorescence," Wiley, New York, N. Y., 1969, pp 157–159.
(16) R. S. Engel and B. M. Monroe, *Advan. Photochem.*, **8**, 245 (1971).
(17) R. C. Sangster and J. W. Irvine, Jr., *J. Chem. Phys.*, **24**, 670 (1956).
(18) R. Dehl and G. K. Fraenkel, *J. Chem. Phys.*, **39**, 1793 (1963); G. A. Russell and R. D. Stephens, *J. Phys. Chem.*, **70**, 1320 (1966).
(19) W. H. Hamill in "Radical Ions," E. T. Kaiser and L. Kevan, Ed., Interscience, New York, N. Y., 1968, p 322.
(20) R. A. Holroyd and C. Capellos, *J. Phys. Chem.*, **76**, 2485 (1972).
(21) A. A. Lamola and N. J. Turro, "Energy Transfer and Organic Photochemistry," Interscience, New York, N. Y., 1969, p 7.

Production of Trapped Electrons in Glassy 3-Methylpentane by Photoionization of Sodium[1]

S. C. Srinivasan and J. E. Willard*

Department of Chemistry, University of Wisconsin, Madison, Wisconsin 53706

(Received April 3, 1973)
Publication costs assisted by the U. S. Atomic Energy Commission

Photoionization of sodium metal dispersed in 3-methylpentane by deposition at 77°K from vapor mixtures yields trapped electrons with esr line width and half-life similar to electrons produced by γ irradiation of 3MP glass at 77°K. An apparatus for transferring samples condensed on a cold finger at 77°K to an esr sample tube at 77°K under vacuum is described. A narrow singlet signal at g near 2.0000, observed earlier *during* illumination of 3MP-metal matrices, and ascribed to weakly trapped electrons, is now known to be an electron cyclotron resonance signal from electrons ejected into the evacuated tube.

Introduction

When 3-methylpentane (3MP) and sodium are deposited from the vapor phase on a cold finger at 77°K in an evacuated tube and the system is irradiated with uv light in the cavity of an esr spectrometer, a narrow resonance signal (0.1 G) is produced which has a lifetime of less than 0.2 sec when the light is turned off.[2] This signal has been attributed to weakly trapped electrons which differ from those produced by γ irradiation of 3MP glass (*ca.* 3 G and >5 min $t_{1/2}$[3]) because of a difference in physical properties of the matrix or differences in the associated cation and method of production. We have now found[4] that the

signal is an electron cyclotron resonance signal of free electrons ejected into the evacuated space surrounding the cold finger by photoionization of a thin deposit of sodium on the walls of the container.

The present note describes further studies which show that trapped electrons with characteristics similar to those formed by γ irradiation of glassy 3MP can be produced by photoionization of sodium dispersed in 3MP deposited from the vapor. The photoionization of dispersed metals in organic glasses has potential as a method for investigating the effect of cationic differences on the properties of trapped electrons, and, by the use of different wavelengths, for investigating effects of varying the average cation-electron separation distances.

A simple apparatus for transferring deposits condensed on a cold finger to a conventional 3-mm i.d. esr tube for irradiation and examination is described.

Experimental Section

The body of the apparatus for matrix preparation (Figure 1) was made from the outer and inner (A) and (A′) portions of a 45/50 standard taper ground glass joint sealed with Apiezon N grease. It was fitted with a stopcock (B) for access to the vacuum line, a 12-mm o.d. cold finger (C) which could be rotated in the 14/20 ground joint (D) (lubricated with silicone grease) while containing liquid nitrogen up to a level slightly below the joint, and a 9-mm o.d. cold finger (E) which could be rotated and moved vertically in the cajon type adapter (F) (sealed into the glass with Picein wax). The cold finger (E) carried a cutting point (G) made from a strip of stainless steel wrapped around a square indentation in the tube and bolted at the point of overlap. A layer of indium metal between the steel and the glass improved thermal contact. An inlet tube (H) connected the deposition chamber to a reservoir of liquid 3MP at −78° from which the rate of flow of vapor to the cold finger (C) was adjusted to 0.1–0.2 ml/hr by a stopcock. When an Na-containing matrix was desired, the vapor was allowed to pass over Na metal placed near the junction of tube (H) with the vessel (A′). The tube (H) was heated with resistance wire for several centimeters prior to this point. About 1 ml of 3MP containing *ca.* 10^{19} atoms of Na (as determined by mass spectrometric analysis for the H_2 evolved when the deposit was treated with water) was deposited on the finger (C). Following the deposition, the finger (E) was filled with liquid nitrogen, the cutting point (G) was forced against the deposit on (C), and (C) was rotated causing the deposit to flake off. A substantial part fell to the bottom of the 3-mm i.d. Suprasil esr tube (I), which was attached to the main vessel by the graded seal (J). During the scraping the entire apparatus was immersed in a large dewar of liquid nitrogen up to about the level of the cutting edge. Following the scraping the dewar was lowered and the Suprasil tube was sealed off at its upper end. To prevent flakes of the matrix which melted on the bottom of the large container from draining into the esr tube, a styrofoam cup filled with liquid nitrogen was positioned at (K) by means of the outer portion of a ground joint cemented to a hole in its base. The pressure in the vessel A–A′ was maintained at 10^{-5} Torr. A stream of He gas bubbled through the liquid nitrogen in the cold finger (E) reduced its temperature to a point where the temperature of the knife was 77°K, whereas it was 90°K without this precaution.

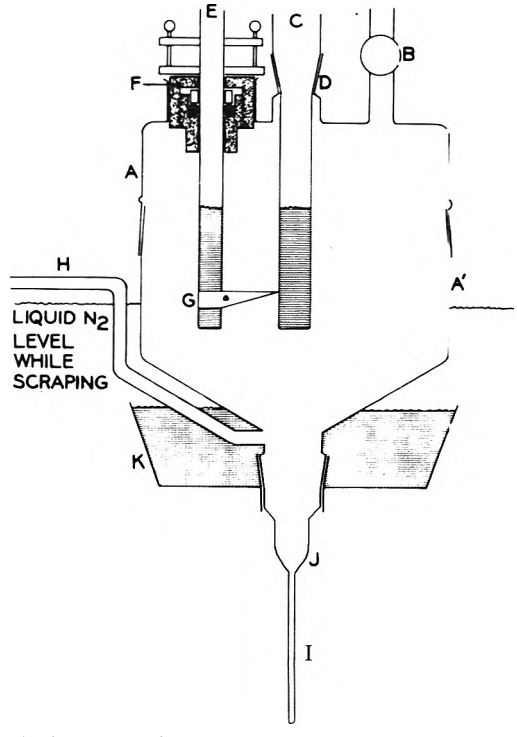

Figure 1. Apparatus for condensation of 3MP vapor and 3MP–Na vapor mixtures on a cold finger and for subsequent removal and transfer to an esr tube. See text for lettering code and discussion of operation.

The 3MP used was Phillips Pure grade, further purified by passage through 5 ft of freshly activated silica gel, storing over Na–K alloy on the vacuum system, and pumping on the liquid to remove CO_2.

Esr measurements were made in the X band with a Varian spectrometer using 10^5-Hz modulation frequency.

Results

Characteristics of 3MP and 3MP-Na Mixtures Condensed from the Vapor Phase. Deposits of 3MP condensed from the vapor phase as described above were white and translucent in the absence of sodium. With sodium incorporated they varied from light to deep purple depending on the temperature of the Na reservoir. The four-line esr signal of Na atoms[5] was not observed in any sample, implying that all of the Na was present in agglomerates, unless line broadening obscured the spectrum. An esr line of 12 G width (ΔH_{ms}) attributable to conduction electrons[6] was observed (Figure 2). This implies agglomeration sufficient to give the particles metallic character, while the symmetric nature of the signal implies that the particle diameters are less than the skin thickness of *ca.* 5 μ for the X-band microwave radiation.

Effects of γ Irradiation. γ-Irradiated (10^{19} eV g^{-1}) samples of 3MP and of 3MP–Na prepared by vapor deposition gave esr spectra similar to those from γ-irradiated 3MP glass formed by immersing the liquid in liquid nitrogen. These consist of the spectrum of trapped electrons superimposed on the spectrum of a free radical produced from the matrix (Figure 3a,b). The electron signal decayed with an initial half-life of about 25 min, similar to that in samples of partially annealed 3MP glass formed from the liquid.[7]

Effects of Uv Irradiation. When samples of 3MP–Na condensed from the vapor state were exposed at 77°K to

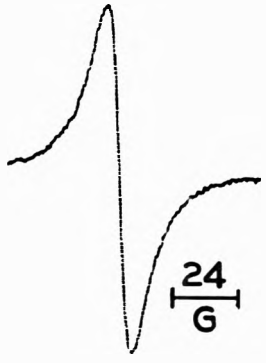

Figure 2. Esr spectrum at 77°K of conduction electrons in 3MP–Na condensate prepared in apparatus of Figure 1. Power, 1.5 mW; modulation amplitude, 2 G; signal level, 2000; recorder scale, 600 mV.

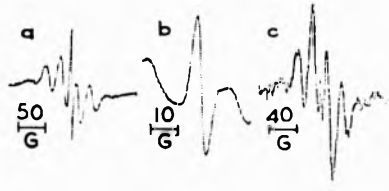

Figure 3. Esr spectra from γ-irradiated and photolyzed 3MP–Na condensate prepared in apparatus of Figure 1. Power, 0.2 mW; modulation amplitude, 2 G; signal level, 100; recorder scale, 60 mV. (a) Trapped electron singlet superimposed on six-line free radical signal from γ irradiation; (b) trapped electron singlet of spectrum (a), shown at slower scan rate; (c) free radical signal, following illumination of 3MP–Na condensate with AH4 lamp at 77°K. Small narrow line is residual electron signal.

Figure 4. Repetitive scans of trapped electron signal produced by photoionization of Na in 3MP. (A) Steady-state illumination with AH4 lamp and 27 mm of 7-54 filter; (B) light turned off; (C) light turned on with no filter; (D) 3-mm 7-54 filter inserted; (E) filter removed; (F) 9-mm 7-54 filter inserted.

the radiation of a quartz-jacketed AH4 medium-pressure mercury arc through a Corning 7-54 filter, an esr signal attributable to trapped electrons grew to a steady-state concentration in *ca.* 3 min (Figure 4). When the light was turned off the signal decayed with an initial half-life of *ca.* 5 min, again in the range observed for electrons formed by γ irradiation of 3MP glass[7] (for which the $t_{1/2}$ varies with time following irradiation and time of preirradiation annealing). The signal bleached rapidly in visible light and, consistent with this, was very weak when the AH4 lamp was used without a filter to reduce the intensity of exposure in the region of trapped electron absorption spectrum (Figure 4). A 3-mm thickness of Corning 7-54 filter has a maximum transmission of *ca.* 85% in a band around 320 nm and removes wavelengths greater than 410 nm except for a relatively weak transmission starting at 680 nm, passing through a maximum of 40% at 730 nm, and falling to 10% at 1000 nm. Figure 4 shows that the concentration of electrons during continuous illumination increases with increasing filter thickness (3, 9, and 27 mm). This is consistent with the decrease in ratio of transmission of the wavelengths which bleach electrons to that of the wavelengths which form electrons.

As observed in the previous work,[2] free radicals are formed by a sodium photosensitized reaction during illumination of the 3MP–Na matrices (Figure 3c).

Discussion

Annealing of 3MP glass at 77°K changes the physical properties in a way to reduce the rate of decay of trapped electrons.[7] Polycrystalline hydrocarbons of low molecular weight are much less efficient in trapping electrons than glassy hydrocarbons.[8] In view of such effects of changes in physical state, it would not be surprising if, as suggested earlier,[2] electrons were much more weakly trapped in 3MP deposited from the vapor phase than in the glass formed by quenching the liquid at 77°K. The present work indicates that the properties of trapped electrons are at least qualitatively similar in the two types of matrices and that trapped electrons with lifetimes convenient for study on the time scale of minutes to hours can be produced in 3MP by photoionization of sodium. This should make possible studies of the relative fates of electrons produced with different energies of activating light, and allow observation of properties of the electrons in the presence of fewer by-product fragments than when γ irradiation is used.

The free radicals formed during photolysis of the 3MP–Na matrix must result from a sodium-photosensitized process utilizing the energy from neutralization of Na^+, or energy transferred from an excited state. The initial free radical spectrum (Figure 3c) is different from that following γ irradiation (Figure 3a). There is evidence[2] that it changes on standing to the type of 3a, suggesting the presence of a second radical, possibly methyl, in addition to the 3-methylpentyl radical.

References and Notes

(1) This work has been supported in part by the U. S. Atomic Energy Commission under Contract No. AT(11-1)-1715 and by the W. F. Vilas Trust of the University of Wisconsin.
(2) F. W. Froben and J. E. Willard, *J. Phys. Chem.*, **75**, 35 (1971).
(3) For references and discussion, see A. Ekstrom, *Radiat. Res. Rev.*, **2**, 381 (1970).
(4) S. C. Srinivasan and J. E. Willard, *J. Chem. Phys.*, in press.
(5) C. K. Jen, V. A. Bowers, E. L. Cochran, and S. N. Foner, *Phys. Rev.*, **126**, 1749 (1962).
(6) G. Feher and A. F. Kip, *Phys. Rev.*, **98**, 343 (1954).
(7) D. Shooter and J. E. Willard, *J. Phys. Chem.*, **76**, 3167 (1972).
(8) N. A. Bonin, J. Lin, K. Tsuji, and F. Williams, *Advan. Chem. Ser.*, **No. 82**, 269 (1968).

Radiation Chemistry of Polyethylene. XII. Alkyl Radical Decay and Amorphous Content[1]

David R. Johnson, Walter Y. Wen, and Malcolm Dole*

Department of Chemistry, Baylor University, Waco, Texas 76703 (Received January 23, 1973)

Publication costs assisted by the U. S. Atomic Energy Commission

The decay of the alkyl free radical, $-CH_2\dot{C}HCH_2-$ in γ-irradiated polyethylene was studied at room temperature and above. No second-order decay component in the total decay process could be observed; instead the decay data were quantitatively interpreted in terms of a fast and slow first-order decay process. It is shown that the slow first-order decay constants increase linearly with the square of the amorphous volume fraction; the fast first-order constants also increase with increase of amorphous fraction, but the data scatter considerably. Hydrogen gas which is soluble only in the amorphous fraction has a marked catalytic effect on both the slow and fast decay processes. The activation energies of both processes are practically identical, so that the large difference in the rates results from differences in the preexponential factor of the Arrhenius equation.

Introduction

In this paper the kinetics of decay at room temperature and above of alkyl free radicals in irradiated polyethylene (PE) are discussed chiefly from the standpoint of the morphological structure of the solid and of the catalytic effect of hydrogen gas. Data obtained by more sophisticated esr techniques and new mathematical approaches are used. Previous studies of radical decay in irradiated PE have been recently reviewed by Dole[2] and Butiagin[3] and such discussions will not be repeated here except where pertinent to the present work.

Experimental Section

In general the technique consisted of irradiating the PE with Co-60 γ rays at 77 K and then heating the sample to a selected temperature where the radical decay was then quantitatively measured. Details of the experimental work are the following.

1. Materials Studied. Marlex-6002 PE, a linear polyethylene containing vinyl end groups was the polymer studied. The density of the initial film was 0.9595 g cm^{-3} at 25° as determined in an ethanol–water density gradient column. Not much scatter was observed from different samples of this film material which indicated that the film was homogeneous with respect to its amorphous content. The volume fraction of amorphous content was calculated from the equations[4]

$$\alpha_v = 6.8882 - 6.8951\rho \quad \text{(at 25°)} \quad \text{(1a)}$$

$$= 6.6973 - 6.7087\rho \quad \text{(at 29°)} \quad \text{(1b)}$$

where ρ is the density of the sample. The numerical factors were calculated taking the specific volumes of the 100% crystalline and amorphous fractions at the different temperatures as given by the equations of Chiang and Flory.[5] Because of changes in volume with temperature of the pure crystalline and amorphous components, α_v will change slightly with temperature, but the changes are negligible compared to uncertainties in the kinetic constants given below.

To prepare samples of different amorphous content illustrated in Figure 1, the PE film was held in a sandwich between two copper plates, degassed in a vacuum oven overnight, and then held at 135° for 2 hr. The samples were then quickly transferred to water baths ranging in temperature from 0 to 100°. After 2.5 hr in these baths they were transferred to room temperature and allowed to stand in air for 24 hr before their densities were measured at 29° in a density gradient column. For some samples both a water–ethanol column and a chlorobenzene–toluene column were used. Agreement between the two methods was good, and average values were taken. As demonstrated by the data of Figure 1 the amorphous volume fraction decreased linearly with increase of temperature of the crystallizing bath. The density and α_v values of the different samples are collected in Table I. The density of the different samples was not changed significantly by the irradiation.

2. Irradiation Techniques. All samples were γ-irradiated *in vacuo* at 77 K at a dose rate of about 0.28 Mrad hr^{-1} using previously described techniques.[6] After the irradiations esr signals in the quartz tube were annealed out by heating one end of the tube while the other end was immersed in liquid nitrogen. The sample was then shaken to the annealed end at 77 K and esr measurements made with the sample in the annealed end.

Before the kinetic experiments at room temperature and above were carried out, the samples were heated to room temperature and the hydrogen produced by the irradiation evacuated. This was accomplished by placing the dewar flask containing the irradiated samples in quartz tubes into a nitrogen atmosphere, then breaking open the tubes and pumping out the hydrogen on a vacuum line as the tubes warmed to room temperature. The tubes were next reinserted into the dewar flask, reheated to room temperature, and again evacuated. This process was repeated until no pressure increase could be detected on heating to room temperature. In the process of evacuating the hydrogen some free radicals decayed, but usually 20–35% of the radicals initially present at 77 K remained. Most of the radicals that had decayed did so during the heating from 77 K to room temperature. Some sample tubes were broken open in air and quickly attached to the vacuum line; no difference in the results could be de-

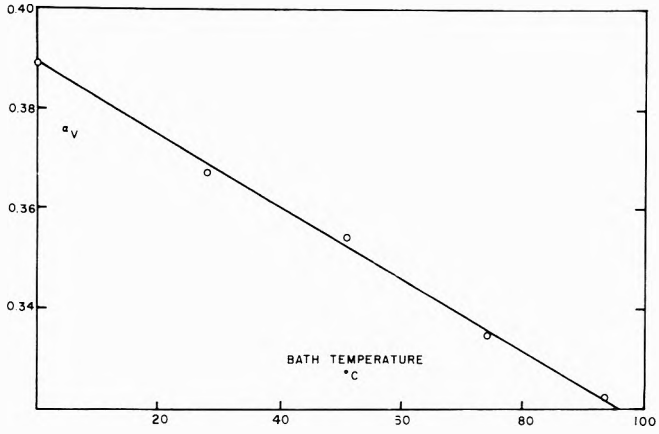

Figure 1. Amorphous volume fraction of bulk polyethylene samples after quenching from the melt at the bath temperature indicated.

TABLE I: Densities and Amorphous Volume Fractions of Polyethylene Samples Studied

Sample no.	Type of sample	Recrystallization temp, °C	Density, g cm^{-3}	Temp of density measurement, °C	Volume fraction, α_v
1	Film as received		0.9595	25	0.272
2	Quenched film	0	0.945 ± 0.005	25	0.373
3	Annealed film	a	0.9566	25	0.223
4	Bulk recrystallized	0	0.9403	29	0.389
5	Bulk recrystallized	28	0.9435	29	0.368
6	Bulk recrystallized	51	0.9455	29	0.354
7	Bulk recrystallized	74	0.9484	29	0.335
8	Bulk recrystallized	93	0.9503	29	0.322

[a] Slowly crystallized below 135°.

tected between these samples and those opened under nitrogen. The tubes were then sealed off while still on the vacuum line and replaced in the liquid nitrogen bath until used in the kinetic experiments. For experiments at 60° it was estimated that about 90 sec was required for the sample in the esr cavity to heat up to 60° from 77 K. About another 2 or 3 min was required to adjust the esr spectrometer before actual measurements could be begun. In all of the figures of the kinetic experiments shown in this paper, zero time was the time at which the esr measurements began.

Hydrogen at known pressures was introduced into the sample tubes while still on the vacuum line in the case of the experiments in which the catalytic effect of hydrogen was studied.

3. Esr Techniques. Esr measurements were made using a Varian E-4 electron spin resonance spectrometer. This spectrometer was interfaced with a Varian Spectro-System 100 computer so that total spin concentrations could be measured at 93 K by scanning the spectrum. Using a computer program supplied by Varian, double integrations of the first derivative curves were carried out. Relative changes in the alkyl radical, $-CH_2\dot{C}HCH_2-$, concentrations were also followed by observing the changes in

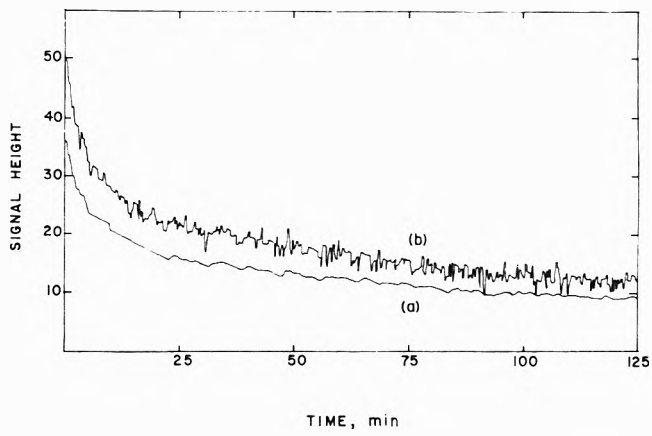

Figure 2. Comparison of a direct esr recording of alkyl decay, curve b, with a computer automatically smoothed curve of the same data, curve a.

the alkyl wing peak as previously described.[6] The alkyl wing peak is the outermost and weakest peak of the six-line alkyl spectrum. Esr signals from allyl radicals present do not overlap with the alkyl wing peak.

During the kinetic experiments a continuous recording of the height of the alkyl wing peak was made. All kinetic data used in the calculations came from these height measurements. By storing in the memory of the computer 19 data points before and after a certain point and averaging them, the computer could then signal the recorder to make a graph of an average or "smoothed" alkyl decay curve. Such an automatic smoothing process is illustrated in Figure 2 where the normal curve is compared with the smoothed curve, the two curves being displaced by a constant factor to avoid overlap. Kinetic data were read off of the smoothed curve. Computer control of the data acquisition also allowed the alkyl decay results to be stored in memory up to 1000 data points. These could then later be printed out by teletype for kinetic analysis.

Power saturation of neither the alkyl nor allyl radical occurred at room temperature at 0.2 mW power, but at 93 K the power had to be reduced to 0.0632 mW to avoid power saturation in the case of the allyl radical.

In order to determine absolute alkyl and allyl radical concentrations, the total area of the allyl radical spectrum which is very stable at room temperature was compared with area measurements of a freshly prepared solution of diphenylpicrylhydrazyl in benzene. By area measurements we mean the area after the double integration of the first derivative spectrum. The PE sample was then cooled to 93 K and the alkyl and allyl areas compared. According to theory[7a] the magnitude of the total area under the absorption curve should increase in proportion to $1/T$ or 3.1 on cooling from 288 to 93 K. In the case of a strong pitch sample the measured ratio was 3.0, but only 2.07 in the case of the allyl radical. The reason for the discrepancy in the case of the allyl radical is unknown, but since the environments of the allyl and alkyl radicals in PE are similar, it was decided to use the allyl radical area at 93 K as the standard, rather than the pitch area.

An experiment was done to compare the relative changes with rise of temperature of the height of the alkyl wing peak and the total area. After measuring these quantities at 93 K, the samples were heated to 253 K for 10 min and then recooled to 93 K where the peak heights and areas were again measured. From the data of Table II it can be seen that the percentage of total radicals remain-

TABLE II: Percentage of Initial Alkyl Radicals Remaining after Heating to 253 K as Measured from Total Areas and Wing Peak Heights[a-c]

Sample no.	Sample type	α_v	% radicals remaining: From peak heights	From area	Ratio area %/ht %
2	Quenched film	0.373	39.2	31.4	0.80
1	Film as received	0.272	53.5	40.2	0.75
3	Annealed film	0.223	60.0	42.0	0.70

[a] All peak heights and areas were measured at 93 K. [b] Samples held at 253 K for 10 min. [c] Hydrogen not evacuated.

TABLE III: Change in Peak Width[a,b] at Half-Height of Alkyl Wing Peak on Heating to 253 K

Sample no.	Sample type	α_v	Peak width[c]: Initial	Final	% change
2	Quenched film	0.373	29.1	21.6	25.7
1	Film as received	0.272	26.5	18.8	29.0
3	Annealed film	0.223	24.9	17.2	31.0

[a] All peak widths measured at 93 K. [b] Hydrogen not evacuated. [c] Arbitrary units.

ing was less as measured by the total area method than by the peak height method. This was surprising as some of the alkyl radicals must have decayed to allyl radicals[6] whose areas would be included in the total area measurements. A possible explanation is that some chain end free radicals $-CH_2CH_2\cdot$ might have been initially present and contributed to the initial total area measurement; as these rapidly decayed out as suggested by Butiagin,[3] the final area might have been reduced. Another possibility is that the esr spectrum of the alkyl radicals may have been different for different radicals; that is, the proton coupling constants may have varied slightly depending on whether the alkyl radicals were in the crystalline or amorphous phase.

The change in peak width of the first derivative spectrum at half height (the positive peak to negative peak distance as measured along the base line) of the alkyl wing peak decreased as measured at 93 K due to the heating to 253 K, see Table III. Nara, *et al.*,[8] also noted a change in line width with temperature in the case of their linear PE samples. By taking difference esr spectra they concluded that the alkyl free radicals that decayed between 77 and 204 K had been trapped in the gauche conformation with a hyperfine splitting constant of 25 G. At higher temperatures the radicals that decayed had the trans zig-zag conformation with a splitting constant of 22 G.

Poole[7b] has discussed and compared Gaussian and Lorentzian line shapes; according to both mathematical formulations the area, A, divided by peak height of the first derivative spectrum, y', and by the square of the peak width at half height (positive peak to negative peak distance as measured along the base line), $(\Delta H_{pp})^2$, should be a constant with the Lorentzian constant 3.5 times the Gaussian. With respect to the data of Tables II and III, this means that the percentage of radicals as calculated from the area measurements divided by the percentage calculated from the peak heights and by the square of the peak widths should be a constant (in arbitrary units). These so-called constants decreased linearly with increase of amorphous content, the total change being about 38%; the area also decreased with increase of α_v but not linearly. As a result of the change in peak shape with temperature and free radical concentration the absolute values of the alkyl radical concentration at room temperature and above may be in error by as much as 38%, but the relative changes in peak height at any one temperature on which all of the following kinetic data are based are much more reliable because in the kinetic experiments neither the amorphous content nor the temperature changed with time.

TABLE IV: G(Alkyl) for γ-Irradiation of Polyethylene Samples *In Vacuo* at 77 K

Sample no.	Type of sample	α_v	No. of samples	G(alkyl)
2	Quenched film	0.373	11	3.74 ± 0.21
1	Film as received	0.272	8	3.32 ± 0.26
3	Annealed film	0.223	1	3.69

4. Temperature Measurements. The variable temperature controller made by Varian Associates was used to control the temperature of the esr spectrometer cavity during the kinetic runs. Cavity temperatures were always checked by means of a copper–constantan thermocouple before and after the kinetic experiments.

5. Alkyl Radical G Values. Eight experiments performed on sample 1 in which the radicals produced in the quartz sample tubes were annealed out resulted in a G(alkyl) value (number of alkyl radicals produced by γ-irradiation at 77 K per 100 eV of energy absorbed) equal to 3.32 ± 0.26. Waterman and Dole[9] previously found G(alkyl) for the film as received to be 3.3 ± 0.5. In 11 experiments of the present work on sample 1 in which the quartz radicals were not annealed out G(alkyl) was 3.60 ± 0.18. In Table IV are collected G(alkyl) values (obtained after annealing out the quartz signals) for the three different types of polyethylene studied. There seems to be no definite trend in G(alkyl) with crystallinity.

6. Fraction of Radicals Surviving the Heating to Room Temperature. Because it has been found by others[8,10] that radicals decay more rapidly in branched than in linear PE one would expect that the samples with the highest amorphous fraction would have a lower free radical concentration on heating to room temperature than highly crystalline samples. This expectation is borne out by the results of this research, see Figure 3.

Kinetics of Alkyl Radical Decay

If the alkyl radicals decayed by a second-order process, then the relative rate of decay c/c_0 with time should be a function of the initial radical concentration or of the radiation dose. By doubling the dose, the relative rate of decay remained unchanged in our work; hence there was no second-order reaction involved in the decay process of our samples. Although Nara, *et al.*,[8] Charlesby, *et al.*,[10] and Auerbach and Sanders[11] observed a second-order decay rate, there could not have been any significant second-order decay in the case of our samples heated to 40 or 60°. Waterman and Dole[6] observed a second-order alkyl decay, but only in the case of alkyl free radicals regenerated from

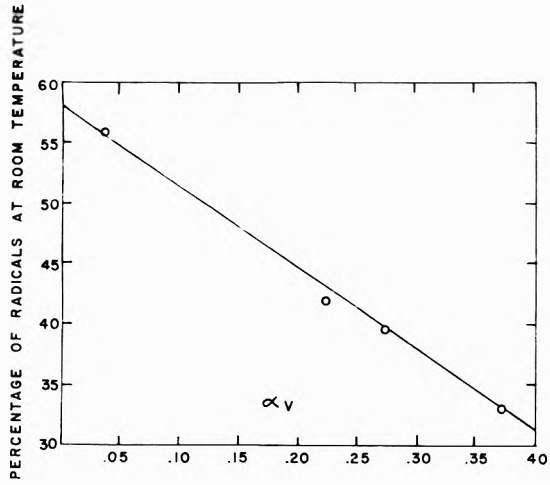

Figure 3. Percentage of alkyl radicals produced by irradiation at 77 K which survived a heating to room temperature after 5 min in samples of different amorphous content. The point at the lowest α_v value represents the percentage of radicals in an extended chain sample of polyethylene whose radical decay kinetics will be discussed in a subsequent paper.

allyl radicals by uv radiation at 77 K. These regenerated alkyl radicals decayed at a measurable rate only in the presence of hydrogen gas.

The decay was first order in dose, but not in time. This type of decay is called composite first order by French and Willard.[12] A first-order plot of our data demonstrated that at long times, the decay rate was first order in time; this suggested that there were two first-order processes occurring simultaneously, but with different first-order decay constants. Let c_s be the concentration of the alkyl radicals decaying slowly and c_f the concentration of the rapidly decaying radicals. We can write then

$$c = c_s + c_f \tag{2}$$

and if c_s and c_f are given by the first-order equations

$$c_s = c_s^0 e^{-k_s t} \tag{3a}$$

$$c_f = c_f^0 e^{-k_f t} \tag{3b}$$

then

$$c = c_s^0 e^{-k_s t} + c_f^0 e^{-k_f t} \tag{4}$$

where c is the total alkyl radical concentration, and t the time. Equation 4 can be rearranged to

$$\ln \frac{c - c_s}{c_s} = \ln \frac{c_f^0}{c_s^0} - (k_f - k_s)t \tag{5}$$

By observing the decay rate at long times, k_s can be determined and c_s then calculated for short times, so that the ratio $(c - c_s)/c_s$ can be evaluated. Figure 4 illustrates the application of eq 4 to alkyl decay data at 60° for the film as received, sample irradiated to two different doses. The agreement between the data for the different doses demonstrates the absence of any significant second-order decay process. Knowing k_s, k_f can be determined from the slope of the straight line of Figure 4 which is equal to $(k_f - k_s)$. From the intercept at zero time on the ordinate, $(c^0 - c_s^0)/c_s^0$ can be calculated and because c^0 is known, then both c_s^0 and c_f^0 can be separately determined. All of these constants were determined by the least-squares method. Data for c_s and c_f in arbitrary units (esr peak heights normalized to unit weight, unit dose, and unit receiver gain) for decay *in vacuo* at 60° are collected in

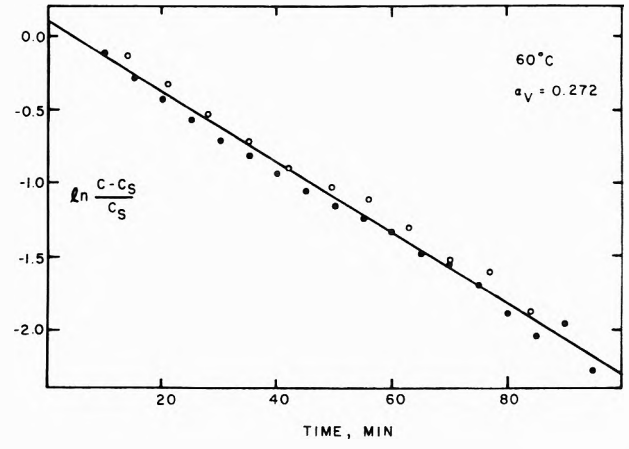

Figure 4. Test of eq 5. Alkyl radical decay at 60° *in vacuo:* open circles, 14 Mrads dose; closed circles, 22 Mrads dose; film as received (sample 1).

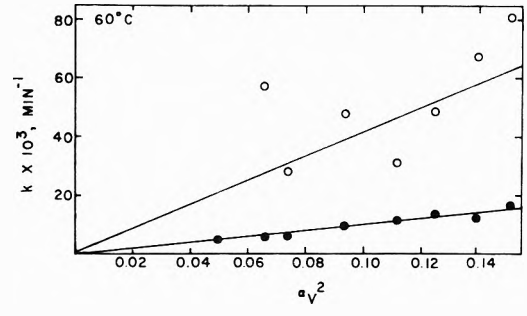

Figure 5. First-order alkyl radical decay constants at 60° as a function of the square of the amorphous volume fraction of the different samples of PE studied: solid circles, k_s values; open circles, k_f values.

TABLE V: Extrapolated Initial Alkyl Free Radical Concentrations at 60° *in Vacuo* after an Irradiation at 77 K[a]

Sample no.	α_v	c_s^0	c_f^0	c_f^0/c_s^0
4	0.389	0.153	0.135	0.9
6	0.354	0.302	0.284	0.9
7	0.335	0.226	0.211	0.9
8	0.322	0.158	0.161	1.0
1	0.272	0.473	0.515	1.1

[a] Concentration in arbitrary units.

Table V. A surprising result was the almost equal initial abundances of the fast and slowly decaying radicals at zero time. This was true also in the experiments with hydrogen present.

We consider first the first-order decay constants in relation to the amorphous content of the samples studied. In the case of k_s the data for the different bulk PE samples can be shown to increase very nearly exactly in proportion to α_v^2 and a least-squares analysis of the data obtained at 60° *in vacuo* yielded the equation

$$k_s = 1.12 \times 10^{-1}\alpha_v^2 - 1.3 \times 10^{-3} \text{ min}^{-1} \tag{6}$$

with an uncertainty in the slope of ±0.012 and in the intercept at zero amorphous fraction of ±0.0012. From Figure 5, however, the k_f values can be seen to scatter considerably due to the difficulty of making exact k_f measurements. Nevertheless the trend of increasing first-order decay constants with increasing amorphous content is clearly seen.

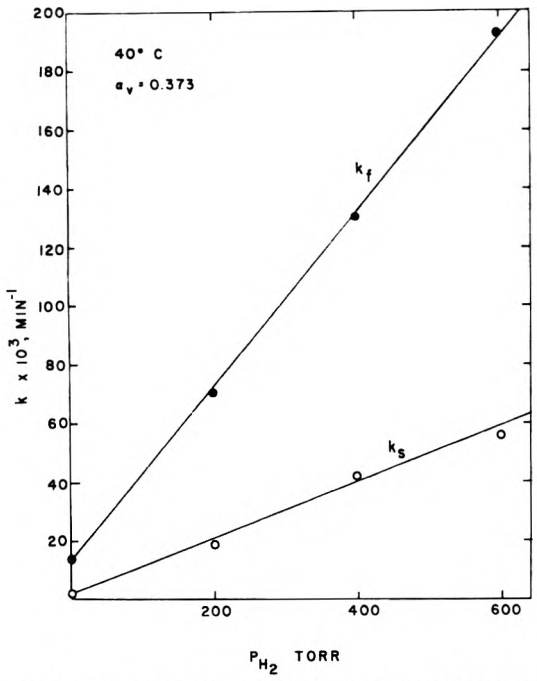

Figure 6. Comparison of the effect of molecular hydrogen on the fast and slow first-order alkyl radical decay constants: sample 2 of PE (quenched film).

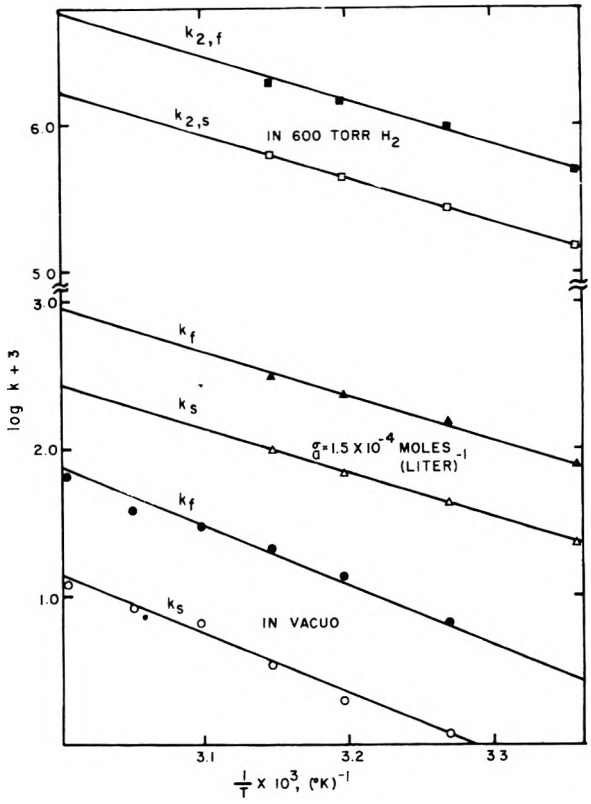

Figure 7. Logarithmic plots of the fast and slow first-order decay constants as a function of reciprocal absolute temperature: open and solid circles, decay *in vacuo*; open and solid squares, second-order decay constants at 600 Torr of hydrogen; open and solid triangles, first-order decay constants at a constant amount of hydrogen dissolved, the hydrogen concentration calculated for the 100% amorphous fraction. Data for the amorphous film sample of α_v equal to 0.373. The units of k_2 are M^{-1} min^{-1} and of the other constants min^{-1}.

It might be supposed that the rate of the slow decay depends upon the rate of diffusion of free radicals from the crystalline to the amorphous phases of the PE; if this were true, then the pronounced catalytic effect of hydrogen gas observed by Waterman and Dole[6] should not be seen in the case of the slowly decaying radicals because the hydrogen is soluble only in the amorphous fraction of the PE.[13] Yet the first-order slow decay constants were definitely increased by the presence of molecular hydrogen although not to the same extent as in the case of the fast decay constants, see Figure 6.

As an explanation of the above facts we propose the following. As Waterman and Dole[6] showed, the last approximately 3% of alkyl radicals remaining at room temperature after an irradiation at 77 K are quantitatively converted to allyl free radicals. However, in the present work the initial concentration of the slowly decaying radicals, Table V, is too high to account for the rather small allyl free radical G values (approximately half of which results from allyl formation during the heating to room temperature). We suggest that the fast decaying radicals are all in the amorphous regions by the time that the upper temperature has been reached so that all of those radicals are immediately affected by the hydrogen dissolved in the amorphous regions. On the other hand, it is possible that the slowly decaying radicals have first to diffuse into the amorphous regions before reacting at which time the catalytic effect of hydrogen would come into play.

The variation of k_s with the square of the amorphous content can be explained on the postulate of a sort of second-order reaction between amorphous zones. If the slowly decaying radical has to diffuse from one amorphous zone through a crystalline zone to another amorphous zone before reacting and another radical has to follow the same mechanism, then the second-order relationship of the amorphous zones would be evident. The first-order decay constant is attributed to the first-order nature of the diffusion process for the alkyl radicals. These radicals are presumed to diffuse by means of a free valency migration through the PE.[6]

Parenthetically, it might be pointed out that the marked catalytic effect of the hydrogen gas is not a general reaction, because there is no catalytic effect of hydrogen in the case of the decay of the $-CH_2OCHOCH_2-$ free radicals in polyoxymethylene.[14] Nor does hydrogen influence the decay of the allyl free radical in PE.

We suggest that the initial almost equal concentrations of the fast and slowly decaying alkyl radicals indicated by the data of Table V may be due to an equal probability of a free radical diffusing immediately into an amorphous zone from a crystalline zone and so becoming a fast decaying radical, or diffusing within the same crystalline zone before diffusing into the amorphous zone and reacting.

We now consider the temperature coefficient of the first-order fast and slow decay constants for the decay *in vacuo*. An Arrhenius plot, Figure 7, demonstrates that the activation energy, equal to 17.1 kcal mol^{-1} is essentially the same for both the slow and rapid decay processes *in vacuo*. This value of 17 kcal mol^{-1} agrees with that found by Waterman and Dole[6] for the alkyl decay *in vacuo*. The marked difference in the fast and slow first-order decay constants is due, therefore, to differences in the preexponential factors of the Arrhenius equation. These values were 3.5×10^7 sec^{-1} for k_s and 19×10^7 sec^{-1} for k_f. If the migration of the free radicals to a reaction zone occurs by the free valency random jumping mechanism discussed

TABLE VI: Values of the Arrhenius Preexponential Factors, *A*

Sample no.	α_v	A_f	A_s	A_f/A_s	ΔS_{fs}^*, eu
		In Vacuo[a]			
2	0.373	19	3.5	5.43	3.4
1	0.272	8.7	1.7	5.12	3.3
		In 600 Torr of H_2[b]			
2	0.373	4.73	1.40	3.37	2.4

[a] A in units of $sec^{-1} \times 10^{-7}$. [b] A in units of $M^{-1} sec^{-1} \times 10^{-10}$.

by Waterman and Dole,[6] then the lower preexponental factor for k_s would have to be explained on the basis of more jumps required for the slow process. In the presence of hydrogen the preexponential factor for the slow decay constant is also lower than that for the fast decay constant, 1.4×10^{10} M^{-1} sec^{-1} as compared to 4.7×10^{10} M^{-1} sec^{-1}. Here the units of the constants are different because in the case of the hydrogen-catalyzed reaction the solubility of the hydrogen changes with the temperature and this must be taken into account which we have done using very recent unpublished data of Kubo and Dole.[15] The latter data were obtained by the same but somewhat improved semimicro method of Deas, Hofer, and Dole.[13]

From Figure 6 we can write

$$k_{s,h} = k_{s,vac} + k_s' P_{H_2} \quad (7)$$

where $k_{s,h}$ and $k_{s,vac}$ are the observed first-order rate constants for the slow decay in the presence of hydrogen and *in vacuo*, respectively, and k_s' is slope of the plot of Figure 6. A similar relation can be written for the fast decay process. The linearities of the plots shown in Figure 6 also imply that the solubility of hydrogen in PE follows Henry's law. Because hydrogen dissolves only in the amorphous regions of the PE we can substitute σ_a/K for P_{H_2} into eq 7 where σ_a is the solubility of hydrogen in moles of hydrogen per liter of amorphous PE, and K is Henry's law constant. Further, k_s'/K can be merged into a single constant $k_{s,2}$ and this second-order constant plotted according to the Arrhenius equation. This has been done in Figure 7 for a hydrogen pressure of 600 Torr where it can be seen that the data all fall on a straight line. The calculations yield an activation energy of 13 kcal mol^{-1} for both the slow and fast decay processes. This value also agrees with that published by Waterman and Dole.[6]

If σ_a is kept constant by decreasing the hydrogen pressure as the temperature is increased, the change of the reaction rates due to the change of hydrogen solubility can be eliminated. The first-order rate constants thus obtained, k_s and k_f for σ_a held constant at σ_a equal to 1.5×10^{-4} M, are also plotted in Figure 7 and straight lines are obtained. This also holds true for σ_a values ranging from 0.5 to 1.5×10^{-4} mol of hydrogen per liter of amorphous PE. The calculated activation energy was also 13 kcal mol^{-1}.

It is interesting to calculate and compare the preexponential factors, A, of the Arrhenius equation, $k = A \exp(-\Delta E^*/RT)$. These have been collected in Table VI in units of $sec^{-1} \times 10^{-7}$ for two different PE samples. The ratio of A_f in sample 2 to that in sample 1 is 2.18 while the ratio of A_s in sample 2 to that in sample 1 is almost the same 2.08. If we assume that the A factors are proportional to $\exp(\Delta S^*/R)$ where ΔS^* is the entropy of activation, then the difference between the entropies for the fast and slow reactions of the same sample can be calculated and their values are also given in Table VI as ΔS_{fs}^*. It will be noted that the entropy differences are practically independent of the amorphous content at least for samples 1 and 2, but not of the presence of 600 Torr of hydrogen. We believe that the preexponential factors are determined by the number of free valency jumps either in the crystalline or amorphous zones or both, but due to the complexity of the solid morphology, no quantitative calculations can be made at this time. However, it is not surprising that the ΔS_{sf}^* value in the 600-Torr hydrogen experiment is lower than the values *in vacuo* because the pronounced catalytic effect of hydrogen lowers the possibility of a radical from diffusing into a crystalline zone once it is in an amorphous zone.

Acknowledgments. This research was supported by the U. S. Atomic Energy Commission and by income from the chair in chemistry at Baylor University endowed by a gift from The Robert A. Welch Foundation. Dr. J. A. Reid of the Phillips Petroleum Co. kindly supplied the Marlex-6002 polyethylene.

References and Notes

(1) Paper XI of this series: M. Budzol and M. Dole, *J. Phys. Chem.*, **75**, 1671 (1971).
(2) M. Dole, "The Radiation Chemistry of Macromolecules," M. Dole, Ed., Academic Press, New York, N. Y., 1972, p 340.
(3) P. Ju. Butiagin, *Pure Appl. Chem.*, **30**, 57 (1972).
(4) A. S. Michaels and J. H. Eixler, *J. Polym. Sci.*, **50**, 393 (1961).
(5) R. Chiang and P. J. Flory, *J. Amer. Chem. Soc.*, **83**, 2857 (1961).
(6) D. C. Waterman and M. Dole, *J. Phys. Chem.*, **74**, 1913 (1970).
(7) C. P. Poole, Jr., "Electron Spin Resonance," Interscience, New York, N. Y., 1967, (a) p 557; (b) p 798.
(8) S. Nara, S. Shimada, H. Kashiwabara, and J. Sohma, *J. Polym. Sci., Part A-2*, **6**, 1435 (1968).
(9) D. C. Waterman and M. Dole, *J. Phys. Chem.*, **74**, 1906 (1970).
(10) A. Charlesby, D. Libby, and M. G. Ormerod, *Proc. Roy. Soc., Ser. A*, **262**, 207 (1961).
(11) I. Auerbach and L. H. Sanders, *Polymer*, **10**, 579 (1969).
(12) W. G. French and J. E. Willard, *J. Phys. Chem.*, **72**, 4604 (1968).
(13) T. M. Deas, Jr., H. H. Hofer, and M. Dole, *Macromolecules*, **5**, 223 (1972).
(14) P. N. Lee and M. Dole, unpublished.
(15) S. Kubo and M. Dole, unpublished.

Free Radical Formation in Hydrocarbon Crystals by γ Irradiation. Anisotropic Hyperfine Couplings in $CH_3\dot{C}H(CH_2)_{33}CH_3$ and Relative Radical Yields in Single Crystal Hexatriacontane

Anders Lund[1] and Larry Kevan*

Department of Chemistry, Wayne State University, Detroit, Michigan 48202 *(Received April 9, 1973)*

Publication costs assisted by U. S. Army Research Office—Durham

The epr spectra of a single crystal of $C_{36}H_{74}$, hexatriacontane, have been analyzed. The radicals $CH_3\dot{C}H(CH_2)_{33}CH_3$ and $R'CH_2\dot{C}HCH_2R''$ are formed after γ irradiation at 195°K in a ratio of approximately 3 to 1. A computer-assisted method was applied to separate the overlapping radical signals. The isotropic and anisotropic coupling constants of $CH_3\dot{C}H(CH_2)_{33}CH_3$ were obtained from a complete single crystal analysis. The parameters are found to agree reasonably well with values derived from the anisotropic couplings of methyl and ethyl radicals and indicate that the radical site is planar.

Introduction

Previous studies[2,3] of free radical formation in alkane crystals by γ irradiation have shown that the predominant species is of the type $CH_3\dot{C}HCH_2R$ (I). Radicals of the type $R'CH_2\dot{C}HCH_2R''$ (II) are present to a smaller extent in the lower *n*-paraffins containing 4–16 carbon atoms as revealed by an estimate from the electron paramagnetic resonance (epr) spectra. In this study an irradiated crystal of $C_{36}H_{74}$, hexatriacontane, was investigated to see whether this observation is valid also for long chain *n*-alkanes. It was also considered to be of interest to evaluate the hyperfine coupling tensors, particularly for the α-proton interaction. Previous measurement of this coupling tensor has mainly been performed on crystals like malonic acid[4] in which some spin delocalization into the carbonyl group occurs. The principal values of the coupling tensor are proportional to the π-electron spin density on the α carbon and thus somewhat larger couplings than in malonic acid are expected for the radical (I) studied here.

A third aspect of this work is the application of a procedure to analyze spectra containing superimposed components from two different radicals. A computer-assisted method is used for this purpose and is described in some detail.

The crystal structure[5] of hexatriacontane is known to consist of two molecules per unit cell and has a space group $P2_1/a$. The carbon chain is regular and periodic with a center of symmetry in each molecule. From this, it follows that radicals centered on carbon atom C_i are magnetically equivalent to those centered on C_{37-i}. There is also a possibility of site splitting from chemically equivalent radicals which are related through a reflection operation.

Experimental Section

Large single crystals (~1 cm^3), grown from the melt,[6] were obtained from 99.8% pure hexatriacontane, *n*-$C_{36}H_{74}$. One of the crystals was dipped into liquid nitrogen to produce cracks along which smaller crystal plates with approximately planar surfaces could be cut out.

The crystals were irradiated at 77, 195, 273, and 300°K by means of ^{60}Co γ rays at a nominal dose rate of 0.2 Mrad/hr for 5–8 hr. Epr measurements were usually made at 77°K with a Varian E-4 spectrometer. The magnetic field sweep was calibrated by the splitting a_N = 13.0 G of Fremy's salt which is accurate to within 1%. All measurements were performed at a microwave power of 1 mW at which level no significant saturation broadening occurred.

A complete set of data for rotation about three orthogonal axes was collected for crystals irradiated at 195°K. Epr spectra were recorded for each 10° of rotation about an axis at right angles to the magnetic field vector. The angular reading was accurate to within 1°. Near the orientations corresponding to the maximum and the minimum splittings, several spectra were recorded or displayed on the oscilloscope so that the extreme positions could be located to within 3°. After a set of data had been collected for one axis of rotation the crystal was reoriented by working at Dry Ice temperature so that a new axis of rotation was aligned at right angles to the previous one. The crystal was properly marked to ensure that a right-handed coordinate system was set up.[7] Due to the rather badly defined surfaces of the crystals the axes of rotation may deviate from orthogonality by as much as 5°. To ensure reproducibility the measurements were therefore repeated using a second crystal.

Results

The spectra obtained after irradiation at 77°K were imperfectly resolved, which made accurate measurement of splitting constants difficult. Irradiation at 273°K produced spectra which had well resolved lines on the wings while the central part was broader. After irradiation at 300°K only rather broad lines were left in the central portion of the spectrum while the outermost lines observed at lower temperature had vanished. Irradiation at 195°K gave the most easily interpretable spectra. They appear to contain predominantly one component which is also the one formed at 77°K. Since the spectral resolution was better with the crystals irradiated at 195°K the detailed analysis was confined to those spectra.

At certain orientations the spectra resembled very closely the type of absorptions found from crystals of decane under similar conditions; compare Figure 1a of this paper with Figure 2 of ref 3. This type of spectrum is readily interpreted as containing contributions from two

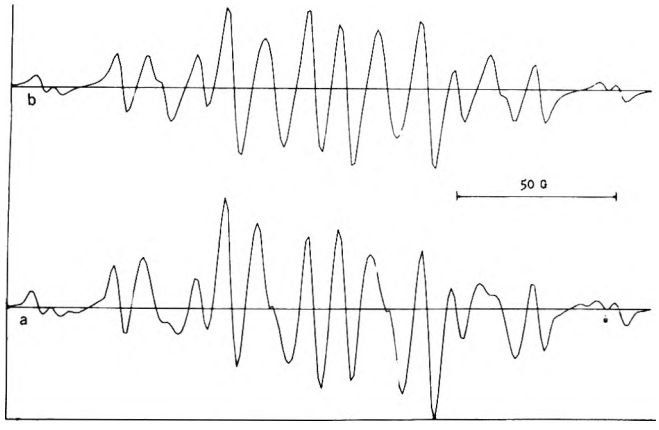

Figure 1. (a) The digitized epr spectrum from a single crystal of hexatriacontane γ-irradiated at 195°K to a dose of ~1 Mrad and oriented to give the maximum hyperfine splitting when the crystal is mounted for rotation about the x axis. (b) spectrum synthesized from 0.67 times radical I spectrum + 0.33 times radical II spectrum as shown in Figure 2 through a least-squares fit to the experimental spectrum; the parameters are given in Table I.

TABLE I: Epr Parameters for Spectra Used to Calculate the Proton Coupling Tensors for Radical I: $CH_3\dot{C}HCH_2R$

Spectrum Axis	Coupling	Radical	$a(CH_3)$, G	$a(CH_2)$, G	$a(\alpha)$, G	W,[b] G
X	max	I[a]	25.5 ± 0.1	34.1 ± 0.1	36.0 ± 0.1	2.6 ± 0.2
		II		33.7	33.5	3.5
X	min	I	24.2	34.9	14.2	4.9
		II		34.5	13.1	4.9
Y	max	I	22.5	32.8	22.5	5.6
		II		32.8	22.5	5.6
Y	min	I	25.0	35.0	11.5	4.3
		II		35.0	11.5	4.3
Z	max	I	25.9	35.0	35.0	3.1
		II		34.3	34.3	3.5
Z	min	I	23.3	33.0	18.0	5.5
		II		32.9	18.2	5.5

[a] The parameters for radical I were computed with the program ESRCON; the quoted errors are standard deviations. Radical II is assigned as $-CH_2\dot{C}HCH_2-$. [b] The line width W is the measured peak-to-peak derivative width.

radicals of which the predominant one most likely is $CH_3\dot{C}HCH_2R$ and the minor one $-CH_2\dot{C}HCH_2-$. The spectra to be anticipated for these radicals for the crystal orientation employed are shown in Figure 2a,b. At other orientations the interpretation is less simple because the magnitude of the α-proton coupling sometimes becomes comparable to the β splitting from the CH_3 and the CH_2 groups. For this reason six spectra were selected for a detailed analysis. Provided that the spectra correspond to the maximum and the minimum couplings in each of the three planes, simple analysis, which does not require that the angle of rotation be known with respect to a crystal fixed coordinate system, allows one to obtain the hyperfine coupling tensor. These spectra were therefore carefully recorded as described in the Experimental Section. Even though these spectra were fairly well resolved the assignment of coupling constants was not obvious in all cases. The methods employed to estimate the couplings are described in the next section.

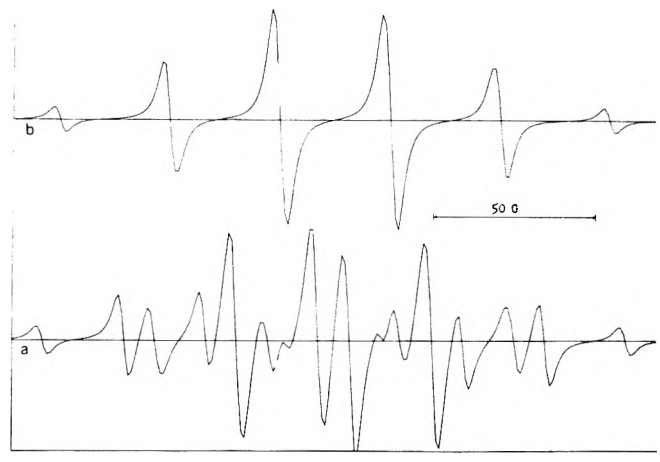

Figure 2. (a) Epr simulated spectrum for radical I: $CH_3CH(CH_2)_{33}CH_3$; (b) simulated spectrum for radical II: $R'CH_2\dot{C}HCH_2R''$.

Spectral Analysis

As has been outlined above, it is essential to obtain accurate measures of the coupling constants of the six spectra selected for analysis. The following procedure to obtain these data proved suitable.

In a first step, reasonable guesses of the coupling constants were made on the basis of the assumed structure of the predominant $CH_3\dot{C}HCH_2R$ radical. The guesses were tested by running several spectral simulations with the computer program MARU.[8] After an approximate set of parameters had been obtained, refined values were computed by employing the treatment devised by Heinzer.[9] In this program (ESRCON) the digitized spectrum is fitted in the least-squares sense to a computed line profile. After several cycles of iteration a set of coupling constants, one line width, and one scaling factor, that provide the smallest standard deviation, are obtained. At this stage a weaker component of the structure $-CH_2\dot{C}HCH_2-$ was introduced and a least-squares estimate of the contribution of each component to the total spectrum was made by employing the program ASESK described previously.[3] For the spectrum shown in Figure 1a, the component spectra were those shown in Figure 2a and b. In this process the line shape was computed for the appropriate mixture of the two components as is illustrated in Figure 1b. A further refinement was attempted by subtracting the weaker component from the experimental spectrum. The remaining spectrum was then analyzed again with ESRCON to obtain a new set of data. Usually the standard deviation dropped somewhat, indicating that unwanted contributions from a second component had diminished. The computed parameters were found to vary only slightly when this process was repeated. Thus the error of the final parameters which are summarized in Table I is probably not greatly affected by the termination of the iteration. Other factors limit the accuracy.

It was not possible to assign different splittings to the methyl protons and the α proton for the Y-max spectrum designated in Table I for radical I due to convergence difficulties. Similar problems arose when $a(\alpha) \approx a(CH_2)$ (see spectrum Z max of Table I) and appear to be quite general for this type of analysis. One further source of error is the uncertainty in the choice of parameters for the weaker component. In the favorable orientation shown in Figure 1a the two spectra are clearly resolved, but for most other

TABLE II: Principal Values and Directions of the Hyperfine Coupling Tensors for the $CH_3\dot{C}HCH_2$–R Radical I in γ-Irradiated Hexatriacontane Single Crystal

Nucleus	Principal values, G	Direction cosines with respect to X	Y	Z
α-H	36.5 ± 1.0	0.186	0.934	0.306
	20.0	0.812	−0.322	0.487
	10.5	−0.553	−0.158	0.818
Methylene-H	36.7	0.145	0.691	−0.708
	34.0	0.841	−0.463	−0.279
	31.6	0.521	0.556	0.648
Methyl-H	27.4	−0.548	0.792	0.268
	23.8	−0.078	−0.367	0.927
	21.7	0.833	0.487	0.263

orientations the weak component is hidden. This tends to introduce errors in the spectrum which remain when the weaker component is subtracted. Imperfections in the subtraction procedure are likely to become worse when the two components have different g factors. That this might be the case was indicated by some asymmetry in a few spectra. This cannot be distinguished from site-splitting effects to be expected for $P2_1/a$ crystal symmetry. In principle it would have been possible to estimate the errors introduced by both of these effects by performing the analysis on each half of the spectra independently. In view of the extra labor that would have been involved this was not done and the ESRCON analysis which requires symmetrical spectra was carried out by measuring one half and generating the other half within the computer.

The elements of the tensor $\mathbf{T} = \mathbf{A}^2$, where $\mathbf{A}$ is the hyperfine coupling tensor for the α proton, were computed from the expressions[7]

$$T_{11} = \alpha_2 + \alpha_3 - \alpha_1;\ T_{22} = \alpha_3 + \alpha_1 - \alpha_2;\ T_{33} = \alpha_1 + \alpha_2 - \alpha_3;\ T_{12} = T_{21} = [\delta_3^2 - (\alpha_1 - \alpha_2)^2]^{1/2};\ T_{23} = T_{32} = [\delta_1^2 - (\alpha_2 - \alpha_3)^2]^{1/2};\ T_{13} = T_{31} = [\delta_2^2 - (\alpha_3 - \alpha_1)^2]^{1/2}$$

Here α and δ are related to the measured maximum and minimum splittings $a_i^{\pm}$ in each plane through $\alpha_i = 0.5[(a_i^+)^2 + (a_i^-)^2]$ and $\delta_i = 0.5[(a_i^+)^2 - (a_i^-)^2]$. The principal values of $\mathbf{A}$ are obtained from the square roots of the elements of the diagonalized $\mathbf{T}$ tensor. The values are given in Table II.

Measurement of the methyl and the methylene couplings permits the coupling tensor to be estimated from the relations

$$T_{11}^{\beta} = 0.5[(a_3^+)^2 + (a_3^-)^2 + (a_2^+)^2 + (a_2^-)^2 - (a_1^+)^2 - (a_1^-)^2]$$

$$T_{22}^{\beta} = 0.5[(a_1^+)^2 + (a_1^-)^2 + (a_3^+)^2 + (a_3^-)^2 - (a_2^+)^2 - (a_2^-)^2]$$

$$T_{33}^{\beta} = 0.5[(a_1^+)^2 + (a_2^-)^2 + (a_1^+)^2 + (a_1^-)^2 - (a_3^+)^2 - (a_3^-)^2]$$

$$T_{12}^{\beta} = T_{21}^{\beta} = [(a_3^+)^2 - (a_3^-)^2 - (T_{11}^{\beta} - T_{22}^{\beta}) \cos 2\theta_3^+]/\sin 2\theta_3^+$$

$$T_{23}^{\beta} = T_{32}^{\beta} = [(a_1^+)^2 - (a_1^-)^2 - (T_{22}^{\beta} - T_{33}^{\beta}) \cos 2\theta_1^+]/\sin 2\theta_1^+$$

$$T_{31}^{\beta} = T_{13}^{\beta} = [(a_2^+)^2 - (a_2^-)^2 - (T_{33}^{\beta} - T_{11}^{\beta}) \cos 2\theta_2^+]/\sin 2\theta_2^+$$

Here θ_i^+ is the angle of rotation at which the α-proton splitting is at a maximum; a_i^+ is the estimated β splitting at this orientation and a_i^- is the value obtained when the sample is rotated 90° about axis i. The angles θ_i^+ can be computed from the equations[7]

$$\sin 2\theta_1^+ = T_{23}|\delta_1 \sin 2\theta_2^+ = T_{13}|\delta_2 \sin 2\theta_3^+ = T_{12}|\delta_3$$

The accuracy with which these tensor elements can be measured from the data is considerably less than that obtainable for the α-proton tensor elements.

The probable error in the determination of the g tensor can be estimated according to the analysis given by Schonland.[7] A similar analysis applies also to the case of hyperfine couplings. The errors are introduced by the uncertainty in the coupling constants. Due to the various factors discussed above, these errors are considerably larger than the typical standard deviations quoted in Table I, and an error of about 0.5 G seems reasonable. Another potential source of error is misalignment of the rotation axes. Numerical estimates of this effect have been made[10] and indicate that an axis which is inclined 5° from its correct position might introduce errors of the order of 3% of the coupling constant under unfavorable conditions. As has been indicated in Table II, errors of the order ±1 G can then be anticipated in the principal values; this is the magnitude of the anisotropy for the methyl and the methylene protons.

Discussion

The largest principal value of the α-proton coupling tensor obtained here seems to deviate somewhat from the largest principal values of the values of 32.5, 21.8, and 10.4 G reported from the radical $\cdot CH(COOH)_2$ formed in irradiated malonic acid.[4] This might be caused by a difference in structure; also spin delocalization into the carboxyl groups cannot be excluded in the latter case. For methyl, ethyl, propyl, and isobutyl radicals the isotropic coupling constants in solution[11] are a = 23.0, 22.4, 22.1, and 22.8 G, respectively compared to a = 22.3 G obtained here. This indicates that the spin density on the α carbon is almost constant for these alkyl radicals.

It would therefore be of interest also to compare the anisotropic couplings of these radicals. Measurement performed on ethyl radical contained in a solid argon matrix[12] at 4°K gave the couplings $A_{\perp}^{\alpha}$ = 19.4 G and $A_{||}^{\alpha}$ = 29.9 G at 77°K.[13] For methyl radical adsorbed on silica gel the values $A_{\perp}$ = 22.6 G and $A_{||}$ = 21.9 G were obtained[13,14] at both 4 and 77°K. At these temperatures the radical is presumed to rotate about its threefold axis. If one assumes that the methyl and ethyl radicals are planar with a valence angle of 120° about the C_{α} position, the dipolar couplings can be obtained[14] by combining these data. The results give B_x = 12.5 G, B_y = −13.0 G, and B_z = 0.5 G where x is along the C–H bond, z is perpendicular to the radical plane, and y is orthogonal to x and z. The absolute values of the dipolar couplings for radical I are obtained as 14.2, 2.3, and 11.8 G. By comparison with the above values we can assign the values to the x, y, and z axes to give B_x = 11.8 G, B_y = −14.2 G and B_z = 2.3 G. The difference between the two sets of data might be attributed to the approximations involved in computing the values in the first case and also to the experimental uncertainties in the second case. This comparison therefore supports the hypothesis that radical I has a planar structure with an approximately sp^2-hybridized α carbon.

The isotropic couplings for the methylene protons a = 34.1 G and for the methyl protons a = 24.3 G are close to the values obtained previously for radicals of type I in crystalline C_6-C_{16} n-alkanes.[2,3] As indicated above, the estimate of the anisotropic interactions for the β protons is probably not too reliable especially since the anisotropy is small. From a simple point dipole model the methylene proton interaction is predicted to be axially symmetric with the parallel direction along the bond C_α-H_β. Provided that the hydrogen atoms occupy fixed positions and that the geometry about C_β is tetrahedral the parallel directions would be different for the two methylene protons. This difference was not resolved in the spectra which limits the accuracy in the determination. The methyl protons are assumed to be equivalent for all orientations due to rapid rotation about the C_α-CH_2 bond. Such a rotation would give an axially symmetric coupling tensor which is approximately observed, but the anisotropy obtained here appears somewhat larger than that from the values of $A_\perp^\beta$ = 26.0 G and $A_\parallel^\beta$ = 27.9–28.7 G obtained for the ethyl radical.[11-13] This difference might be caused by a change in the structure of a secondary radical I compared to a primary radical like ethyl.

The average relative yields of radicals I and II obtained by the computer fits for six different orientations as shown in Figure 1b are approximately 3 to 1. The predominant formation of radical I has been noted previously for shorter chain alkanes.[3] Possible causes for this behavior have been suggested in terms of the charge distribution in the parent molecular ion, but no real understanding of this specificity of radical formation in such long chain alkanes exists. In polyethylene,[15] predominantly radicals of type II are formed at 77°K in addition to 5–10% allylic type radicals. This assignment is well supported by measurements of partly oriented samples,[16] and it seems clear that there is a difference in the predominant type of radicals formed in hexatriacontane, $C_{36}H_{74}$, and polyethylene. It has been suggested[17] that radicals formed in pairs can recombine to form dimers in the solid-state radiolysis of hexadecane. These pairs were considered to react even at 77°K. It is thus possible that the relative yield of radicals initially formed does not correspond to that measured by epr after irradiation at 77 or 195°K. An important extension of this work would therefore be to determine the nature and the yields of the radical pairs in n-alkanes after irradiation at a sufficiently low temperature to prevent radical pair recombination.

Acknowledgment. This research was supported by the U. S. Army Research Office—Durham. A. L. is also grateful for support from the Swedish-American Foundation.

References and Notes

(1) On leave from Swedish Research Council's Laboratory, Studsvik, Nykoping, Sweden.
(2) T. Gillbro, P. O. Kinell, and A. Lund, *J. Phys. Chem.*, **73**, 4167 (1969).
(3) A. Lund, *J. Phys. Chem.*, **76**, 1411 (1972).
(4) T. Cole and H. C. Heller, *J. Chem. Phys.*, **34**, 1035 (1961).
(5) H. M. M. Shearer and V. Vand, *Acta Cryst.*, **9**, 379 (1956).
(6) We thank Dr. J. Silverman, University of Maryland, for providing the crystals.
(7) D. S. Schonland, *Proc. Phys. Soc., London*, **73**, 788 (1959).
(8) R. Lefebvre and J. Maruani, *J. Chem. Phys.*, **42**, 1480 (1965).
(9) J. Heinzer, Quantum Chemistry Program Exchange 197, Indiana University, Bloomington, Ind., 1972.
(10) O. Edlund, Acta Universitatis Upsaliensis, Abstracts of Uppsala Dissertations from the Faculty of Science, Abstract No. 225 1972.
(11) R. W. Fessenden and R. H. Schuler, *J. Chem. Phys.*, **39**, 2147 (1963).
(12) C. A. McDowell, P. Raghunathan, and K. Shimokoshi, *J. Chem. Phys.*, **58**, 114 (1973).
(13) T. Shiga and A. Lund, *J. Phys. Chem.*, **77**, 453 (1973).
(14) T. Shiga, to be published.
(15) S. Ohnishi, *Bull. Chem. Soc. Jap.*, **35**, 254 (1962).
(16) D. Libby and M. G. Ormerod, *J. Phys. Chem. Solids*, **18**, 316 (1961).
(17) W. E. Falconer and R. Salovey, *J. Chem. Phys.*, **44**, 3151 (1966).

Infrared Spectroscopic Investigation of Zeolites and Adsorbed Molecules. VII. Hydroxyl Groups of Erionite

D. F. Best, R. W. Larson, and C. L. Angell*

Union Carbide Corporation, Tarrytown Technical Center, Tarrytown, New York 10591 *(Received April 17, 1973)*
Publication costs assisted by Union Carbide Corporation

Removal of water and ammonium ions and the formation of hydroxyl groups on ammonium-exchanged erionite on gradual heating from room temperature to 700° have been observed. Interaction of the hydroxyl groups with propylene and ammonia has been examined to determine their accessibility and reactivity. The changes of infrared spectra on propylene adsorption are interpreted in terms of accessibility of the two main OH groups—one accessible and one inaccessible.

Many papers have appeared in the literature over the past ten years dealing with infrared spectroscopic studies of the hydroxyl bands observed in the spectra of X- and Y-type zeolites.[1] These studies describe the types of OH bands in deamminated ammonium-exchanged zeolites, as well as their gradual formation and decomposition on heating and their interactions with a variety of molecules. The locations of the OH groups within the zeolite framework have been deduced from the properties of these groups. In the present work we discuss infrared spectro-

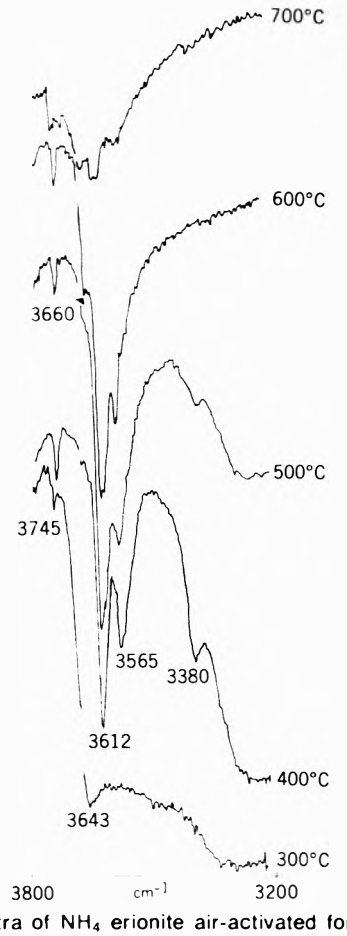

Figure 1. Spectra of NH_4 erionite air-activated for 1 hr at each temperature.

scopic observations on the OH bands in the spectra of calcined ammonium-exchanged erionite.

A sample of erionite, a sedimentary mineral zeolite, was obtained from a deposit in the western United States. Ammonium ion exchange was achieved by repeated treatment with 10% NH_4Cl solution. The chemical analysis of the product, expressed as weight per cent of the dehydrated mineral, is as follows: Al_2O_3, 17.2; SiO_2, 71.5; Na_2O, 0.1; K_2O, 3.7; $(NH_4)_2O$, 6.5; MgO + FeO, 0.9. This corresponds to a SiO_2/Al_2O_3 molar ratio of 7.1 and an ammonium ion exchange of 75%. The infrared cell and the experimental procedure have been described in part I of this series.[2] Spectra presented in Figures 1 and 2 were obtained on the Perkin-Elmer Model 112 single-beam spectrophotometer. All samples were calcined in air. The X-ray diffraction patterns of the materials studied showed complete retention of crystallinity after calcination at 300, 400, 500, 600, and 700°.

Spectra of the hydroxyl stretching region of ammonium-exchanged erionite successively calcined for 1 hr at each temperature are shown in Figure 1. At 300° both water and ammonium ions are present as shown by bands at 1630 and 1420 cm^{-1}. At 400° all the water is removed as indicated by the disappearance of the 1630-cm^{-1} band; therefore the band at 3380 cm^{-1} and the broad band around 3200 cm^{-1}, also evident in the 300° spectrum, must be due to the NH_4^+ ions. These bands are still present after the 500° calcination as is the band at 1420 cm^{-1}, indicating the presence of NH_4^+. This behavior is different from that of ammonium-exchanged type Y where the

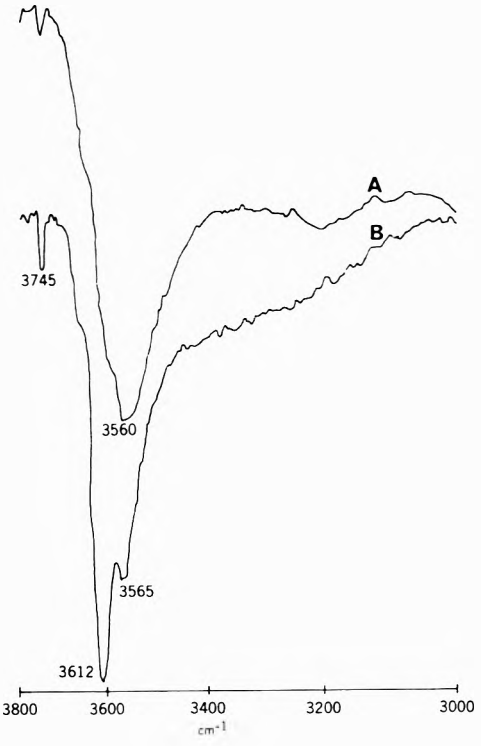

Figure 2. Lower curve: NH_4 erionite air-activated at 600°; upper curve: same exposed to 200 Torr of propylene.

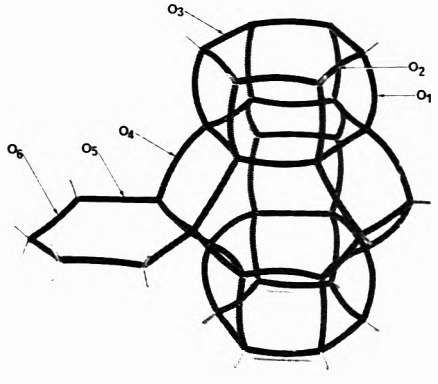

Figure 3. Location of oxygen atoms in erionite structure.

NH_4^+ band is completely removed by 380°.[3] At 600° the NH_4^+ bands of erionite are gone and the spectrum consists of three sharp bands at 3745, 3612, and 3565 cm^{-1} and a shoulder at 3660 cm^{-1}. The intensity of these bands has not decreased from the 500° spectrum, showing higher thermal stability to dehydroxylation by the hydroxyls of erionite in comparison with those developed in ammonium type Y where the OH bands have decreased substantially by 600°.

Since the pore system of erionite prevents the adsorption of benzene or pyridine which are usually employed to investigate adsorbate–hydroxyl interaction in large pore zeolites, we used propylene and ammonia instead.

Changes that occur on the addition of propylene to erionite are shown in Figure 2. The 3612-cm^{-1} band disappears while the 3565-cm^{-1} band is slightly broadened and shifted to 3560 cm^{-1}. A broad band at about 3200 cm^{-1} is presumably the 3612-cm^{-1} band shifted by hydrogen bonding. These results are similar to those observed by Liengme and Hall[4] for calcined ammonium-exchanged

type Y. They obtained a hydrogen bonding shift of 440 cm^{-1}, while in our case this shift is 412 cm^{-1}.

Pyridine has been used in many cases to study the surface acidities of zeolites;[5] the spectra clearly differentiate between Bronsted and Lewis acidities of the sites that interact with pyridine. In this study, ammonia was substituted for pyridine as the adsorbate. When ammonium-exchanged erionite, after activation at 600° was exposed to 70 Torr of ammonia at room temperature, the OH bands, except the 3745 cm^{-1} band, were completely removed and bands appeared at 3380, 3200 (broad), and 1420 cm^{-1}. Evidently the NH_4^+ ion form of erionite was reconstituted on the addition of ammonia.

We may now hypothesize the location of the hydroxyl groups in the erionite structure. The assignment of the hydroxyl bands in type Y zeolite assists in the interpretation of the erionite spectrum. The 3745-cm^{-1} band appears in all zeolite spectra and has been assigned to a siliceous impurity.[2] Of the two main OH bands in the erionite system, that at 3612 cm^{-1} interacts with propylene, while that at 3565 cm^{-1} does not interact significantly. Similar properties of the two main OH bands in the type Y zeolite spectrum have led to the following assignments: the OH group corresponding to the 3640-cm^{-1} band is on the O_1 oxygen pointing into the large cavity and therefore available to interact with adsorbate molecules. The OH group corresponding to the 3540-cm^{-1} band is on the O_3 oxygen pointing into the double six-ring.[6] In the type Y zeolite structure there are four crystallographically different oxygens, while in the erionite structure there are six. Inspection of a model of erionite,[7] Figure 3, allows us to classify these as follows: two different oxygens in the double six-rings (O_2 and O_3), two in the single six-ring (O_5 and O_6), one oxygen making the connection between the six-rings of the double six-ring (O_1), and one connecting the double and single six-rings (O_4). Of these, one oxygen of each type in the double and single six-rings points toward the inside of the six-rings, and the other four types of oxygens all point toward the large channel. Because of this we cannot actually assign the hydroxyl bands to particular oxygen atoms, but we can say that the 3612-cm^{-1} band represents a group that points toward the large channel, while the 3565-cm^{-1} band represents one that points to the inside of a six-ring.

References and Notes

(1) For a recent review, see J. W. Ward, *Advan. Chem. Ser.*, **No. 101**, 380 (1971).
(2) C. L. Angell and P. C. Shaffer, *J. Phys. Chem.*, **69**, 3463 (1965).
(3) J. W. Ward, *J. Catal.*, **9**, 225, 396 (1967).
(4) B. V. Liengme and W. K. Hall, *Trans. Faraday Soc.*, **62**, 3229 (1966).
(5) J. W. Ward, *J. Catal.*, **10**, 34 (1968); **11**, 251 (1968); **13**, 364 (1969); **14**, 365 (1969).
(6) R. L. Stevenson, *J. Catal.*, **21** 113 (1971).
(7) A. Kawahara and H. Curien, *Bull. Soc. Fr. Mineral. Cristallogr.*, **92**, 250 (1969).

Liquid Ammonia Solutions. X. A Raman Study of Interactions in the Liquid State

A. T. Lemley, J. H. Roberts, K. R. Plowman, and J. J. Lagowski*

Department of Chemistry, The University of Texas at Austin, Austin, Texas 78712 *(Received March 5, 1973)*

Publication costs assisted by the National Science Foundation and the Robert A. Welch Foundation

The results of a Raman study of liquid NH_3, ND_3, and ND_2H and of NaI and $NaClO_4$ solutions in liquid NH_3 are reported. The resolution of the experimental envelopes in the N-H and N-D stretching regions suggests a two-species model for the solvent structure. Band positions for the pure liquids and solutions at different temperatures are discussed in terms of the proposed liquid structure model.

Introduction

There has been considerable interest in the liquid structure of hydrogen bonded solvents in recent years.[1-6] Spectroscopic studies on water using near-ir and Raman spectroscopy have suggested various models for its liquid structure. Data obtained in the fundamental stretching and the near-infrared overtone and combination regions of the spectrum have been used to support both a continuum[1-3] and a mixture[4-6] model for the liquid state of H_2O. Recent work[7] with HOD suggests that the mixture model is more consistent with the available experimental data.

Spectroscopic studies of liquid NH_3 are hindered by difficulty with the optics necessary for low-temperature observations and by the basic low intensity of the Raman effect. Corset[8] overcame many of the difficulties encountered in the ir region by recording spectra at room temperature in pressure cells. Recent work[9] in this laboratory made use of similar cells for studies in the near-infrared region. The use of a laser exciting source greatly enhanced the intensity of the Raman spectra of liquid ammonia and its solutions; however, Raman spectra of liquid ammonia had been recorded with a mercury source by Plint, Small, and Welsh[10] and by Kinumaki and Aida.[11] The details of the pressure cells and the laser source used in this work have been previously reported from this laboratory.[12]

Both the resolution and interpretation of the Raman and infrared spectra in the fundamental region at room

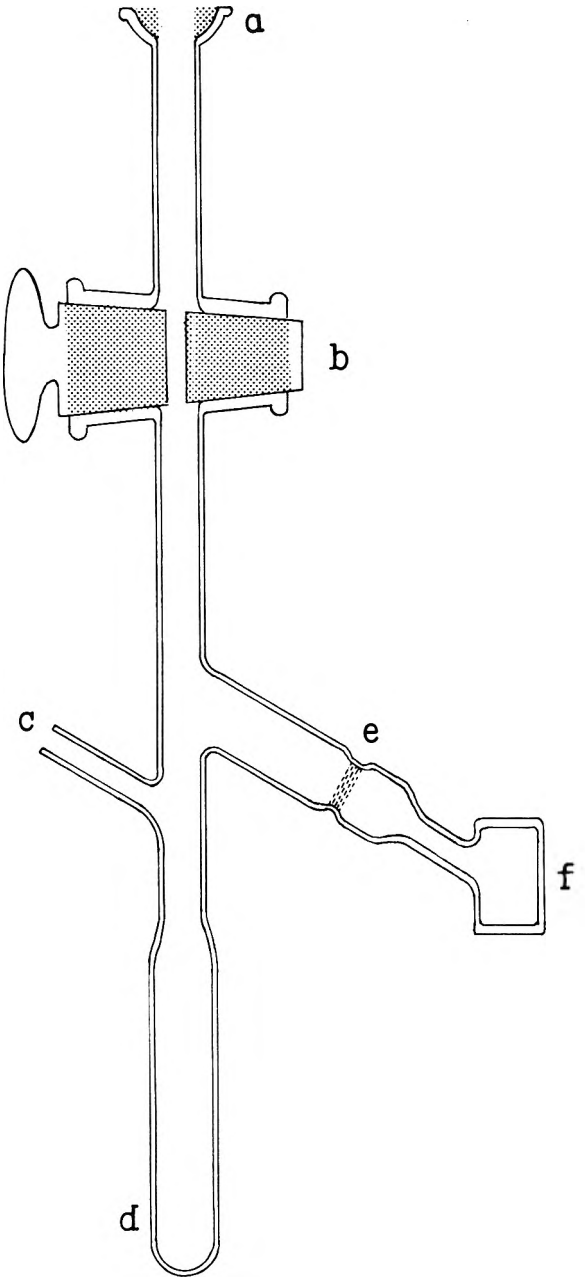

Figure 1. Raman cell assembly. Salt is weighted in through (c) which is then sealed off. Cell is attached to vacuum line at (a) and NH_3 is condensed through (b) into (d) where solution is mixed. Solution is filtered through sintered glass frit (e) to optical cell (f).

and at low temperature have been open to discussion. Considerable disagreement has arisen concerning the assignment of bands in the N–H stretching region of the spectrum.[13,14] This disagreement dealt with the unresolved spectrum and was based on the assignment of the three band maxima in the envelope. Birchall and Drummond[13] assign the maximum at *ca.* 3300 cm^{-1} to $2\nu_4$, the overtone of the asymmetric bending mode. They assign the maximum at *ca.* 3215 cm^{-1} to ν_1, the symmetric stretching mode. de Bettignies and Wallart[14] assign these maxima in the opposite manner as have previous workers.[10,11] It has been suggested[12] that a meaningful statement concerning the structure of liquid ammonia rested on a reliable solution of the N–H stretching region.

We report here (a) the results of a study of the Raman spectra of liquid NH_3, ND_3, and ND_2H, and of salt solutions in liquid NH_3, (b) the resolution of the experimental envelopes, and (c) the assignment of the bands in terms of a model for the solvent structure.

Experimental Section

Ammonia used in these experiments was doubly distilled from a sodium–ammonia solution. The ND_3 was prepared from Mg_3N_2 and D_2O and stored in a lecture bottle over sodium;[15] it was redistilled from sodium before use in these experiments. Salt solutions were prepared with reagent grade anhydrous chemicals weighed into the side arm of a Raman cell assembly in a drybox. The cell assembly, pictured in Figure 1, consisted of the Raman cell proper, a pressure stopcock, and a ball joint which was attached to a vacuum line through which ammonia was distilled into it. The cell and side arm part of the assembly was sealed off under vacuum by means of the pressure stopcock. The Raman cell itself was cylindrically shaped and was made of Pyrex with optical windows on the top and bottom. Samples of anhydrous NH_3 and ND_3 at 25° were prepared in similar cells. The laser beam was directed up through the bottom and the scattered radiation observed at a 90° angle.

The spectrum of liquid NH_3 at low temperatures was obtained with a cell similar in design to that previously described[15] with appropriate modifications for use in the Raman spectrophotometer. The apparatus consists of a solution make-up vessel connected to a Raman cell enclosed in a dewar and a vacuum jacket, respectively. After condensation of NH_3 in the cell, it was pressurized with dry helium which was pumped regularly back and forth to agitate the solution, a process which helped to control the temperature of the solution and to maintain homogeneity. The temperature of the solution was monitored with a thermocouple attached to the Raman cell.

Spectra were measured with a Cary Model 82 Raman spectrophotometer using the 5145-Å line of an argon ion laser (Coherent Radiation Laboratories, Model 53A) as the source.

Computer resolution of the experimental envelopes was performed by a nonlinear least-squares fit of symmetric bands which were Gaussian–Lorentzian combinations.[16] Experience has shown that neither pure Gaussian nor pure Lorentzian bands fit the data as well as the combination bands.

Results

The Raman spectrum of liquid NH_3 at 25 and −71° exhibits a complex envelope between 3100 and 3500 cm^{-1} composed primarily of N–H stretching bands. (See Figures 2 and 3.) The resolution of this envelope was accomplished with a nonlinear least-squares computer program (RESOL).[16] A unique solution for a nonlinear problem does not exist; therefore, resolution of the envelope was attempted with three, four, and five bands The criterion used to decide which assumption, three, four, or five bands, gave the best fit in the statistical sense was the significance tests on the R-factor ratio developed by Hamilton.[17] This test which is generally applicable to nonlinear least-square problems allows one to decide if the addition of parameters or the imposition of fixed relationships between parameters results in improvement between ex-

TABLE I: *R* Factors and *R*-Factor Ratios for Resolution of the N–H Stretching Region

	R_3	R_4	R_5	R_3/R_4	$R_{3,4}$[a]	R_4/R_5	$R_{4,5}$[a]
NH_3 (25°)	0.0915	0.0206	0.0115	4.44	1.042	1.33	1.043
NH_3 (−71°)	0.0734	0.0123	0.0118	5.97	1.043	1.04	1.044
ND_3 (25°)	0.0787	0.0190	0.0227	4.15	1.049	0.837	1.050

[a] The tabulated *R* value from ref 17.

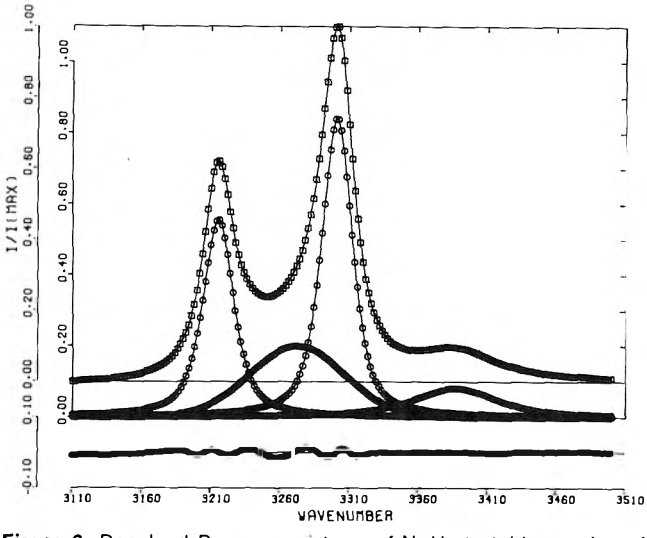

Figure 2. Resolved Raman spectrum of N–H stretching region of NH_3 at 25°.

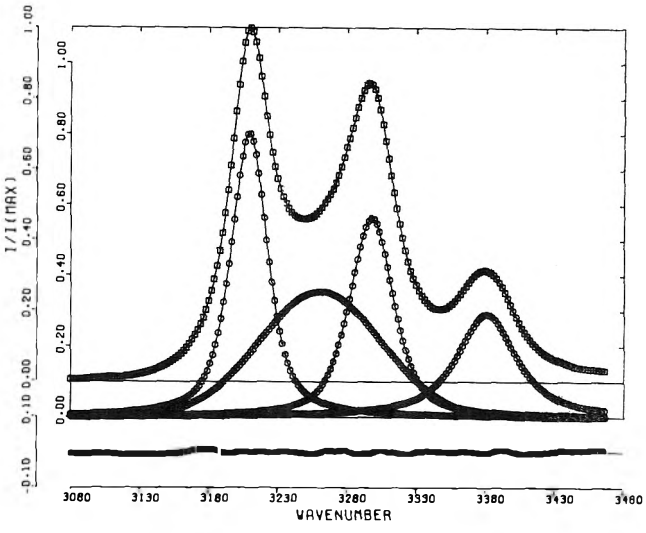

Figure 3. Resolved Raman spectrum of N–H stretching region of NH_3 at −71°.

perimental and calculated values. The hypotheses are made that the three-band fit is better than the four-band fit and that the four-band fit is better than the five-band fit; the *R*-factor ratio of the three-band resolution to that of the four-band resolution and the corresponding ratio of the four- and five-band resolutions were formed and compared to the statistical *R* factor calculated with respect to the number of degrees of freedom, the number of restricted parameters, and the significance level at which the comparison is to be made. These *R* factors are tabulated in Hamilton's paper.[17] If the *R*-factor ratio is greater than the tabulated value the hypothesis is rejected.

The *R*-factor data obtained using combination Gaussian and Lorentzian functions is shown in Table I. Using this test at the 0.005 significance level we observe that when three and four bands are compared, that the four-band resolution is significantly better. The same results obtain for a Gaussian, Lorentzian, or a linear combination of Gaussian and Lorentzian functions, but the fit is significantly better for a combination Gaussian–Lorentzian function.[2] If a five-band resolution (addition of four parameters for a combination function) is attempted, statistically significant improvement does not occur in most cases. In addition, the fifth resolved band contributes very little intensity to the overall band envelope (2%) while the fourth band contributes significantly to the overall intensity (≈30%). The four-band resolution of the envelope gives the best fit for the spectrum of the pure liquid and for spectra of solutions of salts in liquid NH_3 which is the subject of a forthcoming publication. Independent experimental results, discussed later in conjunction with the spectrum of liquid ND_2H, support the validity of the resolution of the liquid NH_3 spectrum into four bands.

The lowest frequency band obtained from the resolution of the spectrum of NH_3 at 25°, *i.e.*, 3214 cm^{-1}, is assigned to the overtone of the fundamental bending mode, ν_4, which occurs at 1638 cm^{-1} in the same spectrum. The remaining three bands are assigned to the fundamental N–H stretching modes of at least two types of NH_3 molecules in the liquid state. The frequencies and band assignments for NH_3, ND_3, ND_2H, and solutions of NaI and $NaClO_4$ in liquid NH_3 are listed in Table II. A notable feature of the data is that the lowest frequency band grows in intensity relative to the band at *ca.* 3300 cm^{-1} with decreasing temperature as do the relative intensities of the bands at *ca.* 3270 and 3385 cm^{-1}. In addition, the 3270-cm^{-1} band becomes broader while that at 3385 cm^{-1} becomes narrower with decreasing temperature. Others[18] have correlated the changing width of the 3385-cm^{-1} band with rotational restriction of NH_3 molecules due to intermolecular association in the liquid state. The N–H stretching region of spectra of solutions of NaI and $NaClO_4$ in NH_3 discussed previously[12] were also resolved into four component bands, the frequencies and assignments of which are also listed in Table II.

A sample of gaseous ND_3 containing a small amount of ND_2H (less than 10%) was examined by high-resolution mass spectrometry to determine if a spectroscopically significant amount of NDH_2 was present. The results confirmed that there was less than 1% NDH_2 in the sample. The Raman spectrum of a liquid sample of this mixture at 25° was measured (Figure 4). This supports the mass spectrometry results indicating very little, if any, NDH_2. The envelope in the ND stretching region measured at a low gain can be considered to consist only of fundamental modes of ND_3 (Figure 5). Equilibrium constants for the

TABLE II: Raman Stretching Frequencies[a] and Assignments

Solution	Symmetry type C_s C_{3v}	$2\nu_4$	Assignment ν_2	ν_1 ν_1	ν_5 ν_3
ND_3 (25°)		2347(p)[b]	2373(p)	2403(p)	2521(dp)
ND_2H (25°)				3342(p),3367(p)	
NH_3 (25°)		3214(p)	3271(p)	3300(p)	3385(dp)
NH_3 (−71°)		3209(p)	3261(p)	3298(p)	3380(dp)
NH_3/NaI[c]		3212(p)	3252(p)	3292(p)	3370(dp)
NH_3/$NaClO_4$[d]		3222(p)	3280(p)	3306(p)	3393(dp)

[a] In cm^{-1}. [b] p = polarized; dp = depolarized. [c] Mole ratio = 12. [d] Mole ratio = 9.

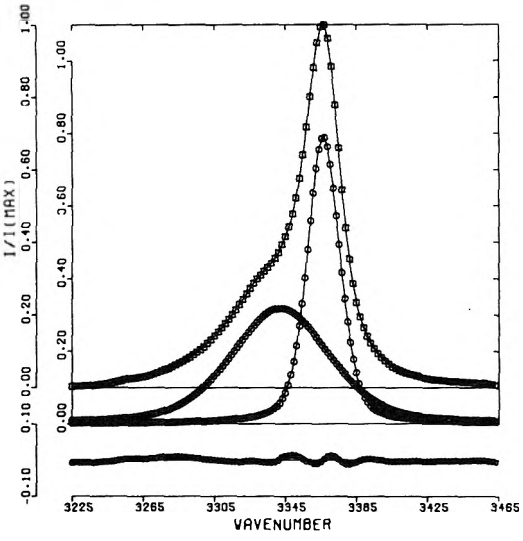

Figure 4. Resolved Raman spectrum of N–H stretching region of ND_2H at 25°.

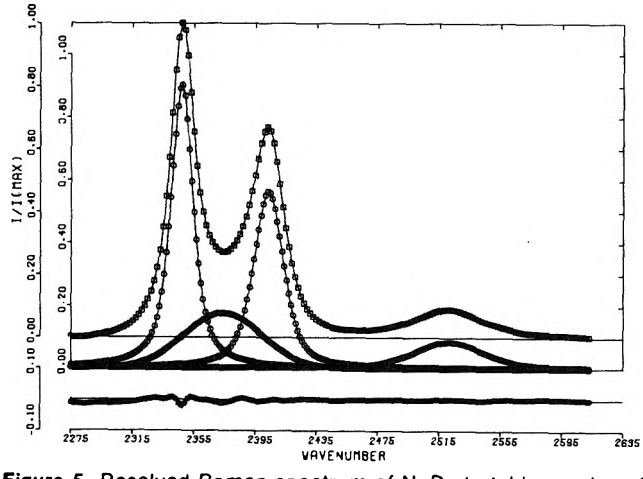

Figure 5. Resolved Raman spectrum of N–D stretching region of ND_3 at 25°.

equilibria between ND_3, ND_2H, NDH_2, and NH_3 have been used by Corset[8] to calculate the amounts of various species present at various ND_3/NH_3 mole ratios. If NH_3 is absent from the mixture, which is the case here based on the absence of NH_3 fundamentals in the Raman spectrum, less than 3% NDH_2 can be present according to these calculations. Therefore, the envelope in the N–H stretching region of this liquid mixture can be attributed solely to ND_2H. The envelope clearly has two maxima,

TABLE III: Raman Bending Frequencies[a] and Assignments

Solution	Assignment ν_4	ν_2
ND_3 (25°)	1198	809
NH_3 (25°)	1638(dp)[b]	1046(p)
NH_3 (−71°)	1638(dp)	1070(p)

[a] In cm^{-1}. [b] p = polarized; dp = depolarized.

TABLE IV: Raman Frequencies[a] Observed below 800 cm^{-1}

Solution	Frequency
NH_3 (25°)	380
NH_3 (−71°)	320
ND_3 (25°)	280

[a] In cm^{-1}.

and has been resolved into two bands, one at 3342 cm^{-1} and one at 3367 cm^{-1}. These bands are assigned to two species of ND_2H.

The ν_2 and ν_4 bending modes of liquid NH_3 at 25°, reported previously, are listed in Table III, as are the fundamental bending modes of liquid NH_3 at −71°. The ν_2 bending mode of NH_3 in the NaI solution occurs at 1092 cm^{-1} rather than at 1067 cm^{-1} which was previously reported incorrectly.[12] The ν_2 and ν_4 bending modes of ND_3–ND_2H mixture are also reported in Table II.

The spectrum of liquid NH_3 exhibits a broad, low intensity band between 150 and 400 cm^{-1}. The band was observed in spectra of NH_3 at 25 and −71°. Band maxima were determined by computer methods using a nonlinear least-squares program with a quadratic background function.[16] The intensity of the low-frequency band increases with a decrease in temperature, and its maximum appears at a lower frequency in ND_3. The band positions are reported in Table IV.

Discussion

An important consideration in the analysis of the NH_3 vibrational spectrum, and thus in a proposed model for the liquid state is the determination of the number and position of bands in the stretching region. As mentioned previously, there has been disagreement about assignments when three bands were used to resolve the envelope. Birchall and Drummond[13] assumed that the overtone band was the higher frequency band (*ca.* 3300 cm^{-1}) and the ν_1 symmetric stretching mode was at *ca.* 3215

cm^{-1} for the 25° data. They cited the changing intensities of these bands at lower temperature with decreasing Fermi resonance as confirmation of their assignment. However, if the opposite assignments are made for the 25° data there would be an increase in Fermi resonance with a lowering in temperature and the same relative intensity changes would be expected. de Bettignies and Wallart[14,19] showed that their assignments are compatible with the changing amount of Fermi resonance which occurs with a change in temperature. They report a temperature at which Fermi resonance would be complete and we will discuss this later in terms of a four-band resolution of the data. Our discussion of the results will be in terms of a four-band resolution with the assumption that the lowest frequency band is the overtone of ν_4.

If one assumes that NH_3 in the liquid state has C_{3v} symmetry, two fundamental stretching modes ($\nu_1(A)_1$ and $\nu_3(E)$) are expected. The overtone of the ν_4 bending mode ($2\nu_4$) exhibits an increased Raman intensity due to a Fermi resonance interaction with ν_1, the symmetric stretching mode, since both modes have A_1 symmetry. This overtone would account for a third band. The fact that a three-band resolution leaves considerable residual intensity around 3270 cm^{-1} indicates either that NH_3 with C_{3v} symmetry is not present or that it is not the only type of NH_3 molecule in the liquid state. The four-band resolution shown in Figure 4 suggests the possibility that two types of NH_3 molecules are present which was confirmed by experiment. The spectrum of ND_2H was measured so that one N-H stretching mode of an ammonia type molecule could be isolated. There should be only one N-H stretching mode for ND_2H under C_s symmetry; the band should be of A′ character, and therefore, polarized. The fact that two bands of comparable intensity were found, both polarized, indicates that two types of ND_2H molecules are present. The two bands (3342 and 3367 cm^{-1}) are separated by 25 cm^{-1} and have half-widths of 65 and 21 cm^{-1}, respectively. In the four-band resolution of NH_3, the bands at 3271 and 3300 cm^{-1} are separated by 20 cm^{-1} and have half-widths of 80 and 26 cm^{-1}, respectively. The similarity of these two pairs of bands suggests that in each case, ND_2H and NH_3, two types of N-H bonds are present; the one having a lower stretching frequency is probably due to a species of the type, D_2N-H—ND_2H, *i.e.*, ND_2H associated through hydrogen to another ND_2H, and the other to a free (unassociated) N-H bond of ND_2H.

To understand the three N-H stretching bands in the four-band resolution of NH_3 in terms of two types of NH_3 molecules, all possible associated and free species should be examined. If none or all of the hydrogen atoms are associated with another NH_3 molecule, C_{3v} symmetry should be maintained, and two stretching modes are expected. It would be unreasonable to expect the structure observed for solid NH_3[20] (*i.e.*, all hydrogens associated) to be maintained in the liquid state, especially at 25°. Two other species are possible, both having C_s symmetry (I and II). Model I should have three stretching modes giving rise to three bands. The lowest frequency band due to the N-H stretch of the associated hydrogen should be polarized. Two stretching modes, one symmetric and the other asymmetric, would be attributed mainly to the free N-H bonds and would probably coincide with the two fundamental stretching modes of NH_3 molecules with C_{3v} symmetry with non-hydrogen-bonded atoms. The symmetric mode should be responsible for the lower frequency of these two bands. Therefore, three bands in addition to the overtone would be predicted, the highest frequency band being depolarized and the two of lower frequency polarized, as is observed experimentally. Model II should exhibit two bands due to the symmetric and asymmetric stretching modes of the associated N-H bonds and a symmetric stretching mode due to the free N-H bond. While the 3271-cm^{-1} band would be attributed to the symmetric stretching mode of the associated N-H bond and the 3300-cm^{-1} band to the symmetric stretching mode of the free N-H bond, the 3385-cm^{-1} band would have to be assigned to the asymmetric stretching mode of the associated N-H bond and to the asymmetric stretching mode of the free N-H bond of C_{3v} NH_3. To account for two species of NH_3 (C_{3v} and Model II) two depolarized bands at frequencies greater than 3300 cm^{-1} would be expected. Lauranson, *et al.*,[21] calculated vibrational frequencies of a Model II type NH_3 association and predicted that the asymmetric stretching mode due to the associated hydrogen atoms would be found at a frequency less than 3385 cm^{-1} and would not be coincident with a depolarized band due to Model I type NH_3 or C_{3v} NH_3. A combination of Model I and Model II would also have less than three bands coincident. While it might be possible for the 3271- and 3300-cm^{-1} bands to account for all the symmetric stretching modes of the associated and free hydrogen atoms of both models, respectively, only the one depolarized band at 3385 cm^{-1} would be left to account for the asymmetric stretching mode of both free and associated hydrogens.

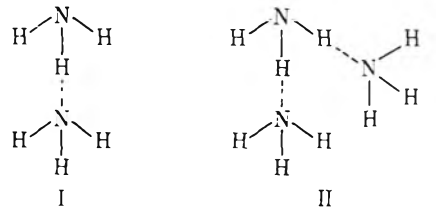

I II

It is reasonable to suggest that NH_3 with all N-H bonds having unassociated hydrogen atoms would have symmetric and asymmetric stretching modes of frequencies very similar to the free N-H stretching modes of Model I. The terminal NH_3 molecule in a species exhibiting Model I-type bonding would also have C_{3v} symmetry. Therefore, from the evidence in the N-H stretching region two types of NH_3, one with C_s symmetry (Model I) and one with C_{3v} symmetry would be expected.

The interpretation of N-D stretching region of ND_3 is very similar to that of the N-H stretching region for NH_3, further supporting the hypothesis and suggesting that ND_3, ND_2H, and NH_3 are alike in the liquid.

The position of the band due to an associated N-H stretching mode should change in frequency with the strength of its association with other molecules. I^- and ClO_4^- were chosen because previous work has suggested that they are representative of two classes of anions which interact differently with NH_3. The presence of iodide ion causes the 3271-cm^{-1} band to shift to a lower frequency implying some interaction between anion and solvent while the perchlorate ion causes this band (3280 cm^{-1}) to move to higher frequency. The suggestion of an interaction of the iodide ion with NH_3 is consistent with evi-

dence obtained from the charge transfer spectrum of I^- in NH_3.[22,23] By contrast, the perchlorate ion seems to have little association with NH_3. The cation should have little effect on these positions as previous data from the near-infrared region suggest.[9]

The lowering of the temperature in liquid NH_3 produces significant changes in the spectrum in the N-H stretching region. de Bettignies and Wallart[14] have explained the changing intensities on the basis of Fermi resonance and have assumed that the envelope is made up of only three bands. Gardiner, *et al.*,[18] have explained similar intensity changes with changing NH_3 concentration in CCl_4 and changing salt concentrations in NH_3 by assigning the 3214-cm^{-1} band to NH_3 molecules associated through hydrogen atoms.

While de Bettignies' theory with regard to two bands in Fermi resonance appears to be reasonable, the situation is complicated by the presence of two species of NH_3, both having overtones of the bending mode at *ca.* 3214 cm^{-1}. Each of these overtones can be in Fermi resonance with a stretching fundamental of the same molecule. NH_3 with all hydrogen atoms unassociated could exhibit resonance between the 3300-cm^{-1} band and the 3214-cm^{-1} band. An ammonia molecule with one hydrogen associated could exhibit resonance between the 3271-cm^{-1} band and the 3214-cm^{-1} band. It is not possible then, to say at what point either species has two bands in perfect resonance and therefore when the mixing of states is complete. To deduce the state of perfect resonance, according to de Bettignies' approach, that part of the intensity of the 3214-cm^{-1} band due to the NH_3 molecules with C_{3v} symmetry would have to be compared to that part of the intensity of the 3300-cm^{-1} band due to the stretching fundamental of this same molecule. When these two intensities are equal, resonance for this molecule would be complete. Similarly, that remaining part of the intensity of the 3214-cm^{-1} band due to the NH_3 molecule with C_s symmetry would have to be compared to the stretching fundamental of the same molecule in order to determine when perfect resonance is reached. At that point each band should represent an eigenfunction which would be an equal mixture of the zero approximation eigenfunctions of the unperturbed ν_1 and $2\nu_4$ states. The problem is complicated by the fact that there is probably an increase in the concentration of NH_3 molecules with C_s symmetry over that of NH_3 molecules with C_{3v} symmetry as the temperature is lowered, or as the NH_3 concentration is increased in CCl_4 solutions. Such factors should change the intensities of the 3300- and 3271-cm^{-1} bands and would cause a change in the amount of Fermi resonance in each of the species.

It has been pointed out that the ν_4 fundamental mode does not change in frequency and therefore does not indicate any changes in Fermi resonance. However, if only the unperturbed stretching fundamental changed in frequency in each case, due to a change in the amount of hydrogen bonding, Fermi resonance would be affected. The expected change in frequency of the symmetric stretching fundamental possibly would not be observed because of a shift in the opposite direction due to the perturbation caused by the resonance. The asymmetric stretching mode, ν_3, which should also shift with a change in hydrogen bonding and which is not involved in Fermi resonance, shifts considerably in the presence of NaI and $NaClO_4$ to lower frequency.

Gardiner, *et al.*,[18] assign the polarized band at *ca.* 3214 cm^{-1} to the symmetric stretching mode of NH_3 molecules with two or three hydrogens associated with another molecule. If this were correct, another depolarized band due to the asymmetric stretching mode of these NH_3 molecules would be expected. The only depolarized band observed is at 3385 cm^{-1}. In addition, if the 3214-cm^{-1} band were a fundamental mode an overtone of this band in the near-ir region of intensity comparable to the overtones and combinations of the other fundamental modes in this region would be expected. The region between 6060 and 6540 cm^{-1} is devoid of bands of the expected intensity; however, bands above 6540 cm^{-1} are of observable intensity.[9] Therefore, the most consistent explanation for the 3214-cm^{-1} band appears to be that it is the first overtone of the ν_4 fundamental bending mode.

The N-H bending region of the ammonia spectrum does not show the presence of NH_3 molecules with C_s symmetry. However, it has been shown that bending vibrations are not as sensitive as are stretching modes[24] to changes in the symmetry of the potential field around a molecule. This is especially true in the case of hydrogen-bonded species.[25] While degeneracies in this region are not lifted, the change in frequency of the symmetric bending mode (ν_2) of NH_3 with a change in the nature of the hydrogen-bonded species or with temperature helps support our general picture of the structure of liquid NH_3. The symmetric bending mode shifts to higher frequency in solutions of NaI, and to lower frequency in solutions of $NaClO_4$, which is consistent with the suggestion that association of I^- with hydrogen atoms in NH_3 occurs and that the interaction between a perchlorate ion and an NH_3 molecule is weaker than the association between two NH_3 molecules. The shift in frequency of the 1046-cm^{-1} band which occurs at lower temperatures can be correlated with an increase in the number of NH_3 molecules associating and a corresponding decrease in the number of NH_3 molecules which have free (unassociated) hydrogen atoms creating a shift in the maximum of this band toward higher frequency.

The unchanging position of the ν_4 bending mode of NH_3 with a change in the amount or type of hydrogen bonding in the system suggests that this fundamental bending mode is not as sensitive as the ν_2 symmetric bending mode to these effects.

The suggestion[26] that the broad, low-intensity band between 150 and 400 cm^{-1} is associated with rotational motion is not borne out by the observation that the intensity of the band increases with a decrease in temperature, since rotation is expected to be hindered by increased hydrogen bonding at lower temperatures. The intensity increase suggests that this band arises from intermolecular interactions which would be expected to increase at lower temperatures. The shift of the band to lower frequency in liquid ND_3 supports this hypothesis since the greater reduced mass of the interacting ND_3 species should result in a lower frequency of interaction. In addition, hydrogen bond-type interactions for deuterium are slightly weaker than similar interactions for hydrogen in similar environments.[27,28] If such weaker interactions are also characteristic in liquid NH_3 and ND_3, one would expect the corresponding bands to shift to lower frequency in ND_3.

The interpretation presented here suggests that liquid NH_3 probably consists of linear polymeric species incorporating NH_3 molecules associated by hydrogen bonding.

The molecule at one end of this entity retains C_{3v} symmetry, while the others have their symmetry lowered to C_s, a perturbation which is discernible in the stretching region but not in the bending region of the spectrum. There may exist also some molecules in the liquid state that are not associated, and which, thus, retain C_{3v} symmetry. The introduction of salts into liquid ammonia affects the structure in different ways depending on the nature of the anion. Evidence of a strong Na^+-NH_3 interaction was not observed.

In order to confirm this model for the structure of liquid NH_3, and possibly to learn more about the structure of liquid H_2O, a Raman study of NH_3-H_2O liquid mixtures has been undertaken. In addition, solutions of other salts in liquid NH_3 at different concentrations are currently being investigated. It is expected that such studies will add to the understanding of the nature of hydrogen-bonded solvents.

Acknowledgments. We gratefully acknowledge the financial support of the National Science Foundation and the Robert A. Welch Foundation. We also wish to extend our appreciation to Dr. Peter F Rusch for his helpful suggestions and discussions concerning computer resolutions.

References and Notes

(1) T. T. Wall and D. F. Horning, *J. Chem. Phys.*, **43**, 2079 (1965).
(2) J. Schiffer and D. F. Hornig, *J. Chem. Phys.*, **49**, 4150 (1968).
(3) E. U. Franck and K. Roth, *Discuss. Faraday Soc.*, **43**, 108 (1967).
(4) J. D. Worley and J. M. Klotz, *J. Chem. Phys.*, **45**, 2868 (1966).
(5) W. A. P. Luck, *Fortschr. Chem. Forsch.*, **4**, 653 (1964).
(6) G. E. Rodgers, Thesis, Cornell University, Ithaca, N. Y., 1971.
(7) G. E. Walrafen, *J. Chem. Phys.*, **52**, 4176 (1970).
(8) J. Corset, Thesis, Universite de Bordeaux, 1967.
(9) J. H. Roberts and J. J. Lagowski, *Metal-Ammonia Solutions; Physicochem. Prop., Colloq. Weyl*, in press.
(10) C. A. Plint, R. M. B. Small, and H. L. Welsh, *Can. J. Phys.*, **32**, 653 (1954).
(11) S. Kinumaki and K. Aida, *Sci. Rep. Res. Inst. Tohoku Univ.*, **6** 186 (1954).
(12) J. H. Roberts, A. T. Lemley, and J. J. Lagowski, *Spectrosc. Lett.*, **5**, 271 (1972).
(13) T. Birchall and I. Drummond, *J. Chem. Soc. A*, 1859 (1970).
(14) B. de Bettignies and Francis Wallart, *C. R. Acad. Sci., Ser. B*, **271**, 640 (1970).
(15) D. Burow, Dissertation, University of Texas at Austin, 1966.
(16) P. F. Rusch, Dissertation, University of Texas at Austin, 1971.
(17) W. C. Hamilton, *Acta Crystallogr.*, **18**, 502 (1965).
(18) D. J. Gardiner, R. E. Hester, and W. E. L. Grossman, private communication.
(19) B. de Bettignies, Thesis, Universite de Lille, 1970.
(20) I. Olovsson and D. H. Templeton, *Acta Crystallogr.*, 12, 832 (1959).
(21) J. Lauranson, J. Corset, and M. Forel, *Ann. Chim.*, **3**, 109 (1968).
(22) M. J. Blandamer, R. Catterall, L. Shields, and M. C. R. Symons, *J. Chem. Soc.*, 4357 (1964).
(23) D. Shapira and A. Treinin, *J. Phys. Chem.*, **70**, 305 (1966).
(24) J. P. Mathieu and M. Lounsbury, *Discuss. Faraday Soc.*, **9**, 196 (1950).
(25) G. C. Pimentel and A. L. McClellan, "The Hydrogen Bond," San Francisco, Calif., 1960.
(26) B. L. Smith and W. H. Koehler, private communication.
(27) O. D. Bonner, *J. Amer. Chem. Soc.*, **92**, 4197 (1970).
(28) A. Grimison, *J. Phys. Chem.*, **67**, 962 (1963).

The Dipole Moments of 4-Aminobicyclo[2.2.2]octane-1-carboxylic Acid and Some α,ω-Amino Acids

J. T. Edward, P. G. Farrell,* and J. L. Job

Department of Chemistry, McGill University, Montreal 101, Canada *(Received April 17, 1973)*

Publication costs assisted by the National Research Council of Canada

The dielectric constants for aqueous solutions of 4-aminobicyclo[2.2.2]octane-1-carboxylic acid, and the α,ω-amino acids, $H_3N^+(CH_2)_nCO_2^-$, $(0 < n < 10)$, have been measured. The dipole moments of these molecules have then been calculated using both Kirkwood's and Buckingham's theories. The values obtained for the rigid molecule are compared with the theoretical dipole length, calculated from the molecular geometry, to give empirical correction factors for these theories. Application of these correction factors to the dipole moments of the flexible molecules gives intercharge distances in close agreement with those calculated for fully extended chains.

Introduction

Much of the early evidence in favor of the dipolar ionic or zwitterionic form for molecules such as amino acids in aqueous solution was provided by measurements of the dielectric constants of their solutions.[1] However, there have been few attempts to calculate dipole moments from such data because of the inherent theoretical problems involved in treating solutions of polar molecules in polar solvents. The magnitudes of the charges forming the dipoles are known and hence the dipole lengths of zwitterionic molecules are readily calculable from the dipole moments. If the molecules have precisely defined geometries, a comparison of the known lengths with those calculated from dipole moments should give an indication of the value of the method used to calculate the latter. For flexible molecules, valuable information on the conformations of these molecules should be obtained.

The early theories of Debye and Onsager may be used to calculate dipole moments from measurements on dilute solutions of dipolar molecules in nonpolar solvents, but

they are not applicable to measurements in polar solvents. Kirkwood[2] modified Onsager's theory by including the effects of electrostatic interactions and short-range intermolecular forces on the rotational behavior of solute and solvent under the influence of an electric field, in order to apply the theory to polar solutes in polar solvents. Although he concluded that the true dipole moment, μ, of an individual molecule could not be obtained from dielectric constant measurements alone, he showed that it was approximated by the expression

$$\mu = 3.30\delta^{1/2} \quad (1)$$

where δ is the molar dielectric increment of the solute. Kirkwood's theory thus provided some theoretical justification for an earlier empirical relationship of Wyman[1]

$$\mu = (10\delta)^{1/2} \quad (2)$$

Using eq 1 Kirkwood obtained values for the dipole moments of the first five homologous α,ω-amino acids and found that these were close to values calculated assuming intercharge distances equal to the free rotation values.[3] This indicated that the α,ω-amino acids did not exist in their most extended forms in aqueous solution.

In 1953, Buckingham[4,5] developed an alternative theory to calculate the dipole moments of polar solutes in polar solvents. In this theory the solute molecules were assumed to be anisotropic ellipsoids surrounded by a homogeneous and continuous medium of dielectric constant equal to that of the bulk solution. He derived an expression for the orientation polarization of the solute, ${}_oP_2$

$${}_oP_2 = \frac{1}{x_2}\left(\frac{\epsilon + (n_2^2 - \epsilon)A_2}{1 + (n_2^2 - 1)A_2}\right)^2\left[\frac{(\epsilon - n^2)(x_1M_1 + x_2M_2)}{\epsilon(2\epsilon + n^2)d} - x_1({}_oP_1)\left(\frac{1 + (n_1^2 - 1)A_1}{\epsilon + (n_1^2 - \epsilon)A_1}\right)^2\right] \quad (3)$$

where subscripts 1 and 2 refer to solvent and solute, respectively, x = mole fraction, A = shape factor, n = refractive index, ϵ = dielectric constant, d = density of solution, M = molecular weight, and ${}_oP$ = orientation polarization. From this the dipole moment can be calculated using the equation

$$\mu^2 = \frac{9kT({}_oP_2)}{4\pi N} \quad (4)$$

Application of this theory to glycine and β-alanine, assuming a free-rotation intercharge distance in the latter,[5] gave results in reasonable agreement with those obtained by Kirkwood.

We have been unable to find any other reports of either theory being tested with a zwitterionic molecule of precisely defined geometry. To this end we have determined the dipole moment of 4-aminobicyclo[2.2.2]octane-1-carboxylic acid (I) in aqueous solution. This molecule closely

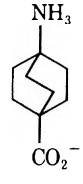

I

approximates an axially symmetric prolate ellipsoid and the intercharge distance can be measured precisely. The ratio of the measured dipole length to that determined from eq 3 and 4 or 1 provides, respectively, empirical correction factors indicating the effectiveness of Buckingham's or Kirkwood's model for zwitterion–water systems.

We have also measured the dielectric constants of aqueous solutions of the flexible α,ω-amino acids, $H_3N^+(CH_2)_nCOO^-$, where $0 < n < 10$, and calculated their dipole moments. Application of the empirical correction factors, derived for 4-aminobicyclo[2.2.2]octane-1-carboxylic acid, to these data indicates the probable degree of extension of these chain molecules in water.

Experimental Section

Materials. 4-Aminobicyclo[2.2.2]octane-1-carboxylic Acid. This compound was synthesized by combining the literature methods of Kauer,[6] Roberts, *et al.*,[7] and Chapman, *et al.*,[8] and was recrystallized several times from water: mp >360° (lit.[6] 365°).

α,ω-Amino Acids. These were commercially obtained, or prepared in accordance with literature methods, and recrystallized at least three times from ethanol or ethanol–water mixtures. Their melting or decomposition points agreed with the literature values.

Water. Doubly distilled water was passed through a mixed-bed deionizing resin (Rexyn I300) immediately before use. The specific conductivity was less than 10^{-6} ohm^{-1} cm^{-1}.

Measurements. Densities were determined using a 10-ml pycnometer and refractive indices using a thermostated Abbé refractometer. Dielectric constant values were determined using a Dipolemeter, Type DMO1 (Wissenschaftlich-Technische Werkstätten) fitted with a water-jacketed cell, Type MFL3/S (WTW, nickel-plated) which functions in the dielectric constant range 21–120 (the latter figure is approximate). The Dipolemeter operates at 2 MHz on the superposition (or beat) principle and is designed to give a linear correlation between capacitance readings and dielectric constants.

All measurements were made at 25°, constant temperatures (±0.01°) being maintained by circulating water from an external bath. Solutions were made up by weight and the same solution specimen was used for all three measurements.

Conductance measurements showed that the maximum specific conductivity which resulted in no decrease in signal amplitude was 1.5×10^{-5} ohm^{-1} cm^{-1}. A linear increase in capacitance readings (and thus dielectric constant values) with amino acid concentration was observed below this specific conductivity and the signal amplitude was at its maximum. When the specific conductivity exceeded 1.5×10^{-5} ohm^{-1} cm^{-1}, the signal amplitude decreased and negative deviations of the ϵ *vs.* molar concentration lines were observed. (See Figure 1.)

Care was taken to ensure thermal equilibration and readings were taken over a 15-min period, the capacitance values being averaged to calculate the dielectric constant.

Calibration of the Dipolemeter. The apparatus was calibrated with water, (treated as described above), nitrobenzene (certified ACS, Fisher Scientific Co.), and acetone (certified ACS Spectroanalysed; Fisher Scientific Co.). The latter two solvents were not further purified but were dried by passage over a column of Linde molecular sieves (Type 4A). The solvents were run directly from the columns into the dielectric cell (rinsed 3 times) to avoid the uptake of atmospheric moisture. Typical calibration data

TABLE I: Experimental Data, Structural Parameters for, and Results of the Calculations of the Dipole Moment of 4-Aminobicyclo[2.2.2]octane-1-carboxylic Acid

Concn, *M*	Dielectric constant	x_2	Refractive index	Density	μ_B
0.0	78.540	0	1.3325	0.99704	
1.388×10^{-2}	79.532	2.511×10^{-4}	1.3329	0.99767	45.7
2.389×10^{-2}	80.233	4.327×10^{-4}	1.3331	0.99805	37.6
3.766×10^{-2}	81.248	6.830×10^{-4}	1.3336	0.99879	32.9
4.895×10^{-2}	82.038	8.890×10^{-4}	1.3340	0.99903	30.8
6.021×10^{-2} [a]	82.853	1.095×10^{-3}	1.3343	0.99951	29.4
7.851×10^{-2} [a]	84.168	1.430×10^{-3}	1.3349	1.00040	27.9
2.058×10^{-1} [a]	93.281	3.803×10^{-3}	1.3392	1.00567	24.6
3.899×10^{-1} [a]	06.47	7.354×10^{-3}	1.3449	1.01388	23.5

[a] The dielectric constants were calculated from the value of the dielectric increment. Molar dielectric increment 71.6 ± 0.3; $n_2^2 = 3.723$; $b/a = 0.60$; $A_2 = 0.21$.

were: slope of ϵ *vs.* capacitance plot, 0.02440 ± 0.00001; intercept, 12.210 ± 0.017; correlation coefficient, 0.99999.

Data Treatment. The dielectric constants, ϵ, of the solutions were calculated from the experimental capacitance readings and the slope and intercept of the calibration plot. From the linear variation of ϵ with concentration, the dielectric increment, δ, was obtained, and the dipole moment was calculated using eq 1.

The calculation of the dipole moments from Buckingham's theory was carried out as in his paper. With the exception of the refractive index,[9] Buckingham's parameters for water were used. The parameters for the solutes were determined as follows.

n_2. The refractive index was calculated from the molar refractivity determined from the data given by Vogel,[10] and the molar volume was calculated from the van der Waals increments tabulated by Edward.[11]

A_2. The shape factor was obtained from a knowledge of the axial ratios of the molecules.[12] For the bicyclooctane derivative these were found from measurements of a space-filling model (Courtauld). The flexible molecules were assumed to be axially symmetric and the parameter λ_0 was calculated from the assumed intercharge distance, R, and the molecular volume, V, using the relationship[13]

$$\lambda_0^3 - \lambda_0 = \frac{6V}{\pi R^3} \qquad (5)$$

This equation was solved for λ_0 using a Newton-Raphson iterative procedure. The major and minor semiaxes, a and b, were then determined from

$$a = \frac{\lambda_0 R}{2}; \quad b^2 = \frac{3V}{2\pi\lambda_0 R}$$

In all cases the charge on the carboxyl group was assumed to lie symmetrically between the oxygen atoms on the extension of the methylene–carboxyl bond. The charge on the ammonium group was taken to be situated 0.25 Å beyond the nitrogen atom on the extension of the carbon–nitrogen bond. The complete experimental data for 4-aminobicyclo[2.2.2]octane-1-carboxylic acid are given in Table I. (See the paragraph at the end of the paper regarding supplementary material.)

Results and Discussion

4-Aminobicyclo[2.2.2]octane-1-carboxylic Acid. The dipole moment of 4-aminobicyclo[2.2.2]octane-1-carboxylic acid in water at various concentrations was calculated from the data in Table I using eq 3 and 4. The dielectric

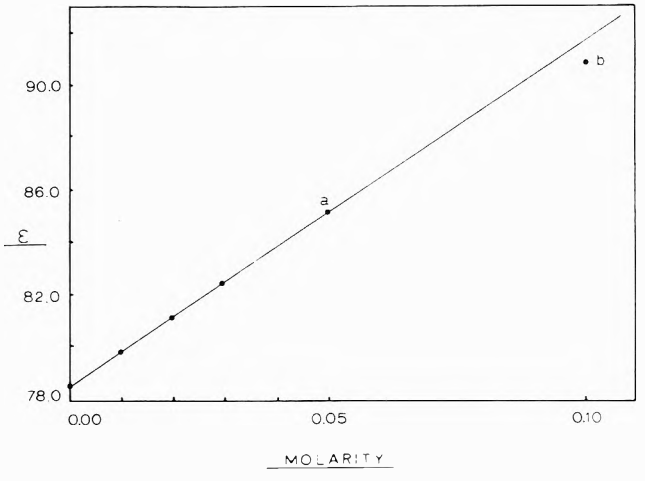

Figure 1. The variation of dielectric constant with the concentration of 9-amino nonanoic acid. Slope of line (excluding point b), 130.8 ± 0.5 l. mol^{-1}; correlation coefficient (excluding point *b*) 0.9996. (a) Last point giving full signal amplitude; specific conductivity 1.10×10^{-5} mho cm^{-1}. (b) Approximately 75% signal amplitude; specific conductivity 1.62×10^{-5} mho cm^{-1}.

constants for the more concentrated solutions were calculated from the value of the molar dielectric increment, as the conductivities of these solutions were too high to allow accurate experimental determination of ϵ with the apparatus used. It was assumed that the dielectric increment was invariant over the concentration range considered for the dipole moment calculations as previous studies on several other amino acids showed that the dielectric constant varied linearly with concentration to values of the latter in excess of 2 *M*.[1]

It is evident that the dipole moments calculated from Buckingham's equation increase with decreasing solute concentration. This effect was not observed in the earlier application of this theory as solute concentrations of 1 *M* only were considered. The variation of the dipole moment with concentration results from the term x_2^{-1} in eq 3 being improperly compensated by the other variables and this constitutes a major limitation of the theory. In order to provide a common basis for the comparison of our results for each compound with the others in the series studied, and with those in the literature,[5] we have plotted the calculated dipole moment against the reciprocal of the solute concentration (Figure 2) and use the value at 1 *M* for discussion (μ_B). Although it is customary when using other dipole moment equations to extrapolate the varia-

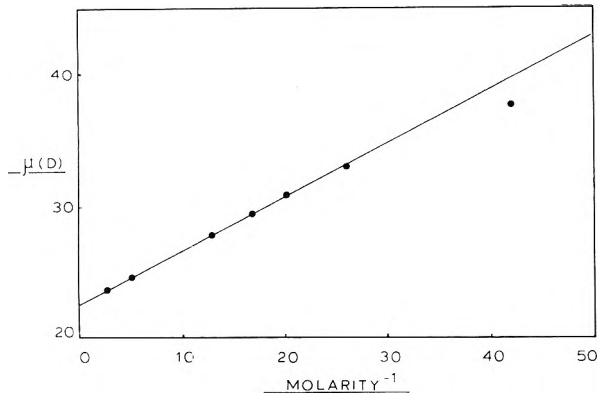

Figure 2. The variation of the dipole moment of 4-aminobicyclo[2.2.2]octane-1-carboxylic acid in aqueous solution, calculated using Buckingham's theory, with the reciprocal of the concentration.

tion of the polarization of the solute with concentration to infinite dilution,[14,15] this is not possible in the present study as ${}_{o}P_2$ and the calculated value of the dipole moment tend to infinity as the solute concentration tends to zero.

The choice of 1 *M* as the standard concentration, in addition to its convenience, is justified by the results obtained for the dipole moment of glycine by this extrapolation procedure and by Buckingham.[5] These are, respectively, 13.4 and 13.3 D. The uncertainty in our dipole moment results at 1 *M* concentration should thus be very small. For β-alanine at 1 *M*, we obtain a dipole moment of 14.9 D when a free-rotation chain model is assumed, whereas Buckingham reported a value of 17.5 D. This difference results from the dielectric increment obtained in the present study and that used by Buckingham (27.9 and 34.5, respectively) and is not caused by our extrapolation procedure.

The value of the dipole moment of 4-aminobicyclo[2.2.2]octane-1-carboxylic acid obtained by the procedure described above is 23.0 D. From this dipole moment the intercharge distance predicted by Buckingham's theory, R_B, is found to be 4.8 Å, whereas the measured dipole length, R, for this compound is 7.1 Å. For this rigid molecule, the ratio $R/R_B \simeq 1.5$ thus provides a quantitative measure of the limitations of Buckingham's theory and a means of adjusting R_B to give agreement with the measured dipole length R.

The molar dielectric increment of 71.6 for this compound, when substituted into eq 1, gives $\mu_K = 27.9$ D, whence $R_K = 5.8$ Å. The analogous correction factor $R/R_K \simeq 1.2$ for Kirkwood's theory.

Flexible α,ω-Amino Acids. In an attempt to assess the value of the empirical parameters derived above we have determined the dielectric constants for aqueous solutions of the first nine homologous α,ω-amino acids.

To calculate the dipole moments for these flexible molecules using eq 3 and 4, A_2 has to be determined. As the degree of chain extension was not known *a priori*, the values for A_2 were calculated (a) assuming fully extended chains ($R = R_{Max}$) and (b) assuming a free-rotation model ($R = R_{Free}$).[16,17] The values of A_2 and μ_B found for these conditions are given in Table II. (For all compounds, the dipole moment varied with concentration and the values for 1 *M* concentration were determined by the extrapolation procedure described above.) The intercharge distances calculated from these dipole moments, $R_B{}^a$ and $R_B{}^b$ (Table III), are much lower for all compounds than those assumed for their determination, R_{Max} and R_{Free}, respectively. This was expected from the results for the bicyclooctane derivative.

TABLE II: Values of A_2 and μ_B for the α,ω-Amino Acids for (a) Maximum Chain Extension and (b) Free Rotation Model

	(a) Maximum extension		(b) Free rotation	
n	A_2	μ_B	A_2	μ_B
1	0.280	13.1	0.272	13.4
2	0.236	15.9	0.260	14.9
3	0.224	17.8	0.252	16.7
4	0.188	23.8	0.245	20.6
5	0.180	26.5	0.242	22.3
6	0.153	31.6	(0.239)[a]	24.5
7	0.147	34.5	(0.237)[a]	26.9
8	0.125	40.6	(0.235)[a]	29.5
9	0.120	44.7	(0.233)[a]	31.5

[a] Values in parentheses were estimated by extrapolating a plot of R_{free} vs. *n*.

Application of the empirical correction factor of 1.5 to the values of $R_B{}^a$ gives intercharge distances which are extremely close to R_{Max} (Table III). The largest discrepancy occurs for glycine which, although it is effectively "rigid," *i.e.*, the intercharge distance is constant, does not closely approximate the ellipsoidal model assumed by Buckingham. In general, however, eq 3 and 4 are internally consistent when full extension of the chains is assumed. If the same empirical factor is applied to $R_B{}^b$, the value obtained from the free rotation model, dipole lengths are obtained which are intermediate between R_{Max} and R_{Free}, and the theory is not self-consistent.

While it must be recognized that the simple model assumed to determine R_{Free} represents a severe approximation to the true rotational motions of a chain molecule,[16] this lack of self-consistency cannot result from this approximation but is a result of the free-rotation model being an incorrect representation of the actual behavior of the α,ω-amino acids in aqueous solution. From the self-consistency of the results obtained assuming maximum chain extension, it is apparent that these flexible amino acids are fully extended in water. This is in agreement with evidence recently obtained from pK data[18] but is contrary to the conclusion drawn by Kirkwood.[2,3]

There is good agreement between the dipole lengths calculated from eq 1 and the R_{Free} values for the first five α,ω-amino acids (Table III). However, the inclusion of the data for the next four homologs shows increasing deviations between the values of R_K and R_{Free}. Application of the correction factor of 1.2 determined above increases the discrepancies between these two measures of the dipole lengths, the corrected R_K values lying between R_{Max} and R_{Free}. This emphasizes that the Kirkwood model is not applicable to the longer chain compounds.

Summary

Thus, an empirical correction factor for dipole moments of amino acids in aqueous solution at 1 *M* concentration, calculated by Buckingham's theory, has been derived from the data for a rigid molecule which closely approximates the assumed ellipsoidal model. The corrected dipole moments for the flexible molecules give intercharge distances in excellent agreement with those measured

TABLE III: Intercharge Distances of the α,ω-Amino Acids

n	R_{Max}[a]	R_E[a]	R_B[a] × 1.5	R_{Free}[b]	R_B[b]	R_B[b] × 1.5	R_K	R_K × 1.2
1	3.25	2.73	4.10	3.56	2.79	4.19	3.35	4.02
2	5.07	3.31	4.97	4.19	3.10	4.65	3.62	4.34
3	5.76	3.71	5.57	4.72	3.48	5.22	4.29	5.15
4	7.58	4.96	7.44	5.19	4.29	6.44	5.27	6.32
5	8.27	5.52	8.28	5.63	4.64	6.96	5.94	7.13
6	10.09	6.58	9.87	(5.98)[b]	5.10	7.65	6.64	7.97
7	10.79	7.18	10.77	(6.30)[b]	5.60	8.40	7.31	8.77
8	12.61	8.45	12.68	(6.59)[b]	6.14	9.21	7.85	9.42
9	13.31	9.31	13.97	(6.84)[b]	6.56	9.84	8.50	10.20

[a] Calculated from known bond lengths and angles. [b] Data taken from ref 14. The value for glycine is larger than R_{Max} because of the slightly different charge placements assumed here and in ref 14. Values in parentheses were estimated by extrapolating a plot of R_{Free} *vs.* n.

from models, assuming maximum chain extension, and the theory is self-consistent. Application of Kirkwood's theory gives closer agreement with the theoretical dipole moment for the rigid molecule, but its application to the flexible molecule does not give intercharge distances in accordance with either free-rotation or maximum extension values.

Acknowledgment. We are grateful to the National Research Council of Canada for financial support. We are also very grateful to Dr. J. C. Kauer for carrying out the Diels-Alder addition for us in the synthesis of the bicyclooctane.

Supplementary Material Available. Listings of refractive indices, dielectric constants, and densities for solutions of the α,ω-amino acids will appear following these pages in the microfilm edition of this volume of the journal. Photocopies of the supplementary material from this paper only or microfiche (105 × 148 mm, 20× reduction, negatives) containing all of the supplementary material for the papers in this issue may be obtained from the Journals Department, American Chemical Society, 1155 16th St., N.W., Washington, D. C. 20036. Remit check or money order for $3.00 for photocopy or $2.00 for microfiche, referring to code number JPC-73-2191.

References and Notes

(1) J. Wyman, *Chem. Rev.*, **19**, 213 (1936).
(2) J. G. Kirkwood, *J. Chem. Phys.*, **7**, 911 (1936).
(3) J. G. Kirkwood, "Proteins, Amino Acids and Peptides," E. J. Cohn and J. T. Edsall, Ed. Hafner, New York, N. Y., 1965, Chapter 12.
(4) A. D. Buckingham, *Aust. J. Chem.*, **6**, 93 (1953).
(5) A. D. Buckingham, *Aust. J. Chem.*, **6**, 323 (1953).
(6) J. C. Kauer, R. E. Berson, and G. W. Parshall, *J. Org. Chem.*, **30**, 1431 (1965).
(7) J. D. Roberts, W. T. Moreland, and W. Frazer, *J. Amer. Chem. Soc.*, **75**, 637 (1953).
(8) N. B. Chapman, J. Sotheeswaran, and K. J. Toyne, *J. Org. Chem.*, **35**, 917 (1970).
(9) "Handbook of Chemistry and Physics," 50th ed, J. Weast, Ed., Chemical Rubber Co., Cleveland, Ohio, 1969, p E232.
(10) A. I. Vogel, *J. Chem. Soc.*, 1842 (1948).
(11) J. T. Edward, *J. Chem. Educ.*, **47**, 261 (1970).
(12) J. A. Osborn, *Phys. Rev.*, **62**, 351 (1945).
(13) J. G. Kirkwood and F. H. Westheimer, *J. Chem. Phys.*, **6**, 513 (1938).
(14) J. W. Smith, "Electric Dipole Moments," Butterworths, London, 1955.
(15) S. Glasstone, "Textbook of Physical Chemistry," 2nd ed, Macmillan, London, 1960, Chapter VIII.
(16) H. Eyring, *Phys. Rev.*, **39**, 746 (1932).
(17) F. H. Westheimer and M. W. Shookhoff, *J. Amer. Chem. Soc.*, **61**, 555 (1939).
(18) J. T. Edward, P. G. Farrell, and J. L. Job, *J. Chem. Phys.*, **57**, 5251 (1972).

Tricritical Points in Three- and Four-Component Fluid Mixtures[1]

B. Widom

Department of Chemistry, Cornell University, Ithaca, New York 14850 *(Received May 17, 1973)*

Publication costs assisted by the National Science Foundation and the Cornell University Materials Science Center

A brief historical account of studies of higher order critical points in multicomponent fluids is given. The connection with tricritical points as observed in ^3He-^4He solutions, in metamagnets, and in NH_4Cl is also mentioned briefly. Most of the paper is devoted to an analysis of the tricritical point in the four-component system $(NH_4)_2SO_4$-water-ethanol-benzene, that was first reported by Radyshevskaya, Nikurashina, and Mertslin. That tricritical point may be understood as arising from a confluence of the two critical solution points that are associated respectively with the two three-component solutions $(NH_4)_2SO_4$-water-ethanol and water-ethanol-benzene. Some experimental observations that help illuminate qualitative features of the three-liquid-phase region for this four-component system are reported.

Kohnstamm,[2] in 1926, suggested that there might exist critical points at which three or more phases become identical, in contrast to ordinary critical points, at which two phases become identical. He, and later Zernike,[3] discussed necessary conditions for the existence of such higher order critical points. A c component solution consisting of p phases has $f = c - p + 2$ degrees of freedom, but each condition of criticality, *i.e.*, each requirement that a prescribed pair of the phases become identical, introduces a further constraint and decreases f by 1. At what we may call a pth order critical point (so that in this notation an ordinary critical point is second order), where all p phases become identical, there are $p - 1$ such conditions of criticality, hence $f = c - p + 2 - (p - 1) = c - 2p + 3$ degrees of freedom. But f cannot be negative, so a pth order critical point requires a minimum of $2p - 3$ components; thus, one component for an ordinary (*i.e.*, second order) critical point, three components for a "tricritical" point (which is a common name for a critical point of third order), five components for a critical point of fourth order, etc. When a mixture consists of that minimum number of components the corresponding higher order critical point is an invariant point; but there is a one-parameter family of such points if the mixture contains one component more than the necessary minimum, a two-parameter family of them if it contains two components more than the minimum, etc.

The experimental discovery of tricritical points has been ascribed to Efremova by her colleagues[4] in the Soviet Union. The first published report of a tricritical point in a three-component system that we are aware of is that by Krichevskii, *et al.*,[5] on the mixture acetic acid-water-butane, while an even earlier paper by Radyshevskaya, Nikurashina, and Mertslin[6] reports the discovery of a tricritical point in the four-component system $(NH_4)_2SO_4$-water-ethanol-benzene. Further three-component systems in which tricritical points have been found are methanol-water-carbon dioxide,[7,8] ethanol-water-carbon dioxide,[9] methanol-ethane-carbon dioxide,[10] and ethane-*n*-hexadecane-*n*-eicosane;[11] while further four-component systems in which tricritical points are known are water-phenol-pyridine-*n*-hexane[12,13] and methanol-ethanol-water-carbon dioxide.[14]

In the three-component systems the tricritical points may be described as of the liquid-liquid-gas type, and, as mentioned, they are invariant points. In the four-component methanol-ethanol-water-carbon dioxide system there is then a one-parameter family of such liquid-liquid-gas tricritical points, extending from that in the three-component system methanol-water-carbon dioxide at one extreme of composition to that in the three-component system ethanol-water-carbon dioxide at another extreme. But the tricritical points in the four-component systems $(NH_4)_2SO_4$-water-ethanol-benzene and water-phenol-pyridine-*n*-hexane may be described as of the liquid-liquid-liquid type, since in those cases the three phases that become identical are three ordinary liquid solutions. In such three-liquid-phase systems it is convenient to look upon the pressure as the parameter that varies along the locus of tricritical points. Then if the system is always at atmospheric pressure, or is always in equilibrium with its vapor (these being the two most common conditions under which such liquid solutions are studied), one point on the locus is thereby singled out. Thus, for practical purposes the tricritical points in such systems are again invariant points; though in principle they do depend on the pressure, and a study of that pressure dependence might someday be of interest.

What are in effect tricritical points, though occurring in contexts that, from the chemical point of view, are less familiar, have been known for some time in certain antiferromagnets (metamagnets), in NH_4Cl, and in ^3He-^4He solutions. In each of those cases the tricritical point is observed as a point at which a first-order phase-transition line in the space of thermodynamic "fields" (variables such as pressure and temperature that assume equal values in coexisting phases) changes into a line of critical points. A unified thermodynamic treatment of those systems has been given.[15] In the thermodynamic analysis the line of first-order phase transitions is seen to be really a line of triple points, yet in practice there is no achievable state of any of those systems in which it can be seen with the eye to consist of the three distinct phases that are to become identical at the tricritical point. The reason for this is that in each of those cases one of the field variables that is presumed to play an important role in the thermodynamics is fixed by nature, and is not (or has not yet been) an independent variable at the experimenter's disposal. This is in contrast to the situation in the multicomponent fluids that we are concerned with here, where all the relevant thermodynamic states are physically realizable.

Figure 1. Three fluid phases in equilibrium.

In Figure 1 are pictured three phases α, β, and γ in equilibrium. The condition in which the phases α and β become identical while they are still in equilibrium with the distinct phase γ is a critical end point, and may be symbolized by $(\alpha\beta)\gamma$. In a three-component system there is a one-parameter family of such states ($c = 3$, $p = 3$, and one condition of criticality, so $f = 1$), that is, they lie on a curve in the full four-dimensional space of thermodynamic fields. The projection of that locus onto the pressure–temperature plane is shown in Figure 2, where it is marked $(\alpha\beta)\gamma$. The second curve in Figure 2, marked $\alpha(\beta\gamma)$, is the projection of the locus of critical end points at which phases β and γ have become identical while still in equilibrium with the distinct phase α. The tricritical point occurs at the confluence of these two loci, for that is where the three phases α, β, and γ all become identical. Note that there is no third locus $(\alpha\gamma)\beta$ in the neighborhood of this tricritical point. In principle there may be such a line of $(\alpha\gamma)\beta$ critical end points elsewhere in the thermodynamic space, and it may meet one of the other lines of critical end points to produce another tricritical point, but at any one tricritical point of the kind under discussion there are only two such lines. Because there is no $(\alpha\gamma)\beta$ locus at the tricritical point pictured in Figure 2, phase β is singled out as playing a role qualitatively different from that played by phases α and γ. As the tricritical point is approached through the three-phase region the properties of phase β remain intermediate between those of phase α and phase γ (and the points representing the three-phase states, when projected onto the pressure–temperature plane, lie in the cusp-shaped region between the two curves shown in Figure 2). The density is one of those properties; so in practice, when the mixture is close to its tricritical point, the special phase β can be identified as the middle one of the three, as in Figure 1.

The qualitative features of Figure 2, including the tangency of the two curves at the tricritical point and the absence of a third locus of critical end points in the neighborhood of that tricritical point, follow from a general phenomenological theory.[16] Experimentally determined lines of critical end points, plotted as in Figure 2, are given by Efremova and Shvarts for methanol–water–carbon dioxide[7] and for ethanol–water–carbon dioxide.[9] The experimental results are in accord with the phenomenological theory, and, in particular, are consistent with the idea that the two loci in Figure 2 are tangent at their point of confluence.

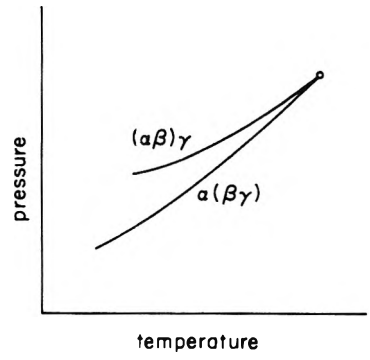

Figure 2. Projection onto the pressure–temperature plane of two loci of critical end points. The curve marked $(\alpha\beta)\gamma$ is the locus of states in which phases α and β have just become identical while in equilibrium with the distinct phase γ, and that marked $\alpha(\beta\gamma)$ is the locus of states in which phases β and γ have just become identical while in equilibrium with the distinct phase α. The tricritical point, marked with a circle, is at the confluence of the two loci.

This paper is intended to be devoted mainly to a discussion of liquid–liquid–liquid tricritical points in four-component systems, with particular reference to $(NH_4)_2SO_4$–water–ethanol–benzene.[6] (The system water–phenol–pyridine–*n*-hexane is rather more complex, and shows two distinct tricritical points.[12,13])

Let the phases α, β, and γ in Figure 1 now represent the three *liquid* phases that can be in equilibrium in the $(NH_4)_2SO_4$–water–ethanol–benzene system. The top layer, α, is always the benzene-rich layer, which is the least dense, while the bottom layer, γ, is always the salt-rich layer, which is the most dense. The $\alpha\beta$ phase equilibrium is essentially the same as that which occurs in the three-component system water–ethanol–benzene, where there is no $(NH_4)_2SO_4$, while the $\beta\gamma$ phase equilibrium is essentially the same as that which occurs in the three-component system $(NH_4)_2SO_4$–water–ethanol, where there is no benzene. These are shown in Figures 3 and 4, respectively.

The $\alpha\beta$ phase equilibrium occurs because of the mutual near insolubility of water and benzene. Both are completely miscible with ethanol, so when there is enough ethanol present the mixture is homogeneous. The one- and two-phase regions are separated by a binodal curve on which there is a plait point (critical solution point), as seen in Figure 3.

The $\beta\gamma$ phase equilibrium is the salting out, by $(NH_4)_2SO_4$, of ethanol from an ethanol–water mixture, as seen in Figure 4. The three-phase region seen in the figure includes the solid salt as one of the phases, but that is quite irrelevant to the three-*liquid*-phase equilibrium to be discussed. The whole of the phenomenon which is ultimately of interest occurs in solutions that are still relatively dilute in the salt and far from being saturated with it. It is sometimes helpful to imagine one of the tielines in the two-liquid-phase salting-out region of Figure 4 to be extended in both directions, so that it meets the $(NH_4)_2SO_4$–water side of the composition triangle in some point A and the water–ethanol side in some point B; and then to imagine a new phase diagram in which A, B, and water are the three components. The result is a diagram entirely analogous to Figure 3, and one which includes only those features of the $(NH_4)_2SO_4$–water–ethanol phase equilibrium that are relevant to the present discussion. In these terms the $\beta\gamma$ phase equilibrium is seen to arise because of the limited miscibility of the two liquids A and

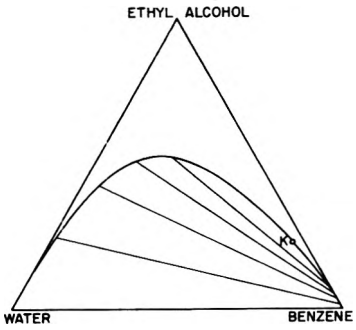

Figure 3. Phase equilibrium in water–ethanol–benzene mixtures at fixed temperature.[17] Compositions are mass fractions. A few tielines are shown in the two-phase region. The plait point K is marked with a circle.

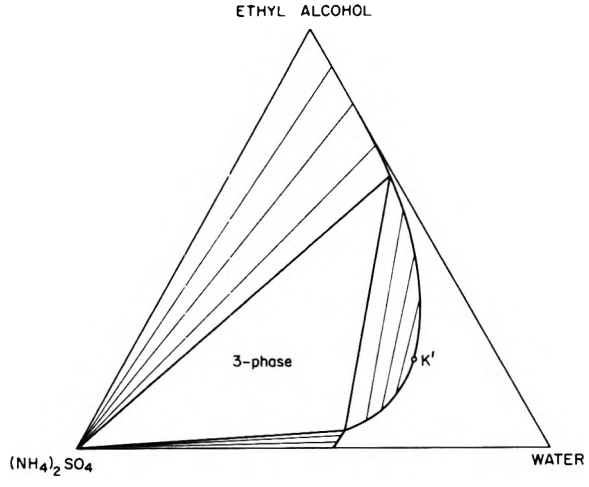

Figure 4. Phase equilibrium in the $(NH_4)_2SO_4$–water–ethanol system, at 50°, from data in Seidell.[18] Compositions are mass fractions. A few tielines are shown in each two-phase region. The plait point K′, on the binodal curve bounding the salting-out region, is marked with a circle. In the region marked 3-phase, solid $(NH_4)_2SO_4$ is in equilibrium with two liquid solutions of fixed composition.

B, while the complete miscibility of A and B with water then gives rise, again, to a binodal curve and plait point.

The four-component mixtures are now to be thought of as represented in a composition tetrahedron inside which (if the temperature is below that of the tricritical point) is a region of three-liquid-phase coexistence. Such a three-phase region as might be found in the interior of the composition tetrahedron is shown in Figure 5. (Another example may be found in ref 6.) It may be thought of as consisting of a stack of infinitely many, infinitely closely spaced triangles, the vertices of any one of which give the compositions of the three liquid phases α, β, and γ that are in coexistence. (The labeling still corresponds to that in Figure 1, with α the benzene-rich layer and γ the salt-rich layer.) The three sides $\alpha\beta$, $\beta\gamma$, and $\gamma\alpha$ of these triangles generate three ruled surfaces which form the faces of the figure. In Figure 5 these are, respectively, the front faces CC′D′ and C′CD, and the back face CDC′D′.

The length of the side $\alpha\beta$ of the generating triangle vanishes at the vertex C. That is a critical point, at which the meniscus separating phases α and β disappears and the two phases become identical. But the phase γ, now represented by D, is still present at that moment, so C is in fact an $(\alpha\beta)\gamma$ critical end point. The vertex C′, where the side $\beta\gamma$ of the generating triangle is of vanishing length, is an $\alpha(\beta\gamma)$ critical end point, for there the phases β and γ

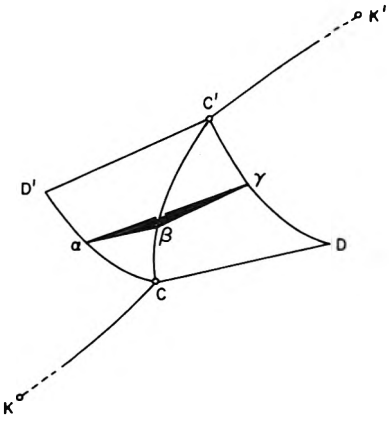

Figure 5. CDC′D′ is the three-liquid-phase region within the composition tetrahedron of the four-component system. It may be imagined as a stack of infinitely many, infinitely closely spaced triangles, of which a representative one, its vertices labeled α, β, and γ, is shown. The vertices C and C′ are critical end points, while the curves KC and K′C′ are the loci of $\alpha\beta$ and $\beta\gamma$ critical points, respectively, where K and K′ are the plait points previously shown in Figures 3 and 4. The whole of this figure is for a single fixed temperature.

are critical but are in equilibrium with phase α which is at D′. The critical end point C is the terminus of a locus of $\alpha\beta$ critical points, shown in Figure 5 as the locus KC. Point K, at which this locus originates, is the water–ethanol–benzene plait point seen in Figure 3, which is now on one of the faces of the composition tetrahedron. Likewise the critical end point C′ is the terminus of a locus K′C′ of $\beta\gamma$ critical points that originates at the $(NH_4)_2SO_4$–water–ethanol plait point K′ on another face of the composition tetrahedron.

The whole of Figure 5 corresponds to a single temperature below that of the tricritical point. As the temperature is raised the three-liquid-phase region shrinks. When the tricritical-point temperature (which is[6] about 49°) is reached, the points C, D, C′, and D′ all coalesce and the three-phase region has shrunk to a point. That is the tricritical point. Whether the tricritical-point composition lies within or without the three-phase region that exists at a temperature slightly below that of the tricritical point, *i.e.*, whether with increasing temperature the three-phase region shrinks to a point contained within itself or to a point that lies just outside itself, is not yet certain, but the phenomenological theory[16] strongly suggests the latter. There is no $(\alpha\gamma)\beta$ critical end point, or locus of $\alpha\gamma$ critical points, in the neighborhood of this tricritical point, so the middle phase β is again singled out as playing a special role, just as in the earlier discussion of tricritical points in three-component systems.

The three-phase region shown in Figure 5 is completely surrounded by two- and one-phase regions. The face CC′D′ abuts a region in which the two liquid phases α and β are in equilibrium, while the faces C′CD and CDC′D′ abut the $\beta\gamma$ and $\gamma\alpha$ two-phase regions, respectively. These three two-phase regions are partly separated by one-phase regions that border on the edges CD′, C′D, and CC′ of the figure. The one-phase region that borders on the edge CD′, thus partly separating the $\alpha\beta$ and $\gamma\alpha$ two-phase regions, is the region of phase α; that which borders on the edge C′D is the region of phase γ; and that which borders on the edge CC′ joining the two critical end points is the region of the special (hence middle) phase β.

The topology of the three-phase region is as shown in Figure 5, but the quantitative aspects of its shape may in

reality be quite different from what is there depicted. From the phenomenological theory[16] there is reason to suppose that near the tricritical-point temperature, where it is of nearly vanishing volume, the real figure is considerably twisted and skewed; and that, independently of that skewness, there is a great discrepancy among the figure's three characteristic dimensions, so that the lengths of the edges CD and C′D′ contribute the figure's greatest dimension, the altitude from the vertex β to the side $\alpha\gamma$ of the representative triangle shown is much less than those lengths and contributes the figure's next greatest dimension, while the distance between the edges CD and C′D′ is much smaller still and contributes the figure's smallest dimension. It will be observed in any case that the figure has four vertices (V), five edges (E), and three faces (F), so that it satisfies Euler's rule $V - E + F = 2$, and does so with the same number of vertices as a tetrahedron has, but with one less edge and one less face. Finally, the figure is chiral, not superimposable on its mirror image, and could have occurred in either of two enantiomorphic forms. It derives its chirality from its unique relation to the four chemical components that label the vertices of the composition tetrahedron. Because those components are all different the labeled tetrahedron has a definite handedness, and so the three-phase region does as well. The arbitrary initial choice of one of the two possible labelings of the tetrahedron then determines which of the two enantiomorphic forms of the three-phase region will arise.

The description of the three-liquid-phase region given in the preceding paragraphs assumes that the region is not interrupted by a four-phase region in which the liquids are saturated with salt. Near the tricritical-point temperature ($\approx 49°$) that assumption is correct, but at sufficiently low temperatures, certainly at room temperature, it is not. That is a distracting complexity that we wish to ignore because it is irrelevant to an understanding of the tricritical point. Therefore, in describing the three-liquid-phase region it has been supposed *either* that the temperature is high enough for there to be no range of compositions in which excess solid salt is in equilibrium with the three liquid phases, *or,* purely hypothetically, that the region under discussion corresponds partly to metastable states in which the liquid solutions are supersaturated with salt, none of which is present as excess solid.

Thus dismissing its possible interruption by a solid phase, we have a picture of the three-phase region as an isolated object within the composition tetrahedron, its faces abutting on two-phase regions. Two simple observations were made to confirm this picture.

For the first, six mixtures were prepared (at room temperature), all containing $(NH_4)_2SO_4$:water:ethanol in the ratios 1:4.2:4.2 by mass, but with varying amounts of benzene, the resulting mass fraction of which, in the six solutions, was 0.05, 0.10, 0.19, 0.35, 0.53, and 0.70. These mixtures are called a, b, c, d, e, and f, respectively, and are shown schematically in Figure 6. In mixture a is so little benzene that there is no α phase, only the β and γ phases associated with the salting out of the aqueous ethanol solution. What little benzene is present is mostly dissolved in the ethanol-rich β phase. Mixture f, by contrast, contains so much benzene that much of the ethanol is dissolved in it, in the α phase, not leaving enough ethanol in the aqueous salt solution γ to salt out, so the β phase is missing. The intermediate mixtures b, c, d, and e show all three phases, and make clear the gradual appearance or

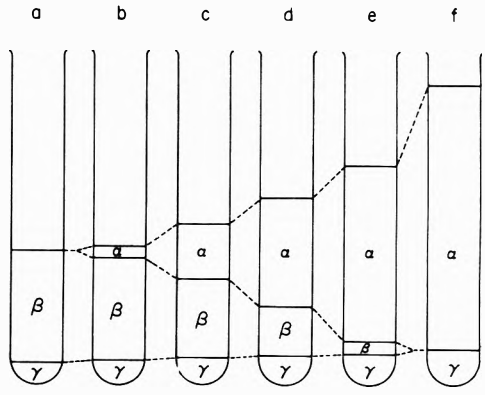

Figure 6. Six mixtures prepared by starting with six identical solutions containing $(NH_4)_2SO_4$, water, and ethanol in the respective ratios 1:4.2:4.2 by mass, and then adding benzene in different and increasing amounts from a to f. The dotted lines trace the changing locations of the meniscuses.

disappearance of the α or β phases at the two extremes of composition. Every $\beta\gamma$ meniscus, associated with the salting-out, is razor sharp, while every $\alpha\beta$ meniscus has a thick and oily appearance. The $\alpha\gamma$ meniscus is in that respect intermediate. The six solutions correspond to six points on a straight line in the composition tetrahedron. The line starts at a point in the two-liquid-phase region on the $(NH_4)_2SO_4$–water–ethanol face (see Figure 4) where the respective mass fractions are 0.11, 0.45, and 0.45, and it ends at the benzene vertex. If the line is followed in that sense, from face to vertex, the points representing the six solutions appear on it in the order a to f. The line enters the three-phase region through the $\beta\gamma$ face (CDC′ in Figure 5) at a point somewhere between those which represent the compositions of the solutions a and b, and it leaves the three-phase region through the $\alpha\gamma$ face (CDC′D′ in Figure 5) at a point somewhere between those which represent the composition of the solutions e and f.

The second observation was in principle rather similar to the first, though arranged to give a quite striking effect as well as to help resolve an apparent paradox. When the β and γ phases are present in a mixture the addition of more salt increases the salting-out effect, that is, it makes the β and γ phases more disparate and thus reinforces the $\beta\gamma$ meniscus. But from the picture of an isolated three-liquid-phase region it must be concluded that if one adds enough salt to a mixture in which all three liquid phases are initially present, supersaturating with salt if necessary, one of the liquid phases will disappear. Then with the $\beta\gamma$ meniscus being, if anything, strengthened by the addition of salt, it must be the α phase that disappears. This seems, at first, quite paradoxical, because it means that the effect of adding salt is to increase the solubility of benzene! The explanation is that the added salt mostly concentrates in the γ phase, and at the same time carries with it into the γ phase a large fraction of whatever water was previously dissolved in the β phase. That leaves the β phase so concentrated in ethanol, that is to say, so dry, that it is a good solvent for benzene, and the α phase disappears. This resolution of the paradox will have been confirmed if it can be demonstrated that the effects of adding $(NH_4)_2SO_4$ are to strengthen, or in the first place to cause the appearance of, a $\beta\gamma$ meniscus, and simultaneously to weaken, or to cause the disappearance of, an $\alpha\beta$ meniscus. To this end there was prepared (again at room temperature) a mixture of water, ethanol, and benzene with the respective mass fractions 0.26, 0.48, and

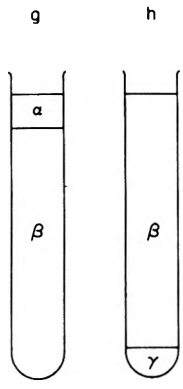

Figure 7. Before (g) and after (h) the addition of a large quantity of $(NH_4)_2SO_4$ to a water–ethanol–benzene mixture in which the respective mass fractions were 0.26, 0.48, and 0.26.

0.26. This composition lies in the two-phase region of Figure 3. The volume of the β phase was roughly eight times that of the α phase, and the $\alpha\beta$ meniscus had its characteristic thick, oily appearance. This initial mixture is shown schematically as g in Figure 7. Next, enough $(NH_4)_2SO_4$ was added to the mixture to saturate it (though rather less salt would have done as well); whereupon there was an immediate disappearance of the $\alpha\beta$ meniscus, accompanied by the simultaneous appearance of a razor-sharp salting-out meniscus near the bottom of the tube, thus demonstrating the predicted effect. The final mixture is shown as h in Figure 7.

The workers who discovered the tricritical point in the $(NH_4)_2SO_4$–water–ethanol–benzene system[6] estimated it to occur at a temperature close to 49° and at a composition in which the mass fraction of $(NH_4)_2SO_4$ is 0.04 ± 0.01 while the ratio of the water and ethanol masses is 1.0 ± 0.2. This still leaves the benzene content unspecified, but using the quoted estimates to help interpolate between the compositions of the two plait points in Figures 3 and 4, one may guess that the mass fraction of benzene at the tricritical point is probably in the range 0.37 ± 0.05. That estimate was then roughly confirmed by observation, as follows. The tricritical-point temperature is the highest temperature at which three liquid phases can coexist (indeed, that is how it was sought and estimated by the original workers[6]), and at that temperature the three-phase region has shrunk to a point; so any mixture that still consists of three liquid phases at a temperature not too far below 49° is probably not far from the tricritical-point composition. A mixture was prepared with the mass fractions $(NH_4)_2SO_4$ = 0.04, water = 0.28, ethanol = 0.33, and benzene = 0.35. At room temperature all three liquid phases were present, with the γ phase occupying about $\frac{1}{5}$ the total volume; but as the temperature was raised the $\beta\gamma$ meniscus rose slowly, the $\alpha\beta$ meniscus fell rapidly, and at 42° they joined, forming an $\alpha\gamma$ meniscus, with the β phase no longer present and with the γ phase now occupying a slightly larger fraction, about $\frac{3}{10}$, of the total volume. (The movements of the meniscuses as described are best seen with increasing temperature, but a determination of the temperature of disappearance of the β phase is best made by watching for the *appearance* of the β phase with *falling* temperature, and that is what was done to make the estimate of 42°.) Thus, the benzene content of that mixture, mass fraction 0.35, cannot have been very far from its value at the tricritical point; especially since much of the difference between 49 and 42° can be ascribed to the water:ethanol ratio having been only 0.8, which is at the edge of the estimated range of possible values of that ratio in the true tricritical-point composition.

It would be of considerable interest to determine the detailed shape of the three-liquid-phase region in the composition tetrahedron at a fixed temperature below that of the tricritical point; to observe the changes in the size and shape of the three-phase region as the tricritical-point temperature is approached; and to determine, by measurement of the angular dissymmetry of the intensity of scattered light, the range of correlation of composition fluctuations in the neighborhood of the tricritical point. These measurements would allow quantitative assessments to be made of some of the ideas that have been outlined here, and would also yield values for some of the critical-point exponents, which are what provide the most deep-going characterization of the tricritical point.[16] We hope soon to undertake such studies in this laboratory.

Acknowledgment. The author is greatly indebted to Professor R. B. Griffiths for enlightening discussions and helpful comments.

References and Notes

(1) Work supported by the National Science Foundation and by the Cornell University Materials Science Center.
(2) Ph. Kohnstamm, "Handbuch der Physik," Vol. 10, Springer Verlag, Berlin, 1926, Chapter 4, § 45.
(3) J. Zernike, *Recl. Trav. Chim. Pays-Bas*, **68**, 585 (1949).
(4) I. R. Krichevskii, *et al.*, *Russ. J. Phys. Chem.*, **46**, 141 (1972).
(5) I. R. Krichevskii, G. D. Efremova, R. O. Pryanikova, and A. V. Serebryakova, *Russ. J. Phys. Chem.*, **37**, 1046 (1963).
(6) G. S. Radyshevskaya, N. I. Nikurashina, and R. V. Mertslin, *J. Gen. Chem. USSR*, **32**, 673 (1962).
(7) G. D. Efremova and A. V. Shvarts, *Russ. J. Phys. Chem.*, **40**, 486 (1966).
(8) G. D. Efremova and A. V. Shvarts, *Russ. J. Phys. Chem.*, **43**, 968 (1969).
(9) A. V. Shvarts and G. D. Efremova, *Russ. J. Phys. Chem.*, **44**, 614 (1970).
(10) G. D. Efremova and A. V. Shvarts, *Russ. J. Phys. Chem.*, **46**, 237 (1972).
(11) J. R. Wagner, Jr., D. S. McCaffrey, Jr., and J. P. Kohn, *J. Chem. Eng. Data*, **13**, 22 (1968). See also G. D. Efremova and A. V. Shvarts, *Russ. J. Phys. Chem.*, **44**, 470 (1970).
(12) K. P. Myasnikova, N. I. Nikurashina, and R. V. Mertslin, *Russ. J. Phys. Chem.*, **43**, 223 (1969).
(13) N. I. Nikurashina, G. I. Kharitonova, and L. M. Pichugina, *Russ. J. Phys. Chem.*, **45**, 444 (1971).
(14) G. D. Efremova and A. V. Shvarts, *Dokl. Chem. Technol.*, **188**, 201 (1969).
(15) R. B. Griffiths, *Phys. Rev. B*, **7**, 545 (1973).
(16) R. B. Griffiths, *J. Chem. Phys.*, submitted for publication.
(17) A. W. Francis, "Liquid–Liquid Equilibriums," Interscience, New York, N. Y., 1963, Figure 30, p 35.
(18) A. Seidell, "Solubilities of Inorganic and Metal-Organic Compounds," 3rd ed, Van Nostrand, Princeton, N. J., 1940, pp 1129–1130.

Similarity Considerations in Facilitated Transport

David Yung and Ronald F. Probstein*

Department of Mechanical Engineering, Massachusetts Institute of Technology, Cambridge, Massachusetts 02139
(Received March 26, 1973)

Publication costs assisted by the National Science Foundation

Similarity parameters are presented for the facilitated transport of a gas through a liquid membrane in which the gas concentration on the downstream side of the membrane is negligible. The membrane facilitation performance is shown to depend on three similarity parameters: a dimensionless initial gas concentration on the upstream face of the membrane; a parameter which measures the diffusion rate of the liquid to the backward chemical reaction rate; and one which measures the diffusion rate of the gas to the forward chemical reaction rate. The process is shown to be characterized theoretically by a single second-order equation. Numerical solutions of this equation are presented. It is shown that the facilitation characteristics of the membrane are easily mapped out in terms of a dependent parameter which measures the degree of chemical disequilibrium of the system, and a parameter which is a ratio of the total to initial carrier concentration. Simple limiting analytic solutions are given for both the chemical disequilibrium parameter and the carrier concentration ratio parameter, which enable the facilitation performance to be described quite accurately over most of the range of interest. The results are found to compare very well with other available solutions and experiments.

Introduction

Facilitated transport is a process in which the permeation of a gas through a liquid membrane is augmented over that due to diffusion alone. The molecules (or ions) in the liquid membrane are capable of chemically reacting with the permeating gas but cannot leave the membrane. The permeating gas, therefore, moves through the membrane with part of it in the free state and part of it in the chemically reacted state. As a result of the added chemical reaction, the gas flux is higher than that from pure diffusion, and the transport is therefore augmented.

This phenomenon is of interest in a number of fields. For example, in the life sciences, in the problem of transporting oxygen through a thin film of hemoglobin solution,[1,2] or in the problem of removing carbon dioxide from a life-supporting environment using a liquid membrane.[3] It has obvious applications in commercial separation processes. Bdzil, *et al.*,[4] have also pointed out that the associated electrically induced ion transport could have uses in concentrating or detecting a gas. The application of the phenomenon to numerous concentration, separation and purification processes is evident.

A number of studies have been directed to this phenomenon. Ward[5] examined the dependence of the transport of nitric oxide on the total ferrous ion concentration in a ferrous chloride film, and obtained good agreement between his experimental data and numerical solution. Kutchai, Jacquez, and Mather,[6] on the other hand, investigated the dependence of facilitated transport on the other physical parameters such as gas concentration, film thickness, and reaction rate coefficients. Good agreement was shown between their numerical solutions and the experimental data obtained by other investigators on the diffusion of oxygen through a thin film of hemoglobin solution. Some asymptotic analytical solutions for "thick" and "thin" membranes have been developed by Smith, Meldon, and Colton[7] to provide an alternative to numerical solutions for these limiting situations. Particular asymptotic analytic solutions have been given by Friedlander and Keller[8] and Murray.[9] Most recently Bdzil, *et al.*,[4] have shown that in facilitated transport, potential differences can be created from a partial pressure difference across the membrane and have experimentally confirmed their predictions.

Despite the extensive work on this problem, all of the authors have been concerned principally with the effects in a given situation of changes in the physical parameters. In facilitated transport, the equivalence between two physical situations which are intrinsically dissimilar, through considerations of the appropriate similarity or scaling parameters and the corresponding similarity rules or solutions, has not been examined in any detail. In the present paper we shall give the dimensionless similarity parameters for facilitated transport, and show that the performance can be characterized theoretically in terms of a single second-order equation and these parameters. Numerical and analytical solutions will be presented and, where possible, compared with other available solutions and experiments.

Governing Equations

We consider a steady one-dimensional problem in which a gaseous solute C is diffusing through a liquid membrane. The gas is taken to have a concentration c_0 on the upstream face of the membrane. The concentration on the downstream face is considered negligibly small, corresponding to a negligible partial pressure in the reservoir adjacent to this face. At the same time that the gas diffuses through the liquid membrane it is assumed to react reversibly with it according to the chemical reaction

$$C + U \underset{k_2}{\overset{k_1}{\rightleftharpoons}} W \qquad (1)$$

where the species W here denotes the complex CU, and where k_1 and k_2 are the forward and backward reaction rate coefficients, respectively.

The species U and W are mobile within the membrane but cannot leave it, and the sum of their concentrations equals the total concentration of U present alone and in

the complex W, that is, the original concentration of U in the liquid membrane prior to the gas adsorption. This is expressed by the relation

$$u + w = u_T \tag{2}$$

where we have used lower case letters to denote the concentrations of the corresponding species, and u_T to denote the total concentration of the carrier U.

From Fick's law applied to the species U and C, detailed balancing, and mass conservation we have (assuming electroneutrality)

$$D(d^2u/d\bar{x}^2) = k_1cu - k_2w \tag{3}$$

$$D_c(d^2c/d\bar{x}^2) = k_1cu - k_2w \tag{4}$$

where D and D_c are the diffusion coefficients of U and C, respectively. If L is the thickness of the film, the boundary conditions corresponding to the absence of any flux of U across the membrane faces are

$$\left.\frac{du}{d\bar{x}}\right|_{\bar{x}=0} = 0, \left.\frac{du}{d\bar{x}}\right|_{\bar{x}=L} = 0 \tag{5}$$

The specification on the solute C of the upstream concentration and of a zero concentration on the downstream face gives

$$c(0) = c_0, c(L) = 0 \tag{6}$$

Equations 2-6 form a closed set of equations and boundary conditions for the problem, under the assumption made by most previous workers[4-9] that the diffusion coefficients of the species U and W are the same.

We normalize the system of equations and boundary conditions through the introduction of the scalings

$$x = \bar{x}/L, y = u/u_0, t = c/c_0 \tag{7}$$

and dimensionless parameters

$$\kappa = c_0k_1/k_2, \epsilon = D/k_2L^2, \delta = D_c/(k_1u_T)L^2 \tag{8}$$

where the subscript 0 denotes conditions at $\bar{x} = 0$. An integral of eq 3 and 4 satisfying the boundary conditions is $Du = A + B\bar{x} + D_cc$, where A and B are constants, so that eq 2-4 can be shown to be reducible to

$$\epsilon(d^2y/dx^2) = (1 + \kappa t)y - \alpha \tag{9}$$

$$t = 1 + \frac{\epsilon/\delta}{\alpha\kappa}(y - 1) - \left[1 + \frac{\epsilon/\delta}{\alpha\kappa}(y_L - 1)\right]x \tag{10}$$

Here

$$\alpha = u_T/u_0 \tag{11}$$

is the ratio of the total to initial carrier concentration, and is an undetermined constant to be determined by the boundary conditions. The subscript L denotes conditions at $\bar{x} = L$. The corresponding nondimensional boundary conditions become

$$\left.\frac{dy}{dx}\right|_{x=0} = 0, \left.\frac{dy}{dx}\right|_{x=1} = 0, y(0) = 1 \tag{12}$$

where by definition $y(1) \equiv y_L$.

For the case where chemical equilibrium exists everywhere throughout the membrane, it is easily shown that the concentration ratio across the film of the species U is given by $y_L = 1 + \kappa$. With this limit as a guide we introduce the following transformations

$$\eta = \frac{y - 1}{\kappa}, \eta_L = \frac{y_L - 1}{\kappa} \tag{13}$$

where η_L has a value of one when the system is in chemical equilibrium and is, of course, zero for a completely frozen condition. The extent to which the parameter η_L falls below unity is therefore a measure of the departure of the system from chemical equilibrium. Introducing the parameter η, eq 9 and 10 may be reduced with some manipulation to the second-order equation

$$\epsilon\frac{d^2\eta}{dx^2} - [1 + \kappa(1 - x)]\eta + \left[\frac{\alpha - (1 + \kappa)}{\kappa} + x\right] = \frac{\epsilon/\delta}{\alpha}(\eta - \eta_L x)(1 + \kappa\eta) \tag{14}$$

The corresponding boundary conditions given by eq 11 are

$$\left.\frac{d\eta}{dx}\right|_{x=0} = 0, \left.\frac{d\eta}{dx}\right|_{x=1} = 0, \eta(0) = 0 \tag{15}$$

Similarly, the total to initial carrier concentration ratio α can be easily shown to have a value of $1 + \kappa$ when the system is in chemical equilibrium. For the frozen condition, that is when $y \to 1$, eq 9 when integrated once shows that α takes on the value $1 + (\kappa/2)$.

The flux of the gaseous solute C across the membrane faces is expressed through

$$J_c = -D_c\left.\frac{dc}{d\bar{x}}\right|_{\bar{x}=0} = -D_c\left.\frac{dc}{d\bar{x}}\right|_{\bar{x}=L} \tag{16}$$

With the aid of eq 10, this flux can be shown to be given by the expression

$$\frac{J_cL}{c_0D_c} = 1 + \Delta\frac{\eta_L}{\alpha} \equiv 1 + F \tag{17}$$

where

$$\Delta = \epsilon/\delta \tag{18}$$

The left-hand side of eq 17 is seen to be a Peclet number for diffusion through the membrane, and F on the right-hand side is the facilitation which is defined as the carrier-mediated flux divided by the flux in the absence of the carrier.

Parameters and Solutions

The second-order nonlinear differential equation (eq 14), characterizing the problem, is seen to contain the three similarity parameters κ, ϵ, and δ (eq 8). The parameter κ is a measure of the initial concentration on the upstream face c_0, while ϵ is a measure of the diffusion rate of the liquid to the reaction rate in the backward sense, and δ is a measure of the diffusion rate of the gas to the reaction rate in the forward sense. Both ϵ and δ are essentially inverse second Damköhler numbers. The effect of these three similarity parameters on the overall transport process will become self-evident once the dependence of the solution behavior on the parameters is shown. It should be remarked in passing that were the concentration of the gaseous solute on the downstream membrane face different from zero, then the problem would contain one more similarity parameter measuring this concentration level.

An exact closed form analytic solution of eq 14 for all values of the similarity parameters cannot be given, although various asymptotic forms and asymptotic expansions[7-9] may be found for a number of limiting cases. Here, we shall concentrate on the mapping of the numerical solution of eq 14 in terms of the similarity parameters discussed above. Detailed analytical procedures will not be emphasized, except insofar as we will present below

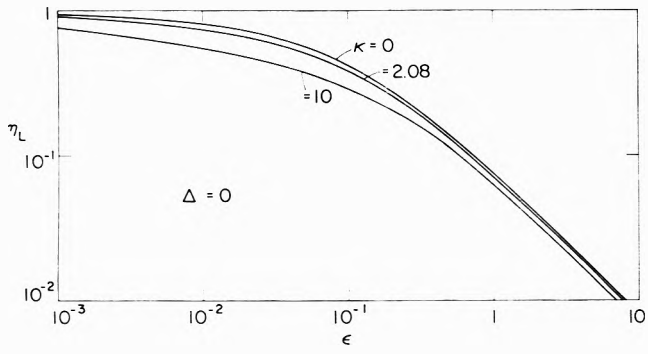

Figure 1. Chemical disequilibrium parameter (η_L) *vs.* parameter measuring liquid diffusion rate to backward reaction rate (ϵ) for different initial gas concentrations (κ). $\Delta = \epsilon/\delta = 0$, where δ is parameter measuring gas diffusion rate to forward reaction rate.

simple limiting analytic solutions, which we shall show describe the facilitation performance quite accurately over most of the range of interest.

The numerical method employed to solve eq 14 is a straightforward step-by-step integration in which the sought after end value η_L and the constant $\alpha = u_T/u_0$ are iterated until the solution satisfies all the boundary conditions (eq 15). A convenient form for the presentation of the results $\eta_L = \eta_L(\kappa, \epsilon, \delta)$ is shown in Figures 1 and 2, which are plots of η_L as a function of ϵ with κ as a parameter for different values of Δ. The reason for choosing Δ rather than δ as a parametric variable is that the curves of η_L *vs.* ϵ for different values of Δ tend to converge in the limits when both $\epsilon \to 0$ and $\epsilon \gg 1$, whereas they will not if δ is chosen. The results shown have been obtained from numerical integrations except those for the case $\kappa = 0$, which are derived from one of the analytic solutions mentioned earlier and discussed below.

The curves of Figures 1 and 2 show clearly that η_L tends to its equilibrium value ($\eta_L \to 1$) when the backward chemical reaction rate dominates over the diffusion rate of the liquid substance ($\epsilon \to 0$). They also show that η_L tends to the frozen condition ($\eta_L \to 0$) when the forward chemical reaction rate dominates over the diffusion rate of the gas ($\epsilon \gg 1$). Also evident from the figures is that η_L is not strongly dependent on the initial gas concentration as expressed through the parameter κ, and that η_L decreases with increasing Δ. However, this dependence on Δ is also not a very strong one and, indeed, as κ becomes large the $\Delta = 0$ solution becomes very closely representative of the complete behavior, provided Δ does not become extremely large.

For the limiting case $\Delta = 0$, an analytic solution of eq 14 is possible because in this case the right-hand side vanishes and the equation becomes linear. What is important to emphasize, and what can be seen from the numerical solutions, is the insensitivity of the solution to Δ even for relatively large values. This can be explained by the character of the right-hand side of eq 14 which vanishes when $\Delta \to 0$. It may be seen that even for finite Δ the right-hand side goes to zero at *both* faces of the membrane because $\eta - \eta_L x = 0$ there, so that generally this term is not large.

For $\Delta = 0$ eq 14 can be reduced by the transformation

$$\xi = [1 + \kappa(1 - x)](\epsilon\kappa^2)^{-1/3} \tag{19}$$

to the linear inhomogeneous form

$$(d^2\eta/d\xi^2) - \xi\eta = \beta \tag{20}$$

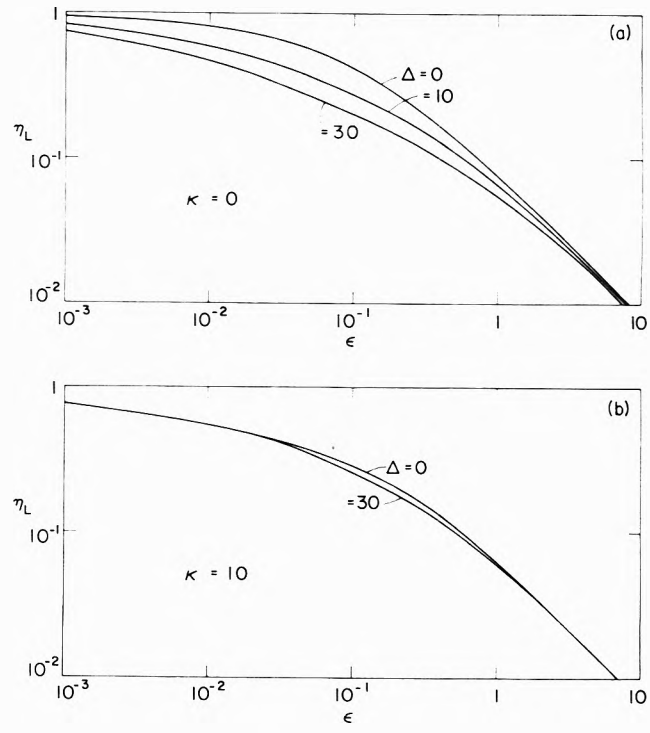

Figure 2. Chemical disequilibrium parameter (η_L) *vs.* parameter measuring liquid diffusion rate to backward reaction rate (ϵ) for different $\Delta = \epsilon/\delta$, where δ is parameter measuring gas diffusion rate to forward reaction rate: (a) $\kappa = 0$, analytic solution; (b) $\kappa = 10$, numerical solution, with κ a measure of initial gas concentration.

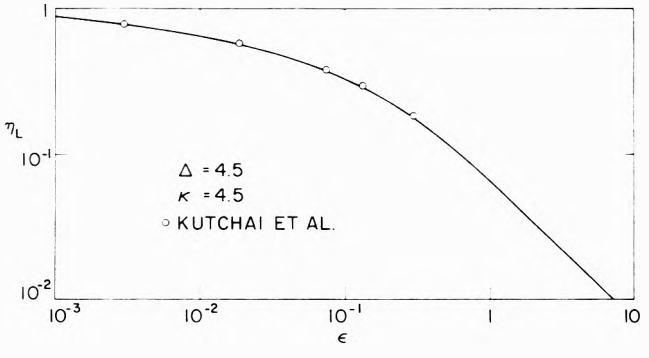

Figure 3. Chemical disequilibrium parameter (η_L) *vs.* parameter measuring liquid diffusion rate to backward reaction rate (ϵ) for $\Delta = \epsilon/\delta = 4.5$, $\kappa = 4.5$, and comparison with numerical results of Kutchai *et al.*[6]

where $\beta = \kappa^{-1}\xi - \alpha\epsilon^{-1/3}\kappa^{-2/5}$. The corresponding boundary conditions are

$$\begin{aligned} d\eta/d\xi &= 0,\ \eta = 0 \quad &\text{for } \xi &= (1+\kappa)(\epsilon\kappa^2)^{-1/3} \\ d\eta/d\xi &= 0 \quad &\text{for } \xi &= (\epsilon\kappa^2)^{-1/3} \end{aligned} \tag{21}$$

Denoting by η_1 the solution to the linear Airy equation, which is the homogeneous part of eq 20, we may express the general solution through the quadrature

$$\eta = \eta_1 \int_0^{\xi} \frac{1}{\eta_1^2} \left[\int_0^{\xi'} \beta\eta_1 \, d\xi'' \right] d\xi' \tag{22}$$

Since only two boundary conditions are required to determine η_1, the solution will not in general satisfy exactly one of the boundary conditions of eq 15. This point will be discussed further in what follows.

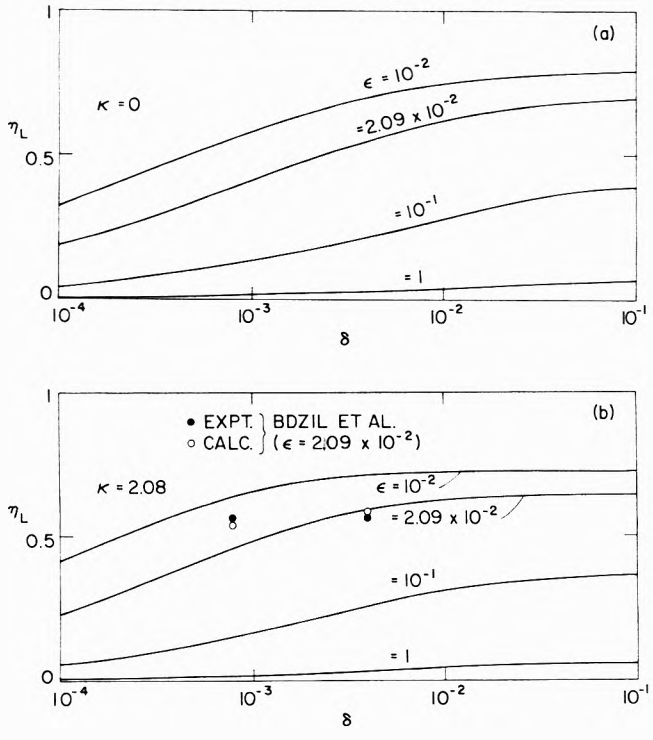

Figure 4. Chemical disecuilibrium parameter (η_L) *vs.* parameter measuring gas diffusion rate to forward reaction rate (δ) for different values of parameter measuring liquid diffusion rate to backward reaction rate (ϵ): (a) $\kappa = 0$, analytic solution; (b) $\kappa = 2.08$, numerical solution and comparison with results of Bdzil, *et al.*,[4] with κ a measure of initial gas concentration.

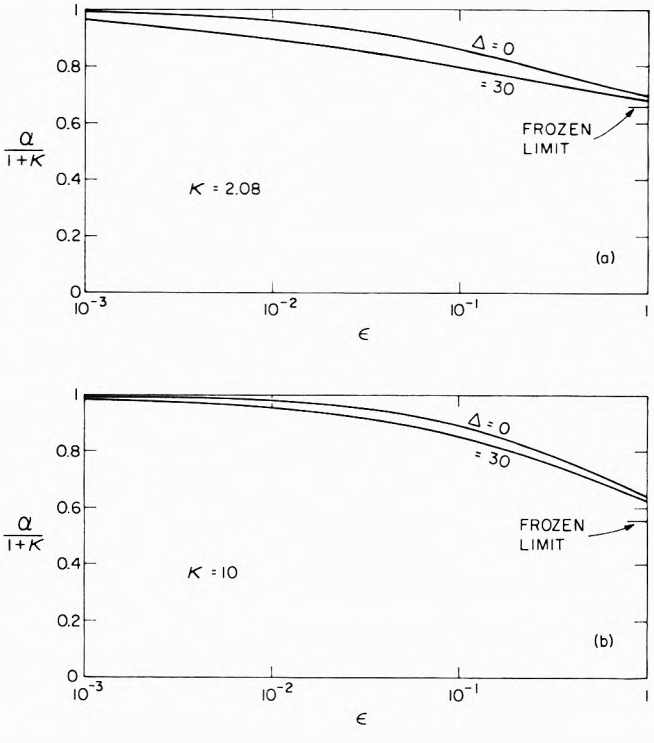

Figure 5. Total to initial carrier concentration ($\alpha = u_T/u_0$) *vs.* parameter measuring liquid diffusion rate to backward reaction rate (ϵ) for different $\Delta = \epsilon/\delta$, where δ is a parameter measuring gas diffusion rate to forward reaction rate: (a) $\kappa = 2.08$. (b) $\kappa = 10$, with κ a measure of initial gas concentration

When $\Delta \neq 0$, but with $\kappa = 0$, eq 14 again becomes linear and a simple analytic solution can be obtained. In this case, eq 14 reduces to

$$\epsilon(d^2\eta/dx^2) - \eta = -\gamma - x + \Delta(\eta - \eta_L x) \quad (23)$$

where α has been set equal to one in the term in Δ, consistent with $\kappa = 0$. The indeterminate constant γ is defined by $\gamma = [\alpha - (1 + \kappa)]/\kappa$, or rearranging

$$\alpha = 1 + \kappa(1 + \gamma) \quad (24)$$

and γ is an undetermined constant to be determined by the boundary conditions. The solution to this equation satisfying the boundary conditions (eq 15) can be shown to be simply

$$\eta_L = [1 - 2\sqrt{\tau}\ \tanh(1/2\sqrt{\tau})]/[1 + \Delta 2\sqrt{\tau}\ \tanh(1/2\sqrt{\tau})] \quad (25)$$

where

$$\tau = \epsilon/(1 + \Delta) \quad (26)$$

The solution has the asymptotic behavior that $\eta_L \sim 1/(1 + 2\Delta\tau^{1/2})$ when $\tau \ll 1$, and $\eta_L \sim 1/[12\tau(1 + \Delta)]$ when $\tau \gg 1$. If Δ is finite, $\eta_L \to 1$ when $\epsilon \to 0$ and $\eta_L \sim 1/12\epsilon$ when $\epsilon \gg 1$. It can be seen from Figures 1 and 2 that eq 25 gives a very adequate representation of the complete solution over a wide range of conditions.

In Figure 3 we have reduced the numerical results of Kutchai, *et al.*,[6] from their Table VI, and compared them with the present solution. As can be seen they are essentially in exact agreement with those of this work.[10] We would point out again that in ref 6 good agreement had been shown between the numerical results and experimental data on diffusion of oxygen through a film of hemoglobin solution.

To complete the picture for the dependence of η_L on all the similarity parameters, solutions are shown in Figure 4 for η_L as a function of δ, with κ and ϵ as parameters. The curves show that η_L tends to a frozen condition ($\eta_L \to 0$) when the forward chemical reaction rate dominates over the diffusion rate of the gas. In Figure 4b we have also shown both numerical and experimental results of Bdzil, *et al.*,[4] which agree reasonably well with the present work. The experimental results were determined from electrical potential measurements of the induced potential resulting from a partial pressure difference across a membrane in which facilitated transport of nitric oxide takes place in a film containing ferrous and ferric ions. The relation between the potential difference and y_L is given by the Donnan potential drop[4]

$$\Delta\phi = (RT/F) \ln y_L \quad (27)$$

The numerical data shown in Figure 4b were obtained by using eq 27 and the values of the potential listed in ref 4 as corresponding to the numerical solution.[11]

In addition to the parameter η_L, the value of the carrier concentration ratio α is also required in order to determine the flux J_c (see eq 17). As mentioned earlier, α has a value of $1 + \kappa$ when the system is everywhere in chemical equilibrium and a value of $1 + (\kappa/2)$ for a completely frozen condition. To show its dependence on the three similarity parameters, $\alpha/(1 + \kappa)$ is mapped out in Figure 5 as a function of ϵ, with κ and Δ as parameters. The curves of Figure 5 show that $\alpha/(1 + \kappa)$ varies very slowly with ϵ and is only weakly dependent on Δ. Although for large ϵ, each curve would eventually go to the indicated frozen limit of

TABLE I: Comparison between Exact Numerical Values for Facilitation Given by Kutchai, *et al.*,[6] and Values Obtained from Approximate Analytic Solution

ϵ	Numerical (ref 6)	Analytic (eq 29)
	F (κ = 4.5, Δ = 4.5)	
2.97×10^{-1}	0.196	0.223
1.32×10^{-1}	0.286	0.333
7.43×10^{-2}	0.351	0.414
1.86×10^{-2}	0.500	0.572
2.97×10^{-3}	0.646	0.706
	F (κ = 35.9, Δ = 1122)	
4.5	0.75	0.36
1.8×10^{-1}	3.75	1.91
4.5×10^{-2}	6.13	3.62
2.0×10^{-2}	7.84	5.15
5.0×10^{-3}	11.44	8.85
1.8×10^{-3}	14.44	12.31

$[1 + (\kappa/2)]/(1 + \kappa)$, in the practical range where ϵ is small the value of $\alpha/(1 + \kappa)$ is also only weakly dependent on the parameter κ.

In obtaining the solution given by eq 25 from eq 23, it is found that $\gamma = (\eta_L - 1)/2$ in order to satisfy all the boundary conditions (eq 15). If γ is related to η_L in this form, then from eq 24 the carrier concentration ratio α would satisfy the relation[12]

$$\alpha = 1 + \kappa[(1 + \eta_L)/2] \tag{28}$$

It is interesting to observe that this expression for α, which is not a general solution, does have the proper limiting behavior with η_L in the sense that when $\eta_L = 1$ (chemical equilibrium) $\alpha = 1 - \kappa$ and when $\eta_L = 0$ (frozen condition) $\alpha = 1 + (\kappa/2)$. That eq 28 is not a valid general solution is evident from the fact that it is a κ-dependent solution derived from a $\kappa \to 0$ limit. This is a manifestation similar to the inability to exactly satisfy all three boundary conditions with the solution obtained from the second-order linear equation obtained by setting $\Delta = 0$. However, comparison with the exact numerical solutions shows that eq 28 does predict quite well the actual values of α over a wide range of conditions. Because of this good agreement, because of the limited range of $\alpha - 1$ (from κ to $\kappa/2$), and because of the fact that eq 28 goes to the correct limits for large and small ϵ, it follows that eq 28 may be applied as a rather accurate "interpolation" formula for α.

If eq 28 is used as the solution for α, then the facilitation performance of the membrane can be expressed by the following simple relation

$$F = \frac{2\eta_L\Delta}{2 + \kappa(\eta_L + 1)} \tag{29}$$

where to good approximation we may take η_L to be given by eq 25, which strictly speaking is valid only for $\kappa \to 0$.

In Table I we have reduced the numerical results of Kutchai, *et al.*,[6] from their Table VI (Δ = 4.5) and their Table V (Δ = 1122) and compared them with the analytic solution given by eq 29 with η_L defined by eq 25. It can be seen that their results are predicted very well, provided κ and Δ are not too large.

The membrane facilitation F, defined by eq 17, can be maximized by making the carrier concentration α as close to 1 as possible, and by making the product of the parameter Δ and the disequilibrium parameter η_L as large as possible. From the present results, α can be made to approach 1 if κ is small enough. Furthermore, when $\kappa \ll 1$ the product $\eta_L\Delta$ can be made indefinitely large by making ϵ as small as possible and Δ as large as possible. This can be seen from the $\kappa = 0$ solution given by eq 25 from which for $\Delta \gg 1$ and $\epsilon \ll 1$ we find $\eta_L\Delta \sim \frac{1}{2}(\Delta/\epsilon)^{1/2}$.

Concluding Remarks

The preceding results show that when considering applications of liquid membranes to problems of facilitated transport, the gas-membrane system should be optimized with respect to the similarity parameters defined in the present paper. The seven independent variables of the system c_0, u_T, L, k_1, k_2, D, and D_c were shown to be reducible to three independent dimensionless similarity parameters. The three parameters κ, ϵ, δ (eq 8) measure, respectively, the initial gas concentration, the liquid diffusion rate to the backward reaction rate, and the gas diffusion rate to the forward reaction rate.

Limiting analytic solutions have been obtained for the facilitation performance of the membrane and they are shown to compare very well with exact numerical solutions over most of the range of interest of the independent similarity parameters. The results also show that the facilitation F can be made very large if both ϵ and κ are small enough and $\Delta \equiv \epsilon/\delta$ is large enough.

Acknowledgments. The authors would like to thank Professor Kenneth A. Smith of M.I.T. for helpful suggestions, and particularly for encouraging them to examine their analytic results as they relate to the facilitation performance. We also wish to thank Professor Jerome S. Schultz and Shyam Suchdeo of The University of Michigan for pointing out some numerical errors in the original manuscript and a simpler form of eq 25.

This research was sponsored by the National Science Foundation, and administered by the Fluid Mechanics Program of the Engineering Division under Grant No. GK-35798X.

References and Notes

(1) J. B. Wittenberg, *Biol. Bull.*, **117**, 402 (1959).
(2) P. F. Scholander, *Science*, **131**, 585 (1960).
(3) W. J. Ward and W. L. Robb, *Science*, **156**, 1481 (1967).
(4) J. Bdzil, C. C. Carlier, H. L. Frisch, W. J. Ward, III, and M. W. Breiter, *J. Phys. Chem.*, **77**, 846 (1973).
(5) W. J. Ward, III, *AIChE J.*, **16**, 405 (1970).
(6) H. Kutchai, J. A. Jaccuez, and F. J. Mather, *Biophys. J.*, **10**, 38 (1970).
(7) K. A. Smith, J. H. Meldon, and C. K. Colton, *AIChE J.*, **19**, 102 (1973).
(8) S. K. Friedlander and K. H. Keller, *Chem. Eng. Sci.*, **20**, 121 (1965).
(9) J. D. Murray, *Proc. Roy. Soc., Ser. B*, **178**, 95 (1971).
(10) A typographical error appears in the value of k_1 in the Appendix of ref 6, the factor multiplying k_1 being given as 10^{+9} instead of 10^{-9}.
(11) In ref 4 it is implied that the theoretical value of y_L can be determined from Figure 5 of ref 5. This figure is a plot of J_c *vs.* u_T (see eq 17). Assuming all the physical constants of the system to be given, it can be seen from eq 17 that y_L cannot be determined without also knowing u_0.
(12) Professor K. A. Smith pointed out this result to the authors for the case $\Delta = 0$, with η_L expressed in terms of ϵ.

Application of Polyelectrolyte Limiting Laws to Potentiometric Titration[1]

Gerald S. Manning*

School of Chemistry, Rutgers University, New Brunswick, New Jersey

and Alfred Holtzer

Department of Chemistry, Washington University, St. Louis, Missouri *(Received February 2, 1973)*

A recently developed theory of polyelectrolyte solutions based on counterion condensation above a critical charge density is applied to the analysis of titration curves of weak-acid polyelectrolytes. For a fixed value of the degree of neutralization α, pK is demonstrated to be a linear function of the logarithm of the salt concentration. Data from the literature on three different polymers are in agreement with this prediction. The slope of the linear function is also given by the theory and is independent of the thermodynamic state of the condensed counterions; thus, the expression for the slope has the same logical status as the successfully applied "limiting laws" for colligative properties which have previously been derived. Observed values of the slopes taken from the literature are not consistently in agreement with the theory, ranging from close agreement for polyacrylic acid (except at low α) to poor agreement for carboxymethylcellulose. At fixed salt concentrations, pK as a function of α is predicted to depend on complex interactions near the polyion chain. An explicit dependence is given, but only at the cost of introducing special assumptions of a somewhat arbitrary nature concerning these interactions. The relationship of the present theory to the Poisson–Boltzmann approach to the same problem is examined, but a clear choice cannot be made at this time. It is also concluded that the Maeda–Oosawa theory for the concentration dependence of pK is equivalent to the present theory for salt-free solutions but is less rigorous for solutions with added salt.

Introduction

We propose in this article to apply the general polyelectrolyte theory developed by one of us[2,3] to the analysis of titration curves of weak-acid polyelectrolytes. Based on a cylindrically symmetric model for the polyion, the theory is rigorous in the limit of zero concentration.

In the zero-concentration limit the polyion model may be described in three equivalent ways: as an infinitely long uniform line charge, a line charge placed along the axis of an infinitely long cylindrical volume of arbitrary radius, or an infinitely long cylinder of arbitrary radius and uniform surface charge density. Again in this limit, the charge need not be assumed continuously distributed along the line or on the cylindrical surface, but may be composed of discrete units; the results are independent of the mode of charge distribution. Furthermore, and again at infinite dilution, the theory depends on no *a priori* assumption about the solvent; in particular, the solvent is *not* assumed to be a dielectric continuum. All these statements may be verified by a careful reading of ref 2b.

The charge density on the polyion is measured by a dimensionless parameter

$$\xi = e^2/\epsilon kTb \tag{1}$$

where e is the charge on a proton, ϵ the bulk dielectric constant of the solvent, k Boltzmann's constant, T the absolute temperature, and b the average distance between charged groups on the polyelectrolyte chain in the configuration of maximum extension; more precisely

$$b = L/\nu \tag{2}$$

where ν is the number of charged groups on the chain and L its maximum end-to-end length.

The appearance of the bulk dielectric constant in eq 1 does not imply any idealized description of the solvent.[2b] Although the situation is somewhat more complex than that which leads to the Debye–Hückel limiting law for simple ionic solutions, it may be useful to recall the rigorous use there of the bulk dielectric constant, in the limit of zero concentration, even for a real, structured solvent.

We will restrict attention to the case for which all counterions are univalent. It follows[2] that if $\xi < 1$, the Debye–Hückel approximation, adapted to cylindrical geometry, is exact in the limit of zero concentration; while if $\xi > 1$, in the same limit,[2b] counterions "condense" on the polyion until its *net* value of ξ is just less than unity.

On this basis we proceed to the derivation of the titration equations. In the following attention should be paid to the major contrasts between the concentration dependence of pH and its dependence on the degree of neutralization α. Indeed we shall show that the former is a colligative property of the system for which an explicit and rigorous limiting law may be derived, while the latter depends crucially on the complex interactions among polyion, solvent molecules, and, for $\xi > 1$, condensed counterions, a circumstance which, at this time, precludes further rigorous development.

Derivation of the Titration Equations

The properties of the titration curve may be derived from an analysis of the equilibrium process

$$P^{-(\nu-1)} \longrightarrow P^{-\nu} + H^+ \tag{3}$$

where $P^{-\nu}$ represents a weak polyacid chain with ν titrated groups.

With μ_i the chemical potential (per molecule) of species i, the equilibrium reaction 3 implies that

$$\mu_\nu - \mu_{\nu-1} + \mu_{H^+} = 0 \tag{4}$$

For greater readability, the subscript ν has been used in-

stead of $P^{-\nu}$. Since μ_i may be written in the form

$$\mu_i = \mu_i^*(T, p) + kT \ln a_i \quad (5)$$

where a_i is the activity of species i, and since

$$a_i = \gamma_i m_i \quad (6)$$

where γ_i is the activity coefficient and m_i the molality, it follows from eq 4 that

$$\Delta\mu_\nu^* + kT \ln (\gamma_\nu/\gamma_{\nu-1}) + \mu_{H^+}^* + kT \ln a_{H^+} = 0 \quad (7)$$

In eq 7

$$\Delta\mu_\nu^* \equiv \mu_\nu^* - \mu_{\nu-1}^* \quad (8)$$

Moreover, in writing eq 7, we have taken

$$m_\nu = m_{\nu-1} \quad (9)$$

that is, the actual solution contains chains which carry a varying number of ionized groups, and we choose ν as the number which maximizes this distribution.

In the general theory[2] it is assumed that interactions among polyions are negligible. This assumption is consistent with the repeated observation for dilute solutions that polyelectrolyte effects on colligative properties are always independent of molecular weight. Moreover, the assumption is required if cylindrical modeling is to be used, since the validity of the model rests on the neglect of interactions between distant segments on the same chain and hence between segments on different chains.[2a,3] The only contribution to the electrostatic free energy, then, stems from interactions of a single polyion with small ions. In that case, the term $kT \ln \gamma_\nu$ is precisely the excess free energy per polyion due to this contribution. It may then be verified from eq 16 of ref 2a that, if $\xi < 1$

$$kT \ln \gamma_\nu = -(\nu^2 e^2/\epsilon L) \ln \kappa \quad \xi < 1 \quad (10)$$

where κ is the Debye screening parameter. The right-hand side of eq 10, correctly, does not contain the self-energy of the polyion, but only its interaction free energy with small ions.

Since ν is a large number, the second term on the left-hand side of eq 7 works out to be

$$kT \ln (\gamma_\nu/\gamma_{\nu-1}) = -kT\xi \ln (\kappa^2) \quad \xi < 1 \quad (11)$$

If the titration has proceeded into the region $\xi > 1$, it is the *net* value of ξ, namely, unity, which must be used in eq 11, since it is that value which determines the interaction of the polyion with uncondensed small ions

$$kT \ln (\gamma_\nu/\gamma_{\nu-1}) = -kT \ln (\kappa^2) \quad \xi > 1 \quad (12)$$

The standard definition of pK (sometimes called the "apparent pK") is

$$pK \equiv pH + \log [(1 - \alpha)/\alpha] \quad (13)$$

where α is the degree of neutralization of the polyacid, that is, the ratio of total number of titrated groups to total number of titratable groups. The relation between ξ and α is

$$\xi = \alpha/\alpha_1 \quad (14)$$

where α_1 is that value of α which gives a linear charge density corresponding to $\xi = 1$. The notation becomes less cluttered if we define the function $g(\alpha)$

$$g(\alpha) \equiv \begin{cases} \alpha/\alpha_1 & \alpha < \alpha_1 \\ 1 & \alpha > \alpha_1 \end{cases} \quad (15)$$

With these definitions, the standard definition of pH, and respective substitution of eq 11 and 12 into eq 7, the relation for pK is

$$pK = -g(\alpha) \log(\kappa^2) + 0.434(\Delta\mu_\nu^* + \mu_{H^+}^*)/kT + \log [(1 - \alpha)/\alpha] \quad (16)$$

note the conversion to common logarithms. We also note in passing that the proper α to be employed here, since ν refers to the maximum in the distribution of charges, is the most probable α. In practice, the experimental value of α is the number average α. It is customary to suppose that the distribution is sufficiently symmetric that the difference is slight.

Concentration Dependence of pK. Since the reference state chemical potentials μ_i^* are, by definition, independent of concentration, the entire concentration dependence of pK resides in the first term of the right-hand side of eq 16. If all small ions are univalent, κ is given by

$$\kappa^2 = (4\pi e^2/\epsilon kT) \sum_i n_i \quad (17)$$

where the sum runs over all small ionic species and n_i is the concentration expressed in (molecule cm^{-3}). A common system is a solution which contains a simple univalent salt of concentration n_s and a weak polyacid partially neutralized by a strong base with n_m the concentration of titratable groups. Then, upon neglect of hydrogen and hydroxide ion concentrations

$$\sum n_i = \begin{cases} 2n_s + \alpha n_m & \alpha < \alpha_1 \\ 2n_s + \alpha_1 n_m & \alpha > \alpha_1 \end{cases} \quad (18)$$

For $\alpha > \alpha_1$, the factor α_1 appears in this relation because the remaining $(\alpha - \alpha_1)N_m$ counterions are condensed on the polyions and are not in the ionic atmosphere. Equation 16 then implies that values of pK extrapolated to zero polyion concentration are linear in the logarithm of the salt concentration

$$(\partial pK/\partial \log n_s)_\alpha = -g(\alpha) \quad n_m \longrightarrow 0 \quad (19)$$

Similarly, for a titration in the absence of added salt

$$(\partial pK/\partial \log n_m)_\alpha = -g(\alpha) \quad n_s = 0 \quad (20)$$

It is recalled that $g(\alpha)$ is defined by eq 15.

Because eq 19 and 20 originate in eq 11 and 12 (which, in their turn, are derived from eq 16 of ref 2a) they are fully rigorous in the limit of infinite dilution. They are limiting laws for what has turned out to be a colligative property of the system, in the same sense as the limiting laws given in ref 2a for activity and osmotic coefficients. In particular, for the region $\alpha > \alpha_1$, they depend on no special assumption concerning the behavior of the condensed counterions but only on their number.

Dependence of pK on α. To study the effect of the degree of neutralization it is necessary to assume that the term $\Delta\mu_\nu^*$ in eq 16 is additively composed of three contributions

$$\Delta\mu_\nu^* = \Delta\mu^0 + \Delta\mu_\nu^*(H^+) + \Delta\mu_{\nu\,self}^* \quad (21)$$

The first term is the contribution from the ionization of a single group at zero charge density along the polyelectrolyte chain. By standard definition, then

$$0.434(\Delta\mu_\nu^0 + \mu_{H^+}^*)/kT \equiv pK_0 \quad (22)$$

note that pK_0 is independent of α.

The second term is the contribution from the entropy of mixing of protons among the ionizable groups. If it is as-

sumed that the mixing is fully random, that is, that the presence of a proton on one group does not affect the probability that a neighboring group is ionized, then a well-known calculation[4] provides the expression

$$\Delta\mu_\nu^*(H^+) = -kT \ln [(1 - \alpha)/\alpha] \quad (23)$$

The third term, $\Delta\mu_\nu^*{}_{self}$ is the contribution from the change in the self-energy of the solvated polyelectrolyte (over and above that included in the term $\Delta\mu^0$) when the total number of charged groups is increased from $\nu - 1$ to ν. In the region $\xi > 1$, or $\alpha > \alpha_1$, the condensed counterions must be considered as a part of the polyelectrolyte and $\Delta\mu_\nu^*{}_{self}$ includes a very complex set of interactions among polyion charged groups, solvent molecules, and condensed counterions; in general, of course, it depends on α.

Substitution of eq 21-23 into eq 16 yields

$$pK = pK_0 - g(\alpha) \log \kappa^2 + W(\alpha) \quad (24)$$

where

$$W(\alpha) \equiv 0.434\Delta\mu_\nu^*{}_{self}/kT \quad (25)$$

According to the definition, eq 15, of $g(\alpha)$, the sole source of dependence of pK on α for $\alpha > \alpha_1$, is the self-energy term $W(\alpha)$. This circumstance does not mean that $W(\alpha)$ is an extraneous term grafted onto the theory to account for the empirically observed variation of pK with α (see the following discussion), a variation which otherwise could not be explained by means of the counterion condensation theory alone. The term $\Delta\mu_\nu^*$ in eq 16 follows from a rigorous thermodynamic analysis of the ionization equilibrium represented by eq 3; that $\Delta\mu_\nu^*$ contains a contribution $\Delta\mu_\nu^*{}_{self}$, as indicated in eq 21, from the change due to ionization of the self- (free) energy of the polyion is part of the physical reality of the system quite apart from considerations of counterion condensation.

Special Assumptions for the Explicit Evaluation of W (α). Suppose it is assumed that the solvent is a uniform dielectric continuum with dielectric constant ϵ (the bulk value of the real solvent); this assumption has not been introduced until this point. The polyion is, moreover, assumed to be an infinitely long cylinder with radius a and uniform surface charge density. For $\alpha > \alpha_1$, the condensed counterions are assumed to have zero radius and to "melt" into the surface of the cylinder, maintaining the surface charge density at a value corresponding to $\xi = 1$. With these assumptions $W(\alpha)$ is given by the Born approximation for charged cylinders in a uniform dielectric

$$W(\alpha) = -g(\alpha) \log \alpha^2 \quad (26)$$

This relation is obtained by charging a cylinder in a manner exactly analogous to the well-known Born calculation for spheres.[5] Thus, with $\Delta pK = pK - pK_0$

$$\Delta pK = -g(\alpha) \log \kappa^2 a^2 \quad (27)$$

a relation which indicates that ΔpK is independent of α for $\alpha > \alpha_1$.

An explicit dependence of pK on α for $\alpha > \alpha_1$ may be obtained by relaxing the assumption that the condensed counterions have zero radius. Suppose each counterion is assigned the radius d (or, equivalently, the average location of point condensed counterions may be assumed to be at the finite distance d from the polyion surface). For $\alpha < \alpha_1$, eq 26 would be unchanged by this assumption, since no counterions are condensed, and the self-energy term, by definition, does not contain the interaction energy with uncondensed ions (it is the log κ term which contains the latter). But for $\alpha > \alpha_1$, the situation is different. There will be a cylindrical surface at $r = a$ with charge density corresponding to the full value of ξ as given by eq 1. There will be another cylindrical surface at $r = a + d$ characterized by a charge density due to the condensed counterions of magnitude such that the *total* charge contained within a surface of radius just greater than $a + d$ corresponds to $\xi = 1$. The cylindrical shell between $r = a$ and $r = a + d$ is free of charge. Now $W(\alpha)$ corresponds to the work required to bring a unit point charge from infinity to the surface $r = a$, in the absence of uncondensed ions. It is composed of two terms, the work required to bring the charge from infinity to $r = a + d$ and the work required to bring the charge from $r = a + d$ to $r = a$. Thus, for $\alpha > \alpha_1$

$$W(\alpha) = -\log (a + d)^2 - (\alpha/\alpha_1) \log [a/(a + d)]^2$$
$$= -\log a^2 - [(\alpha/\alpha_1) - 1] \log [a/(a + d)]^2 \quad (28)$$

The result for ΔpK, written as a single formula valid over the whole range of α, is

$$\Delta pK = -g(\alpha) \log \kappa^2 a^2 - [(a/a_1) - g(\alpha)] \log [a/(a + d)]^2 \quad (29)$$

the second term is zero for $\alpha < \alpha_1$, while, for $\alpha > \alpha_1$, it increases linearly with α. Equation 29 still incorporates the assumption of a uniform dielectric right up to the surface $r = a$.

A more realistic model for the solvent may be obtained by assuming that the region between the surface $r = a$ and $r = a + d$ is a uniform dielectric with dielectric constant ϵ', where ϵ' does not equal ϵ, the bulk value; the dielectric outside $r = a + d$ continues to be characterized by the value ϵ. From the physical point of view we are assuming the existence of a hydration layer of thickness d. Since there is no reason to suppose that the hydration layer suddenly disappears when α drops below α_1, we adopt the same step function for the dielectric constant for all values of α, even though the choice of the thickness as equal to the counterion radius, sufficiently arbitrary for $\alpha > \alpha_1$, becomes totally so when there are no condensed counterions ($\alpha < \alpha_1$). The modification required in the above calculation is obvious and leads to the result

$$\Delta pK = -g(\alpha) \log \kappa^2 a^2 - [(a/a_1)(\epsilon/\epsilon') - g(\alpha)] \log [a/(a + d)]^2 \quad (30)$$

This game can be extended. It is entirely "reasonable" that the thickness of the "hydration layer" should be chosen as $d' \neq d$. Moreover, it is "apparent" that d' and ϵ' are really functions of α; for that matter, d is also a function of α since d is a "hydrated radius" which grows smaller as the condensed counterion is drawn closer to the polyion "surface" with increasing α (not to speak of the wealth of parameters we can use to describe the discrete-charge effect close to the polyion surface). We hope, however, that we have already succeeded in making the point that there is very little at this time of a convincing nature that can be said about the function $W(\alpha)$ in eq 24.

Comparison with Other Theories

Comparison with Theories Based on the Poisson-Boltzmann Equation. Many previous theories of the titration curve are based on solutions of the Poisson-Boltzmann (PB) equation for a uniformly charged cylinder in a uniform dielectric.[6-8] The starting point is the equation

$$\Delta pK = 0.434e\psi(a)/kT \quad (31)$$

where $\psi(a)$ is the value of the electrostatic potential at the surface of the cylinder. The value of $\psi(a)$ is then obtained from the solution of the PB equation.

Since eq 24 is rigorously valid only in the limit of zero concentration, direct comparison of eq 31 with eq 24 requires that the value of $\psi(a)$ at infinite dilution be used. MacGillivray[9] has been able to prove analytically the following asymptotic relation for the solution of the PB equation with point counterions in the limit of infinite dilution: in the present notation

$$0.434e\psi(a)/kT \approx -g(\alpha) \log \kappa^2 a^2 \qquad (32)$$

Thus, the PB theory with point counterions at infinite dilution is equivalent to the special case of the present theory represented by eq 27. The condensation of counterions for $\alpha > \alpha_1$ has been accurately built into the PB theory, but, unfortunately, at least insofar as the PB theory is conventionally applied, the crude Born approximation has been built in as well. If a "distance of closest approach" greater than $r = a$ is assumed, it is easily seen that the PB theory[10] at infinite dilution leads to eq 29. Our conclusion is that the PB theory at infinite dilution is a special case of the more general eq 24.

In practice, however, the PB theory is not used at infinite dilution. The PB equation has the virtue that a solution may be found at any concentration, so the surface potential used to correlate experimental data is properly taken at the concentration employed in the experiment. In contrast with the asymptotic result, eq 32, the solution $\psi(a)$ of the PB equation at experimentally typical concentrations, even for point counterions, is an increasing function of α over the whole range. Indeed, the major triumph of the PB theory is this ability to explain the observed, and pronounced, increase of pK with increasing charge that is such a characteristic feature of polyacids and polybases.

It is recognized, however, that solutions to the PB equation have been obtained by assuming that the solvent is a dielectric continuum that retains its bulk properties right up to the surface of the polyion; *i.e.*, the usual PB treatment is within the regime of the Born approximation. It is the hope of advocates of the PB approach that effects due to departures from this idealized model are small and that these and effects due to the inconsistency of the nonlinearized PB equation can be corrected for by a judicious choice of values for the rod and counterion radii, which are somewhat arbitrary.

The counterion condensation theory developed here, on the other hand, presents a completely different physical picture for the variation of pK with α. This view attributes the *entire* α dependence of pK for $\alpha > \alpha_1$ to effects, considered small in the PB treatment, such as those represented by the second term on the right-hand side of eq 30, namely, the finite size of the counterion, or finite average distance of the condensed counterions from the polyion surface, and the distortion of the solvent structure near the polyion from its bulk characteristics. The fact that the theory is rigorous only in the infinitely dilute limit is not *necessarily* a difficulty, although we recognize that it may be. It is possible that, at least for the more dilute concentrations used in experiments, the general eq 24 remains a reasonably accurate description.

The choice between the two theories must ultimately be made by experiment. In that connection, Ikegami[11] concluded from his experiments on refractivity of poly(acrylic acid) solutions that several predicted aspects of counterion condensation are observed at experimentally practical concentrations and that the condensed counterions strongly modify the molecular structure of the solvation shell about the polyions. In a similarly conceived experiment Zana, Tondre, Rinaudo, and Milas[12] have found the onset of ultrasonic absorption increments at $\alpha = \alpha_1$ for a series of carboxymethylcelluloses of varying degrees of substitution. Dilatometry[13] and density[14] measurements may be similarly interpreted. All these measurements suggest the penetration of counterions into the hydration region of the polyion. The description given by the PB treatment of a time-average continuous ionic atmosphere comprising *all* small ions simultaneously and embedded in a uniform dielectric continuum does not, therefore, seem to be deeply rooted in available empirical evidence.

Nevertheless, it is our opinion that the matter cannot be considered closed; bulk properties, such as refractive indexes, are notoriously refractory to unique molecular interpretation. It is, in our judgment, not likely that the question will be satisfactorily resolved until reliable spectroscopic probes of the water structure local to the polyion are developed and employed. A promising start to such a program has been made by Glasel.[15]

Comparison of the Concentration Dependence of pK with the Maeda-Oosawa Theory. Maeda and Oosawa[16] have recently published an approximate thermodynamic analysis which leads, in our notation, to the relation

$$(\partial pK/\partial \log n_m)_\alpha = -1 + \partial(\phi_p\alpha)/\partial\alpha \qquad n_s = 0 \qquad (33)$$

where ϕ_p is the osmotic coefficient of the salt-free polyacid solution at the degree of neutralization α. At first glance, it appears that eq 33 differs from the corresponding conclusion of the present theory, eq 20. We can show, however, that, with the assumption on which eq 33 is based, it is strictly identical with eq 20.

The assumption explicitly used by Maeda and Oosawa to obtain eq 33 is that the activity coefficient of the counterion in a salt-free polyelectrolyte solution is independent of polyelectrolyte concentration. The authors cite the theory of Lifson and Katchalsky[17] as theoretical justification for this assumption. In fact, however, the Lifson-Katchalsky theory can only predict the osmotic coefficient and not the counterion activity coefficient. The reason is that the counterion concentration is not an independent variable in the Lifson-Katchalsky expression for the free energy; it is effectively identified with the polyion concentration. Thus, the required derivative of the free energy, with respect to the counterion concentration at fixed polyion concentration, cannot be taken.

The only rigorous theory of single-ion activity coefficients yet to be published is contained in ref 2a. There, for a system of charged rods at infinite dilution, it is indeed demonstrated that the counterion activity coefficient in salt-free solution is independent of concentration, thereby justifying the Maeda-Oosawa assumption. However, under exactly the same conditions, a relation for the osmotic coefficient ϕ_p is also derived in ref 2a; for weak polyacids

$$\phi_p = \begin{cases} 1 - (\alpha/2\alpha_1) & \alpha < \alpha_1 \\ \alpha_1/2\alpha & \alpha > \alpha_1 \end{cases} \qquad (34)$$

This expression for ϕ_p coincides with the Lifson-Katchalsky result at infinite dilution, but does not equal the counterion activity coefficient. When it is substituted into eq 33, the latter immediately collapses to eq 20. Thus, a

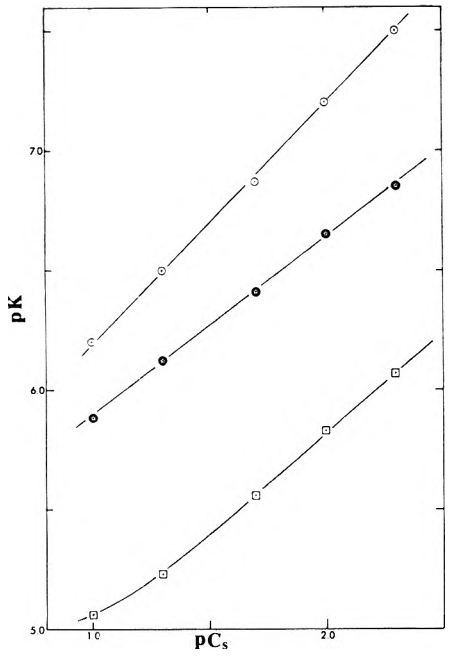

Figure 1. Sample plots of pK *vs.* pC_s: circles, polyacrylic acid, at α = 0.9; squares, at α = 0.3;[18,19] starred dots, polymethacrylic acid at α = 0.5.[18,19] Lines for the upper two sets and for the linear portion of the lowest set are by least squares.

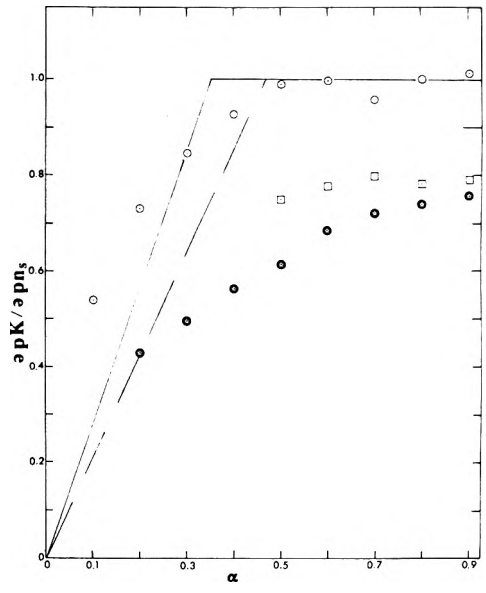

Figure 2. Slopes of pK *vs.* pC_s [*i.e.*, $(\partial pK/\partial pn_s)_\alpha$] *vs.* α: circles, polyacrylic acid;[18,19] squares, polymethacrylic acid;[18,19] starred dots, carboxymethylcellulose of degree of esterification 1.54.[8,19] Solid line is the prediction of counterion condensation theory for acrylic polymers, using α_1 = 0.35. Dashed line is for CMC from the same theory, with α_1 = 0.47. Above α_1, theory predicts a value of unity for both.

self-consistent application of the assumption necessary to eq 33 shows the equivalence of that relation with eq 20.

Maeda and Oosawa also give results for the concentration dependence of pH in salt-containing solutions which differ from the general dependence given in eq 24. The present theory must be considered the more rigorous of the two, for the following reason. To obtain their relations in the presence of added salt, Maeda and Oosawa assume the validity of the so-called additivity rules for both the osmotic pressure and the counterion activity. They correctly cite ref 2a as providing a proof of the additivity of osmotic pressures for infinitely long rods at infinite dilution; however, the same reference shows that the additivity of counterion activities does *not* hold (equivalently, it is proved that the coion activity coefficient does not equal unity). Further critical discussion of the additivity rules may be found in ref 3.

Comparison with Experiment

Comparison of the Concentration Effect with Data. For comparison of eq 19 with experiment, we have chosen three sets of data: (1) those of Nagasawa, Murase, and Kondo[18,19] on atactic poly(acrylic acid) (PAA) at 15°, for which α_1 = 0.35; (2) those of the same authors for atactic poly(methacrylic acid) (PMA) at 23° with essentially the same α_1; and those of Muroga, Suzuki, Kawaguchi, and Nagasawa[8,19] for a carboxymethylcellulose (CMC) having an average of 1.54 carboxyls per glucose unit, at 25°, for which α_1 = 0.468. Dr. Nagasawa was able, and kind enough, to provide us his data for PAA and PMA in tabular form. We obtained the pK values for CMC, from Figure 5 of ref 19. In all three studies, proper attention was paid to extrapolation to zero polyion concentration, so eq 19 is presumably applicable. The PMA data were only used for $\alpha \geq 0.5$ because of the conformation change that complicates the situation outside that range.

The pK values for given degree of ionization were plotted *vs.* $-\log C_s$ (NaCl is the added salt), where C_s is the molarity of salt. Some sample plots are shown in Figure 1 for PAA and PMA. A similar plot for CMC is Figure 6 of ref 19. The plots for PMA and CMC are linear over the entire studied range of salt concentration (0.005–0.1 M for PMA, 0.01–0.2 M for CMC) and α (0.5–0.9 for PMA, 0.2–0.9 for CMC). The graphs for PAA are linear over the whole range of C_s (0.005–0.1 M) for $\alpha \geq 0.7$, but deviate from linearity at the highest C_s (0.1 M) if $\alpha < 0.7$. The reason for the deviation at high salt in the case of PAA (or, perhaps, since the prediction of linearity comes from a limiting law, one should say "the reason for the nondeviation at high salt of PMA and CMC") is unclear.

The counterion condensation theory thus provides the correct *form* for the salt dependence of pK at given α. Unfortunately, Nagasawa, *et al.*,[18,19] find that the salt-concentration dependence of the PB surface potential at fixed α also fits the data, so this result alone can do little to help decide between the two approaches.

To investigate the accuracy of eq 19 in more detail, the linear portions of the pK *vs.* pC_s plots were fit by least squares and slopes, *i.e.*, $\partial pK/\partial pC_s = -\partial pK/\partial \log n_s$, plotted *vs.* α as in Figure 2. The behavior expected from counterion condensation theory, eq 19, is also shown. The curve for PAA levels off at unity as predicted by theory; but the initial rise is not linear as predicted and no sharp corner is apparent. The data for PMA level off as predicted, but at a value of ~0.8 rather than 1.0. The CMC data show no redeeming features whatever; the values of $-\partial pK/\partial \log n_s$ rise monotonically and nonlinearly with α.

The limiting laws for other colligative properties have also been found to diverge from measured values for PAA at low degrees of neutralization,[2a] possibly because the polyion is more tightly coiled at low α, making the cylindrical geometry of the model no longer applicable. The problem with the CMC data may be that they were obtained at concentrations higher than the range needed to satisfy the theoretical requirement of "zero concentration." It is to be expected that for CMC the required con-

TABLE I: Attempted Correlation of Mandel's Data on CMC[a]

α	$\Delta pK_x - \Delta pK_y$	$-(\alpha/\alpha_1) \log (\kappa_x^2/\kappa_y^2)$	δ
0.2	0.24	0.41	0.17
0.3	0.34	0.54	0.20
0.4	0.42	0.66	0.24
0.5	0.48	0.76	0.28
0.6	0.52	0.85	0.33
0.7	0.54	0.93	0.39

[a] ΔpK values according to Mandel's empirical interpolation formulas, $\Delta pK_x = 2.9\alpha - 0.9\alpha^2$ and $\Delta pK_y = 1.5\alpha$.

centration range may be lower than that which gives agreement for PAA, since the former is a much thicker molecule than the latter. Yet the lowest salt concentration for the CMC data was 0.01 *M*, while the PAA data extended down to 0.005 *M*.

Mandel[20] has also published titration data for a sample of CMC, but one which had one carboxyl group per monomer. For this structure, $\alpha_1 = 0.72$ (using $b = 5.15$ Å at $\alpha = 1$) so that over nearly the entire range of α, the system is in the Debye-Hückel region with no condensation of counterions. One of Mandel's titration curves, here called curve x, was taken at the concentrations $n_s = 0$, $n_m = 1.85 \times 10^{-3}$ *M*; another, curve y, at $n_s = 5.00 \times 10^{-3}$ *M*, $n_m = 1.85 \times 10^{-3}$ *M*. In the second column of Table I we list Mandel's measured values of the difference $\Delta pK_x - \Delta pK_y$ for fixed values of α less than α_1.

According to eq 24, for $\alpha < \alpha_1$

$$\Delta pK_x - \Delta pK_y = -(\alpha/\alpha_1) \log (\kappa_x^2/\kappa_y^2) \quad (35)$$

Values for the right-hand side of eq 35 are given in the third column of Table I, with eq 18 and 19 having been used to calculate κ^2. Finally, the fourth column lists values of δ, the difference between the entries in the third and second columns, *i.e.*, the discrepancy between theory and experiment. As α increases from 0.2 to 0.7, δ increases from just under 0.2 p*K* unit to just under 0.4 p*K* unit.

The discrepancy cannot be laid to a poor choice of adjustable parameters, because there are none in eq 35. Possible explanations are (1) the low charge densities involved ($\xi < 1$ in each case) may give rise to sufficient coiling of the CMC chain to render invalid the assumed cylindrical symmetry; (2) there may be residual polyion-polyion interactions at the experimental concentration for curve x, taken in the absence of added salt (although the limiting laws have successfully predicted a number of other properties in the absence of salt[2a,3]); (3) the liquid junction potential, an inevitable feature of the experimental apparatus, may not remain invariant as the sample solution is changed from one free of added salt (curve x) to one characterized by excess salt (curve y).

Comparison of the α Dependence with Data. This section can be brief, since we hope that the reader has already been convinced by the previous discussion that we are capable of fitting any simple titration curve as a function of α by introducing a large number of flexible parameters, all properly justified by appeal to physical intuition. As examples, let us consider the titration curves for PAA[18,19] and CMC[8,19] in excess added NaCl of concentration 0.01 *M*. These are compared with theory in Figure 3, using appropriate values for *a* and *d*. As is seen in each case, the Born regime (eq 29) provides too mild a dependence of ΔpK on α; but, if we assume $\epsilon/\epsilon' = 2$, a perfectly

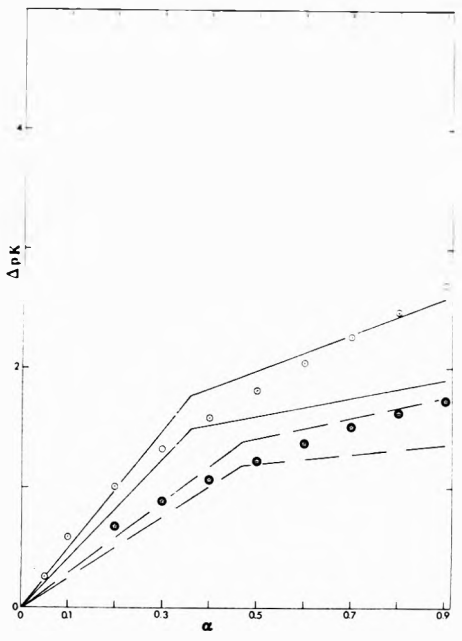

Figure 3. Plots of ΔpK *vs.* α in 0.01 *M* NaCl: open circles, data for polyacrylic acid.[18,19] Solid lines, theory for polyacrylic acid with $a = 5.5$ Å, $d = 2.0$ Å, $\alpha_1 = 0.358$, $pK_0 = 4.5$. Lower solid line is eq 29, upper solid line is eq 30 with $\epsilon/\epsilon' = 2$; starred circles, data for CMC;[8,19] dashed lines, theory for CMC with $a = 7.8$ Å, $d = 2.0$ Å, $\alpha_1 = 0.468$, $pK_0 = 3.34$. Lower dashed line is eq 29, upper dashed line is eq 30 with $\epsilon/\epsilon' = 2$.

reasonable relation for an electrostricted dielectric constant, the theory (eq 30), while not perfect, fits the data as well as the PB theory does.[8,18,19] Furthermore, certain features of the data are well described by the theory. In particular, the linear form of the data at high α is predicted by theory; and, while the data can be fit by a smooth curve, they are also compatible with a break that, in each case, would have to come very near $\alpha = \alpha_1$.

One final difficulty must be noted. Schultz and Strauss[21] have recently published titration curves for two maleic acid copolymers which deviate strikingly from the predictions of the Poisson-Boltzmann equation. These authors suggest that the assumption of independent proton binding which underlies eq 23 is not valid for their case, and, indeed, the nonvalidity of eq 23 would provide a source of dependence on α considered neither in the usual applications of the PB equation nor in the present approach.

Acknowledgments. We wish to thank M. Nagasawa for comments on the original manuscript and U. P. Strauss for several fruitful discussions. One of us (G. S. M.) was an Alfred P. Sloan Fellow during the time most of this work was accomplished and wishes to express his appreciation to the Sloan Foundation for their support.

References and Notes

(1) Supported in part by Biomedical Sciences Support Grant No. RR-07054 from the General Research Support Branch, Division of Research Resources, Bureau of Health Professions Education & Manpower Training, National Institutes of Health and by a grant from the Alfred P. Sloan Foundation.
(2) (a) G. S. Manning, *J. Chem. Phys.*, **51**, 924 (1969); (b) *ibid.*, **51**, 3249 (1969).
(3) G. S. Manning, *Annu. Rev. Phys. Chem.*, **23**, 117 (1972).
(4) S. A. Rice and M. Nagasawa, "Polyelectrolyte Solutions," Academic Press, New York, N. Y., 1961.
(5) N. R. Davidson, "Statistical Mechanics," McGraw-Hill, New York, N. Y., 1962.

(6) L. Kotin and M. Nagasawa, *J. Chem. Phys.*, **36**, 873 (1962).
(7) A. Katchalsky, Z. Alexandrowicz, and O. Kedem, "Chemical Physics of Ionic Solutions," B. E. Conway and R. G. Barradas, Ed., Wiley, New York, N. Y., 1966, Chapter 15.
(8) Y. Muroga, K. Suzuki, Y. Kawaguchi, and M. Nagasawa, *Biopolymers*, **11**, 137 (1972).
(9) A. D. MacGillivray, *J. Chem. Phys.*, **56**, 80, 83 (1972); **57**, 4071, 4075 (1972).
(10) M. Nagasawa and A. Holtzer, *J. Amer. Chem. Soc.*, **86**, 531 (1964).
(11) A. Ikegami, *J. Polym. Sci., Part A2*, 907 (1964).
(12) R. Zana, C. Tondre M. Rinaudo, and M. Milas, *J. Chim. Phys., Physicochim. Biol.*, **68**, 1258 (1971).
(13) U. P. Strauss and Y. P. Leung, *J. Amer. Chem. Soc.*, **87**, 1476 (1965).
(14) C. Tondre and R. Zana, *J. Phys. Chem.*, **76**, 3451 (1972).
(15) J. A. Glasel, *J. Amer. Chem. Soc.*, **92**, 375 (1970).
(16) H. Maeda and F. Oosawa, *J. Phys. Chem.*, **76**, 3445 (1972).
(17) S. Lifson and A. Katchalsky, *J. Polym. Sci.*, **13**, 43 (1954).
(18) M. Nagasawa, T. Murase, and K. Kondo, *J. Phys. Chem.*, **69**, 4005 (1965).
(19) M. Nagasawa, *Pure Appl. Chem.* **26**, 519 (1971).
(20) M. Mandel, *J. Polym. Sci., Part A-2*, **8**, 1841 (1970).
(21) A. W. Schultz and U. P. Strauss, *J. Phys. Chem.*, **76**, 1767 (1972).

Thermodynamic Properties of Conformal Mixtures Calculated from the Hard-Sphere Equation of State

Aleksander Kreglewski,* Randolph C. Wilhoit, and Bruno J. Zwolinski

Thermodynamics Research Center, Department of Chemistry, Texas A&M University, College Station, Texas 77843
(Received April 19, 1973)

Publication costs assisted by the Texas A&M Research Foundation

The equation of state for hard spheres with a van der Waals term $a(T)$ for intermolecular attraction was applied to the evaluation of thermodynamic excess functions of conformal mixtures of inert components. The combining rule for mixed pair interactions, applicable for evaluation of gas–liquid critical constants of mixtures, was used in the present calculations with satisfactory results. Comparisons were made for 23 binary systems of spherical, chain, disk-like molecules including cases of very different as well as similar sizes of the components.

The hard-sphere equation of state has been repeatedly applied in recent years to the calculation of thermodynamic functions of mixtures of nonelectrolytes, particularly the excess functions.[1-7] In all these calculations, the combining rule for the mixed total pair potential $\bar{u}_{ij}$ was expressed by the geometric mean rule multiplied by an empirical constant c_{ij}, which is not the same for different systems and must be evaluated from one or more known properties of the mixture. An exception is the work of Snider and Herrington,[1] who derived a general combining rule for the van der Waals constant a_{ij} closely conforming to that of the actual systems. This rule, however, does not permit a direct calculation of critical constants of mixtures.

If the van der Waals attraction term $a(T)$ (in general a function of the temperature) is taken as proportional to the product of critical constants, T^cV^c, and the geometric mean rule for $\bar{u}_{ij}$ is used, the constant c_{ij} adjusted to the critical temperatures of the mixtures is very close to the values required to fit the excess functions.[2] It can be shown, however, that this internal agreement is limited only to the case of components of similar sizes.

In case of large size differences of the components, the excess functions become asymmetrical. The calculated and the observed curves were compared by Marsh[4b] for mixtures of disk-like molecules such as cyclopentane + octamethylcyclotetrasiloxane (OMCTS). The effect of various factors on the asymmetry of excess functions is again examined more closely in the present paper.

As shown by Rogers and Prausnitz,[6] the term $a(T)$ can be evaluated exactly on the basis of the theory of Barker and Henderson, and the results are in good agreement with experimental data for liquid–vapor equilibrium at high pressures including the critical region. However, excessive computing-time requirements restrict the usefulness of this method in practice, at least at the present time. For this reason, empirical treatments of $a(T)$ can still be useful in applications to fluids and their mixtures.

Since we have recently found[8] that the hard-sphere equation of state with an attraction term $a(T) = a'(1 + c'/RT)$ holds with the same accuracy for spherical as for the chain molecules, the present calculations include mixtures of the latter. The comparisons are limited to mixtures of inert components, *i.e.*, whose molecules interact through London forces only.

The thermodynamic functions were evaluated in two ways, briefly called method A and B, from the equation

$$PV/(RT) = \phi(\xi) - a(T)/(RTV) \qquad (1)$$

where P is the pressure, T is the temperature, and V is the molar volume either of the mixture (V_m) or of a pure component (V_i^0). Equation 1 is a van der Waals-type equation with the compressibility factor $\phi(\xi)$ derived from recent theories of hard-sphere fluids. Since the proper relations are dispersed in numerous papers, they are briefly summarized below.

Method A. For an m-component mixture of hard spheres, Mansoori, *et al.*,[9] derived the relation

$$\phi(\xi)_m = [1 + \xi(1 - 3z_1) + \xi^2(1 - 3z_2) - \xi^3 z_3](1 - \xi)^{-3} \quad (2)$$

where

$$\xi = \sum_{i=1}^{m} \xi_i; \xi_i = (1/6)\pi N_0 \sigma_{ii}^3 x_i / V; \sum_{i=1}^{m} x_i = 1$$

and σ_{ii} is the hard-sphere diameter, N_0 is the Avogadro number, and x_i is the mole fraction of the ith component.

The relations for z_1, z_2, and z_3 were obtained by Lebowitz[10]

$$z_1 = \sum_{j>i=1}^{m} \Delta_{ij}(\sigma_{ii} + \sigma_{jj})(\sigma_{ii}\sigma_{jj})^{-1/2}$$

$$z_2 = \sum_{j>i=1}^{m} \Delta_{ij} \sum_{k=1}^{m} \left(\frac{\xi_k}{\xi}\right) \frac{(\sigma_{ii}\sigma_{jj})^{1/2}}{\sigma_{kk}} \quad (3)$$

$$z_3 = \left[\sum_{i=1}^{m} \left(\frac{\xi_i}{\xi}\right)^{2/3} x_i^{1/3}\right]^3$$

where $\Delta_{ij} = [(\xi_i\xi_j)^{1/2}/\xi][(\sigma_{ii} - \sigma_{jj})^2/(\sigma_{ii}\sigma_{jj})](x_i x_j)^{1/2}$.

The residual molar Helmholtz energy $A_m{}^{rh}$ of a hard-sphere mixture, defined as that of a hard-sphere mixture, $A_m{}^h$, minus that of a perfect gas, A^{id}, at the same T and V_m of the liquid mixture, obtained from eq 2, is[9]

$$A_m{}^{rh}/(RT) = -\frac{3}{2}(1 - z_1 + z_2 + z_3) + (3z_2 + 2z_3)(1 - \xi)^{-1} + \frac{3}{2}(1 - z_1 - z_2 - \frac{1}{3}z_3)(1 - \xi)^{-2} + (z_3 - 1)\ln(1 - \xi) \quad (4)$$

Method B. Equations 2 and 4 become for the pure components

$$\phi(\xi) = (1 + \xi + \xi^2 - \xi^3)(1 - \xi)^{-3} \quad (5)$$

and

$$A^{rh}/(RT) = -3 + 2(1 - \xi)^{-1} + (1 - \xi)^{-2} \quad (6)$$

According to van der Waals, the average collision diameter in the mixture is

$$\langle\sigma_x{}^3\rangle = \sum_{i=1}^{m}\sum_{j=1}^{m} \sigma_{ij}{}^3 x_i x_j \quad (7)$$

where $\sigma_{ij} = (\sigma_{ii} + \sigma_{jj})/2$. By this method, the quantities $\phi(\xi)_m$ and $A_m{}^{rh}/(RT)$ were evaluated by inserting $\xi = (1/6)\pi N_0\langle\sigma_x{}^3\rangle/V_m$ into eq 5 and 6.

For a given $P/(RT)$ and σ_{22}/σ_{11}, method B yields much more negative excess volumes than method A and, as shown later, the van der Waals approximation 7 is a source of serious errors in the excess functions when $\sigma_{22} \gg \sigma_{11}$. Both methods yield, of course, the same liquid volumes of the pure components. For $P/(RT) = 0.2055$ mol/cm^3, so chosen to fit $V_1{}^0 = 38.55$ cm^3/mol for methane at 115.8 K, one obtains $V_2{}^0 = 108$ for 2-methylpentane (system 1 in Table I) while the observed value[11] is 106.7 cm^3/mol. The error is small, considering that at $P = 1980$ bars (for this $P/(RT)$ and T) the state of the fluids lies beyond the range of validity of eq 5.[8] The results are similar when the high density is due to an intermolecular attraction $a(T)$ such that the external $P = 0$.

Empirical Approximations for σ and $a(T)$. It is usually assumed that $(\sigma_{ii}/\sigma_{jj})^3$ may be expressed by the ratio of critical volumes $V_i{}^c/V_j{}^c$. One of us proposed to use for practical reasons[12] the ratio of liquid molar volumes at the reduced temperature $T/T^c = 0.6$ for this purpose. It is well known that for the light molecules the data on second virial coefficients $\beta(T)$ require much smaller values of σ than the liquid molar volumes or V^c suggest. The quantum corrections depend on T, T^c(T^c is subject to corrections itself), and the molecular mass.[13] We have simplified it to a dependence on T^c alone and, by using the values of σ resulting from $\beta(T)$ data, obtained the following empirical relation for corrected liquid molar volumes

$$V^* = V^o[1 - \exp(-0.5 - 0.017T^c)] \quad (8)$$

where V^o is the *observed* liquid molar volume at $T/T^c = 0.6$ and T^c is the *observed* critical temperature in K. With this notation, the symbols in formerly used[14,15] relations remain the same, but all the values of V^* should be calculated from eq 8. In agreement with theory,[13] the correction evaluated from eq 8 is large for H_2, and not negligible for Ar, CH_4, or N_2. Both the theory[16] and experimental PVT data[3,6,8] show that σ and $a(T)$ decrease with increasing temperature. The value of $a(T) = a'[1 + c'/(RT)]$ at the critical point is proportional to T^cV^c or T^cV^*. The values of σ (at $T = 0$), a', and c', obtained from PVT data for nine gaseous substances[8] (Ar, six alkanes, two perfluoroalkanes), are related to T^c and V^* as follows

$$(1/6)\pi N_0\sigma^3 \approx 0.434V^*; a^c \approx 4.7RT^cV^* \quad (9)$$

where a^c is the value of $a(T)$ at the critical point. Hence $\xi_i = 0.434V_i^*x_i/V_m$. In this paper it is assumed that σ and $a(T) = a^c$ are independent of the temperature.

We note that by inserting critical constants into eq 1 and from experimental values of the derivative $(\partial \ln P/\partial \ln T)_{Tc,Vc}$ we obtain a different pair of numerical coefficients in eq 9: 0.39 and 4.33, respectively. The volumes $V_i{}^0$ (the relevant root of eq 1) obtained with these coefficients are much too small, whereas the coefficients in eq 9 yield $V_i{}^0$ close to the experimental values for all the liquids given in Table I.

For a conformal mixture, a^c will be given by

$$a_m{}^c = 4.7RT_\varphi{}^cV_m^* \quad (10)$$

where $T_\varphi{}^c$ is the pseudo-critical temperature. The meaning of V_m^* is considered below.

Kreglewski and Kay[14] have achieved very satisfactory results by expressing $T_\varphi{}^c$ as a function of pair interactions per equivalent surface ϵ_{ii}, ϵ_{jj}, and ϵ_{ij}, and the surface fractions

$$\varphi_i = N_i(V_i^*)^{2/3}/\sum_{k=1}^{m} N_k(V_k^*)^{2/3}$$

where

$$\frac{\epsilon_{ii}}{\epsilon_{jj}} = \frac{T_i{}^c}{T_j{}^c}\left(\frac{V_j^*}{V_i^*}\right)^{1/3}; \frac{T_\varphi{}^c}{(V_x^*)^{1/3}} = \sum_i\sum_j \frac{T_{ij}{}^c}{(V_{ij}^*)^{1/3}}\varphi_i\varphi_j \quad (11)$$

and

$$(V_x^*)^{1/3} = \sum_{i=1}^{m}(V_i^*)^{1/3}x_i \quad (12)$$

In order to secure the agreement with critical state of mixtures, relations 11 are retained, but two different approximations are used for V_m^*.

Method B. In accordance with eq 7 and denoting V_m^* by V_B^* for this case

TABLE I: Comparison of Calculated and Observed Values of the Excess Functions for Equimolar Binary Mixtures

No.	V_2^*/V_1^*	System	T, K	Method A γ	Method A G^E, J mol^{-1}	Method A H^E, J mol^{-1}	Method A I^E, cm^3 mol^{-1}	Method B γ	Method B G^E, J mol^{-1}	Method B H^E, J mol^{-1}	Method B V^E, cm^3 mol^{-1}	Observed values G^E, J mol^{-1}	Observed values H^E, J mol^{-1}	Observed values V^E, cm^3 mol^{-1}
1	3.54	Methane + 2-methylpentane	115.8	0.980	(310)	270	−0.64	0.960	(310)	20	−3.85	310[a]		−1.1[a]
		Methane + 2-methylpentane	155	0.980	350	10[b]	−4.11	0.960	430	−150	−7.39			−3.6[a]
2	3.48	Cyclopentane + octamethylcyclotetrasiloxane	298.15	1.0716	(−208)	480	0.07[c]	1.074	(−208)	130	−8.10	−208[d]	212[d]	0.046[d]
3	2.55	*n*-Hexane + *n*-hexadecane	293.15	1.0036	(−65)	160	1.13	1.0018	(−65)	−80	−3.98	−65[e]	129[e]	−0.48[f]
		n-Hexane + *n*-hexadecane	333.15	1.0036	−90	90	0.96	1.0018	−60	−110	−4.25	−84[e]	10[e]	−0.97[f]
		n-Hexane + *n*-hexadecane	373.15	1.0036	−100	−20	0.09	1.0018	−50	−180	−5.20		−96[g]	
4	2.00	Methane + propane	100	0.996	(190)	140	−0.45	0.991	(190)	65	−1.20	190[h]	113[h]	
5	1.96	2,2,4-Trimethylpentane + *n*-hexadecane	293.15	1	−20	90	0.60	1	−40	−70	−2.44	0[i]	230[i]	−0.49[j]
6	1.92	*n*-Hexane + *n*-dodecane	293.15	1	−20	70	0.45	1	−30	−60	−1.77	−25[k]	46[l]	−0.31[m]
7	1.58	*n*-Decane + *n*-hexadecane	293.15	1	10	100	0.46	1	0	20	−1.09		42[i]	−0.07[m]
8	1.55	Cyclopentane + cyclooctane	298.15	1	0	−10	−0.14	1	0	−70	−0.79	2[o]	−40[o]	−0.283[o]
9	1.39	Argon + methane	91	1	10	0	−0.11	1	10	−10	−0.20	74[n]	103[p]	0.17[p]
10	1.31	Argon + krypton	115.77	1	70	−10	−1.03	1	70	−10	−1.09	84[q]		−0.53[q]
11	1.21	*n*-Pentane + *n*-hexane	298.15	1	−10	0	−0.01	1	−10	−10	−0.13	−37[r]		−0.109[r]
12	1.19	Carbon monoxide + methane	91	1	100	70	−0.75	1	100	70	−0.77	115[s]	107[s]	−0.32[s]
13	1.17	Argon + carbon monoxide	83.82	1	40	60	−0.13	1	40	50	−0.15	57[q]		0.099[q]
14	1.16	Oxygen + nitrogen	83.82	1	70	90	−0.33	1	70	90	−0.34	38[t]	42[t]	−0.313[t]
15	1.16	Cyclohexane + *n*-hexane	293.15	1	90	140	−0.23	1	90	130	−0.30	70[u]	220[u]	0.10[v]
16	1.14	Argon + nitrogen	83.82	1	50	70	−0.26	1	50	70	−0.27	34[t]	51[t]	−0.178[t]
17	1.03	Nitrogen + carbon monoxide	83.82	1	0	0	−0.02	1	0	0	−0.02	23[t]		0.1[t]
18	1.02	Oxygen + argon	83.82	1	0	0	0	1	0	0	0	37[t]	60[t]	0.14[t]
19	1.01	3-Methylpentane + *n*-hexane	298.15	1	0	0	0	1	0	0	0	21[r]		−0.068[r]
20	1.01	2,3-Dimethylbutane + *n*-hexane	298.15	1	0	0	−0.01	1	0	0	−0.01	−4[r]		−0.041[r]
21	1.00	2-Methylpentane + *n*-hexane	298.15	1	0	0	−0.01	1	0	0	−0.01	30[r]		−0.054[r]
22	1.00	2,2-Dimethylbutane + *n*-hexane	298.15	1	0	0	−0.05	1	0	0	−0.05	−10[r]		−0.051[r]
23	1.00	Neopentane + cyclohexane	273.15	1	220	220	−1.30	1	220	220	−1.30	184[w]		−1.1[w]

[a] See ref 11. [b] H^E is negative in methane rich mixtures (system 1). [c] V^E is negative in cyclopentane rich mixtures in agreement with experimental data[d] (system 2). [d] K. N. Marsh, *J. Chem. Thermodyn.*, **2**, 359 (1970). [e] M. L. McGlashan and A. G. Williamson, *Trans. Faraday Soc.*, **57**, 588 (1961); M. L. McGlashan and K. W. Morcom, *ibid.*, **57**, 581 (1961). [f] M. Diaz Peña and M. Benitez de Soto, *An. Real Soc. Espan. Fis. Quim. Ser. B*, **61**, 1163 (1965). [g] J. A. Friend, J. A. Larkin, A. Maroudas, and M. L. McGlashan, *Nature*, **198**, 683 (1963). [h] A. J. B. Cutler and J. A. Morrison, *Trans. Faraday Soc.*, **61**, 429 (1965). [i] J. H. van der Waals and J. J. Hermans, *Rec. Trav. Chim. Pays-Bas*, **69**, 949, 971 (1950). [j] J. H. van der Waals, *Trans. Faraday Soc.*, **52**, 916 (1956). [k] J. N. Brønsted and J. K. Koefoed, *Kgl. Dan. Vidensk. Selsk. Mat. Fys. Medd.*, **22**, 1 (1946). [l] J. H. van der Waals, *Rec. Trav. Chim. Pays-Bas*, **70**, 101 (1951). [m] A. Desmyter and J. H. van der Waals, *Rec. Trav. Chim. Pays-Bas*, **77**, 53 (1958). [n] J. C. G. Calado and L. A. K. Staveley, *J. Chem. Phys.*, **56**, 4718 (1972). [o] M. B. Ewing, B. J. Levien, K. N. Marsh, and R. H. Stokes, *J. Chem. Thermodyn.*, **2**, 589 (1970). [p] F. Sprow and J. M. Prausnitz, *A.I.Ch.E.J.*, **12**, 780 (1966); V. Mathot, *Nuovo Cimento*, **9**, 356 (1958); M. Lambert and M. Simon, *Physica Utrecht*, **28**, 1191 H. Stokes, A. G. Duncan and L. A. K. Staveley, *Trans. Faraday Soc.*, **62**, 519, 548 (1966); R. H. Davies, A. G. Duncan, G. Saville, and L. A. K. Staveley, *ibid.*, **63**, 855 (1967); *Nature*, **209**, 1236 (1966). [r] S.-S. Chen and B. J. Zwolinski, submitted for publication. [s] R. A. H. Pool and L. A. K. Staveley, *Trans. Faraday Soc.*, **53**, 1186 (1957). [t] R. A. H. Pool, G. Saville, T. M. Herrington, B. D. C. Shields, and L. A. K. Staveley, *Trans. Faraday Soc.*, **58**, 1692 (1962). [u] V. Mathot, *Bull. Soc. Chim. Belg.*, **59**, 111 (1950); A. R. Mathieson and J. C. Thynne, *J. Chem. Soc.*, 3708 (1956). [v] H. Klapproth, *Nova Acta Leopold.*, **9**, 305 (1940), quoted by Rowlinson, ref 16. [w] V. Mathot and A. Desmyter, *J. Chem. Phys.*, **21**, 782 (1953).

$$V_B^* = \sum_i \sum_j V_{ij}^* x_i x_j \quad (13)$$

and

$$a_m{}^c = 4.7RT_\varphi{}^c V_B^* \quad (14)$$

These relations and eq 5 and 6 were used to obtain the results given in Table I (method B).

Method A. As mentioned above, the van der Waals approximation (7 or 13) yields volume contractions upon mixing that are much too large. A better approximation for V_m^* that conforms more closely for hard spheres to the exact Lebowitz's relations is, after inserting into eq 10

$$a_m{}^c = 4.7R(V_B^*)^{2/3}\left[\sum_{i=1}^{m}(V_i^*)^{2/3}x_i\right]\left[\sum_i\sum_j \frac{T_{ij}{}^c}{(V_{ij}^*)^{1/3}}\varphi_i\varphi_j\right] \quad (15)$$

where V_B^* is given by eq 13. Equation 15 was coupled with eq 2-4 of method A and the results are given in Table I (method A).

The excess functions are evaluated as follows. The pressure in eq 1 is set equal to $P_0 = 0$, *i.e.*, the high density of the fluid is achieved by intermolecular attraction alone. V_m or V_i^0 is then given by the relevant root of eq 1, found by an iteration. The excess volume

$$V^E = V_m - \sum_{i=1}^{m} V_i{}^0 x_i$$

The deviations of $A_m{}^h$ from additivity are very small, and it is a good approximation to assume that they are the same for hard spheres in the absence of attraction (high P) as in its presence ($P_0 = 0$). However, A^{id} changes considerably as the volume of the perfect gas varies from V_m to RT/P_0 for the mixture and from V_i^0 to RT/P_0 for the pure components. Thus, the excess Helmholtz energy of the mixture of hard spheres at T and P_0

$$\left(\frac{A^{Eh}}{RT}\right)_p = \frac{A_m{}^{rh}}{RT} - \ln V_m - \sum_{i=1}^{m}\left(\frac{A_i{}^{rh}}{RT} - \ln V_i{}^0\right)x_i \quad (16)$$

where $A_m{}^{rh}$ and $A_i{}^{rh}$ are given by eq 4 and 6.

The excess function due to attraction is

$$\left(\frac{A^{Ea}}{RT}\right)_p = -\frac{a_m{}^c}{RTV_m} + \sum_{i=1}^{m}\frac{a_i{}^c x_i}{RTV_i{}^0} \quad (17)$$

where $a_m{}^c$ and $a_i{}^c$ are the values of a^c for the mixture and the pure components, respectively. The total excess function

$$(A^E)_p = (A^{Eh})_p + (A^{Ea})_p \quad (18)$$

and the excess Gibbs energy of mixing at constant P and T

$$G^E = (A^E)_p + P_0V^E = (A^E)_p \quad (19)$$

at $P_0 = 0$.

If σ and $a(T)$ are independent of the temperature, the excess enthalpy is

$$H^E = (A^{Ea})_p \quad (20)$$

given by eq 17. The relative variation of σ with the temperature is similar for different substances and should not be a source of errors in H^E. However, the variation of $a(T)$ may be very different for the components if $T_i{}^c \gg T_j{}^c$ (or rather, $|\bar{u}_{ii}| \gg |\bar{u}_{jj}|$) and part of the errors in H^E and V^E may be attributed to the assumption that $a(T) = a^c$ is independent of the temperature.[16]

The polarizability of the molecules which interact through London forces alone is a linear function of V^0 or V^*.[15] The known London formula simplifies for ϵ_{ij} (per equal $(V^*)^{2/3}$) to the harmonic mean rule

$$\epsilon_{ij} = 2\gamma[(1/\epsilon_{ii}) + (1/\epsilon_{jj})]^{-1} \quad (21)$$

where for a mixture of inert liquids $\gamma = 1$. The use of the ϵ's and the surface fractions is limited to the evaluation of $T_\varphi{}^c$ in eq 14 or 15.

Discussion

The systems are arranged in the order of decreasing size differences of the components where $V_1^* \leq V_2^*$. For $V_2^*/V_1^* > 2$, the value of γ was adjusted to fit the observed value of G^E at $x = 0.5$, and the asymmetry of the functions was studied more closely (Figure 1).

For systems 1 to 4, method B gives values that are much too low for V^E and, consequently, also H^E, whereas method A is much more satisfactory except for systems 3, 6, and 7, where V^E and H^E are too high. We have no satisfactory explanations for the low value of γ required for system 1. However, by considering method A only, it is possible to explain why $\gamma > 1$ for systems 2 and 3. The value of $H^E = 480$ J/mol (system 2) is very close to that calculated by Marsh[4b] by using the method of Snider and Herrington. The observed value of H^E and the excess entropy S^E is much lower. If S^E may be considered a measure of order in a mixture, the disk-like species tend to be ordered parallel at low T and high density of the fluid. The effective $|\epsilon_{22}|$ of OMCTS at this T is much larger than the value of T^c suggests (calculated from T^c it is much smaller than $|\epsilon_{11}|$ of cyclopentane). This error in ϵ_{22} is "corrected" by assuming $\gamma > 1$. At the critical point most of the order vanishes and T^c calculated for $\gamma = 1$ by the method of Kreglewski and Kay[14] conforms to the experimental data[17] (Figure 1). We exclude the possibility of any specific interactions between an alkane and a siloxane (as an explanation for $\gamma > 1$) because it is known that alkanes do not interact specifically with even very strong electron donors or acceptors. The ordering effects are also noticeable for mixtures of chain molecules (systems 3, 6, and 7), though to a lesser extent.

For systems with $V_2^*/V_1^* < 2$, calculations were made assuming $\gamma = 1$. For all these systems the agreement between the calculated and the observed T^c, for $\gamma = 1$, is very satisfactory[14,15] (the validity of the relations for T^c is limited to $\bar{u}_{22}/\bar{u}_{11} \leq 2$ and depends less on V_i^* of the components). The excess functions are more sensitive to errors in ϵ's, and the agreement cannot be expected to be better than ±30 J/mol. We note that for this group of systems, the simple theory of conformal mixtures gives similar results.[15] Two of the systems, 9 and 18, deviate more than "allowed," both with argon as a component. Perhaps the value of ϵ is incorrect, or the deviation is due to a very slight tendency of argon to form Ar_2, and the proper value of γ at low temperatures is less than unity.

For $V_2^*/V_1^* < 1.5$, the results by the two methods are practically identical. If $V_1^* = V_2^*$ but $\epsilon_{11} \neq \epsilon_{22}$, the excess volume is always negative and decreases with increasing differences in ϵ of the components. Thus, system 23 is not an exception, as it was believed earlier, but rather follows a rule.

We note that, except systems 2 and 5, wherever the calculated value of V^E is approximately correct, the value of H^E is also satisfactory. The errors in V^E range from about

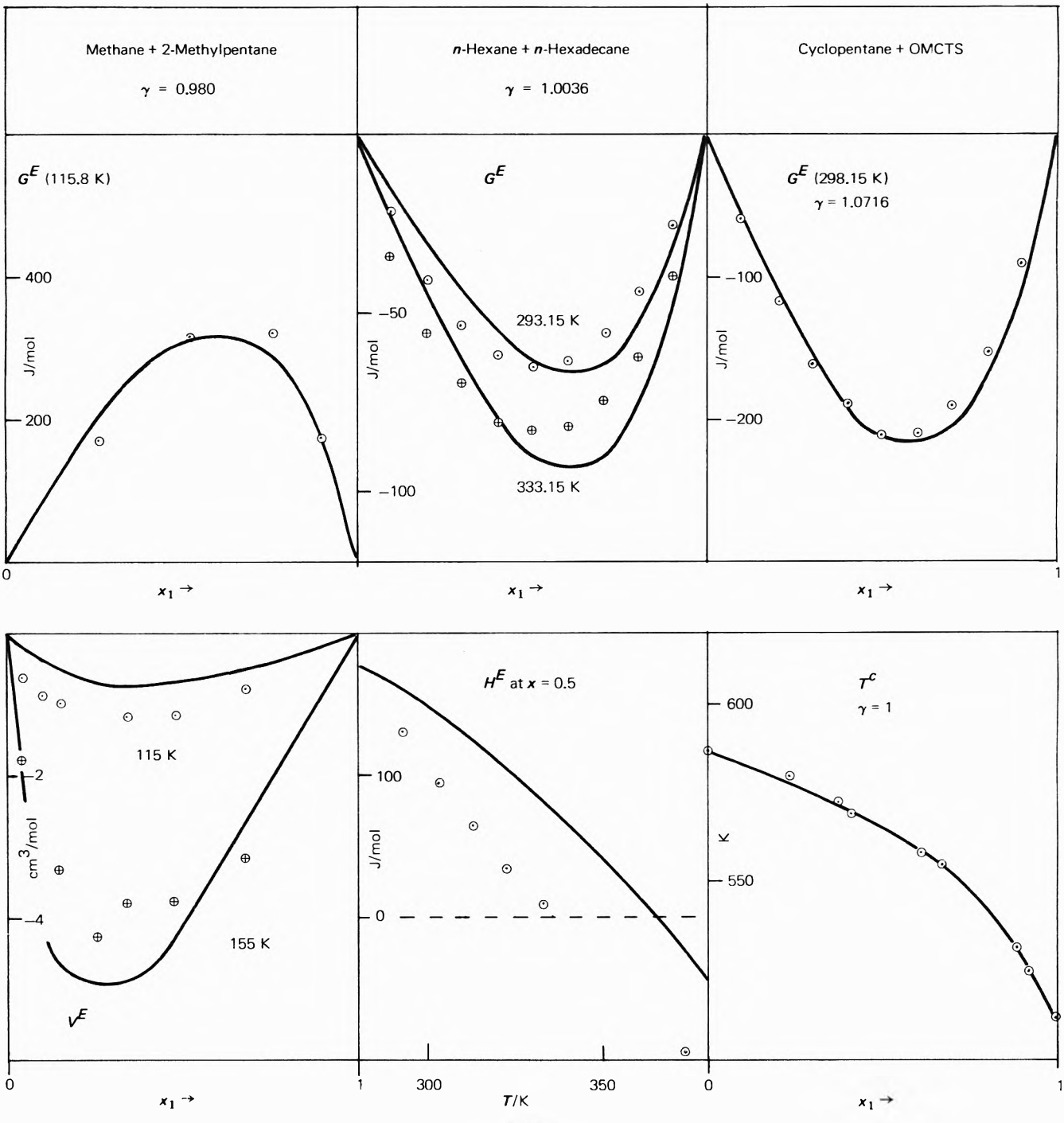

Figure 1. The excess functions for three binary systems (OMCTS = octamethylcyclotetrasiloxane). x_1 is the mole fraction of the first component of each pair. The curves were calculated by method A. The references to the experimental points are given under Table I. For the T^c data of the third system, see ref 17.

±0.05 cm³/mol (if $V_1^* \approx V_2^*$) to about ±0.3 cm³/mol (if $V_2^*/V_1^* > 2$), and one of the reasons is that the ratio $b = (1/6)\pi N_0 \sigma^3/V^*$ is only approximately constant (0.434 in eq 9). If the "packing factors" b would be evaluated for each system separately by iteration to fit the observed V_1^0, V_2^0 (b_1 and b_2, respectively), and V_m (b_{12} in a simple quadratic formula), most of the errors in the values of H^E could be eliminated.

In conclusion we may state that method A permits prediction of reasonably accurate liquid-vapor equilibriums and critical constants of mixtures from the properties (T^c and V^*) of the pure components alone, if the size differences of the components are not too large. If either of the ratios $\tilde{u}_{ii}/\tilde{u}_{jj}$ or V_i^*/V_j^* exceeds 2, the value of γ must be adjusted to fit one of the properties of the mixture even if the components are inert solvents.

Acknowledgment. This investigation was supported in part by the Thermodynamics Research Center Data project of the Thermodynamics Research Center and the Texas Engineering Experimental Station of Texas A&M University.

References and Notes

(1) N. S. Snider and T. M. Herrington, *J. Chem. Phys.*, **47**, 2248 (1967).
(2) T. W. Leland, Jr., J. S. Rowlinson, and G. A. Sather, *Trans. Faraday Soc.*, **64**, 1447 (1968).
(3) D. Henderson and J. A. Barker, *J. Chem. Phys.*, **49**, 3377 (1968); P. J. Leonard, D. Henderson, and J. A. Barker, *Trans. Faraday Soc.*, **66**, 2439 (1970).
(4) (a) K. N. Marsh, M. L. McGlashan, and C. Warr, *Trans. Faraday Soc.*, **66**, 2453 (1970); (b) K. N. Marsh, *J. Chem. Thermodyn.*, **3**, 355 (1971).
(5) R. C. Miller, *J. Chem. Phys.*, **55**, 1613 (1971).
(6) B. L. Rogers and J. M. Prausnitz, *Trans. Faraday Soc.*, **67**, 3474 (1971).
(7) G. A. Mansoori and T. W. Leland, Jr., *J. Chem. Soc., Faraday Trans. 2*, 320 (1972).
(8) A. Kreglewski, R. C. Wilhoit, and B. J. Zwolinski, *J. Chem. Eng. Data*, in press.
(9) G. A. Mansoori, N. F. Carnahan, K. E. Starling, and T. W. Leland, Jr., *J. Chem. Phys.*, **54**, 1523 (1971).
(10) J. L. Lebowitz, *Phys. Rev. A*, **133**, 895 (1964).
(11) A. J. Davenport, J. S. Rowlinson, and G. Saville, *Trans. Faraday Soc.*, **62**, 322 (1966).
(12) A. Kreglewski, *J. Phys. Chem.*, **72**, 1897 (1968).
(13) J. O. Hirschfelder, C. F. Curtiss, and R. B. Bird, "Molecular Theory of Gases and Liquids," Wiley, New York, N. Y., 1954.
(14) A. Kreglewski and W. B. Kay, *J. Phys. Chem.*, **73**, 3359 (1969).
(15) A. Kreglewski, "Mixtures of Fluids," API44—TRC Publications in Science and Engineering, Thermodynamics Research Center, Texas A&M University, College Station, Texas, 1973.
(16) J. S. Rowlinson, "Liquids and Liquid Mixtures," Butterworths, London, 1959; see the theory of non-central forces and *Mol. Phys.*, **7**, 349 (1964); 8, 107 (1964).
(17) C. P. Hicks and C. L. Young, *Trans. Faraday Soc.*, **67**, 1598 (1971).

Electrolytic Conductance in Isodielectric Mixtures of Polystyrene and Diphenylmethane

James E. Scheirer and Walter Dannhauser*

Department of Chemistry, State University of New York at Buffalo, Buffalo, New York 14214 (Received May 3, 1973)

Publication costs assisted by the Petroleum Research Fund

The equivalent conductance of $(n\text{-Bu})_4$NSCN has been measured as a function of electrolyte concentration (10^{-5}–10^{-2} *m*) in solvents comprising 0–71% (weight) polystyrene in the temperature range 70–100°. The solvent viscosity varied from 10^{-2} to 10^{5} P. For solvents with per cent polymer < 50 ($\eta < 10^3$ P), the data are sufficiently precise to show that Λ exhibits a minimum which depends on temperature, dielectric constant, and also on viscosity. Walden's rule is inapplicable even as a crude approximation, the ionic mobility decreasing much less rapidly than the viscosity increases. The mobility is discussed in terms of a free-volume-dependent friction coefficient. Electrolyte solution theory appears entirely adequate to account for electrical conductance in amorphous polymeric systems.

Introduction

The basic equation for electrical conduction is

$$\kappa = \Sigma_j n_j e_j u_j \qquad (1)$$

where κ is the specific conductance (mho/cm), n_j is the number density of charge carriers of the jth type (cm^{-3}) carrying charge e_j (coulombs) with mobility u_j (cm^2/V sec). In amorphous or partly crystalline organic polymers, a commercially important class of electrical insulators, the charge carriers at low applied electric field are probably adventitious ions originating from impure monomers and plasticizers and various polymerization catalysts. Despite the practical importance of such highly viscous electrolyte solutions, there has never been a careful study of electrolytic conduction in amorphous polymeric systems.[1]

In a previous paper,[2] we reported results of experiments on the electrolytic conductance of $(n\text{-Bu})_4$NSCN in amorphous polystyrene (PS) plasticized with 20% by weight of diphenylmethane (DPM). These components form nearly isodielectric mixtures over the entire range of composition. For example, at 70°, $\epsilon = 2.51 \pm 0.04$ and at 100° $\epsilon = 2.48 \pm 0.03$. The equivalent conductance was orders of magnitude greater than predicted by Walden's rule. Also, it apparently decreased with increasing electrolyte concentration over the entire range measured (10^{-4}–10^{-1} *m*). This is contrary to the expected behavior in a solvent of low dielectric constant and we rationalized the observation on the basis of a hydrodynamic argument; we proposed that the mobility of triple ions and higher-aggregate ions was vanishingly low in such an extremely viscous solvent so that, insofar as transport of charge was concerned, the electrolyte effectively consisted only of ions and ion pairs.

However, very little is really known about the effect of enormously high viscosity on electrolytic conduction and it was conceivable that the electrolyte solution theory of Debye, Onsager, Fuoss, etc., which works so well in fluid solvents, might need to be altered in a fundamental qualitative manner for highly viscous systems. Furthermore, our previous experiments were not unambiguous; because the conductance was so very low, we had to utilize dc techniques and these were plagued with interference from polarization processes. We proposed that the principal one of these was due to dielectric relaxation of the solvent and consequently utilized the steady-state (infinite time) leakage currents as the basis of our calculations and discussion. This point of view has been challenged; [3] it was sug-

gested that the instantaneous (zero-time) current be used as the intrinsic measure of bulk transport of charge as, for example, in aqueous electrolytes. Since the two limiting currents may differ by orders of magnitude, there certainly was room for conjecture about the results.

In the previous paper, we proposed a test of the hydrodynamic interpretation, namely, measurement of equivalent conductance as a function of electrolyte concentration in solvents ranging from pure diphenylmethane to (ultimately) pure polystyrene. Conductance experiments in a fluid solvent such as diphenylmethane should be relatively routine; sample preparation can be precise and the conductance presumably would be large enough to measure by well-established unambiguous ac techniques. The results could then be compared with those of conductance experiments in other fluid solvents of similar, low, dielectric constant and with the predictions of well-tested theory. Incremental changes of solvent composition would then permit (hopefully) a confident extrapolation of experimental results and their interpretation to the 80% polymer range and beyond.

We report the results of such an investigation in this paper.

Experimental Section

Materials. Diphenylmethane (Matheson Coleman and Bell reagent grade) was vacuum factionated from activated alumina. The specific conductance of freshly distilled DPM was about 10^{-14} mho/cm at 70° which compares favorably with Sharbaugh's results.[4]

The polystyrene was from the same sample employed previously.[2] It is thermally polymerized, has a $\overline{DP} \approx 1200$, and contains extremely small amounts of metallic impurities.

The electrolyte was $(n\text{-Bu})_4$NSCN, prepared according to Copenhafer and Kraus' method.[5] The salt was recrystallized repeatedly from benzene and then dried in a vacuum oven. Its melting point was 124–125°; Copenhafer and Kraus report 126.4–126.9°.

Instrumentation. For the dc conductance measurements, we used virtually the same apparatus and techniques described by Price and Dannhauser.[2] The input resistors of the General Radio Type 1230A electrometer were calibrated against the instrument's internal standards and we feel confident that the dc conductance is accurate to better than 1%.

Two ac bridges were utilized. A General Radio Type 1615A bridge was used for $f > 500$ Hz. The conductance accuracy claimed by the manufacturer is about 1%, which is more than adequate for our purpose. For the ultra-low-frequency range, 0.01–20 Hz, we used a greatly simplified version of Berberian and Cole's capacitance–conductance bridge.[6] Because the bridge is designed for three-terminal measurements, the conductance standards are delta networks in which none of the constituent resistors need be greater than 10^9 ohms (available[7] in ±1% tolerance) in order to obtain an effective "high-to-low" full-scale conductance as low as 10^{-13} mho. A shielded 10^{13}-ohm Victoreen High-Meg resistor was intercompared from time to time with the dc electrometer and the ulf bridge operating at 1 Hz, always with good agreement.

For the less viscous solutions, Balsbaugh[8] Type 2N50 or 2N25 concentric cylinder, two-terminal conductance cells were used. The cell constant of each electrode assembly in the appropriate jacket, about 500 or 250 cm, respectively, was determined precisely from the measured capacitance of each cell when filled with standard dielectric fluids such as air, *n*-hexane, and cyclohexane. The conductance cell was immersed in a vigorously stirred oil bath whose temperature was regulated to ±0.1° by a proportional temperature regulator. A thermocouple well was situated close to the electrode assembly to permit precise temperature monitoring. Repeatability of sample test temperatures to 0.1° was routine.

For the very viscous 71% PS solutions, Price's[2] parallel-plate conductance cell was used. The cell constant was calculated from the electrode geometry (very thin samples minimized fringing errors) and verified by capacitance measurements with standard fluids. Also, some conductance measurements of 50% PS samples were performed in both types of cells in order to maintain internal consistency. While temperature constancy to ±0.1° was feasible during any one run with the parallel-plate cell, repeatability of a test temperature from run to run was difficult. Therefore, for the 71% PS system we made measurements as close to the four fixed test temperatures as possible and then corrected for the inevitable small temperature difference by means of the well-established temperature coefficient of conductance.

The viscosity of the 0–30% PS solvent ($\eta < 30$ P for $t > 70°$) was measured with calibrated Cannon-Fenske[9] capillary viscometers. The viscosity of the 40 and 50% solvents was obtained by falling-ball viscometry in precision-bore tubes of 1 cm diameter. The ratio of ball diameter to tube diameter was always less than 0.02, so that corrections for wall effects[10] were negligible. The viscosity of 65 and 71% PS solvents was also measured by a falling-ball technique but with considerable less precision because of severe sample size limitations. The shear viscosity (poise) was taken to equal the kinematic viscosity (stokes) which is obtained from the falling-ball experiments. The density of diphenylmethane is 1.003 at 25°[4] and at this temperature we determined that the density of the polymer solutions increased very slightly and linearly with polymer concentration for 1–30% PS. Because the density of amorphous PS is slightly greater than 1.0, we believe that the error incurred by assuming the density of the solutions to be 1.0 in the interval 70–100° is small compared to the overall precision of the viscometry experiments with the most viscous solutions.

Procedure. For the pure DPM solvent runs, stock solutions of $(n\text{-Bu})_4$NSCN in DPM were prepared by weight. By means of a weight buret, aliquots of this solution were added to weighed amounts of DPM already in the conductance cell. Up to six data points could be obtained for a single solvent loading of the cell. The capacitance and conductance was measured as a function of frequency at 70.0, 80.0, 90.0, and 100.0°.

For the 20 and 30% PS solutions, appropriately weighed amounts of PS and DPM were mixed to prepare the "solvent." Stock solutions of $(n\text{-Bu})_4$NSCN in this solvent were prepared by weight and were subsequently added, by weight, to solvent in the conductance cell. For the 0–30% PS solutions, the conductance cell was fitted with a stirrer to ensure thorough mixing and temperature uniformity. Electrical measurements were performed as a function of frequency and temperature.

The 40 and 50% PS solvents were so viscous, and PS sample limitations precluded preparation of large amounts of solvent, that a different technique was used. *Each* sample was prepared separately; the appropriate amount of PS, DPM, and salt was added by weight to a

small flask containing a Teflon-covered magnetic stirring bar. The flask was stoppered, attached to the shaft of a 6-rpm motor, and rotated for several days between the poles of a powerful magnet while simultaneously being heated to about 80° with a heat lamp. This procedure facilitated thorough mixing; all the solutions appeared homogeneous at $t > 70°$, but upon cooling to room temperature some of the solutions became definitely cloudy, this being most noticeable for the 50% PS system. Upon reheating to $t > 70°$, the turbidity always disappeared. [It is evident, however, that the solubility of $(n\text{-Bu})_4$NSCN decreases as the concentration of PS increases. The solubility of $(n\text{-Bu})_4$NSCN in benzene is >1 M[11a] at 25°, but we find it to be less than 0.012 M in pure DPM. The apparent further decrease in solubility with added PS raises serious doubts about the homogeneity of solution for which the per cent PS → 100, even for $t > 70°$.] The flask containing the thoroughly mixed solution was attached to the conductance cell jacket, tilted, and placed under the heat lamp so that the sample slowly flowed into the jacket. At this temperature the solutions were fluid enough that adventitious bubbles from the stirring and pouring disappeared easily, resulting in a homogeneous, crystal clear test solution. The mixing flask was removed from the cell jacket and the electrode assembly was inserted quickly into the cell. Conductance experiments at the four test temperatures were then carried out, but the solutions could not be agitated to hasten and ensure thermal equilibration.

The 71% PS solutions are much too viscous to prepare by this method. Attempts to use Price's method[2] of evaporating the appropriate amount of DPM into a freeze-dried PS-electrolyte matrix failed, presumably because the sample is not self-supporting at *ca.* 50° (this elevated temperature had been used by Price to speed the absorption-diffusion process) and the method is too slow to be practical at room temperature. We finally settled on the following technique: a 50% PS sample was made as described above and about 2 g of the sample was weighed into a Petri dish. This was placed into a vacuum oven at *ca.* 60° where the sample flowed to form a thin layer. The sample weight was monitored until a solution of 71% PS was obtained. These samples (of leathery consistency at room temperature) were repeatedly cut into small pieces which were then pressed between warm ferro-type plates in an attempt to ensure sample homogeneity. The samples were stored in sealed containers until they were put in the parallel-plate conductance cell. At $t > 60°$, under pressure of the electrode assembly, the samples flowed to fill the electrode gap. At the test temperatures the solutions had the consistency of old rubber cement and stuck tenaciously to the polished electrodes. After a run was completed, the cell was dismantled and the electrode assembly, with the sample still in place, was cooled to *ca.* −70°. At this temperature the samples were brittle and could usually be removed nearly intact from between the electrodes. The sample thickness was then micrometered to check that the electrode separation had been uniform (0.025 cm) and that the sample had indeed filled the entire interelectrode volume.

Results

For the 0–50% PS solutions the sample conductance and capacitance was essentially independent of frequency from dc to 10 kHz in the temperature interval 70–100°. We report the 1-kHz results since the GR 1615A bridge appears most reliable there. For these solutions the solvent conductance was always less than 2% that of the solution, usually considerably less. In Table I[11b] we report our principal results: equivalent conductance of $(n\text{-Bu})_4$NSCN as a function of concentration, temperature, and solvent composition. The viscosity and dielectric constant of the solvent are tabulated in Table II.[11b]

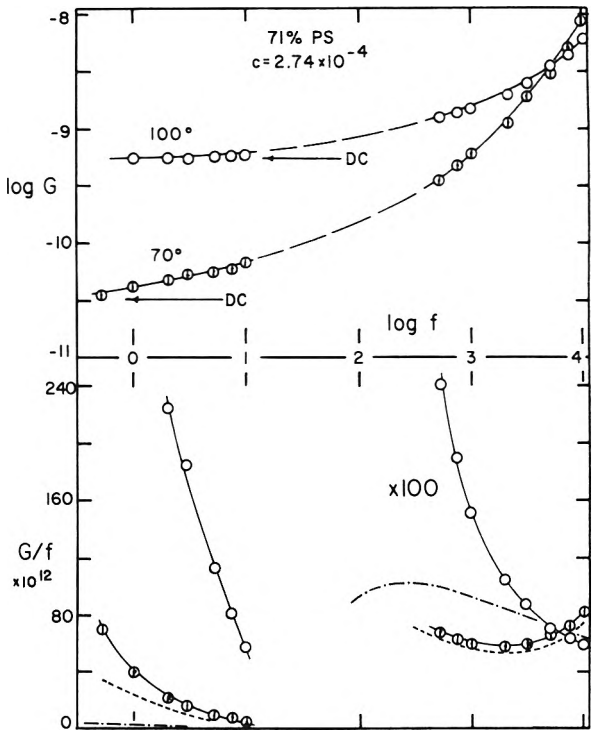

Figure 1. Top: logarithm of sample conductance (mhos) at two temperatures as a function of logarithm of test frequency (Hertz). The arrows marked DC are the steady-state dc conductance values. Note that the conductance curves cross at high frequencies. Bottom: conductance/frequency (mhos/Hertz) as a function of the logarithm of the test frequency. The ordinate is expanded 100 times for log $f > 2$. Note that the 70° isotherm goes through a minimum. The short-dash line refers to an 80% PS–20% DPM solvent (c = 0) sample at 100°; this curve has a well-defined maximum at log $f = 4.7$. The dot-dash line refers to the same 80% PS sample at 70°.

The conductance of the 71% PS solutions, and of pure 71% PS solvent also, increased rapidly with increasing frequency for $f > 0.5$ kHz, the frequency dependence being most pronounced at the lower temperatures. There was a concomitant slight decrease of the capacitance. The availability of the ulf bridge permitted extrapolation of the conductance to $f < 1$ Hz and, as illustrated in Figure 1, this low-frequency asymptote equaled the steady-state dc conductance. The dc conductance was slightly time dependent; application of the voltage resulted in a transient current which attained a steady-state value within a few seconds. This time dependence was most evident at the lower temperatures and is similar to that previously reported[2] for 80% PS–20% DPM samples but is not nearly so pronounced either in its magnitude or in its duration. The present results substantiate our previous contention that the steady-state dc conductance in these samples is truly a measure of charge transport in the bulk of the sample and is not distorted because of electrode polarization processes.

In fact, as indicated by the curves of Figure 1, it is absolutely necessary to extrapolate ac measurements in

these very viscous solutions to *zero* frequency rather than to infinite frequency as in conventional conductance measurements. Alternatively, dc measurements must be extrapolated to *infinite* time, *i.e.*, steady-state values most conveniently obtained for long-lived transients by the charge-discharge technique, rather than to zero time as in conventional studies. The reason for the difference in the extrapolation is due to the different nature of the phenomenon interfering with the conductance measurement. In conventional experiments, various, primarily capacitative, electrode impedances[12] are eliminated by extrapolation to infinite frequency where their impedance is negligible compared to the resistance of the solution. In our experiments the interference is undoubtedly due to the dielectric relaxation of the solvent, as is illustrated by the G/f curves in Figure 1. As the solvent becomes increasingly viscous, either as a result of decreasing the temperature and/or increasing the polymer concentration, the dielectric relaxation process moves to progressively lower frequencies and completely masks the contribution from the intrinsic conduction process. The well-known superposition of time, temperature, and composition is illustrated by the 71% PS data at 70° which virtually coincide with the 80% PS data at 100°.

We believe that such interference will be universal, irrespective of the nature of the "solvent," since there is no such thing as a nonpolar highly viscous solvent. And while the dielectric loss of a "nonpolar" material like polystyrene or diphenylmethane is very small, it nevertheless corresponds to a conductance which is high compared to the true steady-state dc value.

Thus, the reported[13] "break" in conductance–temperature curves at the glass-transition temperature is probably due, not to any essential change in the ionic conduction process as $T \rightarrow T_g$, but to the fact that an entirely different phenomenon (the dielectric relaxation of the solvent) is being measured.

To summarize: in order to measure the intrinsic ionic conductance of a highly viscous sample, it is necessary to make the measurements at $f \ll f_{max}$ (dielectric relaxation) and to extrapolate to $f \rightarrow 0$. But the temperature dependence of the relaxation process near T_g is usually very large so it quickly becomes prohibitively tedious to extend the conductance experiments to the required long times as $T \rightarrow T_g$.

While the specific conductance[14] of the 71% PS solvent (*ca.* 1×10^{-14} mho cm^{-1} at 70°; 1×10^{-13} at 100°) was only slightly lower than that of the 50% PS solvent (6×10^{-14} at 70; 2×10^{-13} at 100°), the specific conductance of 71% PS solutions was relatively much less than that of 50% PS solutions of the same electrolyte concentration. Indeed, the conductance of the solutions was so depressed on going from 50 to 71% PS that it became impossible to make meaningful measurements with $c < 3 \times 10^{-4}$; the relatively ill-defined solvent corrections were already 15% or more at that concentration. This unfortunately high lower limit to the electrolyte concentration, the questionable homogeneity of the more concentrated solutions and our inability to reproduce the solvent composition precisely from sample to sample (see Procedure section), and the lower precision of the parallel-plate cell constant determination, all conspire to preclude a detailed analysis of the 71% PS solution conductance data. We report results for the more dilute solutions in Table III[11b] but emphasize that they are very much less significant than the data for the 0–50% PS solutions.

Because the melting point of $(n\text{-Am})_4$NSCN is 50.5°,[11a] well below our test temperatures, we hoped that this salt would be more soluble than $(n\text{-Bu})_4$NSCN in our solvents, especially in 71% PS. Our expectation seems ill founded; while $(n\text{-Am})_4$NSCN seems quite soluble in pure DPM (>1 *M*), its solubility apparently decreases with increasing polymer concentration so that the homogeneity of 50% PS having $c > 5 \times 10^{-3}$ is questionable. The conductance of the most dilute $(n\text{-Am})_4$NSCN–71% PS solutions we studied is similar to that of $(n\text{-Bu})_4$NSCN solutions of the same concentration. Some data are listed in Table III;[11b] the same reservations as mentioned above apply.

Discussion

In the simplest form of the sphere-in-continuum theory of electrolyte conduction, only two parameters (the dielectric constant and the coefficient of viscosity) define the solvent and another two parameters (the charge and radius) specify each ion. Ion–solvent interaction is expressed in terms of macroscopic hydrodynamics, *i.e.*, the assumption of the validity of Stokes' law, and ion–ion interaction is strictly electrostatic.

Following Fuoss and Accascina,[15] for solvents of very low dielectric constant at low electrolyte concentrations, the simplest analysis takes cognizance of ions, ion pairs, and ion triples all in dynamic equilibrium, *viz.*

$$C^+ + A^- \rightleftharpoons C^+A^- \qquad K_A \qquad (2)$$

$$\left.\begin{aligned} C^+A^- + A^- &\rightleftharpoons A^-C^+A^- \\ C^+A^- + C^+ &\rightleftharpoons C^+A^-C^+ \end{aligned}\right\} \quad k^{-1} \qquad (3)$$

The distinction between the two types of association to triples is neglected, as usual. Free ions and triple ions migrate in the applied field and transport charge while the neutral ion pairs do not. If Λ_0 and λ_0 denote the limiting equivalent conductance of the free ions and the triple ions, respectively, one generalizes the Arrhenius equation and obtains

$$\Lambda = \gamma_1\Lambda_0 + \gamma_3\lambda_0 \qquad (4a)$$

$$\Lambda = \Lambda_0(K_Ac)^{-1/2} + \lambda_0(k^2K_A)^{-1/2}c^{1/2} \qquad (4b)$$

where γ_1 and γ_3 are the fraction of single ions and triple ions, respectively, c is the stoichiometric concentration of electrolyte, K_A is the association constant to form ion pairs, k^{-1} that to form ion triples, activities have been approximated by concentrations, and interionic corrections to the mobilities have been neglected. Equation 4b predicts that a log Λ *vs.* log c plot has a slope of −0.5 for very low c and that the curve exhibits a minimum at

$$c_{min} = (\Lambda_0/\lambda_0)k \qquad (5)$$

with

$$\Lambda_{min} = 2(\gamma_1\Lambda_0)_{min} = 2(\gamma_3\lambda_0)_{min} \qquad (6)$$

This predicted behavior has been amply confirmed for fluid solvents and mixed-solvent systems[15] but has not been demonstrated previously in highly viscous media. In one of the pioneering studies of electrolytic conduction in plastics, Mead and Fuoss[1] suggested that "the molecular mechanics of ion association in media of such high viscosity [80% by weight poly(vinyl chloride) plasticized with DPM; viscosity not determined] will probably turn out to be quite different from those of ordinary liquids." Our results for the 0–50% PS solvent systems, which cover a 10^5-fold range of viscosity ($0.01 < \eta < 1000$ P), suggest

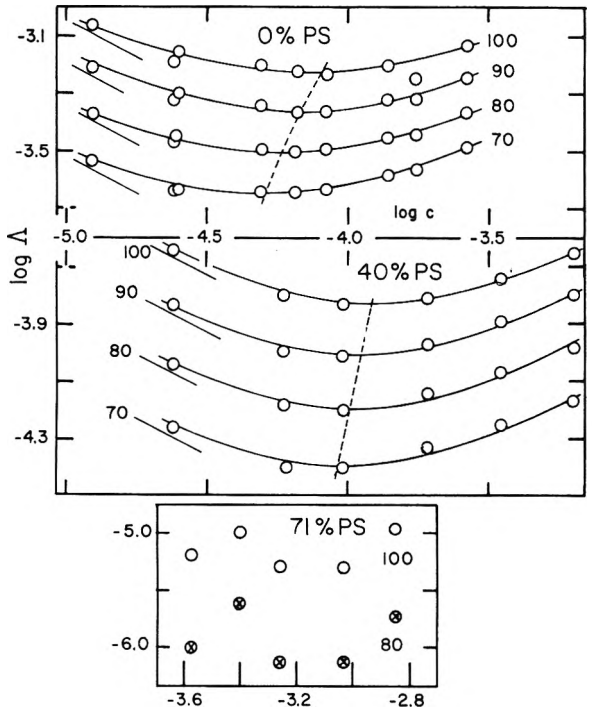

Figure 2. Logarithm of equivalent conductance (mhos kg/cm equiv) as a function of the logarithm of $(n\text{-Bu})_4$NSCN concentration (equiv/kg). The Celcius temperature is indicated. The dashed line denotes the locus of c_{min}. The short line segments at the left are drawn with slope −0.5. Note the large change in scale for the 71% PS sample.

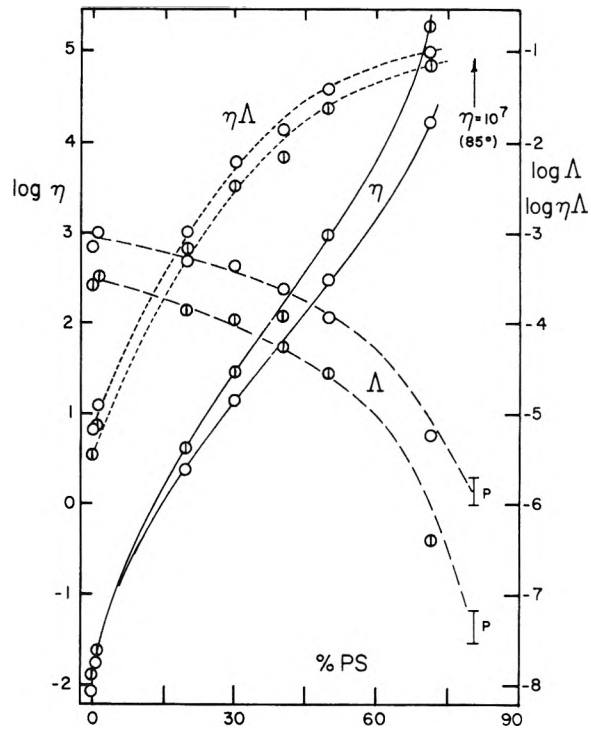

Figure 3. Left ordinate: logarithm of the solvent viscosity (poise) as a function of weight per cent polystyrene: ⊕ = 70°; ○ = 100°. Right ordinate: logarithm of equivalent conductance ($c \approx 2 \times 10^{-4}$) and logarithm of conductance × viscosity as a function of per cent PS: ⊕ = 70°; ○ = 100°. The conductance data marked P at 80% PS are from Price, ref 2, at $c \approx 3 \times 10^{-4}$. The solvent viscosity at 80% PS and 85° is also from Price.

that eq 4b applies irrespective of the solvent's viscosity. See Figure 2 for typical results.

Equation 5 is the basis for the motivation for this investigation. If Walden's rule held for the free ions and the triple ions, or if deviations therefrom were such as to keep Λ_0/λ_0 constant, c_{min} would vary directly as k. And since our simplest model assumes ion association to be strictly electrostatic in nature (no specific solute-solvent interactions) the key parameter determining the extent of ion association is the ratio of the Coulombic energy to the thermal energy. One then finds[15]

$$\log c_{min} = \log (\Lambda_0/\lambda_0) + \log k = \text{constant} - (\epsilon T)^{-1} \quad (7)$$

where ϵ is the dielectric constant of the solvent and with the implicit assumption of constant Λ_0/λ_0.

For a given solvent composition, *i.e.*, PS/DPM ratio, (ϵT) increases with increasing temperature since $d\epsilon/dT$, while negative, is very small for essentially nonpolar substances. The increase in c_{min} with increasing temperature is well illustrated in Figure 2. The model predicts that dc_{min}/dT is the same for all solvent compositions; within the rather large experimental uncertainty of our results we find this to be so, the average increase in c_{min} being 50% in the range 70–100°.

For isothermal changes in solvent composition which are truly isodielectric, we anticipate that c_{min} will be constant *if* Λ_0/λ_0 remains constant. The 0% PS and 40% PS data shown in Figure 2 suggest, and an analysis of all the data confirms, that c_{min} increases with increasing per cent PS, the increase being perhaps more pronounced at the lower temperatures: at 70°, c_{min} approximately doubles as the per cent PS 0 → 50; at 100°, c_{min} increases by about 50%. Part of this change must be attributed to the fact that the isothermal variation of the PS-DPM solvent composition is not strictly isodielectric. Our results (Table II[11b]) are inadequately precise to define the composition dependence of the solvent's dielectric constant but it appears that the dielectric constant increases very slightly with increasing polymer concentration.[16] However, it seems that c_{min} depends on solvent composition to a larger extent than can be accounted for by the small change in dielectric constant. Two possibilities, at least, may be considered: the constancy of (Λ_0/λ_0) with increasing viscosity seems extremely unlikely, as we have discussed previously,[2] and the possibility of specific ion-solvent interactions also cannot be discounted.[17] We see no way to resolve these possibilities with only our present data; different electrolytes in the PS-DPM solvent system and other isodielectric variable viscosity solvents will have to be studied.

We now turn to a discussion of ion mobility in this system. It is often surmised that polymers are good electrical insulators because ionic mobility in these "solvents" is extremely low. The basis for such speculation is the assumed validity of Walden's rule, *i.e.*, the applicability of Stokes' law. However, for the PS-DPM system, Walden's rule fails utterly as is suggested by the data in Table I[11b] and illustrated in Figure 3. It is obvious that the ionic mobility is not diminished nearly so much as the solvent viscosity is increased, especially for the solvents of relatively low viscosity. In fact, for solvents with $\eta < 1000$ P (per cent PS < 50) a better, albeit very crude, approximation would be that the mobility is essentially *independent* of the macroscopic viscosity. Various simple modifications of Walden's rule, such as $\Lambda\eta^{\gamma}$ = constant, with p less[18] than or greater[19] than unity, are all inapplicable for this large

range of viscosity. "The theoretical problem to be considered is the motion of ions around segments of much larger molecules";[18] by definition, the sphere-in-*continuum* model is no longer applicable.

In dilute polymer solutions, some version of an obstruction model would seem most appropriate. Polymer chains repel one another entropically in dilute solutions. Under these conditions, one assumes that the solution consists of discrete regions of pure solvent and smaller regions, pervaded by the polymer molecules, in which the ions' mobility are much less[20] or possibly even zero.[21] Such models lead to the expectation that the initial conductance decrease is in proportion to the volume fraction of the obstructant. With increasing polymer concentration the conductance decreases somewhat more rapidly because the polymer segment density within the random coil increases (unless the experiments are carried out in a Θ solvent) and the ion mobility within the coil presumably decreases. This model can be expected to hold until the polymer concentration is so great that the polymer coils begin to interpenetrate; at this critical concentration, which depends on the polymer's molecular weight in an inverse manner, the concept of distinct regions of the solution having different hydrodynamic properties becomes invalid and a different approach is needed.

A critical concentration for conductance of polystyrene–styrene solutions was found by Purdon and Morton[22] to be about 7% polymer for MW $\simeq 10^5$. The interpenetration of polymer coils is also manifest in viscoelastic experiments as "entanglement couplings" and Ferry[23] suggests that for polystyrene of MW $\simeq 10^5$ the critical concentration is about 20%, in agreement with 15% suggested by Onogi, *et al.*,[24] from solution viscosity measurements. We conclude that for per cent PS > 20, the obstruction model will certainly not be applicable.

Insofar as ionic conduction is an electric-field-biased diffusion, we anticipate that the free-volume concept which has been applied quite successfully to the problem of diffusion in polymeric systems[25] might also be applicable for conduction in an isodielectric, variable viscosity solvent. Following Ferry,[26] we assume that the mean translational friction coefficient of an ion, $\zeta_\pm$, will be similar to the monomeric friction coefficient of the polymer, ζ_0, for test temperatures far above the glass-transition temperature of the solvent.[27]

The glass-transition temperature may be defined[28] operationally as the temperature where $\eta \approx 10^{13}$ P. For pure PS it is 100° but it decreases rapidly with addition of a highly fluid diluent. Jenckel and Heusch's results[29] indicate that 20% by weight of benzene or toluene depresses T_g of PS by about 80°, and we assume that plasticization by DPM will not be substantially different. Thus, all of our samples with per cent PS < 80 and t > 70° should be well above T_g. Referring to Figure 3, it is clear that the viscosity isotherm at 100° must increase enormously for per cent PS > 71; the 70° isotherm will have to increase even more rapidly (nearly vertically on the scale of Figure 3) since the glass transition at this temperature will occur at per cent PS < 100.

For a 1-1 electrolyte, the equivalent conductance is related to the mean ionic friction coefficient by combining the Nernst-Hartley relation[30] between the diffusion coefficient and Λ°

$$D = RT\Lambda^\circ/2F^2 \tag{8}$$

and Einstein's result

$$D = kT/\zeta_\pm \tag{9}$$

Equating these relations, we find for the 71% PS solution at the lowest electrolyte concentrations that log $\zeta_\pm$ (dyn sec/cm) = −7.1 at 70° and −8.2 at 100°. The glass-transition temperatures of PS–DPM solutions are not known. Jenckel and Heusch's results for PS–benzene and PS–toluene suggest that 30% plasticizer lowers T_g by about 110°, so our results at 70 and 100° probably bracket T_g + 100 for the 71% PS system. Ferry[31] quotes log ζ = −6.95 for polystyrene at $T = T_g + 100$. This order-of-magnitude agreement is encouraging so we next investigate the possibility of using the free-volume concept to explain the viscosity dependence of the conductivity.

Free-volume theory[32] relates the monomeric friction coefficient in a polymer solution to that in the pure polymer at the same temperature and pressure as

$$[\zeta_0]_v/[\zeta_0]_0 = \exp[B(f_v^{-1} - f_0^{-1})] \tag{10}$$

where f_0 is the fractional free volume in the pure polymer, f_v is the fractional free volume in a solution whose volume fraction of dilutent is v, and B is a constant of order unity related to the size of the "hole" required for diffusion. Next, one invokes a linear dependence of f_v on v, *viz.*

$$f_v = f_0 + \beta v \tag{11}$$

which implies a linear decrease of T_g with v and therefore serves as a guide to the range of applicability of the subsequent results. Substituting (11) into (10), making the assumption that $\zeta_\pm$ depends on fractional free volume in the same way as ζ_0 does, and recognizing that $\Lambda \propto \zeta_\pm^{-1}$ we obtain

$$\ln \Lambda_v = \ln \Lambda_0 + (B/f_0)\frac{v}{v + f_0/\beta} \tag{12}$$

where the subscript on Λ refers to the volume fraction of DPM in the solvent. Because of the near identity of the densities of PS and DPM, weight fractions may be substituted for v in eq 12.

We expect f_0 to be about 0.05 or less. At T_g of 100% PS, $f_0 \approx 0.03$; it will decrease slowly with decreasing temperature but appears to be somewhat greater when measured in solution than in the pure polymer. From eq 11, when $v = 1$, $(f_0 + \beta)$ is the fractional free volume of the pure monomeric diluent which characteristically ranges from about 0.2 to 0.4. Thus we may expect $0.1 < f_0/\beta < 0.4$ and test plots of eq 12 were tried for this range. The linearity is most sensitive at small v's, a range where we do not have much data, but a subjective estimate is that $f_0/\beta = 0.2 \pm 0.05$ gives the "best" fit and examples are shown in Figure 4.

The slope of the lines of Figure 4 is B/f_0. At 100°, for $f_0/\beta = 0.2$, $B/f_0 = 20$. With $f_0 = 0.04$ this yields $B = 0.8$ which is the expected order of magnitude. (While B in eq 10 is about unity for monomeric friction coefficients, analyses[25] of small-molecule diffusion experiments indicate that $B < 1$ for the diffusant's friction coefficient.) Since B, β, and f_0 are average quantities estimated from a wide variety of viscoelastic and dilatometric experiments, completely independent of conductance, we are encouraged to believe that the free-volume model is an appropriate way to analyze conductance data in polymeric, highly viscous solvents.

With $f_0/\beta = 0.2$, and $B/f_0 = 20$, eq 10 yields log Λ_0 = −10.2 at 100°. However, since the glass-transition temperature of polystyrene is 100°, equating $\zeta_\pm$ to ζ_0 is no longer

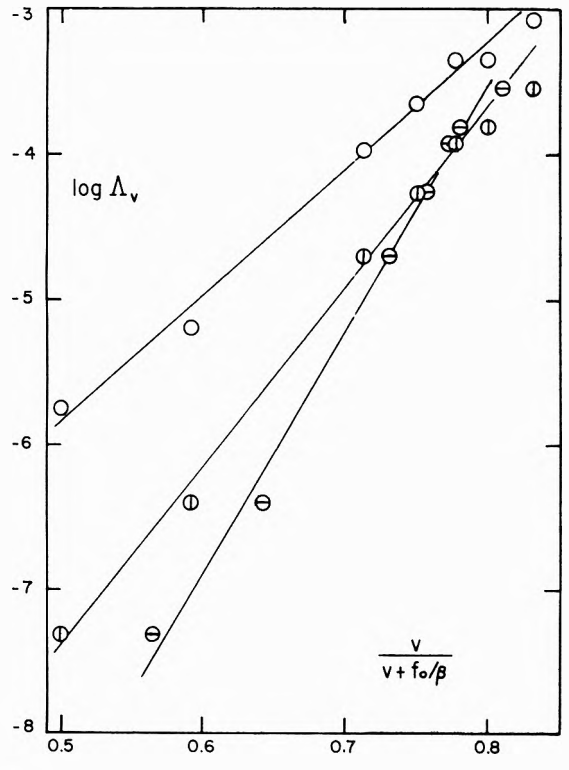

Figure 4. Logarithm of equivalent conductance of $(n\text{-Bu})_4NSCN$ ($c \approx 2 \times 10^{-4}$) in a solvent of v volume fraction diphenylmethane as a function of $v/(v + f_0/\beta)$: O = 100° and ⊕ = 70° with $f_0/\beta = 0.2$; ⊖ = 70° with $f_0/\beta = 0.1$, these points shifted 0.1 unit to the left for plotting purposes. Reading from right to left, data points refer to solvent composition of 0, 20, 30, 40, 50, 71, and 80% by weight polystyrene. 80% points from Price, ref 2.

valid[33] and eq 12 cannot be expected to hold. The extrapolated value is probably an upper limit. Even so, for $c = 10^{-4}$ it corresponds to a specific conductance of 10^{-17} mho/cm at T_g! The prospects for definitive conductance measurements in such a solvent system appear slim.

Since $v = 1 - 0.01$(per cent PS), eq 12 provides the basis for the shape of the log Λ *vs.* per cent PS isotherms of Figure 3. In particular, we estimate the limiting slope of the 100° isotherm as per cent PS → 100 to be −0.43, which is nearly vertical on the scale of Figure 3. The 70° isotherm decreases even more rapidly because of a smaller f_0. We have already noted that the viscosity isotherms must increase enormously rapidly for per cent PS > 70 so we now come to the surprising conclusion that for *very* viscous solutions, as for very fluid ones, Walden's rule will be a useful approximation.

On the basis of the model developed above, we anticipate that the temperature dependence, *i.e.*, activation energy, for conductance and viscous flow should show a parallel dependence on the PS concentration since the temperature dependence of the friction coefficients provides a common basis. We use conductance data at the lowest electrolyte concentrations (where log Λ is nearly proportional to −0.5 log c) so that only the ion-pair equilibrium will be considered. Following eq 4b we have

$$\ln \Lambda = -\tfrac{1}{2} \ln (K_A c) + \ln \Lambda_0 \qquad (13)$$

and

$$\frac{d \ln \Lambda}{dT^{-1}} = -\frac{E_\Lambda}{R} = -\frac{1}{2}\frac{d \ln K_A}{dT^{-1}} + \frac{d \ln \Lambda_0}{dT^{-1}} \qquad (14)$$

For a 1-1 electrolyte with only electrostatic interaction to form ion pairs

$$K_A = (\text{constant}) \exp(e^2/a\epsilon kT) \qquad (15)$$

where e is the electronic charge, a is the distance of closest approach, assumed ≈5 Å[15] in this calculation, and $\epsilon = 2.5$ is the dielectric constant of the isodielectric solvent. With $\Lambda_0 \propto (\zeta_\pm)^{-1}$ we have

$$E_\Lambda = E_\eta + 13.4 \text{ kcal} \qquad (16)$$

where E_η, the activation energy for viscous flow as determined by the monomeric friction coefficient, depends on the polymer concentration because of free volume considerations.[34] For $T \gg T_g$, ζ_0 and $\zeta_\pm$ are again expected to have a similar dependence on fractional free volume, and thus E_Λ and E_η should differ by a constant amount. Our experimental results are shown in Figure 5.[35] As the polymer concentration is increased and the glass-transition region is approached this parallel cannot continue, and on the basis of diffusion experiments one expects ultimately that $E_\eta > E_\Lambda$.[36] The pitfalls of conductance experiments near T_g have been outlined above; we are unaware of reliable conductance and viscosity data for the same system with which to test this prediction.

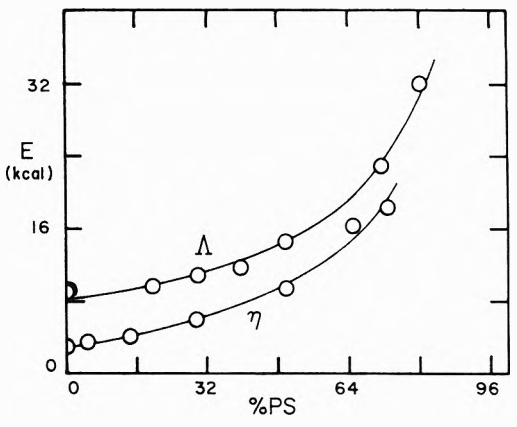

Figure 5. Apparent activation energy (kcal/mol) for equivalent conductance and shear viscosity as a function of weight per cent polystyrene. Temperature range is 70-100°. E_Λ at 80% PS is from Price, ref 2.

To conclude this discussion of ionic mobility in highly viscous solvents, we suggest that an interpretation of the decreased mobility of ions in terms of viscous hindrance in the Stokesian manner is misleading. Rather, "an alternative possibility is that the increased viscosity and the increased resistance experienced by the moving [ion] are not related as cause and effect, but are two parallel effects of a common cause."[21] That common cause is the obstruction action of the polymer, distorting the stream lines of flow for solvent molecules and ions in the concentration range where the polymer chains do not overlap; it is the common influence of free volume on the friction coefficients of the ions and the polymer segments when the polymer concentration becomes sufficiently large.

Acknowledgment. Grateful acknowledgment is made to the donors of the Petroleum Research Fund, administered by the American Chemical Society, for the support of this research.

Supplementary Material Available. Tables I-III will appear following these pages in the microfilm edition of this volume of the journal. Photocopies of the supplementary material from this paper only or microfiche (105 × 148 mm, 20× reduction, negatives) containing all of the sup-

plementary material for the papers in this issue may be obtained from the Journals Department, American Chemical Society, 1155 16th St., N.W., Washington, D. C. 20036. Remit check or money order for $3.00 for photocopy or $2.00 for microfiche, referring to code number JPC-73-2217.

References and Notes

(1) Prior to World War II, R. M. Fuoss and his collaborators began a systematic study of the dielectric and electrolytic properties of some polymeric systems. Most of the results were published after the war but the work had been discontinued by then. Particularly pertinent is the paper by D. J. Mead and R. M. Fuoss, *J. Amer. Chem. Soc.*, **67**, 1566 (1945).

(2) J. R. Price and W. Dannhauser, *J. Phys. Chem.*, **71**, 3570 (1967). Several reviews of the literature are cited in this paper.

(3) A referee objected to our interpretation and pointed out alternatives. Similar comments were made by Fuoss during the discussion following presentation of the paper to the 1967 Conference on Electrical Insulation and Dielectric Phenomena. Publication No. 1578, National Academy of Sciences, 1968, p 32.

(4) A. H. Sharbaugh, Jr., H. C. Eckstrom, and C. A. Kraus, *J. Chem. Phys.*, **15**, 54 (1947).

(5) D. T. Copenhafer and C. A. Kraus, *J. Amer. Chem. Soc.*, **73**, 4557 (1951).

(6) J. G. Berberian and R. H. Cole, *Rev. Sci. Instrum.*, **40**, 811 (1969).

(7) Victoreen Instrument Co., Cleveland, Ohio.

(8) Balsbaugh Laboratories, South Hingham, Mass.

(9) Cannon Instrument Co., State College, Pa.

(10) L. R. Bacon, *J. Franklin Inst.*, **221**, 251 (1936).

(11) (a) L. C. Kenausis, E. C. Evers, and C. A. Kraus, *Proc. Nat. Acad. Sci.*, **48**, 121 (1962). (b) See paragraph at end of paper regarding supplementary material.

(12) R. A. Robinson and R. H. Stokes, "Electrolyte Solutions," 2nd ed, Academic Press, New York, N. Y., 1959, p 91 ff.

(13) See, for example, R. W. Warfield and M. C. Petree, *Polymer*, **1**, 178 (1960); R. W. Warfield, *SPE (Soc. Plast. Eng.) J.*, **15** (8), 1, 1959.

(14) The specific conductance of the "solvent" varied considerably, depending on time interval since distillation of the DPM, length of time since mixing PS and DPM, time left in the cell, and the thermal history of the sample. The values quoted are meant to be comparative rather than definitive.

(15) R. M. Fuoss and F. Accascina, "Electrolytic Conductance," Interscience, New York, N. Y., 1959.

(16) The dielectric constants reported in Table II are those of the solvent. With increasing electrolyte concentration the dielectric constant increases slightly, presumably because of the ion-pair dipoles. We have not attempted to include the small variation in our analysis of the isothermal data.

(17) W. R. Gilkerson, *J. Chem. Phys.*, **25**, 1199 (1956); ref 15, p 260.

(18) C. Treiner and R. M. Fuoss, *J. Phys. Chem.*, **69**, 2576 (1965).

(19) B. I. Sazhin and V. P. Shavayev, *Vysokomol. Soedin.*, **7** (6), 962 (1965); *Polym. Sci. USSR*, **7**, 1062 (1965).

(20) V. P. Budtov, *Vysokomol. Soedin.*, **10**, 776 (1967); *Polym. Sci. USSR*, **10**, 900 (1968).

(21) Reference 12, p 310 ff.

(22) J. R. Purdon and H. Morton, *J. Polym. Sci.*, **57**, 453 (1962).

(23) J. D. Ferry, "Viscoelastic Properties of Polymers," 2nd ed, Wiley, New York, N. Y., 1970, p 536.

(24) S. Onogi, T. Kobayashi, Y. Kojima, and Y. Taniguchi, *J. Appl. Polym. Sci.*, **7**, 847 (1963).

(25) H. Fujita, *Advan. Polym. Sci.*, **3**, 1 (1961).

(26) Reference 23, pp 332 and 371.

(27) The situation is more complex for conductance than for diffusion since there are at least two ions that migrate (near the minimum of the log Λ–log c plot, there are, in addition to the single ions, substantial concentrations of triple ions) and they are generally of different size and may interact differently with the solvent. The quaternary ammonium ion is probably larger than the styrene repeat unit but its charge is well shielded; SCN^- is smaller, but presumably interacts strongly with the polarizable solvent because of its higher charge density. The triple ions are all much larger than the monomer residue. As $T \rightarrow T_g$, the diffusant's friction coefficient becomes increasingly sensitive to the size and shape of the diffusing species.

(28) T. Alfrey, Jr., "Mechanical Behavior of High Polymers," Interscience, New York, N. Y., 1948, p 83 ff.

(29) E. Jenckel and R. Heusch, *Kolloid-Z.*, **130**, 89 (1953). Their value of $T_g = 80°$ is low compared to more recent data but the effect of diluent is qualitatively correct, we believe. Berry and Fox, ref 34, show that 20% by volume of dibenzyl ether lowers T_g of PS by about 80°; 30% by about 100°.

(30) Reference 12, p 286. We assume that the conductance at the lowest electrolyte concentration is due primarily to single ions and, in lieu of any information, that the ions have equal mobility. At the extremely low effective ion concentrations, substitution of Λ for Λ^0 seems quite reasonable.

(31) Reference 23, p 363.

(32) Reference 23, p 518 ff.

(33) Ferry, ref 23, p 373, states: "when the temperature is closer to T_g, however, the friction coefficient for the smaller molecule is considerably smaller than that for a chain unit, to a degree which is ... quite large for $T - T_g < 40$. This effect is accompanied by a growing discrepancy between the apparent activities energy for diffusion and viscoelastic relaxation, the former always being the smaller."

(34) G. C. Berry and T. G. Fox, *Advan. Polym. Sci.*, **5**, 262 (1968). See especially p 317 ff.

(35) Our data yield $E_\Lambda - E_\eta \approx 6$ kcal rather than 13.4 kcal as predicted from the electrostatic model. If the ion pairs are solvent separated rather than intimate, the distance of closest approach will be substantially larger than the 5 Å used in our calculations, thus decreasing the energy. Also, the complete neglect of solute–solvent interactions seems naive. Ions and the highly dipolar ion pairs are expected to interact strongly with the polarizable solvent; the difference of these two terms can easily account for a few kcal.

(36) The apparent activation energy for viscous flow of high molecular weight polystyrene near T_g is quoted as ca. 55 kcal by V. Semjonow, *Advan. Polym. Sci.*, **5**, 387 (1968), but there is a wide range of values available in the literature. Free volume considerations, as embodied in the WLF equation (ref 23, p 374 ff), predict $E_a = 160$ kcal at T_g for polystyrene! Whatever the actual value, it is obvious that the extrapolation of E_η vs. per cent PS in Figure 5 must increase very rapidly for per cent PS > 71.

Concentration Dependence of the Apparent Molal Volumes of Polyelectrolytes

J. Škerjanc

Department of Chemistry, University of Ljubljana, Ljubljana, Yugoslavia *(Received December 27, 1972)*

The volume changes on dilution of aqueous solutions of polystyrenesulfonic acid and its sodium and magnesium salts have been determined by dilatometry in the concentration range 1.5–0.01 mono*M*. An approximately linear dependence of the apparent molal volumes of polyelectrolytes, Φ_v, on the logarithm of concentration has been found at concentrations lower than 0.2 mono*M*, whereas a positive deviation from linearity appears for all three polyelectrolytes at higher concentrations. A theoretical expression for the concentration dependence of Φ_v has been derived for the simplified cell model of polyelectrolyte solution and compared with the experimental results. Agreement between theory and experiment is good for all three polystyrenesulfonates up to concentration 0.2 mono*M*; at higher concentrations, however, experimental values are higher than theoretical ones.

Introduction

In spite of their importance, a few years ago only the first data on the apparent molal volumes of synthetic polyelectrolytes were reported.[1,2] Very recently more attention was paid to the measurements of this thermodynamic property.[3-9] The articles by Ise and Okubo[8] and Tondre and Zana[9] excel by their approach to the problem and the amount of data presented. For most polysalts a more or less pronounced increase of the apparent molal volume with polymer concentration has been observed. Although such a behavior has been interpreted in some papers in terms of charge and hydrophobic effects, there has been no attempt to give the concentration dependence of the apparent molal volume a theoretical background, not even for those polyelectrolytes for which charge effect plays a dominant role. Such an attempt has been made in this paper.

For the purpose of comparing theoretical and experimental values we carefully examined the published results. Unfortunately, we have found out that most of the published data are unsuitable for an unbiased comparison with theory because the scattering of the experimental points is too large or because they are limited to a narrow concentration range. Therefore, in the present work we have focused attention exclusively on the accurate determination of concentration dependence of the apparent molal volume. For this purpose, we did not measure densities of solutions as has been done in all previous studies, but we rather used the dilatometric method. By applying this method it is not possible to obtain absolute values of the apparent molal volumes but the method enables one to determine small volume changes on dilution with great accuracy.

For these studies polystyrenesulfonic acid and its sodium and magnesium salts were chosen, the polyelectrolytes which have thus far been extensively studied in this laboratory. It seems that these polyelectrolytes are especially suitable for testing a purely electrostatic theory, since in this case no significant specific binding of counterions to the polyion has been detected.[10-12]

Experimental Section

(a) Materials. As starting material sodium polystyrenesulfonate, NaPSS (mol wt = 100,000; degree of sulfonation, 1.00; purchased from Polysciences Inc., Rydal, Pa.) was applied. The method of purification has been described previously.[13] A dialyzed solution of NaPSS was converted to the acid (HPSS) by ion exchange and the concentration was determined by potentiometric titration to within 2 °/₀₀. The salts were prepared from solutions of acid by adding the corresponding metal hydroxide or carbonate to acid until pH was about 5. During the operation nitrogen was blown through the solution. In this way a small amount of free acid (less than 1 °/₀₀) was left in the solution. Preliminary experiments showed that a slight excess of acid had no influence on results, whereas an excess of metal hydroxide or carbonate might affect experimental values appreciably. The same experimental observation has been reported elsewhere.[9]

(b) Dilatometry. Volume changes were measured at 25° in Linderstrom-Lang dilatometers purchased from F. C. Jacob Glasteknik (Copenhagen, Denmark) which have the form of an inverted Y. Freshly prepared solutions, diluting water, and kerosene were degassed prior to use. Then 4.00 ml of water was pipetted into one arm of each dilatometer and 4.00 ml of the polyelectrolyte solution was pipetted into the other. This volume was changed at the lowest concentrations to 12.0 ml in order to increase the sensitivity. The solution and water were covered with kerosene and the capillary was affixed. The dilatometers were then immersed in a 25° thermostat controlled within ±0.001° where they remained for several hours. After thermal equilibration, mixing was performed and readings were recorded at intervals of 1 min. All other details concerning the experimental technique have been described previously.[14]

In all runs parallel blank experiments, in which 4.00 ml of water or polyelectrolyte solution of final concentration was mixed with the same volume of water or the same polyelectrolyte solution, respectively, were performed. These small blank volume changes ΔV_b (usually between −0.02 and + 0.02 μl) were subtracted from the average volume change ΔV observed upon mixing water with the solution. The resulting corrected volume change of dilution ΔV_d ($=\Delta V - \Delta V_b$) divided by the number of monomoles n_p is equal to the difference between the apparent monomolal volumes of polyelectrolyte at the initial (Φ_v^i) and final concentrations (Φ_v^f)

$$\Phi_v^f - \Phi_v^i = \Delta V_d / n_p \qquad (1)$$

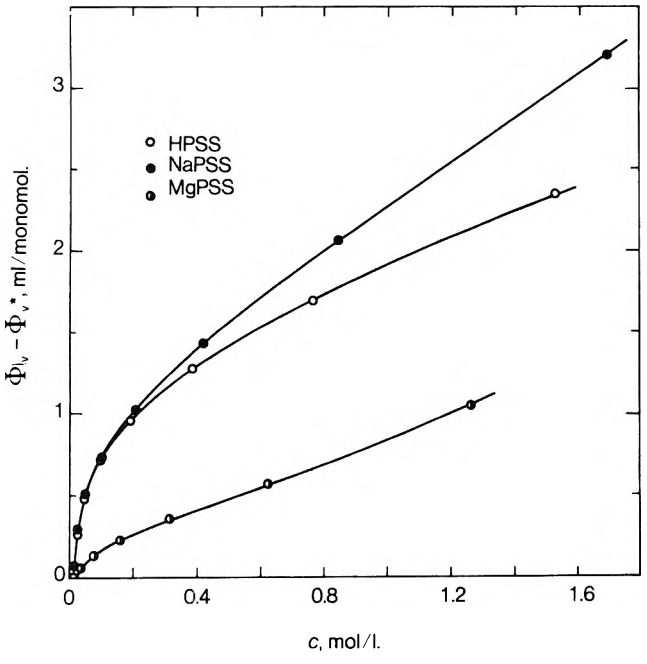

Figure 1. Apparent molal volumes of polystyrenesulfonates in water at 25° as a function of polyelectrolyte monomolarity. Φ_v^* refers to the concentration 0.0120 mol of $-SO_3^-$/l.

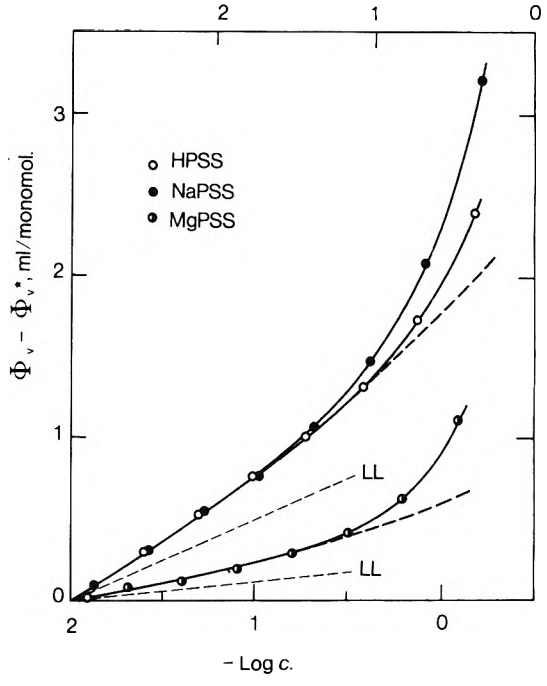

Figure 2. Comparison of the experimental apparent molal volumes of polystyrenesulfonates in water with those predicted by theory. Φ_v^* is the value in the 0.01 mono*M* solution. Points: experimental values; dashed lines: calculated values (eq 9); LL: limiting law (eq 13) for monovalent (upper line) and divalent counterions (lower line).

The final solution from each experiment was used as the initial solution for the subsequent experiment. By linear combination of the volume changes accompanying successive dilutions the concentration dependence of Φ_v over a larger concentration range was obtained.

Results and Discussion

The concentration dependence of the apparent molal volumes of HPSS, NaPSS, and MgPSS at 25° is shown in Figure 1. Perhaps the most striking aspect of these results is a sharp fall of Φ_v with decreasing polymer concentration. This diagram evidently shows that there is no linear relation between Φ_v and concentration, a functional dependence which is usual for many thermodynamic properties of uncharged particles in diluted solutions,[15-18] but which would be quite strange for charged particles.[15,16,19,20] Therefore, in such plots a linear extrapolation of Φ_v to zero concentration which has been applied in some previous studies is not justified and Φ_v's obtained by such extrapolations should be accepted with a great deal of precaution.

For reasons similar to those mentioned in the paper on the relative apparent molal enthalpies[21] which are theoretically closely related to the relative apparent molal volumes, we have not tried to extrapolate the experimental data to zero concentration. Instead, a common reference point has been chosen in Figures 1 and 2 for all polystyrenesulfonates (10^{-2} mol of $-SO_3^-$/l.) in order to obtain a clearer comparison. The logarithmic scale in the diagram has been chosen because the theory in the first approximation predicts such concentration dependence of Φ_v.

The concentration dependence of apparent molal quantities of simple electrolytes has been satisfactorily explained, at least at low concentration, considering only the electrostatic interaction among ions. Analogously, the concentration dependence of the apparent molal enthalpies (more often referred to as heats of dilution) of polyelectrolytes has been recently interpreted[21] on the basis of a purely electrostatic theory.[22] In the following a similar attempt will be made for the apparent molal volumes.

For the calculation we have applied, as previously,[21] the theory based on the cell model.[23] For such a model Lifson and Katchalsky[22] have calculated the electrostatic free energy, F_e, of polyelectrolyte solution, which is the difference between the free energies of the real solution and of the same solution in a hypothetical reference state in which all ions are discharged. Their expression for F_e calculated per monomole of polyelectrolyte would read

$$F_e = \frac{\alpha z_1 RT}{z_2} \int_0^\lambda \frac{u}{\lambda^2} d\lambda \qquad (2)$$

where z_1 and z_2 are the number of charges of the ionized group on the polyion and those on the counterion, respectively, α is the degree of ionization, while R and T have their usual significance. The charge-density parameter, λ, is defined by

$$\lambda = \frac{\alpha z_1 z_2 e_0^2}{\epsilon k T b} \qquad (3)$$

where e_0 is the protonic charge, ϵ is the dielectric constant of the solvent, k is the Boltzmann constant, and b is the length of a monomeric unit. The dimensionless function u, which is proportional to the electrostatic energy of the solution, is given by

$$u = (1 + \beta^2)\gamma + \ln \frac{(1 - \lambda)^2 - \beta^2}{1 - \beta^2} + \lambda \qquad (4)$$

where γ is a concentration parameter, proportional to $-\log c$, and β is a constant related to λ and γ.

The electrostatic free energy, F_e, given by eq 2, has been obtained as the electrostatic work in the charging process in which it has been assumed that the volume of the solution is invariable, that is unaffected by pressure

and by charges of the ions. In the charging process at experimental conditions, *i.e.*, at constant temperature and at constant pressure, the electrostatic work done on the system is equal to the electrostatic free enthalpy, G_e.[24] Hence, it is more accurate to write G_e instead of F_e on the left-hand side of eq 2 at experimental conditions. For simple electrolytes it has been shown by Fowler and Guggenheim[24] that the inaccuracy in the expression for electrostatic work due to the neglect of the slight volume change during the charging process at constant pressure (in comparison with the total volume) is entirely negligible. Following their arguments it can easily be verified that this is also true for polyelectrolyte solutions.

With the above as background, we can now derive an expression for the difference between the apparent molal volumes of polyelectrolyte in the real (Φ_v) and in the hypothetical uncharged solution (Φ_v^0) by means of the thermodynamic relation

$$(\partial G_e/\partial P)_T = V - V^0 = \Phi_v - \Phi_v^0 \qquad (5)$$

where V and V^0 are the volumes of the real and of the uncharged solutions, respectively, containing one monomole of polyelectrolyte.

Differentiating eq 2 with respect to P at constant temperature, we get

$$\Phi_v - \Phi_v^0 = \frac{\alpha z_1 RT}{z_2}\left[\frac{\partial}{\partial\lambda}\int_0^\lambda \frac{u}{\lambda^2}d\lambda\right]_{T,\gamma}\cdot\frac{d\lambda}{dP} \qquad (6)$$

where

$$\frac{d\lambda}{dP} = -\lambda\frac{d\ln\epsilon}{dP} \qquad (7)$$

To emphasize the dimensions of the equation we introduce $V_m \equiv RT/P$, and so we have

$$\Phi_v - \Phi_v^0 = -\frac{\alpha z_1 V_m}{z_2\lambda}u\frac{d\ln\epsilon}{d\ln P} \qquad (8)$$

In order to simplify the derivation the differentiation in eq 6 has been made at constant γ. By a lengthy but exact differentiation of the final expression for F_e, given in ref 22, in which dependence of γ on pressure is taken into account, we get the expression

$$\Phi_v - \Phi_v^0 = -\frac{\alpha z_1 V_m}{z_2\lambda}u\frac{d\ln\epsilon}{d\ln P} - \frac{\alpha z_1 V_m}{2z_2\lambda}v\left(\frac{d\ln V}{d\ln P} - 2\frac{d\ln a}{d\ln P}\right) \qquad (9)$$

where a is the radius of the macromolecular rod and v is given by

$$v = 1 - \beta^2 - 2\lambda\frac{e^{2\gamma}}{e^{2\gamma} - 1} \qquad (10)$$

In an actual experiment we measure the difference between Φ_v's of a real solution at final and initial concentrations (*cf.* eq 1). However, from the theory the difference between the apparent molal volumes of polyelectrolyte in the real solution and in the hypothetical uncharged solution at these two concentrations is obtained. In the present calculations it is assumed that

$$\Phi_v^{0f} \approx \Phi_v^{0i} = \Phi_v^0 \qquad (11)$$

in the whole concentration range studied. With this simplification we have

$$(\Phi_v^f - \Phi_v^i)_{expt} = (\Phi_v^f - \Phi_v^0)_{theor} - (\Phi_v^i - \Phi_v^0)_{theor} \qquad (12)$$

which enables comparison of experimental and theoretical data.

Inspection of eq 8 and 9 has shown that values of ($\Phi_v^f - \Phi_v^i$) calculated from eq 8 are approximately 8% lower than those calculated from eq 9 with d ln a/d ln P = 0. Thus, eq 8 may be used for only rough estimations, whereas for exact calculations eq 9 should be used.

In Figure 2 the theoretical curves for monovalent and divalent counterions, calculated according to eq 9, 4, 10, and 12, are presented. The following values have been chosen in these computations. For the parameter λ its structural values were used (λ = 2.83 for monovalent, z_2 = 1, and λ = 5.66 for divalent counterions, z_2 = 2). These values, typical of highly charged vinylic polyelectrolytes, were obtained by putting α = 1, T = 298.15 K, and b = 2.52 Å in eq 3. For parameters characteristic for solvent, the values for water at 298.15 K were used:[25] ϵ = 78.54, d ln ϵ/d ln $P = 4.71 \times 10^{-5}$, d ln V/d ln $P = -4.54 \times 10^{-5}$. At present, we have no information whatever regarding the coefficient d ln a/d ln P, so that this term of eq 9 may be considered as an adjustable parameter. In these calculations it was assumed to be negligible and set equal to zero. The value 8.0 Å was taken for the macromolecular radius, a, needed for obtaining the relation between γ and c.[22] It was estimated from structural data on polystyrenesulfonates.

Figure 2 shows excellent agreement between theory and experiment for HPSS up to concentration 0.4 monomol/l.; at higher concentrations, however, experimental values are higher than theoretical ones. For the sodium and magnesium salts similar deviations appear at lower concentrations. Exactly the same situation has been observed when experimental values of heats of dilution of polystyrenesulfonates have been compared with theoretical values.[26]

The observed deviations of the experimental values of Φ_v from the theoretical ones at high concentration are not unexpected. One would be naive to expect that at concentrations as high as 2 *m*, where distances between neighboring polymer molecules become comparable to their thickness, a purely electrostatic theory would satisfactorily explain experimental results. Studies of the apparent molal quantities of solutions of simple electrolytes[15] have disclosed that the dependence of the ionic radius on temperature and pressure is decisive in determining the concentration dependence of the apparent molal enthalpies and volumes, respectively, in the region of higher concentrations. We have shown[26] that it is possible to obtain a good correlation between theoretical and experimental values of heats of dilution of alkali polystyrenesulfonates by choosing for d ln a/d ln T arbitrary but reasonable values. Such speculations have failed in this case. For instance, suing for λ the value 3.40 which is 1.2 times higher than the structural one, and by choosing for the term d ln a/d ln P an appropriate value 5.0×10^{-5}, we have nearly the same theoretical curve as with the structural value of λ = 2.83 and d ln a/d ln P = 0. It is certainly true that the answer to the discrepancy between theory and experiment has to be sought in the increasing noncoulombic interactions between ions at higher concentrations, in other words, in the simplification made in going from eq 11 to eq 12. Therefore, an approach to this problem considering also the noncoulombic interactions between the polyion and its counterions will have to be attempted in the future.

One thing more has to be pointed out concerning the theoretical model. The predicted increase of Φ_v with con-

centration might be surprising at first sight, since in the model the molar volume of the rodlike polyion and its counterions does not depend on concentration. However, inspection of the theoretical expression for Φ_v shows that Φ_v is proportional to the electrostatic energy of the solution u, which reflects electrostatic interactions between the polyion and counterions. These interactions depend on the properties of the solvent and decrease with increasing concentration. As a consequence, the structural properties of a medium around ions change. Thus, according to the model the whole concentration dependence of Φ_v is attributed to changing of solvent structure in polyelectrolyte solution. A similar interpretation has been given in some papers in order to explain the concentration dependence of Φ_v in a real polyelectrolyte solution. In this case "changing of solvent structure" implies overlapping of the electrostricted regions of water around ions. This results in a reduced constrictive effect per polyion and, therefore, in a positive concentration dependence of Φ_v.

According to the theory of Manning[27] there are limiting laws for thermodynamic properties of pure polyelectrolyte solutions at high dilutions (not at zero concentration for real flexible polymers). Using Manning's equations we have found that the limiting law for the apparent molal volume in our notation would read

$$\frac{d\Phi_v}{d \ln c} = \frac{\alpha z_1 V_m}{2 z_2 \lambda} \frac{d \ln \epsilon}{d \ln P} \qquad (\lambda > 1) \qquad (13)$$

where λ has the structural value (2.83 for monovalent and 5.66 for divalent salts of HPSS). The same result follows from eq 9, 10, and 4 in the limit $c \rightarrow 0$ ($\beta \rightarrow 0$). It can be seen that the experimental slopes in Figure 2 appear to approach the limiting slopes calculated from eq 13 as the concentration decreases. Furthermore, by rewriting the limiting slope in the form $d\Phi_v/dc = (1/c)(d\Phi_v/d \ln c)$ it becomes obvious that the theoretical slope $d\Phi_v/dc$ has to increase drastically with increasing dilution, a conclusion which is amply supported by experimental observations (*cf.* Figure 1).

Finally, it should be mentioned that although this work does not propose any method of obtaining the apparent molal volumes of polysalts, Φ_v^∞, at zero concentration it does not deny a physical significance of Φ_v^∞. The reported approximative logarithmic decrease of Φ_v with decreasing concentration may apparently suggest a nonlimiting behavior of Φ_v. However, it has to be borne in mind that the cell model, which predicts such concentration dependence of Φ_v, breaks down at concentrations at which the average intermolecular distances become larger than the length of the macromolecule. The possibility is also admitted for real polyelectrolyte solutions[27] that the "limiting laws" are limited to final concentrations. Therefore, one may conclude that neither the experimental nor the theoretical results given in this work exclude possible levelling off of Φ_v in the logarithmic diagram at extremely low concentrations

Acknowledgments. I wish to express my thanks to Professors D. Dolar and S. Lapanje for careful reading and commenting on the manuscript. I appreciate very much a critical review of the manuscript by Professor Z. Alexandrowicz. I also wish to acknowledge the technical assistance of Mr. G. Trtnik, who performed most of the dilatometric measurements. This study was partially supported by the Boris Kidrič Fund.

References and Notes

(1) H. Inagaki and A. Teramoto, *Makromol. Chem.*, **47**, 185 (1961).
(2) B. E. Conway, J. E. Desnoyers, and A. C. Smith, *Phil. Trans. Roy. Soc. London*, **256**, 389 (1964).
(3) M. Rinaudo and C. Pierre, *C. R. Acad. Sci., Ser. C*, **269**, 1280 (1969).
(4) P. Roy-Chowdhury, *J. Appl. Polym. Sci.*, **12**, 751 (1968); *J. Polym. Sci., A-2*, **7**, 1451 (1969).
(5) P. Roy-Chowdhury and K. M. Kale, *J. Appl. Polym. Sci.*, **14**, 2937 (1970).
(6) S. Friedman, A. Caillé, and H. Daoust, *Macromolecules*, **3**, 700 (1970).
(7) J. Lawrence and B. Conway, *J. Phys. Chem.*, **75**, 2353 (1971).
(8) N. Ise and T. Okubo, *J. Amer. Chem. Soc.*, **90**, 4527 (1968); *Macromolecules*, **2**, 401 (1969).
(9) C. Tondre and R. Zana, *J. Phys. Chem.*, **76**, 3451 (1972).
(10) U. P. Strauss and Y. P. Leung, *J. Amer. Chem. Soc.*, **87**, 1476 (1965).
(11) S. Lapanje and S. A. Rice, *J. Amer. Chem. Soc.*, **83**, 496 (1961).
(12) L. Kotin and M. Nagasawa, *J. Amer. Chem. Soc.*, **83**, 1026 (1961).
(13) D. Kozak, J. Kristan, and D. Dolar, *Z. Phys. Chem. (Frankfurt am Main)*, **76**, 85 (1971).
(14) J. Škerjanc, V. Doleček, and S. Lapanje, *Eur. J. Biochem.*, **17**, 160 (1970).
(15) H. S. Harned and B. B. Owen, "The Physical Chemistry of Electrolytic Solutions," 3rd ed, Reinhold, New York, N. Y., 1958, Chapter 8.
(16) R. A. Robinson and R. H. Stokes, "Electrolyte Solutions," Butterworths, London, 1959, Chapter 9, pp 478–481.
(17) P. J. Flory, "Principles of Polymer Chemistry," Cornell University Press, Ithaca, N. Y., 1953, pp 534, 633, interpreted in terms of osmotic coefficients; *cf.* eq 29 of ref 20.
(18) G. V. Schulz and M. Hoffman, *Makromol. Chem.*, **23**, 220 (1957).
(19) A. Katchalsky, "Polyelectrolytes," in "International Symposium on Macromolecules," M. J. Voorn, Ed., Butterworths, London, 1971, pp 336, 343.
(20) R. W. Armstrong and U. P. Strauss, "Polyelectrolytes," in "Encyclopedia of Polymer Science and Technology," Vol. 10, H. F. Mark, N. G. Gaylord, and N. M. Bikales, Ed., Interscience, New York, N. Y., 1968, pp 789, 810–815.
(21) J. Škerjanc, D. Dolar, and D. Leskovšek, *Z. Phys. Chem. (Frankfurt am Main)*, **56**, 208 (1967).
(22) S. Lifson and A. Katchalsky, *J. Polym. Sci.*, **13**, 43 (1954).
(23) (a) R. M. Fuoss, A. Katchalsky, and S. Lifson, *Proc. Nat. Acad. Sci. U. S.*, **37**, 579 (1951); (b) T. Alfrey, Jr., P. W. Berg, and H. Morawetz, *J. Polym. Sci.*, **7**, 543 (1951).
(24) R. Fowler and E. A. Guggenheim, "Statistical Thermodynamics," Cambridge University Press, Cambridge, 1949, p 398.
(25) E. A. Guggenheim and R. H. Stokes, "Equilibrium Properties of Aqueous Solutions of Single Strong Electrolytes," in "The International Encyclopedia of Physical Chemistry and Chemical Physics," Topic 15, Vol. 1, D. D. Eley, J. E. Mayer, and F. C. Tompkins, Ed., Pergamon Press, Oxford, 1969, pp 25, 43.
(26) J. Škerjanc, D. Dolar, and D. Leskovšek, *Z. Phys. Chem. (Frankfurt am Main)*, **70**, 31 (1970).
(27) G. S. Manning, *J. Chem. Phys.*, **51**, 924 (1969).

Correlation of Orthopositronium Annihilation with Surface Tension in Liquids and Liquid Mixtures

B. Lévay, A. Vértes,

Department of Physical Chemistry and Radiology, L. Eötvös University, 1088 Budapest, Hungary

and P. Hautojarvi*

Department of Technical Physics, Helsinki University of Technology, SF-02150 Otaniemi, Finland *(Received April 2, 1973)*

The empirical relationship between the pick-off annihilation rate of the orthopositronium atom and the surface tension of molecular liquids published recently by Tao was found to be valid also in binary mixtures of water with methanol and dioxane. With the aid of the surface tension the pick-off rate was correlated with the parachor. From the additivity of the parachor a new additivity rule was derived for the pick-off rate. It is valid for both molecular liquids and binary mixtures. The connection to the parachor indicates also that the square root of the pick-off lifetime is a linear function of temperature and of the inverse of the viscosity. This simple law was found to be compatible with several earlier experimental results.

Introduction

The positronium atom is formed when the positron while slowing down captures an electron from a molecule. The two-quantum annihilation of an electron–positron pair is not possible in the spin triplet state. Therefore, in a condensed medium, if no other interactions, *e.g.*, ortho–para conversion or chemical quenching, take place the lifetime of the orthopositronium atom is determined by the so-called pick-off quenching. In this process the positron in the positronium atom annihilates with an electron of the medium, the spin of which is antiparallel to the spin of the positron. Thus the lifetime of 140 nsec of the orthopositronium atom *in vacuo* is reduced to a few nanoseconds.[1,2]

Many authors have attempted to explain theoretically this general annihilation phenomenon which occurs in all substances where positronium atoms are formed. Ferrell[3] has taken into consideration the different intermolecular forces acting in liquid helium on positronium atoms. He has concluded that positronium atoms form cavities inside the liquid helium. This "bubble" model for helium was improved by Roellig[4] and extended recently by Buchikhin, *et al.*,[5,6] to molecular liquids. Another theoretical model, the free volume theory, has been worked out by Brandt, *et al.*[7] Similar models have also been used by Ogata and Tao[8] and Thosar, *et al.*[9]

The phenomenon has also been investigated experimentally by many workers and efforts have been made to find a correlation between pick-off rate and the structural properties of molecular liquids. Gray, *et al.*,[10] have found the pick-off quenching cross section in organic liquids to be additive and to be affected by the structural properties of the molecules. Bisi, *et al.*,[11] have attributed to each atom in the molecule an effective number of electrons, whose spin is antiparallel to the spin of the positron in the positronium atom. This number, however, has not been observed to be affected by the structural properties of the molecules.

The behavior of pick-off quenching in liquid mixtures has been investigated only by a few workers. Tao and Green[12,13] have assumed and also verified in aqueous oxyacid solutions that the pick-off quenching cross section was additive in binary liquid mixtures. Lévay and Hautojärvi,[14] however, have not found additivity in methanol–water mixtures.

Recently Tao[15] has published an empirical relation between the pick-off rate and the surface tension of molecular liquids. This relationship was also found to have a theoretical foundation and to be able to explain other relationships between the pick-off rate and the various properties of the medium.

In the present work we shall show the validity of this relationship for the case of binary liquid mixtures. By using the parachor we suggest for the pick-off quenching rate a new additivity rule, which seems to be valid for both simple molecular liquids and binary mixtures. Correlations of the lifetime of the orthopositronium atom with temperature and viscosity are also derived.

Binary Liquid Mixtures

The pick-off quenching rate was measured in binary mixtures of water with dioxane and methanol, respectively. The experimental conditions of lifetime measurements have been published elsewhere.[14] The results are presented in Tables I and II together with surface tension data taken from the literature.[16]

The empirical relationship between pick-off rate λ_p and surface tension γ found by Tao[15] was

$$\lambda_p = \kappa\gamma^{\nu} \tag{1}$$

where κ and ν were constants, and their values were found to be 0.061 and 0.50, respectively, for a number of substances. For alcohols, however, a better fit was found using values of 0.046 and 0.55 for κ and ν. (λ_p was measured in $nsec^{-1}$ and γ in dyn/cm.)

Our results for the water–methanol and water–dioxane mixtures were analyzed by a least-squares fit from the log λ_p *vs.* log γ diagram in Figure 1. Values of κ and ν were calculated from the intercept and slope of the straight line and were found to be 0.057 and 0.55, respectively. These values are in quite good agreement with those found by Tao.

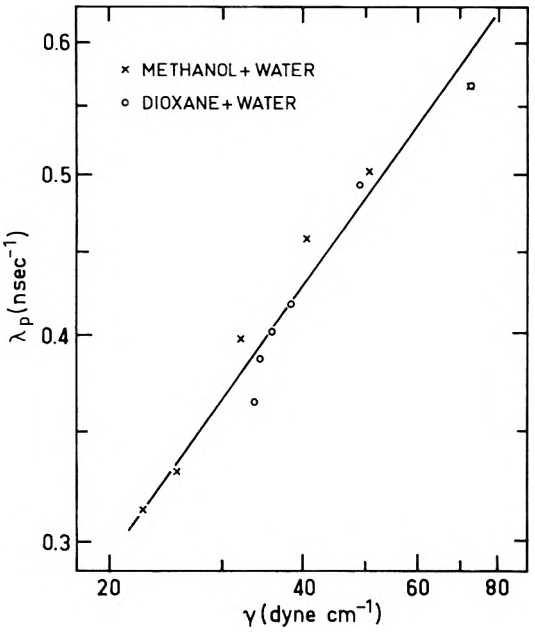

Figure 1. Pick-off quenching rate as a function of surface tension in methanol–water and dioxane–water systems. The solid straight line represents the least-squares fit of the data. Note that both axes have a logarithmic scale.

The change in the pick-off rate in these two different binary mixtures can thus be described by a single parameter, namely, the surface tension. This means, that the surface tension plays an important role, determining the pick-off rate even in very nonideal hydrogen bonding liquid mixtures in which there are strong and special interactions between the molecules of different components. In other words the pick-off quenching rate is very sensitive to all types of molecular forces and interactions which manifest themselves macroscopically in the surface tension.

As the surface tension is an easily measurable parameter its relationship to the pick-off rate seems to be very applicable for practical purposes. In the following we will derive new relationships between the pick-off rate and different physical quantities of molecular liquids from Tao's empirical law (1) by taking $\nu = \frac{1}{2}$.

Pick-Off Rate and the Parachor

On the basis of the empirically observed temperature dependence of the surface tension, Sugden[17] has given the definition of the parachor

$$P = (M/\rho)\gamma^{1/4} = V\gamma^{1/4} \tag{2}$$

where M is the molecular weight, ρ is the density, and V is the molar volume of the liquid.

The parachor was found to be temperature independent in a large temperature interval. Furthermore it proved to be additive, *i.e.*, given parachor increments were attributed to each atom in a given type of bond. Therefore, a given characteristic parachor value belongs to each molecule.

The theoretical explanation of temperature independence of the parachor was not given until quite recently, when Burstein[18] proved it on the basis of the free volume theory.

Now let us examine the correlation of the pick-off rate with the parachor. Combining eq 1 and 2 and taking into account that $\nu = \frac{1}{2}$, we obtain

TABLE I: Pick-Off Quenching Rate and Surface Tension in the Methanol–Water System

H_2O, mol %	λ_p, nsec^{-1}	γ,[a] dyn/cm	$\lambda_{AB}^{1/2}V_{AB}$,[b] nsec$^{-1/2}$ cm^3 M^{-1}
0	0.314 ± 0.004	22.5	22.7
4.86	0.316 ± 0.004	23.0	22.2
30.0	0.331 ± 0.005	25.5	19.5
60.2	0.399 ± 0.005	32.0	16.9
80.2	0.457 ± 0.006	40.5	15.2
90.2	0.502 ± 0.006	50.6	14.4
100	0.567 ± 0.007	72.75	13.5

[a] Reference 16. [b] Calculated from density data in ref 16.

TABLE II: Pick-Off Quenching Rate and Surface Tension in the Dioxane–Water System

H_2O, mol %	λ_p, nsec^{-1}	γ,[a] dyn/cm	$\lambda_{AB}^{1/2}V_{AB}$,[b] nsec$^{-1/2}$ cm^3 M^{-1}
0	0.365 ± 0.004	33.6	51.6
29.6	0.387 ± 0.005	34.25	40.2
50.2	0.402 ± 0.005	35.75	32.3
69.8	0.418 ± 0.006	38.3	24.7
89.8	0.493 ± 0.006	49.0	17.5
100	0.567 ± 0.007	72.75	13.5

[a,b] See corresponding footnote to Table I.

$$\lambda_p = \kappa(P^2/V^2) \tag{3}$$

The pick-off rate can also be expressed by the pick-off quenching cross section σ_p

$$\lambda_p = n\upsilon\sigma_p = (N_A/V)\upsilon\sigma_p \tag{4}$$

where υ is the velocity of the positronium atom in the medium and N_A is Avogadro's number.

Gray, *et al.*,[10] have found that in the separate families of compounds, *e.g.*, the *n*-alkanes, normal primary alcohols, 1-chloro-substituted *n*-alkanes, etc., the quenching cross section ($\upsilon\sigma_p$) was a linear function of the length of the molecule, *i.e.*, the number of carbon atoms in the molecule. They were able to calculate partial quenching cross sections for the various component groups. The empirical cross sections calculated from partial ones were in good agreement with those found experimentally.

This additivity rule, however, seems to contrast with formula 3 as P, and not P^2, is additive.

Equation 3 can be transformed to be formally similar to eq 4

$$\sqrt{\lambda_p} = (\sqrt{\kappa}/V)P = (N_A/V)P' \tag{5}$$

if we define P' as relative parachor, which is additive.

Then there is the following relation between P' and the cross section

$$P' = \upsilon\sigma_p/\sqrt{\lambda_p} \tag{6}$$

We shall show that the new additivity rule expressed by eq 5 gives better agreement between calculated and experimentally found results than eq 4, both for simple liquids and liquid mixtures.

We calculated the P' values from the cross sections measured by Gray, *et al.*,[10] for *n*-alkanes, normal primary alcohols, and water by using eq 6. Then the partial P' values were calculated for the component groups which

TABLE III: Relative Parachor Values for *n*-Alkanes, Normal Primary Alcohols, and Water

Compound	P', 10^{-18} cm^3/sec$^{1/2}$ Obsvd[a]	Calcd[b]	% error[c] This work	Ref 10
n-Butane	2.48	2.484	−0.16	0.00
n-Pentane	3.01	2.997	+0.43	1.49
n-Hexane	3.49	3.510	−0.57	−0.72
n-Heptane	4.03	4.023	+0.17	0.90
n-Octane	4.54	4.536	+0.09	0.53
n-Nonane	5.07	5.049	+0.41	0.93
n-Decane	5.56	5.562	−0.04	−0.11
n-Undecane	6.08	6.075	+0.08	0.48
n-Dodecane	6.59	6.588	+0.03	1.13
n-Tridecane	7.10	7.101	−0.01	−0.16
n-Tetradecane	7.63	7.614	+0.21	0.30
n-Pentadecane	8.13	8.127	+0.04	−0.07
n-Hexadecane	8.67	8.640	+0.35	0.46
n-Heptadecane	9.16	9.153	+0.08	−0.25
n-Octadecane	9.65	9.666	−0.17	−1.00
		Av	0.19	0.57
Methyl alcohol	1.08	1.075	+0.46	6.98
Ethyl alcohol	1.58	1.588	−0.51	−0.78
n-Propyl alcohol	2.11	2.101	+0.43	0.28
n-Butyl alcohol	2.65	2.614	+1.36	1.09
n-Octyl alcohol	4.66	4.666	−0.13	−1.82
n-Dodecyl alcohol	6.76	6.718	+0.62	−0.33
		Av	0.59	1.88
Water	0.66	0.562	14.85	39.31

[a] Calculated from Gray's data by eq 6. [b] Calculated from partial P' values in Table IV. [c] $100(P'_{obsvd} - P'_{calcd})/P_{obsvd}$.

TABLE IV: Partial Relative Parachor Values for Component Groups

Group	P', 10^{-18} cm^3 sec$^{-1/2}$	Group	P', 10^{-18} cm^3 sec$^{-1/2}$
H	0.216	CH_3	0.729
CH_2	0.513	OH	0.346

were used to calculate empirical P' values. The results are presented in Tables III and IV, where for comparison Gray's per cent error are also included.

As can be seen the calculated P' values are in better agreement with the experimental ones, than the cross sections. Not only is the average error (in per cent) about three times less for the P' values than for the cross sections but Gray's extremely scattered calculated value for methanol and even for water are in much better agreement with the measured ones.

Furthermore, the partial cross sections calculated by Gray show an unexpected relation to each other.

For example, the cross section of the CH_3 group is less than the cross section of the CH_2 group, which means that the cross section of H has to be negative for *n*-alkanes.

Our P' values, however, show a normal relation to each other (Table IV). It seems that the new additivity rule is supported by this fact also.

The difference between the two additivity rules perhaps manifests itself most clearly in binary mixtures of water with methanol and dioxane.

By assuming that the cross sections themselves were directly additive, it was shown by us[14] that the $\lambda_p V$ product would have to be a linear function of the mole fraction in binary mixtures. This relation, however, was not found to be valid for the methanol–water system, where a large negative deviation from linearity was observed.

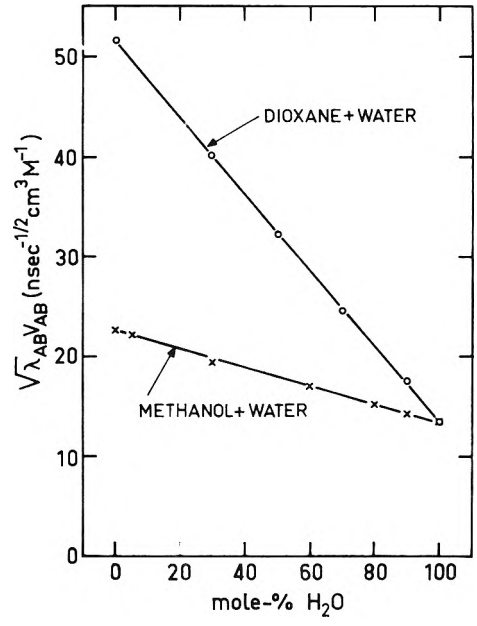

Figure 2. Variation of $\lambda_{AB}^{1/2}V_{AB}$ with composition in binary mixtures of water with methanol (×) and dioxane (○).

Using the new additivity rule, we can write

$$\sqrt{\lambda_{AB}}V_{AB} = \sqrt{\lambda_A}V_A - (\sqrt{\lambda_A}V_A - \sqrt{\lambda_B}V_B)X_B \qquad (7)$$

where the subscripts A, B, and AB refer to components A and B and the mixtures, respectively, and X_B is the mole fraction.

Our results give an excellent fit to eq 7. The $\lambda_{AB}^{1/2}V_{AB}$ values of both the water–methanol and water–dioxane systems lie on straight lines in the whole concentration range as can be seen in Figure 2. This fact again confirms the validity of the new additivity rule.

Finally, it is worth mentioning, that there is a theoretical correlation between the parachor and the polarizability α of molecules[18]

$$P = (\text{constant})\sqrt{\alpha} \qquad (8)$$

Burstein[18] has pointed out that this relationship contains a contradiction in the sense that both P and α have empirically proved to be additive.

Comparing eq 8 with eq 3 one can conclude that the pick-off rate is directly proportional to the polarizability and thus it is additive. This relationship was found empirically by Gray, *et al.*[10]

Thus both additivity rules have a theoretical foundation and both of them are more or less valid. At any rate, in the case of pick-off annihilation the additivity rule derived from the correlation with parachor proved to be much more applicable.

The Free Volume Model and the Temperature Dependence

The parachor is essentially proportional to the zero molar volume V_0 of the substance[19]

$$P = k'V_0 \qquad (9)$$

where k' is a constant.

From this relationship a direct correlation can be derived between pick-off rate and the "free volume" available for the molecules.

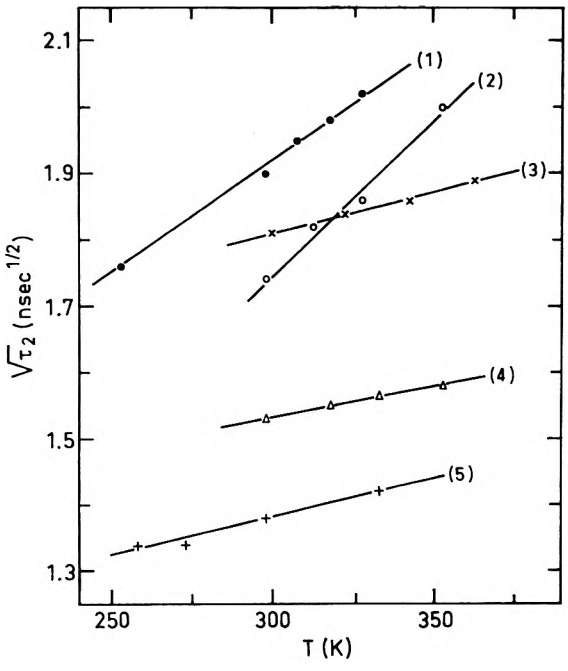

Figure 3. Temperature dependence of the pick-off lifetime in liquids: (1) *n*-octane, (2) iodobenzene, (3) *n*-tridecane, (4) aniline, (5) glycerol.

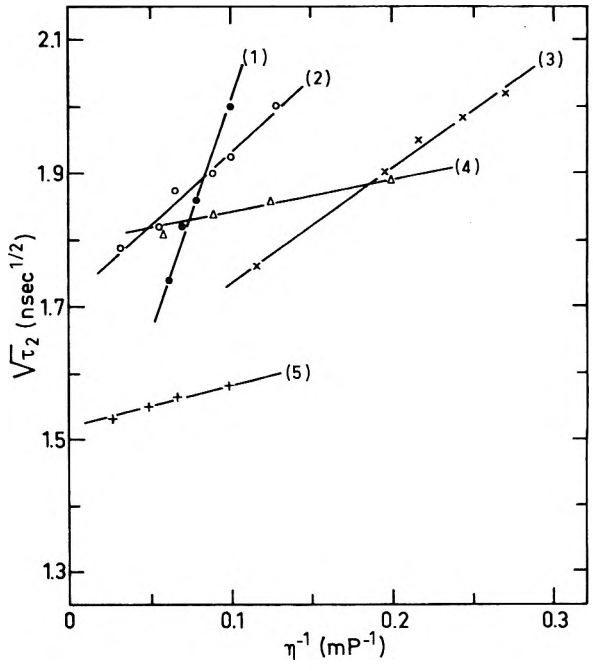

Figure 4. Correlation of the pick-off lifetime with viscosity change of liquids: (1) iodobenzene, (2) n-hexadecane, (3) *n*-octane, (4) *n*-tridecane, (5) aniline.

Substituting eq 9 into eq 3 we obtain

$$\lambda_p = K(V_0/V)^2 \tag{10}$$

where K is a constant.

The free volume V_f for 1 mol of a substance by definition is

$$V_f = V - V_0 \tag{11}$$

Substituting eq 11 into eq 10 we obtain the relationship between the pick-off lifetime τ_p and the free volume

$$\tau_p = \frac{1}{\lambda_p} = K'\left(1 + \frac{V_f}{V_0}\right)^2 \tag{12}$$

where K' is a constant.

The free volume is proportional to the temperature and can be expressed by the thermal expansion coefficient β of the substance in the form[15]

$$V_f = \beta T \tag{13}$$

and then from eq 12 and 13 a direct correlation of the lifetime to the temperature can be found

$$\sqrt{\tau_p} = K''[1 + (\beta T/V_0)] \tag{14}$$

where K'' is a constant.

The square root of the pick-off lifetime have to vary linearly with temperature. Equation 14 proved to be valid for all the substances for which lifetime data as a function of temperature were available from the literature, that is, for *n*-tridecane,[10] *n*-octane, *n*-hexadecane, iodobenzene, aniline, glycerol,[9] ethanol, and 1-propanol.[6] This is presented in Figure 3.

It is worth mentioning that Thosar, *et al.*,[9] have tried to correlate the temperature dependence of the pick-off rate with the viscosity of the liquids.

In the case of associating liquids, *e.g.*, aniline and glycerol, they were not able to find any correlation.

Now we shall show that from eq 3 a simple and direct relationship between the pick-off lifetime and the viscosity change of liquids can be derived. For nonassociating liquids the molecular volume is directly proportional to reciprocal viscosity η^{-1} [19b]

$$V = A + B\eta^{-1} \tag{15}$$

where A and B are constants for a given liquid. Substituting eq 15 into eq 3 we obtain

$$\sqrt{\tau_p} = A' + B'\eta^{-1} \tag{16}$$

where A' and B' are constants.

Using data from ref 9 we have found the linear relationship between the square root of pick-off lifetime and reciprocal viscosity to be valid for all the liquids. This is presented in Figure 4.

Summary

The empirical relationship between the pick-off rate and the surface tension discovered by Tao[15] was found to hold also for binary liquid mixtures, namely, for water–methanol and water–dioxane systems.

With the aid of the surface tension the pick-off rate could be correlated with the parachor. This relationship proved to be useful in deriving other simple relationships between the pick-off rate and temperature or viscosity. Furthermore, it resulted in a new additivity rule, which proves valid not only for simple molecular liquids but for their binary mixtures as well.

Tao's empirical relationship is very applicable for practical purposes as it contains only one parameter, namely, surface tension. This is easily measurable experimentally, and represents the resultants of different molecular forces acting in molecular liquids.

References and Notes

(1) J. H. Green and J. Lee, "Positronium Chemistry," Academic Press, New York, N. Y., 1964.
(2) V. I. Goldanskii, *At. Energy Rev.*, **6**, 3 (1968).
(3) R. A. Ferrell, *Phys. Rev.*, **108**, 167 (1957).
(4) L. O. Roellig in "Positron Annihilation," L. O. Roellig and A. T. Stewart, Ed., Academic Press, New York, N. Y., 1965, p 127.
(5) A. P. Buchikhin, V. I. Goldanskii, A. O. Tatur, and V. P. Shantarov-

ich, *Zh. Eksp. Theor. Fiz.*, **60**, 1136 (1971) [*Sov. Phys. -JETP*, **33**, 615 (1971)].
(6) A. P. Buchikhin, V. I. Goldanskii, and V. P. Shantarovich, *Pis. Zh. Eksp. Theor. Fiz.*, **13**, 624 (1971) [*JETP Lett.*, **13**, 444 (1971)].
(7) W. Brandt, S. Berko, and W. W. Walker, *Phys. Rev.*, **120**, 1289 (1960).
(8) A. Ogata, and S. J. Tao, *J. Appl. Phys.*, **41**, 4261 (1970).
(9) B. V. Thosar, V. G. Kulkarni, R. G. Lagu, and G. Chandra, *Indian J. Pure Appl. Phys.*, **9**, 1008 (1971).
(10) P. Gray, C. F. Cook, and G. P. Stu-m, *J. Chem. Phys.*, **48**, 1145 (1968).
(11) A. Bisi, G. Gambrini, and L. Zappa, *Nuovo Cimento B*, **67**, 75 (1970).
(12) S. J. Tao and J. H. Green, *J. Chem. Soc. A*, 408 (1968).
(13) S. J. Tao and J. H. Green, *J. Phys. Chem.*, **73**, 882 (1969).
(14) B. Lévay and P. Hautojärvi, *Radiochem. Radioanal. Lett.*, **10**, 309 (1972).
(15) S. J. Tao, *J. Chem. Phys.*, **56**, 5499 (1972).
(16) J. Timmermans, "The Physico-Chemical Constants of Binary Systems in Concentrated So utions," Vol. 4, Interscience, New York, N. Y., 1960.
(17) S. Sugden, *J. Chem. Soc.*, **125**, 32 (1924).
(18) A. J. Burstein, *Dokl. Akad. Nauk SSSR*, **205**, 615 (1972).
(19) J. R. Partington, "An Advanced Treatise on Physical Chemistry, The Properties of Liquids," Vol. 3, Longmans, Green and Co., London, 1955, (a) p 146; (b) p 90.

Tracer Diffusion Coefficients in Aqueous Solutions. I. The Method. Sodium in Sodium Chloride

Henry C. Thomas* and James C. Ku[1]

Department of Chemistry, University of North Carolina, Chapel Hill, North Carolina 27514 *(Received February 15, 1973)*

Publication costs assisted by the National Science Foundation

A variant of a method for measuring tracer diffusion coefficients in gels which is applicable to aqueous solutions of ions with hard γ emitting isotopes is described. The coefficient for sodium chloride solutions in the range 0–0.5 M at 25° is given by $D \times 10^5 = 1.330 - 0.1568C^{1/2} + 0.1252C$.

In our studies[2] of self diffusion in gels and colloidal suspensions, we have been badly hindered in interpretation by the lack of reliable values of the coefficients in aqueous solution. Most of the data in the literature are both inadequate in scope and highly suspect in accuracy. It is well known that diffusion coefficients are difficult to measure. Probably the best results for sodium are those of Mills and Adamson[3] obtained from a diaphragm cell, which necessarily required calibration. At one time we thought[4] erroneously that measurements in agar gels could be accurately extrapolated to zero agar content. This misapprehension resulted from a failure to recognize that the gels were not quite in chemical equilibrium with the solution into which the diffusion took place. Some sort of compensation of errors misled us.

A recent technological advance has made possible an experiment which we believe gives reliable determinations of tracer diffusion coefficients in aqueous solution. It is the purpose of this communication to describe the experiment and present results for sodium in solutions of sodium chloride.

The Method

In principle the experiment differs little from that described much earlier[5] in which the diffusion takes place from a short rod through a confining membrane into an "infinite" bath. In all of the previous work the short rod consisted of a gel or a highly viscous colloidal suspension. The method fails with aqueous solutions because of unavoidable mixing. The technological advance mentioned above which has enabled us to go further is the production of what is known as a Collimated Holes Structure[6] (CHS). A piece of this material makes up the "short rod" from which diffusion takes place. It is 0.3084 cm in length, about 0.25 in. across, and is perforated by some 5500 hexagonal holes of nominal diameter 0.002 in. Aqueous solutions in these fine capillaries are essentially stiff to the mechanical and thermal disturbances in our equipment, as will be seen from the self-consistency of the results.

In our previous work an approximation in the mathematical description of the experiment had been introduced; namely, it was assumed that the concentration gradient through the confining cellophane membrane was linear, in effect that the membrane was thin as compared to the short rod of gel. This was experimentally shown to be sufficiently near the truth. But with the CHS the fraction free space is only about 50%, and the amount of solution in the wet cellophane is comparable in amount to that in the short capillaries of the CHS. It has therefore been necessary to enlarge the boundary value problem for the experiment without introducing any approximations as to relative void volume of CHS and cellophane or making any assumption as to the gradient in the cellophane. A summary is given here of the boundary value problem and its solution. This will serve to list all assumptions and approximations which we still must make. In Figure 1 is given the model assumed for the experiment. We assume that there is no ionic adsorption in either section of the cell and that the whole contents of the cell are at chemical equilibrium with the solution of the infinite bath, with which the cell is in contact only at $x = a + b$. Assuming

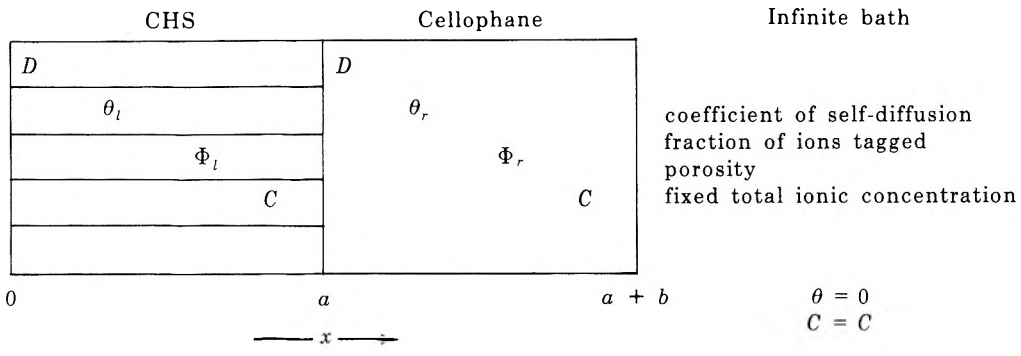

Figure 1.

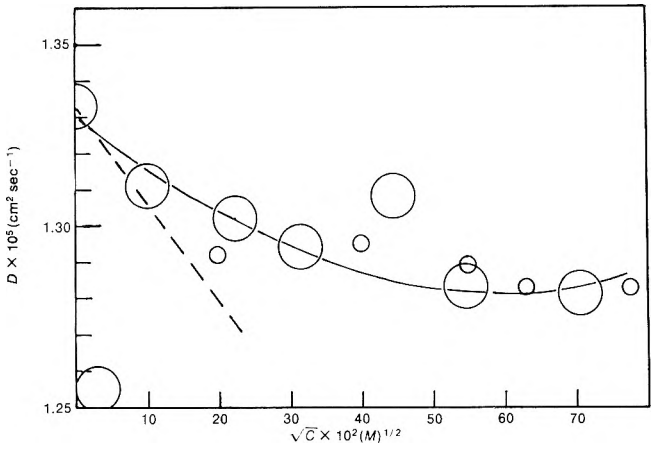

Figure 2. Tracer diffusion coefficient of Na^+ in NaCl at 25°: large circles (diameter 1% of D), present work; small circles, Mills and Adamson;[3] dashed line, Onsager limiting law; solid curve, $D = 1.330 - 0.1568C^{1/2} + 0.1252C$.

Ficks' laws the diffusion problem is

$$DC\Phi_l \frac{\partial^2\theta_l}{\partial x^2} = C\Phi_l \frac{\partial\theta_l}{\partial t} \qquad 0 < x < a,\ t > 0 \qquad (1)$$

$$DC\Phi_r \frac{\partial^2\theta_r}{\partial x^2} = C\Phi_r \frac{\partial\theta_r}{\partial t} \qquad a < x < a + b,\ t > 0 \qquad (2)$$

$$\partial\theta_l/\partial x = 0 \qquad x = 0,\ t \geq 0 \qquad (3)$$

$$\theta_l = \theta_r \qquad x = a,\ t \geq 0 \qquad (4)$$

$$DC\Phi_l \frac{\partial\theta_l}{\partial x} = DC\Phi_r \frac{\partial\theta_r}{\partial x} \qquad x = a,\ t \geq 0 \qquad (5)$$

$$\theta_r = 0 \qquad x = a + b,\ t > 0 \qquad (6)$$

$$\theta_l = \theta_r = \theta_0 \qquad 0 \leq x \leq a + b,\ t = 0 \qquad (7)$$

Equation 3 demands no flux through the left boundary. Equation 4 demands instantaneous isotopic equilibrium at the interface between the two sections, and eq 5 expresses the continuity of flux at this point. Equation 7 effectively demands a large rapidly stirred bath in contact with the open end of the cell. Of these requirements only that of eq 5 is somewhat suspicious. The cellophane rests on the metal separating the capillaries. There must be some disturbance of the boundary condition 5 due to this as well as to the ring of cellophane supported on metal around the capillary matrix. There is no practical way to take these into account; we must accept the uncertainty.

In the actual experiment we measure a quantity, which we call Q, proportional to the total rate of radiation of the tagged atoms in the cell. If Q_0 is the value of Q at the start of the experiment, $t = 0$, then

$$\frac{Q}{Q_0} = \frac{\Phi_l \int_0^a \theta_l\,dx + \Phi_r \int_a^{a+b} \theta_r\,dx}{\Phi_l a\theta_0 + \Phi_r b\theta_0} = \frac{1}{a\theta_0} \frac{\psi \int_0^a \theta_l\,dx + \int_a^{a+b} \theta_r\,dx}{\psi + r} \qquad (8)$$

where

$$\psi \equiv \Phi_l/\Phi_r \qquad (9)$$

and

$$r \equiv b/a \qquad (10)$$

We have to determine D and ψ from measured values of Q/Q_0 and the time.

Since the problem is linear throughout, it is perhaps most easily handled by the method of the Laplace transform. On inverting the transforms for the contents of the left and right parts of the cell we eventually find

$$\frac{Q}{Q_0} = \frac{2}{\psi + r} \sum_{n=1}^{\infty} \frac{e^{-Dt\alpha_n^2/a^2}}{\alpha_n^2} \frac{\psi \tan\alpha_n + \tan r\alpha_n}{(1 + \psi r)\tan\alpha_n + (\psi + r)\tan r\alpha_n} \qquad (11)$$

Here the α_n are the positive roots of

$$\psi \tan y \tan ry = 1 \qquad (12)$$

Putting $\omega = r\psi$ it is immediately seen that to the approximation $\tan r\alpha = r\alpha$ this result reduces to that previously used.[5]

Equation 11 is applied to the data in much the same way as previously described except that the computer now does all the work and gives us the best value of D and ψ together with a print-out of the calculated and experimental values of Q/Q_0 and their differences.

Experimental Section

The only difficult part of the experiment is the filling of the capillaries with the radioactive solution. After a goodly number of abortive attempts the following procedure was developed.

The CHS is cleaned by soaking for several hours in concentrated nitric acid. It is washed and dried along with the other parts of the stainless steel cell in which it is mounted. The cell is then clamped in an inverted position so that the bottom of the CHS ($x = 0$) is exposed and the lower end of the cell is closed with a rubber stopper. Now 200–300 λ of radioactive solution are placed on the exposed ends of the capillaries. With the aid of a medical

syringe the solution is sucked into the capillaries until they are full. Excess solution is removed with a bit of tissue and the cell assembled. A glass plate closes the bottom, and presoaked cellophane is clamped over the top. Great care must be taken to avoid introducing air bubbles.

The least-squares values of the parameter ψ vary from 0.8 to 1.2, probably because of the impossibility of assembling and filling the cell in a completely reproducible manner. A rough estimate based on weights and thicknesses of dry and wet cellophane gives for the ratio of the porosities about 0.7. Fortunately the values of D are insensitive to the quantity.

Results

Figure 2 shows the results of 18 runs using Na-22 as the tracer in sodium chloride solutions from 0.01 to 0.5 M at 25.00 ± 0.01°. The points represent the average results of two to five runs. The average agreement of replicate runs with their averages is 0.019. We do have greater troubles than this. Possibly from some undetected instrumental fault the point at 0.2 M (an average of five runs) seems to be grossly out of line and was omitted in the calculation of the empirical equation below. Fifty pairs, Q/Q_0 and t, were recorded for each run. The details of carrying out the experiment have been described.[5]

Our experiment is apparently unsatisfactory at concentrations much below 0.01 M, possibly due to some adsorption effect. Using the Nernst limiting point, $RT\lambda_0/F^2 = 1.333 \times 10^{-5}$ cm^2 sec^{-1}, as a piece of data and omitting the points at 0.001 and 0.2 M, the least-squares best parabola in $C^{1/2}$ representing the results is

$$D \times 10^5 = 1.330 - 0.1568C^{1/2} + 0.1252C$$

This is given by the solid line in Figure 2. The larger circles are our experimental points. The diameter of these is 1% of the diffusion coefficient. The dashed line is for the Onsager limiting law for this case

$$D \times 10^5 = 1.333 - 0.2679C^{1/2}$$

In our present equipment it is impossible to measure the thickness, b, of the wet cellophane after it has been clamped over the CHS. We have, therefore, for one run at 0.01 M forced the data to agree with the Onsager limiting law by altering the value of b (as measured with a micrometer outside the cell) from 0.0251 to 0.0282 cm. This altered the measured coefficient from 1.285×10^{-5} to 1.306×10^{-5}, about the experimental error. The membrane thickness $b = 0.0282$ was used in the calculations for the remaining 19 experiments. Here the method loses its absolute character, although this could be remedied, if it is desired to push the accuracy further.

The small circles in Figure 2 (the diameter of which has no significance) are for the data of Mills and Adamson,[3] as obtained with a calibrated diaphragm cell. The agreement is all that could be expected.

We believe that we have shown that we have an reliable and rapid method for measuring tracer diffusion coefficients in aqueous solution of which have hard γ emitting isotopes.

Acknowledgment. It is a pleasure again to thank the National Science Foundation for the support of this work.

References and Notes

(1) Post doctoral research associate.
(2) *E.g.*, A. G. Langdon and H. C. Thomas, *J. Phys. Chem.*, **75**, 1821 (1971), where other references are given.
(3) R. Mills and A. W. Adamson, *J. Amer. Chem. Soc.*, **77**, 3454 (1955).
(4) A. L. Slade, A. E. Cremers, and H. C. Thomas, *J. Phys. Chem.*, **70**, 2840 (1966).
(5) G. F. Allen, H. Schurig, L. Slade, and H. C. Thomas, *J. Phys. Chem.*, **67**, 1402 (1963).
(6) Manufactured by the Brunswick Corporation, Technical Products Division, Skokie, Ill. 60076.

Mechanism of the Reaction of Hydrogen with Uranium

Tomoyasu Hashino* and Yasuharu Okajima

Institute of Atomic Energy, Kyoto University, Kyoto, Japan

(Received August 29, 1972; Revised Manuscript Received April 11, 1973)

Publication costs assisted by the Institute of Atomic Energy, Kyoto University, Kyoto, Japan

The reaction mechanism of the formation and decomposition of uranium hydride has been developed in terms of an absolute rate equation. The equation derived was sufficient to describe characteristic features of the system, the explanation of which is beyond the scope of the classical approach based on the macroscopic treatment of chemical kinetics. The treatment proposed was justified by the fact that the equilibrium condition is of the same form as Lacher's isotherm, which is the most reliable equilibrium equation for transition metal–hydrogen systems, including the uranium–hydrogen system. The kinetic parameters of the simplified equation were determined from the experimental results, and the validity condition was tested.

Introduction

A mass of uranium metal heated in hydrogen gas absorbs hydrogen until its concentration in the metal attains an equilibrium value which is dependent on the temperature of the specimen and the pressure of the atmosphere.[1] The hydrogen in uranium can easily be removed by vacuum and/or heat treatment. Thus, the reaction of uranium with hydrogen is chemically reversible. The nonstoichiometrical character of uranium hydride has been interpreted as being due to the vacancies within the sublattice accessible for occupation by hydrogen.[2] Accordingly, the reaction between hydrogen and uranium may in effect be reduced to the problem of putting in or taking out hydrogen from the sublattice position.

Uranium hydride is considered to be a true chemical compound with the formula UH_3 when it is completely saturated with hydrogen.[3,4] According to the phase diagram of the system,[5,6] α-phase and β-phase solid solutions exist in small regions of low and high hydrogen concentration, respectively, while the two phases coexist in the large intermediate region. Thus, the system may be envisaged as a solid solution having a tendency of hydrogen aggregation, so that the mutual attraction between hydrogen atoms in the solid system, although the origin of this attraction has not yet clearly been explained, must affect the chemical process, as suggested by Lacher's isotherm.[2,6] In the argument of lattice defects in uranium hydride it has been emphasized that transition metal hydrides in general, including uranium hydride, are to a large extent ionic rather than interstitial compounds.[2] However, it does not seem to be adequate that the interaction force is interpreted as due to occurrence of an electric field associated with the presence of lattice vacancy, because the hydride has the same order of electric conductivity as the parent metal.[3,4]

The formation of the hydride results in the complete disintegration of the structure of the original metal, and the hydride appears as voluminous, finely divided black powder. This fracture is thought to be caused by the internal stress produced by introducing hydrogen atoms as inclusions into the small interstices between the uranium atoms in the metal lattice, because the density of the β phase is nearly one-half that of the α phase. Thus, it may be recognized that the parent uranium lattice suffers considerable deformation which is sufficient to change the crystal configuration.[4] On the other hand, the continuum theory of lattice defects[7] has proved that a pronounced interaction occurs between the inclusions ejected by the stress field which is associated with the presence of the inclusions. Thus, it is probable that the parent-lattice deformation accompanying the reaction is related not only to the hysteresis phenomena of the process,[6,8] but also to the stability with respect to the distribution of hydrogen atoms over the sublattice points.

Empirical or half-empirical rate equations have been presented, mainly based on a diffusion model.[9-11] However, they do not predict the aggregation of hydrogen, the occurrence of hysteresis, and various lattice deformation effects. To be satisfactory, the equation must ensure the attainment of Lacher's isotherm at equiliblium conditions.[2,6] This suggests that a satisfactory approach must be based on a microscopical rather than macroscopical treatment. Wicke, *et al.*,[8] have pointed out the difficulties which arise from the classical approach, and suggest a statistical mechanical approach to the problem. Thus, it seems that the theory of rate processes is appropriate for handling the problem. In the theory, both the diffusion process and the chemical reaction may be treated in the same way, the diffusion process being considered simply as the making and breaking of bonds between a diffusing particle and an empty site.[12] Furthermore, in accordance with the fundamental postulates of statistical mechanics, the region under consideration, while much smaller than a macroscopic scale, is much larger than the molecule dimensions. Therefore, as long as the absolute rate equation is derived for the case where the rate-determining stage is within the solid phase, it can be used to represent the rate of the jump process at some arbitrary point in the solid phase.

The purpose of this paper is to obtain an absolute rate equation which is satisfactory to describe the characteristic features of the system. This theory may be applicable to other transition metal–hydrogen systems.

Theory

Rate Equations of Hydrogenation Reaction. It has been reported that the reaction rate of the hydrogenation of

uranium is proportional to $P^{1/2}/(b + aP)^{1/2}$ under ordinary conditions, where P is the pressure of the hydrogen atmosphere and constants a and b are determined experimentally.[8] This result suggests that the rate of the overall hydrogenation reaction is determined by the stage at which a hydrogen atom jumps from its chemisorption site on the metal surface to a site below the surface.

Before discussing the approach based on the theory of rate processes, let us consider the interaction arising between hydrogen atoms in the solid phase. As mentioned before, it has been proved that the interaction between the inclusions inserted into a continuum is related to the stress field associated with the presence of a set of inclusions.[7] Thus, the potential energy associated with the interaction between the hydrogen atoms may be specified in terms of the solution of a problem in elasticity theory. An exact solution can hardly be expected at the present stage of development of elasticity theory, and even if a solution could be obtained, it would be too unwieldy. Rather, a simplified expression would be more useful.

It is found in the order–disorder theory of statistical mechanics that a satisfactory approximation can be obtained by considering that the entropy remains almost unaffected by the potential energy terms. Moreover, in a simplified treatment of mutual interaction, it is permissible to represent the interaction energy of a particle by the potential energy with respect to the average number of its nearest neighbors.[13]

When a uranium lattice cell is expanded by the introduction of hydrogen atoms, the lattice cell meshes of surrounding cells are naturally stretched in a direction parallel to the boundary between them and the central cell, especially at the boundary itself. Because the hydrogen atom in the uranium becomes stable as the parent lattice is expanded to the dimension of the UH_3 structure, this effect will facilitate clusterwise occupation of sites adjacent to an occupied site with respect to the hydrogen sublattice accessible for occupation by hydrogen. In consideration of the resulting lattice deformation, the field seems to act as if the hydrogen atoms were mutually attractive.

At each stage of the insertion process, the number of occupants adjacent to any given site is, on the average, $z\theta$, where z is the number of adjacent sites (8 in the case of uranium hydride), and θ is the ratio of occupants to hydrogen sublattice positions. Thus, the influence of atoms occupying $z\theta$ sites will diminish the potential energy ϵ_i for the forward process of a single hydrogen atom by an amount $\alpha z\theta\epsilon$, where ϵ is the reduced mutual interaction energy, and α is a jump-in fraction, in a similar way to the kinetic theory for an adsorption process accompanied by interaction forces.[13] (See Figure 1.)

According to the theory of rate processes, the rate of the forward process of jump-in may then be written as

$$\vec{v} = \frac{kT}{h}\frac{c_a c_p}{c_s}\frac{f_* f_s}{f_a f_p} e^{-(\epsilon_i - \alpha z\theta\epsilon)/kT} \tag{1}$$

because the activated complex may be regarded as a special form of the interstitial state, where c_a is the adsorbed hydrogen concentration in atoms per unit area, c_s is the empty adsorption site concentration in sites per unit area, c_p is the empty sublattice site concentration in sites per unit volume, f_* is the partition function for the activated complex, which does not include the contribution to the degree of translational freedom in the reaction coordinate, f_a is the complete partition function for an adsorbed hydrogen atom, f_s is the complete partition function for an empty adsorption site, and f_p is the complete partition function for an empty sublattice point in the crystal.

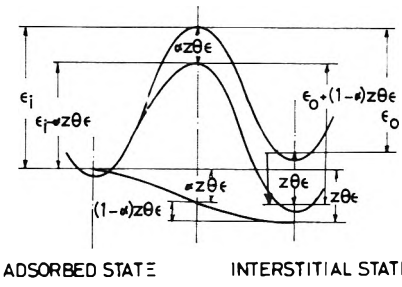

Figure 1. Potential energy curve for hydrogenation reaction in the presence of lattice deformation.

For the reverse process, the attractive effect will tend to increase the activation energy ϵ_0 by the fraction $(1 - \alpha)$ of total interaction energy, and the activation energy then becomes $\epsilon_0 + (1 - \alpha)z\theta\epsilon$. It follows that the rate of the reverse process in the hydrogenation reaction is

$$\overleftarrow{v} = \frac{kT}{h} c_H \frac{f_*}{f_H} e^{-[\epsilon_0 + (1-\alpha)z\theta\epsilon]/kT} \tag{2}$$

where c_H is the hydrogen atom concentration on the sublattice points in atoms per unit volume and f_H is the complete partition function for hydrogen atoms on the sublattice points. Here we have assumed that the state of the activated complex is the same in both processes.

As long as the jump stage is assumed to be rate determining, the adsorption stage is in equilibrium. The equilibrium equation for adsorption with dissociation may be expressed in the following way.[6,12]

$$\frac{c_a}{c_s} = c_g^{1/2}\frac{f_a}{F_g^{1/2} f_s} e^{\epsilon_{ad}/kT} \tag{3}$$

where c_g is the hydrogen gas concentration in molecules per unit volume, F_g is the partition function per unit volume of hydrogen gas, and ϵ_{ad} is the adsorption energy per hydrogen atom. Substituting eq 3 into eq 1, we obtain

$$\vec{v} = \frac{kT}{h} c_g^{1/2} c_p \frac{f_*}{F_g^{1/2} f_p} e^{-(\epsilon_i - \alpha z\theta\epsilon - \epsilon_{ad})/kT} \tag{4}$$

Thus, the overall reaction rate R can be specified by the use of eq 2 and 4 as

$$R = \vec{v} - \overleftarrow{v} \tag{5}$$

It is convenient that the reaction rate is measured at conditions of constant volume (*i.e.*, combined volume of solid and gas phase).[8-10] Let us convert eq 4 into a more convenient form for our experiments. Under the conditions the law of mass conservation requires that

$$\frac{1}{2} c_H V' + c_g V = c_g^0 V \tag{6}$$

where V is the volume of gas phase, V' is the volume of solid phase, and c_g^0 is the initial concentration of hydrogen gas. Because the mass of hydrogen in the hydride is negligible in comparison with that of the uranium, we have

$$V' = \frac{W(\theta)}{D(\theta)} \approx \frac{w}{D(\theta)} \tag{7}$$

where w is the mass of uranium metal in the reaction system, $W(\theta)$ is the mass of hydride system converted from w, and $D(\theta)$ is the density of the uranium hydride system.

A linear relation was obtained from the experimental data[1] as follows: $D(\theta) = 11.0 - 8.0\theta$ (g/cm³). Using relation 7 and

$$c_g = \frac{P}{kT};\ c_g^0 = \frac{P_0}{kT} \tag{8}$$

we have from eq 6

$$c_H = \frac{2(P_0 - P)V}{kT}\frac{D(\theta)}{w} \tag{9}$$

where P_0 is the initial pressure of hydrogen gas and P is the pressure of hydrogen gas at an arbitrary instant. Because the number of sublattice positions in the uranium metal may be written as

$$\frac{(c_p + c_H)w}{D(\theta)} = \frac{3Nw}{A} \tag{10}$$

Substitution of eq 9 into eq 10 yields

$$c_p = \left\{\frac{3Nw}{A} - \frac{2(P_0 - P)V}{kT}\right\}\frac{D(\theta)}{w} \tag{11}$$

where N is Avogadro's number and A is the atomic weight of uranium. Thus, we have

$$\theta = \frac{c_H}{c_H + c_p} = \frac{2(P_0 - P)AV}{3NwkT} \tag{12}$$

From eq 2, 4, 5, 8. 9, 11, and 12 the rate of the overall hydrogenation reaction may be represented by

$$-\frac{dP}{dt} = P^{1/2}\left\{\frac{3Nw}{2AV} - \frac{(P_0 - P)}{kT}\right\} \times \frac{(kT)^{3/2}}{h}\frac{f_*}{F_g^{1/2}f_p}e^{(\epsilon_{ad} - \epsilon_i + \alpha z\theta\epsilon)/kT} - (P_0 - P)\frac{kT}{h}\frac{f_*}{f_H}e^{-(\epsilon_0 + (1-\alpha)z\theta\epsilon)/kT} \tag{13}$$

Isotherm Equation. In equilibrium at any temperature, the rates of the forward and reverse processes must be equal. Hence, from eq 2, 4, and 8

$$P_{eq}^{1/2} = \frac{\theta}{1-\theta}(kT)^{1/2}\frac{F_g^{1/2}f_p}{f_H}e^{-(\epsilon_{ad} + \epsilon_j + z\theta\epsilon)/kT} = P^{0\,1/2}\frac{\theta}{1-\theta}e^{-z\theta\epsilon/kT} \tag{14}$$

where

$$\epsilon_j = \epsilon_0 - \epsilon_i;\ P^0 = kT\frac{F_g f_p^{\,2}}{f_H^{\,2}}e^{2(\epsilon_{ad} + \epsilon_j)/kT} \tag{15}$$

The general scheme of eq 14 is represented by curve A in Figure 2. In the case where $z\epsilon/kT > 4$ we have the plateau pressure $P_{eq(plateau)}$ $(\theta_L \leq \theta \leq \theta_K) = P^0 \exp(-z\epsilon/kT)$. However, there is no plateau in the case where $z\epsilon/kT \leq 4$, as shown by curve B in Figure 2. This is in good agreement with the experimental results that as temperature is increased, the width of plateau decreases and finally vanishes.

It will be noticed that eq 14 is just Lacher's isotherm which has been justified by the fact that it satisfactorily describes the characteristic features of the transition metal-hydrogen systems,[6] including the uranium-hydrogen system.[2] As the rate equation derived here is of a form similar to Lacher's isotherm, it suggests that our approach is probably adequate.

Dehydrogenation Reaction. Note that eq 13 was derived for the case of a hydrogenation reaction in which the hydrogen is pushed into the crystal by the excess gas pressure. In the dehydrogenation reaction, it is sucked out by lowering the pressure in the gas phase. Therefore there is an essential difference in the resulting deformation corresponding to each reaction, as illustrated in Figure 3. In the dehydrogenation reaction, the escape of hydrogen from the interior of the crystal may be slightly reduced by excessive shrinkage of the uranium lattice near the surface. Thus, the energy term in eq 2 must be modified to account for this effect; *i.e.*, as a first approximation

$$\epsilon_0 + (1-\alpha)z\theta\epsilon + z\theta\epsilon' = \epsilon_0 + (1 - \alpha + \beta)z\theta\epsilon \tag{16}$$

in which

$$\beta = \epsilon'/\epsilon \tag{17}$$

where ϵ' is the energy related to the impeding effect due to the excessive shrinkage; obviously $\epsilon' > 0$. In the case of the dehydrogenation reaction, the rate of the forward process may then be rewritten from eq 2

$$v = \frac{kT}{h}c_H\frac{f_*}{f_H}e^{-(\epsilon_0 + (1-\alpha+\beta)z\theta\epsilon)/kT} \tag{18}$$

so that it conforms with the isotherm equation

$$P_{eq}^{1/2} = \frac{\theta}{1-\theta}P^{0\,1/2}e^{-z\theta\epsilon(1+\beta)/kT} \tag{19}$$

for the dehydrogenation reaction. Equation 19 is in agreement with the equation presented on the basis of thermodynamics.[14] From eq 14 and 19 we have the interesting relation

$$\left(\frac{P_{eq(hydrogenation)}}{P_{eq'(dehydrogenation)}}\right)_{\theta=0.5} = e^{z\epsilon/kT} \geq 1 \tag{20}$$

This explains the experimental results[8,9,15] in which the plateau pressure of the hydrogenation reaction is higher than that of the dehydrogenation reaction in the isotherm, and that the difference, *i.e.*, hysteresis, vanishes at higher temperatures.

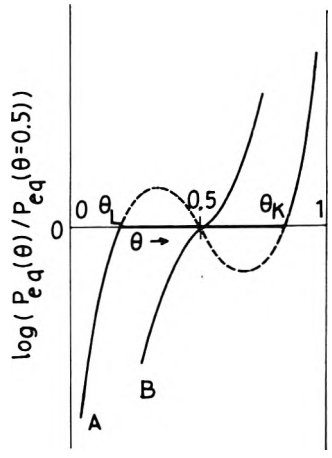

Figure 2. Relation between pressure and concentration in the isotherm.

Effect of Crystal Fracture. So far we have considered the solid phase as a continuous system. In the state corresponding to the plateau in the isotherm, the system is actually discontinuous because it is composed of two phases. As a first approximation, this effect may be related to the recrystallization which may be characterized by the energy terms in the equation.[8] When a mass of uranium metal or an incompletely disintegrated metal reacts with hydrogen gas, the energy term in eq 4 must be modified by an

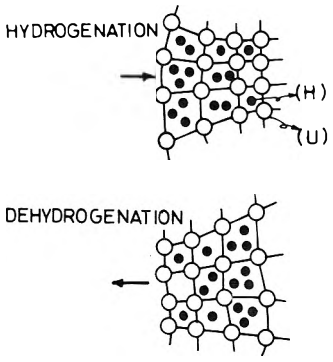

Figure 3. Difference in lattice deformations between hydrogenation reaction and dehydrogenation reaction.

amount associated with the work of fracture. The nature of this correction is naturally uncertain because the work depends on crystal size, shape, etc. If the correction can be represented by ϵ_f, ignoring the complications, we have

$$\bar{v} = \frac{kT}{h} c_g^{1/2} c_p \frac{f_*}{F_g^{1/2} f_p} e^{(\epsilon_{ad} - \epsilon_i + \alpha z f \epsilon - \epsilon_f)/kT} \quad (21)$$

for the hydrogenation reaction instead of eq 4.

If $P_{eq}*$ is the equilibrium pressure for the hydrogenation reaction with crystal fracture, it follows from eq 14 and 21 that

$$\frac{P_{eq^*(\text{hydrogenation})}}{P_{eq(\text{hydrogenation})}} = e^{2\epsilon_f/kT} \geqq 1 \quad (22)$$

because $\epsilon_f \geqq 0$.

Kinetic Parameters. In isotherm experiments[15] it has been found that the solubility of hydrogen decreases with temperature at a constant pressure, the decrease being especially steep in a particular temperature range. According to statistical thermodynamics, this result means that an entropy change occurs as a result of the change in the parent lattice configuration.[6] That is, the partition function f_p of the empty site may increase with temperature, whereas the partition function f_H of the hydrogen atom in the state of occupation may decrease. Clearly, the change in f_p and f_H with temperature contributes to the rise in the equilibrium pressure represented by eq 14 and to the decrease in the adsorption rate represented by eq 13 as well as eq 4 or 21. However, an exact calculation of the contribution to f_p, f_H, and $f*$ terms has not yet been developed in statistical thermodynamics.[6] A satisfactory approximation of the theory of rate processes is to consider that the parent-lattice configuration makes the most important contribution only to the energy term and that the entropy remains almost unaffected.[13] Therefore, the condition where the potential energies are independent of temperature in the rate equation no longer holds. In order that the rate equation may actually be used, the temperature dependence of the individual kinetic parameters should be determined experimentally.

Experimental Section

Apparatus. The apparatus, shown in Figure 4, consisted of a sample container A, resistance furnace B with temperature measurement C and control system D, pressure measurement system E, gas buret F, and hydrogen purification train G.

Materials. The uranium metal used was high-purity reactor grade (99.9%). A small piece of metal was weighed and cleaned successively in 1 N HNO_3 solution, isopropyl alcohol, and n-hexane, transferred to the sample container as quickly as possible and kept in an atmosphere of purified argon.

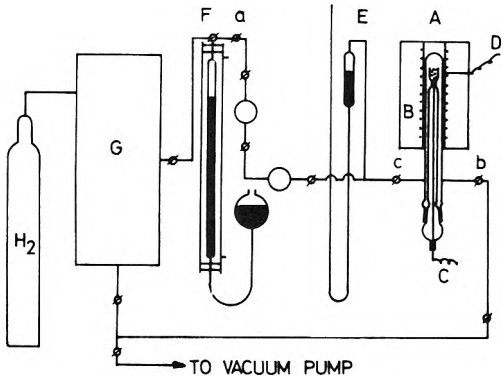

Figure 4. Apparatus for the study of the reaction of a constant volume system of hydrogen gas and uranium metal.

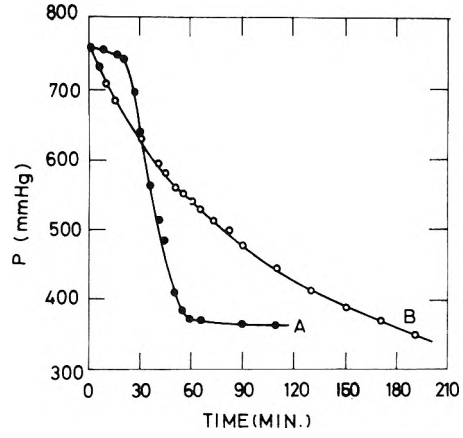

Figure 5. Typical hydrogenation rate of a mass of uranium metal: A, w = 0.640 g, T 49° °K; (B) w = 0.979 g, T 591°K.

Experimental Method. The reaction was carried out at various temperatures under constant volume conditions. The hydrogen gas was purified by passing over hot spongy titanium metal after the usual preliminary purification procedures, measured by means of the gas buret, and stored in the reservoirs (between bulbs a and c which had been previously evacuated. The reaction was initiated by opening bulb c to the reactor which had previously been completely evacuated and heated. The extent of the reaction was observed by measuring the change in pressure.

Correction to the Pressure Reading. Although the reaction was carried out at elevated temperatures, the mercury manometer used for measuring the pressure was kept at room temperature for convenience of operation, so a correction to the pressure reading was necessary. The calibration chart was prepared by carrying out blank tests.

Experimental Results

Typical results of pressure change against time are shown in Figure 5. In the hydrogenation of a mass of uranium metal, we observed an induction period at lower temperatures, probably caused by the formation of an oxide film.[8] This period, the length of which was poorly reproducible, became shorter as the temperature increased and vanished above 300°. In calculating the results, the induction period was omitted on the assumption that it is independent of the normal reaction. The hydrogenation rate of completely powdered uranium is summa-

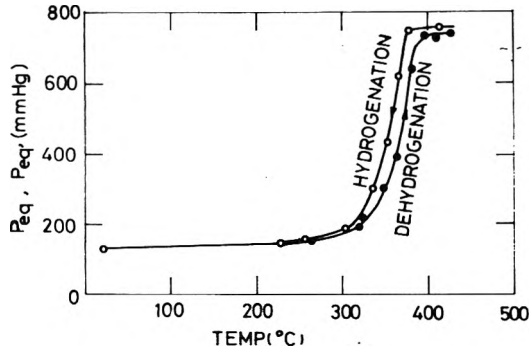

Figure 6. Equilibrium pressure to various temperatures at constant volume (w = 0.9829 g (block), P_0 = 762.4 mm, T_0 684°K).

TABLE I: Hydrogenation Rate of Powdered Uranium Metal, Prepared by the Thermal Dissociation of Hydride, at Various Temperatures under Constant Volume Conditions

T, °K	w, g	P_0, mm	$-(dP/dt)_{t=0}$, mm/min
452	0.400	688	11.8
463	0.538	637	11.2
491	0.641	755	15.9
541	0.631	750	9.26
585	0.612	765	2.72
624	0.484	758	1.20

rized in Table I. It has been reported that the rate appears to be at a maximum near 225° and falls off sharply.[3] This tendency has been observed in our experiment as well.

In the experiments conducted at equilibrium at constant volume, the system was regarded as being in equilibrium when the pressure change fell to less than 1 mm in the final 1 hr at a given temperature. The equilibrium curves for the hydrogenation of mass of uranium to $UH_{2.9}$ and the successive dehydrogenation at constant volume are shown in Figure 6. It took 24–48 hr to establish equilibrium conditions at any given temperature.

Determination of the Kinetic Parameters

ϵ *Values.* Since we have the relation

$$P_{eq'(\theta=0.5)} = P_{eq'(\theta=\theta_K)} \tag{23}$$

it follows by equating eq 4 and 18 for the hydrogenation reaction

$$\epsilon = \frac{2.3kT}{z(1+\beta)(\theta_K - 0.5)} \log \frac{\theta}{1-\theta} \tag{24}$$

where θ_K is the break point between the plateau and the sloping part, as shown in Figure 2. It is convenient to use eq 24 at temperatures >400° since the hysteresis disappears,[15] *i.e.*, $\beta = 0$. By using the θ_K values estimated from experimental data for the hydrogenation reaction of Libowitz, *et al.*,[15] we have obtained the ϵ values at temperatures of 450, 500, 550, 600, and 650° as shown by curve A in Figure 7. In order to determine the remaining kinetic parameters, we have graphically extrapolated the ϵ values observed to the lower temperature range where the ϵ values exclude β. It was found that the relation between log ϵ and T could be conveniently represented by a straight line A in Figure 7.

$(\epsilon_j + \epsilon_{ad})$ *Values.* From eq 14, taking β into account, we have

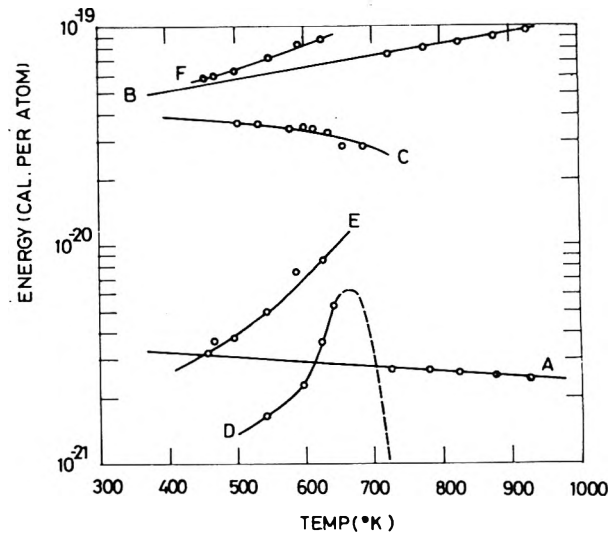

Figure 7. Kinetic parameters at various temperatures: curve A, ϵ curve B, $\epsilon_j + \epsilon_{ad}$; curve C, ϵ_f; curve D, ϵ'; curve E, $\epsilon_i - \epsilon_{ad}$; curve F, ϵ_0.

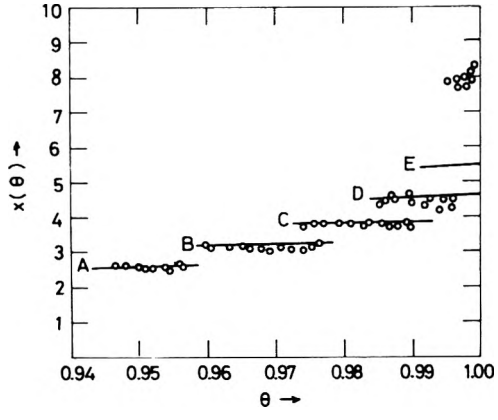

Figure 8. Comparison of experimental results and calculated values (for β = 0): curve A, 650°; curve B, 600°; curve C, 550°; curve D, 500°; curve E, 450°.

$$\epsilon_j + \epsilon_{ad} = 1.55kT \log \left[\frac{kT}{P_{eq'(\theta=0.5)}} \frac{F_g f_p^2}{f_H^2} \right] - \frac{z\epsilon(1+\beta)}{2} \tag{25}$$

for the dehydrogenation reaction. As a first approximation, the ratio f_D/f_H is assumed to be unity, which is unusual in statistical mechanics.[13] The partition function F_g per unit volume may be split into the translational contribution for three degrees of freedom and the rotational factor, *i.e.*

$$F_g = \frac{(2\pi mkT)^{3/2}}{h^3} \frac{8\pi^2 IkT}{\sigma h^2} \tag{26}$$

on the assumption that the vibrational contribution is unity,[13] where σ is the symmetry number of the hydrogen molecule, I is the moment of inertia of the molecule, and m is the hydrogenation isotherm by molecule. Use of the data for the hydrogenation isotherm by Libowitz, *et al.*[15] and of known ϵ values yielded the $(\epsilon_j + \epsilon_{ad})$ values shown in curve B in Figure 7.

ϵ_f *Values.* The condition of constant volume requires that

$$\left(c_g - \frac{P_0}{kT_0}\right)V + \frac{c_H w}{2D(\theta)} = 0 \tag{27}$$

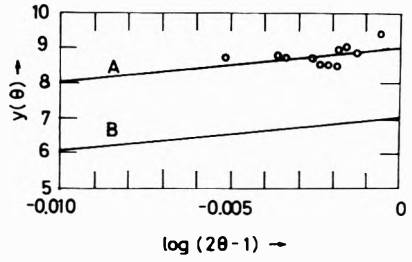

Figure 9. Graphical determination of β value at 450°: curve A, $\beta = 0.3$; curve B, $\beta = 0$.

Using eq 2, 21, and 27 and setting the equilibrium condition, we can determine ϵ_f values based on the hydrogenation curve in Figure 6, as shown by curve C in Figure 7.

ϵ' Values. From eq 19 with the condition (27) we obtained curve *D* in Figure 7 based on the dehydrogenation curve in Figure 6.

$(\epsilon_i - \epsilon_{ad})$ Values. At the beginning of the hydrogenation reaction, we have from eq 13 the relation

$$\epsilon_i - \epsilon_{ad} = 2.3kT \log \left[\frac{P_0^{1/2}}{-\left(\frac{dP}{dt}\right)_{t=0}} \frac{(kT)^{3/2}}{h} \frac{1}{F_g^{1/2}} \frac{3Nw}{2AV} \right] \quad (28)$$

Using the data shown in Table I, we obtain curve E in Figure 7.

ϵ_0 Values. From relation 15, ϵ_0 values were determined as curve F in Figure 7.

Discussion

Thus far, the kinetic parameters have been determined from some particular points on the isotherm, *i.e.*, intersection points, with the aid of the other experimental data, but it remains to show that the practical rate equations can sufficiently describe the complete isotherm curve. A comparison will be made on the sloping part of the isotherm for the dehydrogenation reaction. By equating eq 4 and 18 and by taking the logarithm we get

$$2\log \frac{\theta}{1-\theta} - \log P_{eq'} = \frac{0.870(1+\beta)z\epsilon}{kT}\theta + \left\{\frac{0.870(\epsilon_i + \epsilon_{ad})}{kT} - \log (F_g kT)\right\} \quad (29)$$

or simply

$$x(\theta) = a(T)\theta + b(T) \quad (30)$$

The calculation was made on the assumption that $\beta = 0$, because the ϵ' values at the temperatures $\geq$450° were so small that they could not be determined as accurately as at the lower temperatures. Our data were found to be in good agreement with the results calculated from Libowitz's data at temperatures $\geq$500°, as shown in Figure 8. The deviation at temperatures <500° may be interpreted as being due to the effect of recrystallization. In order to determine the exact β value at 450°, we convert eq 29 or 30 with eq 25 as

$$\log \{x(\theta) + \log P_{eq'(\theta=0.5)}\} = \log (2\theta - 1) + \log \frac{z\epsilon(1+\beta)}{2.3kT} \quad (31)$$

or simply

$$y(\theta) = \log (2\theta - 1) + d(T,\beta) \quad (32)$$

In Figure 9 we find that the calculated values from eq 32 for $\beta = 0.3$ ($\epsilon = 2.80 \times 10^{-21}$ cal/atom, $\epsilon' = 7.60 \times 10^{-22}$ cal/atom) agree with the experimental results at 450°.

References and Notes

(1) F. H. Spedding, N. S. Newton, J. C. Warf, O. Johnson, R. W. Nottorf, I. B. Johns, and A. H. Daane, *Nucleonics*, **4**, 4 (1949).
(2) G. G. Libowitz, *J. Chem. Phys.*, **27**, 514 (1957).
(3) J. J. Katz and G. T. Seaborg, "The Chemistry of the Actinide Elements," Wiley, New York, N. Y., 1957, p 133.
(4) D. D. Hurt, "An Introduction of Chemistry of the Hydrides," Chapman-Hall, London, 1952, p 172.
(5) M. W. Mallet, M. J. Trzeciak, and C. B. Griffith, Reprint No. 334, *Nucl. Eng. Sci. Conf., 5th, Cleveland*, (1955).
(6) R. H. Fowler, E. A. Guggenheim, "Statistical Thermodynamics," Cambridge University Press, Cambridge, 1965, p 421.
(7) J. D. Eshelby, *Solid State Phys.*, **3**, 79 (1956).
(8) Z. Wicke and K. Otto, *Z. Phys. Chem. (Frankfurt am Main)*, **31**, 222 (1962).
(9) W. M. Albert and M. W. Mallet, *J. Electrochem. Soc.*, **103**, 404 (1956).
(10) F. Amilliat and M. Destriau, *Bull. Soc. Chim. Fr.*, 3471 (1956).
(11) R. M. Barrer, "Diffusion in and through Solids," Cambridge University Press, Cambridge 1951, p 144.
(12) S. Glasstone, K. J. Laidler, and H. Eyring, "The Theory of Rate Processes," Chapters IV and IX, McGraw-Hill, New York, N. Y., 1941.
(13) Reference 12, Chapter VII.
(14) N. A. Scholtus and W. K. Hall, *J. Chem. Phys.*, **39**, 868 (1963).
(15) G. G. Libowitz and R. P. Gibbs, Jr., *J. Phys. Chem.*, **61**, 793 (1957).

Structural and Textural Studies in Molybdenum Sulfide Systems

P. Ratnasamy,*

Indian Institute of Petroleum, Dehra Dun (U.P.) India

L. Rodrique, and A. J. Leonard

Laboratoire de Physico-Chemie Minerale, Institut des Sciences de la Terre, de Croylaan 42, 3030 Heverlee, Belgium
(Received March 1, 1973)

The structural and textural evolution of MoS_2 from MoS_3 has been investigated. Changes in the crystallite size and crystalline fraction have been estimated from X-ray line broadening and electron microscopy. The evolution of the short-range order around the molybdenum and sulfur atoms has been evaluated from X-ray scattering experiments. Differential thermal analysis has been used to follow the thermal changes accompanying the structural evolution. In MoS_3 which is amorphous to X-rays, the immediate environment (within 6 Å) of both the Mo^{4+} and S^{2-} ions is not much different from that in hexagonal MoS_2. Small fragments of randomly oriented layers exist. At higher temperatures of reduction, two crystalline forms of MoS_2, namely, the hexagonal and rhombohedral, are formed. The latter is formed only at a reduction temperature of about 800°. The structural and textural differences between the two forms are discussed.

Introduction

The surface and structural properties of MoS_3 and MoS_2 have recently been investigated using ir[1] and X-ray[2] techniques. When MoS_3 is reduced in hydrogen at successively higher temperatures, crystallization of the hexagonal MoS_2 starts around 350°. The resulting crystalline phase contains many defects and stacking faults as deduced from the line profiles in the X-ray patterns. Beyond about 600°, however, another crystalline form of MoS_2 (rhombohedral MoS_2) is formed with a more ordered structure.[2] Both the surface area and catalytic activity for thiophene desulfurization pass through a maximum around 500°.[2,3] This maximum is related to the presence of crystal defects and stacking faults in the hexagonal phase of MoS_2. In order to probe deeper into the nature of these defects, a detailed analaysis of the textural evolution of MoS_2 was carried out in this study using electron microscopic, differential thermal analysis, and radial electron distribution[4] techniques. In addition, the average crystallite size and crystalline fraction in the various reduction products have been calculated from a quantitative analysis of the X-ray line widths and intensities. The results, together with those published earlier,[1,2] enable us to visualize the structural and textural evolution of the molybdenum disulfide catalysts in a coherent manner.

Experimental Section

Materials. Sample A was MoS_3 prepared according to the methods of Moldavski, *et al.*[5] Samples C, D, E, and F were prepared as detailed earlier[2] by reduction in a stream of dry H_2 at 350, 450, 550, and 800°, respectively for 24 hr. Sample B of the previous study[2] has not been examined in the present contribution.

Apparatus. The X-ray patterns were obtained using a Philips diffractometer (Cu Kα radiation with Ni filter). The X-ray scattering technique used in the radial electron distribution has already been described in detail.[4] A AEI EM6G electron microscope was used for the electron-optical study, with an accelerating potential of 60 kV and a 50-μm contrast aperture. The powdered samples were first ultrasonically dispersed in distilled water; a droplet of the suspension was then deposited on a copper support grid of the AEI (Smethurst High-Light, Ltd), covered with a thin carbon film, and dried in a desiccator. For the differential thermal analysis measurements a Netzsch Model 406 apparatus was used and α-Al_2O_3 was taken as the standard. A linear heating rate of 12°/min was selected.

X-Ray Diffraction.

The X-ray diffraction patterns and their structural interpretation have already been published.[2] In this section only textural aspects, such as crystallite size and the relative content of amorphous and crystalline material, will be detailed. The crystallite sizes were calculated from the profile width at half its maximum height using the Scherrer equation. A value of 1.84 (for hexagonal particles) was retained for the Scherrer constant K. The profile width due to instrumental broadening was corrected by using a commercial sample of MoS_2 of crystallite size greater than 2000 Å. It should be noted that though the Scherrer equation was derived for a sample of cubic crystals, it is not a bad approximation for hexagonal crystals, if, for each hkl reflection, the crystallite size D is interpreted as an average crystal dimension perpendicular to the corresponding reflecting planes.[6] The crystallite sizes for samples C, D, E, and F are given in Table I. Sample A was completely amorphous and did not exhibit any line at all in the X-ray pattern,[2] hence it was not possible to calculate any crystallite size value. X-Ray line broadening is caused not only by very small crystallite size but also by the presence of strain in the lattice. Hall[7] has derived a general relationship between the broadening of the lines in the X-ray diagram and the size and lattice strain in the crystallites. The use of Hall's equation in the determination of crystallite size, D_{Hall}, has already been detailed.[8]

The values of D_{Hall} are given in Table I. The fraction of the total MoS_2 in the crystalline form was estimated from the variation in the integrated intensity values of the different *hkl* planes. The values (Table I) have been normalized with respect to that of sample E.

There is a regular increase in crystallite size as we go from sample C to F. For sample F, the rhombohedral crystals have a larger crystallite size than the hexagonal crystals. In the former, all layers are in parallel orientation and neighboring layers are related to each other by a translation only. In hexagonal MoS_2, on the other hand, adjacent layers are oriented in an antiparallel manner. That is, each layer is related to its neighbor by a translation followed by a rotation of 180° around the *C* axis. The parallel orientation of the layers in rhombohedral MoS_2 is an additional factor causing the larger crystallite size values. Similar results were also obtained by Wildervanck and Jellinek[9] who found that rhombohedral MoS_2 crystals, prepared by Guichard's method,[10] were larger than the hexagonal crystals.

Another feature of Table I is the change in the crystalline fraction. From sample C (0.78, 0.65), it increases through sample D (0.99, 0.86, 0.99, 0.63) and reaches a maximum for sample E (1.0). There is a decrease in the intensity of the 101, 103, and 110 lines on going from sample E to F. That is, part of the crystalline hexagonal MoS_2 is being transformed to the rhombohedral phase of crystallite size around 700 Å. There is also a decrease in the total amorphous material content in this temperature region as was shown by the decrease in surface area and increase in total crystalline (hexagonal and rhombohedral) content.[2] The significance of these results is discussed later.

TABLE I: Crystallite Size and Crystalline Fraction Derived from X-Ray Line Broadening

Sample	*hkl*	*D*, Å	D_{Hall}, Å	Rel. crystalline fraction[a]
C	101	98 ± 10	103 ± 10	0.78
	110	67 ± 16		0.65
D	101	106 ± 19	111 ± 12	0.99
	103	112 ± 18		0.86
	006	180 ± 18		
	110	115 ± 14		0.99
	105	121 ± 10		0.63
E	101	112 ± 14	236 ± 28	1.0
	103	117 ± 13		1.0
	105	86 ± 12		1.0
	110	227 ± 15		1.0
F				
hexagonal	101	530 ± 20	*b*	0.50
	103	518 ± 19		0.86
	110	554 ± 20		0.95
	005	515 ± 25		
	006	600 ± 26		
	007	470 ± 29		
rhombohedral	106	690 ± 31	800 ± 62	
	006	735 ± 38		
	009	583 ± 30		

[a] In arbitrary relative units. [b] For this sample, the standard deviation was so high that no meaningful value of D_{Hall} could be obtained.

Electron Microscopy

The electron micrographs[11a] of samples A, C, D, E, and F are shown in Figures 1–5, respectively. Sample A (amorphous MoS_3) consists essentially of thin plate-like particles of about a 1–2 μm (Figure 1a); sometimes also very small particles appear more or less agglomerated between themselves (Figure 1b). On some of the thin particles dark spots of varying shapes and sizes of about 500–2000 Å are seen (Figure 1a). In general, the edges of the particles are not sharp. The specimen shows no lines at all in the X-ray pattern. The same size and shape are more or less preserved in sample C also (Figure 2). However, they differ from sample A in two respects: first the particles are more transparent indicating that they are thinner, and second, the edges are better defined. These changes are due to the removal of the excess amorphous sulfur[11b] and the beginnings of the crystallization[2] of hexagonal MoS_2 (Figure 7). The "holes" that are shown on some of the particles are also probably due to the elimination of sulfur. At 450° (sample D) there is a growth in the average dimension of the particles to 2–4 μm. Both transparent (thin) and opaque platelets are seen (Figure 3). The edges are now much sharper and the hexagonal form can be discerned in some of the platelets. However, there are still many particles with diffuse edges characteristic of amorphous matter. At 550° an admixture of large (1–2 μm) and very small (200–300 Å) particles is seen (Figure 4). The latter dimension agrees well with the average crystallite size determined by X-rays (D_{Hall} = 236 Å, Table I).

It may be noted here that the surface area increases from sample A, reaches a maximum for sample E, and then decreases when the reduction in H_2 is carried out at 800°[2] (sample F). The presence of a large number of small poorly agglomerated crystallites of dimensions about 200–300 Å accounts for the large surface area of sample E. Sample F (Figure 5) consists almost entirely of crystalline material; the X-ray diffraction pattern indicated the presence of both hexagonal and rhombohedral forms of MoS_2. For these two forms the average crystallite sizes (from X-ray line broadening) are about 500–600 and 700–800 Å, respectively (Table I). Well-defined hexagonal plates are seen along with some triangular plates (Figure 5). Dickinson and Pauling[12] have also reported similar results though their sample of MoS_2 was prepared by a different method. Triangular plates are now known[13] to be characteristic of the rhombohedral form of MoS_2. Their detection by electron microscopy lends additional support to the conclusions derived from X-ray diffraction data.

Radial Electron Distribution (RED)

The method of calculating the RED distributions and their significance have already been published.[4] The RED curves (Figure 6) were calculated in the region 0–7 Å. Table II identifies the various peaks observed with interatomic distances in crystalline MoS_2.[12] It should be mentioned here that thus far no crystalline form of MoS_3 has ever been prepared. Wildervanck and Jellinek[9] prepared MoS_3 by different methods and in all cases the products obtained were always amorphous to X-rays in agreement with our results.[2] At present, there is no conclusive evidence to show that MoS_3 is a definite chemical compound rather than an intimate mixture of subcrystalline MoS_2 and amorphous sulfur. Our RED studies reveal that the Mo–S distance in MoS_3 (2.39 ± 0.04 Å) is almost identical with that in MoS_2 (2.41 Å). But the strong peak around 3.1–3.2 Å present in the patterns of samples C, D, and E (Figure 6) occurs only as a shoulder in sample A. This peak is characteristic of the edge (3.15 Å) and altitude (3.17 Å) of the triangular prism[12] in which one mo-

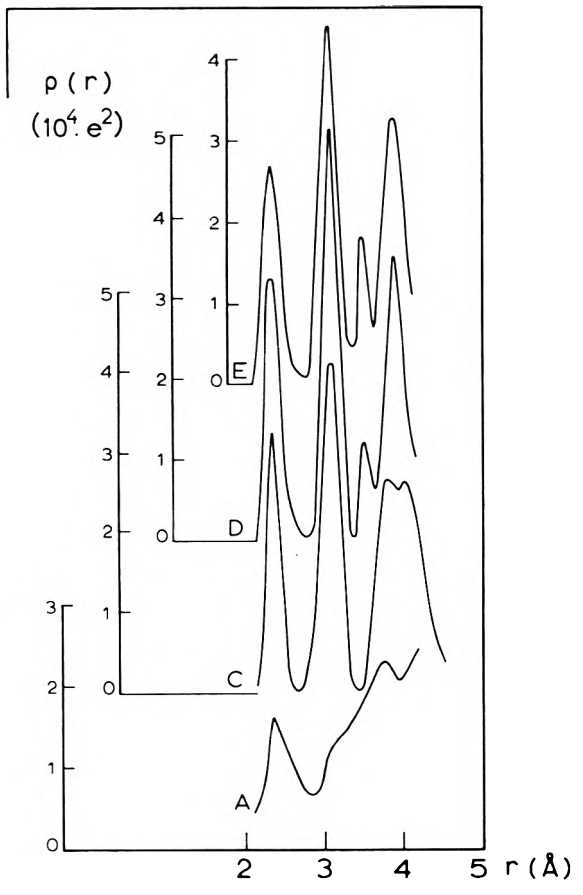

Figure 6. Radial electron d stribution in samples A, C, D, and E.

lybdenum ion is surrounded by six sulfide ions at the corners of a trigonal prism. Similarly the peak around 3.50 Å, only apparent in the profiles of samples D and E (and which is characteristic of the interlayer S-S distance in MoS_2 (3.49 Å)), is only faintly visible in MoS_3. The peak around 3.85 Å resembles the Mo-S peak in MoS_2 though of a much diminished intensity. All these features lead to the conclusion that though the immediate environment of the molybdenum ions (with respect to the sulfide ions) in MoS_3 may bear structural similarities to MoS_2, the long-range order present in MoS_2, such as *hcp* layer structure, antiparallel orientation of adjacent layers, etc., is absent in MoS_3 thus causing its amorphous character.

Sample C differs qualitatively in two respects from samples D and E as may be seen in Figure 6. First, the interlayer S-S peak around 3.5 Å is absent and second, the Mo-S peak around 4.0 Å is split into doublets. On the other hand, both the 2.41- and 3.15-Å peaks are well defined. Thus at 350°, though the MoS_2 layers are well developed, they are oriented in a random manner around the *C* axis. A similar conclusion was arrived at in an earlier paper[2] from an analysis of the relative changes in the shape and intensity of the X-ray diffraction lines.

Differential Thermal Analysis

The differential thermogram of sample A in the temperature range 25-900°C is shown in Figure 7. The decomposition of $(NH_4)_2MoS_4$ to MoS_3 was apparently complete since sample A did not exhibit the N-H stretching band in the infrared region (KBr pellet) and conventional wet methods did not evolve NH_3 from the sample. The broad, shallow endothermic peak between 50 and 200° is due to the removal of H_2S, NH_3, as well as H_2O, the former two

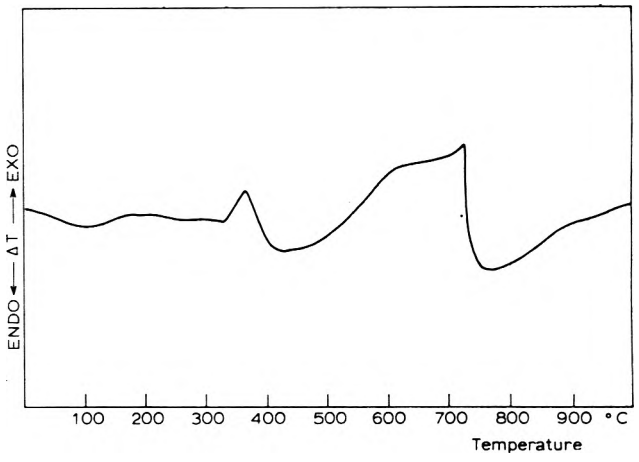

Figure 7. Differential thermogram of sample A.

TABLE II: Radial Electron Distribution[a] in Samples A, C, D, and E[b]

Vector	Sample A	C	D	E	MoS_2[c]
Mo-S	2.39	2.37	2.36	2.38	2.41
Mo-Mo (S-S)	3.13	3.12	3.11	3.12	3.15
S-S	3.50		3.55	3.54	3.49
Mo-S	3.85	3.83	3.94	3.93	4.12
		4.07			
S-S	4.56	4.53	4.51	4.47	4.46
Mo-S	4.93	4.98	5.01	5.01	5.02
Mo-Mo (S-S)	5.30	5.44	5.47	5.49	5.43
Mo-Mo	6.41	6.29	6.30	6.30	6.30
Mo-Mo	6.72	6.73	6.74	6.75	6.66

[a] The values are accurate to about ± 0.03 Å. [b] Length of the bonds in Å. [c] Taken from ref 12.

being evolved earlier. Rode and Lebedev[11b] who studied the thermal decomposition of $(NH_4)_2MoS_4$ had also observed a similar phenomenon, but around 250°. Since our samples were reduced in a stream of dry H_2 the removal of free S as H_2S is facilitated. Hence the endothermic peak due to sulfur removal occurs at a lower temperature.

The exothermic peak at 350° is due to the crystallization of hexagonal MoS_2. This is confirmed by the X-ray data[2] where the 101 and 110 lines are observed at 350°. The crystallites formed at 350°, however, are small in size (Table I), about 70-100 Å. The formation of the new hexagonal MoS_2 phase causes the shift in baseline seen around 400°.

An interesting feature of Figure 7 is the broad asymmetric exothermic band between 500 and 730°. This band can be resolved into a broad band centered around 600° and a narrow peak at 720°. Now, from X-ray results,[2] we know that in this temperature region two phenomena occur; the small hexagonal crystallites (of size, about 120 Å) sinter to form larger crystallites (of about 520-550 Å in size). In addition, a new phase, namely, rhombohedral MoS_2, is formed. These two processes together give rise to the observed thermogram. The former probably accounts for the broad band while the crystallization of the new phase is responsible for the superimposed narrow peak. Formation of the new phase also explains the shift in baseline around 750°.

Discussion

The structure of hexagonal MoS_2 consists of sheets of Mo^{2+} and S^{2-} ions. Each Mo^{2+} sheet is sandwiched between two S^{2-} sheets but each S^{2-} sheet is located between one Mo^{2+} sheet and another S^{2-} sheet.[2] Within each sheet hexagonal close packing prevails and the forces are purely ionic in nature giving a strong binding. The stacking sequence of the sheets is ABA, BAB, ABA, etc. The unit cell which comprises the sequence ABABAB has a C parameter[9] of 12.29 Å. Each Mo^{2+} sheet, together with two S^{2-} sheets (one above, another below), form one MoS_2 layer. The layers are held together by weak van der Walls forces of attraction. Rhombohedral MoS_2 also consists of sheets of Mo^{2+} and S^{2-} ions and the packing within a sheet is identical with that in the hexagonal form. Here also each Mo^{2+} sheet is sandwiched between two S^{2-} sheets and each S^{2-} sheet between one S^{2-} and one Mo^{2+} sheet. However, the stacking sequence is ABA, BCB, CAC, ABA, etc. The unit cell now comprises the longer sequence ABABCBCAC and hence has a correspondingly larger C value of 18.37 Å. The "structure" of MoS_3 as well as other amorphous phases present in our study (Figure 6, Table II) may be summarized as follows. The immediate environment (within 6 Å) of both the Mo^{4+} and S^{2-} ions is not much different from that in hexagonal MoS_2. Small fragments of layers exist. Even within a layer there is a large amount of defects and distortions of the individual sheets. (For example, the peak at 3.1–3.2 Å characteristic of the edge and altitude of the trigonal prism is only vaguely present in Figure 6 for sample A.) The layers are oriented in a completely random manner as evidenced by the absence of peaks in the X-ray pattern of sample A.[2] The presence of a faint shoulder around 3.5 Å in the RED pattern (Figure 6) indicates that a few layers are piled on top of one another, their number, however, being insufficient to give rise to a X-ray pattern.

Some of the solid-state transformations involved in our study are the following: amorphous to hexagonal MoS_2, amorphous to rhombohedral MoS_2, and hexagonal to rhombohedral MoS_2. Since even the amorphous material consists of fragments of layers (Figure 6, sample A) it seems that the major physical phenomena involved in all the above transformations are the fusion of the fragments of the layers as well as the crystal growth by successive stacking of the fused unit layers. The mechanism by which this occurs is not clear. Diffusion of the sulfur atoms in the solid state to the site of crystal growth is definitely one of the important processes. An additional possibility is the following: under conditions of reduction in H_2 used in this study, S-H groups are known to exist on the surface as evidenced by ir spectroscopy.[1] Probably, hydrogen reacts with the sulfur atoms forming some mobile intermediate species which diffuse to the site of crystal growth. In addition, slip phenomena will also play an important role, especially in crystalline transformations such as hexagonal to rhombohedral MoS_2.

When MoS_3 (obtained from $(NH_4)_2MoS_4$) is reduced in hydrogen, the product consists of small fragments of randomly oriented layers. Around 350° these fragments are converted to larger layers. They also grow by successive stacking of the layers. Due to the elimination of excess sulfur (which blocks the pores) the surface area increases.[2] Some amorphous sulfur is, however, still present (Figure 2). At this stage, the stacking sequence ABABAB, etc., is preferred in the crystalline portion (Table I). This process continues at higher temperatures. The crystallite size increases (Table 1 and Figures 3 and 4). Due to further elimination of sulfur from the pores, the larger amorphous particles are converted to smaller crystallites (Figure 4) thus accounting for the maximum in the surface area for the material reduced at 550°. Above this temperature, crystal growth is highly accelerated (Figure 7 and Table I) and part of the crystals grow with a different stacking sequence, namely, ABABCBCACABA, etc. Kinetic factors probably cause this phenomenon because on prolonged heating at 1000° *in vacuo* rhombohedral MoS_2 is converted[9] into hexagonal MoS_2. Initial formation of the unstable rhombohedral MoS_2 which transforms into the more stable hexagonal MoS_2 at higher temperatures had also been observed by Rode and Lebedev.[11b]

An interesting feature of our results is the decrease in the intensity of the hexagonal MoS_2 lines on going from sample E to F (Table I). Now, hexagonal crystallites (in sample E, for example) are separated from each other by amorphous MoS_2 (Figure 4). During the growth of the rhombohedral phase from this amorphous portion, fusion of the crystallites of the hexagonal phase is also going on simultaneously (Figure 7). Apparently, at intercrystallite or particle boundaries part of the diffusing atoms (taking part in the sintering of the hexagonal crystallites) are incorporated into the growing rhombohedral phase thus accounting for the observed phenomenon.

Acknowledgment. We thank Professor J. J. Fripiat and Dr. M. G. Krishna for encouragement and support.

Supplementary Material Available. Electron micrographs (Figures 1–5) will appear following these pages in the microfilm edition of this volume of the journal. Photocopies of the supplementary material from this paper only or microfiche (105 × 148 mm, 20× reduction, negatives) containing all of the supplementary material for the papers in this issue may be obtained from the Journals Department, American Chemical Society, 1155 Sixteenth St., N.W., Washington, D. C. 20036. Remit check or money order for $3.00 for photocopy or $2.00 for microfiche, referring to code number JPC-73-2242.

References and Notes

(1) P. Ratnasamy and J. J. Fripiat, *Trans. Faraday Soc.*, **66**, 2897 (1970).
(2) P. Ratnasamy and A. J. Leonard, *J. Catal.*, **26**, 352 (1972).
(3) R. S. Mann, *Ind. J. Tech.*, 3, 53 (1965).
(4) P. Ratnasamy and A. J. Leonard, *Catal. Rev.*, **6(2)**, 293 (1972).
(5) B. L. Moldavski, *et al. J. Gen. Chem. (USSR)*, 3, 603 (1933).
(6) B. E. Warren, "X-Ray Diffraction," Addison Wesley, Reading, Mass., 1969, p 251.
(7) W. K. Hall, *Proc. Phys. Soc.*, **A62**, 741 (1949).
(8) P. Ratnasamy and A. J. Leonard, *J. Phys. Chem.*, **76**, 1838 (1972).
(9) J. C. Wildervanck and F. Jellinek, *Z. Anorg. Allg. Chem.*, **328**, 309 (1964).
(10) M. Guichard, *Ann. Chim. Phys.*, **23(7)**, 557 (1901).
(11) (a) See paragraph at end of paper regarding supplementary material. (b) E. Y. A. Rode and B. A. Lebedev, *Zh. Neorgan. Khim.*, **6**, 1189 (1963).
(12) R. G. Dickinson and L. Pauling, *J. Amer. Chem. Soc.*, **45**, 1466 (1923).
(13) R. E. Bell and R. E. Herfort, *J. Amer. Chem. Soc.*, **79**, 3351 (1957).

Temperature Studies for Quenching of Pyrimidine Triplet States

A. Fenster and H. E. Johns*

Physics Division, Ontario Cancer Institute, Toronto, Ontario M4X 1K9, Canada *(Received March 9, 1973)*

Publication costs assisted by Ontario Cancer Institute, Physics Division

The bimolecular rate constant for quenching of the triplet state of thymine and orotic acid was determined over the temperature range 15–90° using flash photolysis. The rate constants were smaller by factors from 2 to 10 than k_{diff}, the value predicted by diffusion theory. Furthermore, they did not vary with temperature the same way as k_{diff}. From these data, a rate constant *not* including the diffusion contribution was determined. This rate constant implies that the diffusing molecules on encounter must collide many times and overcome a small activation energy barrier before a reaction occurs. From this rate constant, the activation energy for both thymine and orotic acid was calculated to be 1.3 kcal/mol and a preexponential factor was calculated to be $5.9 \pm 0.9 \times 10^{10}$ and $1.7 \pm 0.2 \times 10^{10}$ sec^{-1}, respectively. The preexponential factor is larger for thymine than for orotic acid by a factor of 4, suggesting that there are 4 times as many suitable orientations for dimerization in thymine than in orotic acid. We have also determined that the triplet yield for thymine decreases by about 15% over the temperature range from 20 to 90°.

Introduction

Measurements carried out in our laboratory and in many others have shown that when pyrimidines are irradiated in aqueous solutions they give rise to two classes of photoproducts, the dimer and the hydrate.[1-6] It has also been shown that the hydrate arises from reactions of the singlet state,[7,8] whereas dimers in solution arise through the reaction between a molecule in triplet state, with one in a ground state. The necessity for involving the triplet state is largely due to the fact that the excited species must live long enough in solution to find a ground state molecule in the right configuration so that a dimer can be formed. Most of the studies of the excited state precursor to the dimer have been carried out using the technique of flash photolysis. With a powerful flash of uv light it is possible to populate the triplet state to a high enough concentration so that it can be seen in absorption spectroscopy and observed as it decays. The various pathways which are involved in this photochemistry are indicated in Figure 1.

The absorption of a photon ($h\nu$) raises a ground state pyrimidine, P, to one of the many vibrational levels of the singlet manifold. This energy is mainly lost by fluorescence leading to the ground state but a small portion of the levels are depopulated to produce hydrates or triplet states through intersystem crossing with probability ϕ_{isc}.

In this reaction scheme we have shown three pathways for deactivation of the triplet state. It may lose its energy through radiationless transition to the ground state, by pathway k_3. It may be deactivated by a ground state molecule with a bimolecular rate constant k_1, leading to a dimer. Unfortunately, we have a third pathway, represented by k_1', in which the triplet state is quenched by a ground-state molecule but does not lead to a stable dimer. To date, no one has precisely determined the relative magnitude to k_1 and k_1', and in all of our studies all that we have been able to measure is the sum of the two. Lamola[9] has evidence that k_1' may be considerably larger than k_1 in thymine, but probably of the same order of magnitude as k_1' in orotic acid. Wagner and Bucheck[10] have also investigated this problem for related compounds and find that in certain solvents k_1' can be as much as 10 times k_1. In this paper we will deal only with the sum of these two coefficients ($k_1 + k_1'$).

With the development of our flash photolysis system,[11-13] we have been able to study the triplet state in considerable detail and we therefore studied its decay rate as a function of temperature. We have also measured the total yield of thymine triplets as a function of temperature. Some of this work was initiated because of an earlier finding by Fisher, *et al.*,[14] who showed that for thymine in aqueous solution four isomeric dimers could be formed and that the yield of these did not vary in a logical manner with respect to temperature. The yield of one type of dimer increased with temperature, whereas the others decreased with temperature.

In this paper, we have shown that the yield of triplet state in thymine is essentially independent of temperature over the range 20–90° with the yield decreasing by some 15% as the temperature is increased from 20 to 90°. We have also shown that the deactivation of the triplet state is *not* solely controlled by diffusion. Other mechanisms are involved in the quenching of the triplet.

Experimental Section

Using a dual beam[11-13] flash photolysis system, we observed the decay of the absorption signal from the triplet state of orotic acid[15] and thymine.[16] The orotic acid (Cyclo Chemical Grade I) and thymine (Calbiochem A grade) solutions were prepared from four times distilled water.[15] The concentration of the solutions were determined by absorbance measurements using an extinction coefficient for orotic acid of 7.4×10^3 M^{-1} cm^{-1} at 278 nm and for thymine of 7.9×10^3 M^{-1} cm^{-1} at 264 nm. The solutions were deoxygenated by bubbling nitrogen gas (prepurified grade, Canadian Anaesthetic Gases) through the solutions for about 0.5 hr prior to the experiment. The pH of the orotic acid solutions was adjusted to 3.2 using Analar grade $HClO_4$. The pH of the thymine solutions was not adjusted and was measured to be about 6.0. The

temperature of the solutions which was held constant to 0.5° was varied from 15 to 90° by passing water through the jacket around the quartz cell[11] containing the solution.

Results

In deoxygenated solutions and in the absence of additional quenchers, the triplet state disappears at a rate k_{obs} with lifetime τ_{obs} given by

$$\frac{1}{\tau_{obs}} = k_{obs} = k_3 + (k_1 + k_1')[P] \quad (1)$$

The pathways corresponding to the various rate constants are given in Figure 1. In the above expression [P] is the concentration of the pyrimidine in the solution.

In Figure 2, k_{obs} is plotted against the concentration of orotic acid at pH 3.2 for several temperatures, to give straight lines as predicted by eq 1. Similar data were obtained for thymine. The bimolecular rate constant $(k_1 + k_1')$ was determined from the slopes of these lines.

In Figure 3, $(k_1 + k_1')$ is plotted as a function of temperature for orotic acid and thymine. On the same graph is plotted a theoretical curve for the rate constant for diffusion, as calculated by eq 2.

Discussion

If we assume that the quenching of the triplet state is determined solely by diffusion, we predict the curve marked k_{diff} shown in Figure 3. This was calculated using the modified Smoluchowski equation[17] given by

$$k_{diff} = \frac{8RT}{3000\eta(T)} \left(\frac{1}{\text{mol-sec}}\right) \quad (2)$$

where $\eta(T)$ is the viscosity of the water in poises, R is the gas constant in ergs deg^{-1} mol^{-1}, and T is the absolute temperature.

Clearly k_{diff} does not agree with $(k_1 + k_1')$. In the first place it is larger by a factor of 2-10 and in the second place it shows a more rapid variation with temperature. Before discussing this observation we consider the validity of eq 2. Equation 2 is derived from the Smoluchowski equation[18]

$$k_{diff} = 4\pi N(r_A + r_B)(D_A + D_B) \times 10^{-3} \frac{1}{\text{mol-sec}} \quad (3)$$

where N is Avogadrò's number, $(r_A + r_B)$ is the sum of the radii of the spherical colliding molecules, and $(D_A + D_B)$ is the sum of the diffusion coefficients of the two molecules, the triplet and the ground-state molecule. Since these are not known for orotic acid or thymine we are forced to use the Stokes-Einstein equation to relate the diffusion coefficients to temperature and viscosity thus

$$D = \frac{kT}{6\pi\eta r} \quad (4)$$

where D is the diffusion coefficient of a spherical molecule of radius r and k is the Boltzmann constant. Assuming that $D_A = D_B$ and is given by eq 4 and that $r_A = r_B$, eq 3 reduces to the simpler form of eq 2.

Equation 2 is probably accurate to within ±25% in describing the diffusion of a triplet and ground-state molecule to one another for the following reasons. Diffusion coefficients are tabulated in the International Critical Tables for numerous cyclic compounds such as pyridine, alloxan, picric acid, phenol, hydroquinone, resorcinol, and pyrogallol. They all have $D \simeq 0.6 \times 10^{-5}$ cm^2/sec at 15° in agreement with the calculated value using eq 4 assuming $r = 3 \times 10^{-8}$ cm. Furthermore, it has also been shown[19,20] that the quantity $D\eta(T)/T$ remains constant

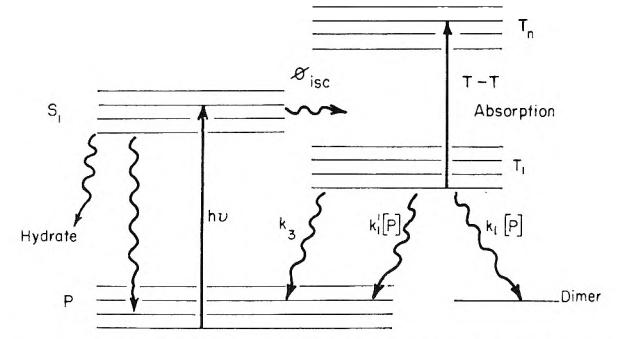

Figure 1. Model for excited-state reactions of pyrimidines, showing the rate constants for the various pathways.

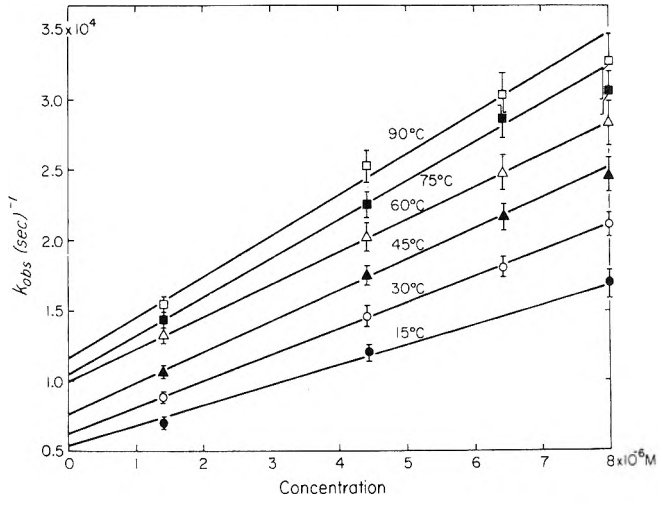

Figure 2. Graph showing k_{obs} (see eq 1) as a function of concentration for orotic acid in aqueous deoxygenated solutions at six different temperatures.

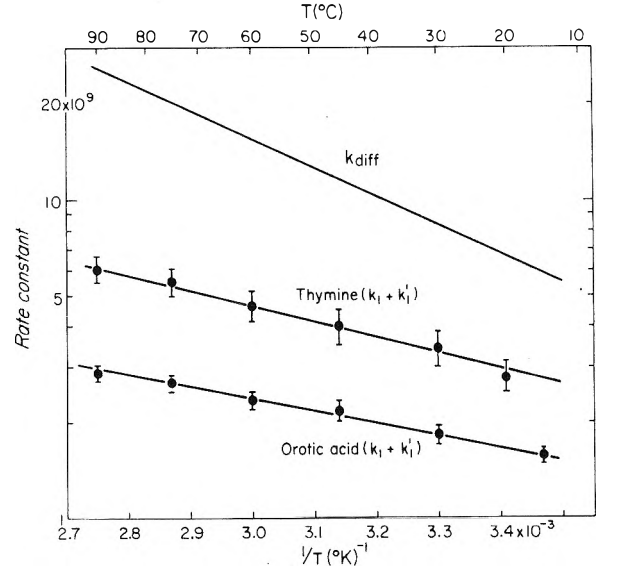

Figure 3. Rate constant $(k_1 + k_1')$ as a function of the reciprocal of the absolute temperature for orotic acid and thymine. Also shown is k_{diff} calculated assuming that the rate is determined solely by diffusion and given by eq 2.

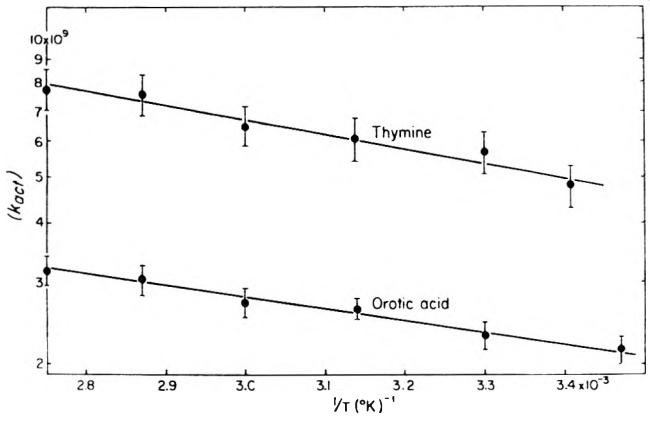

Figure 4. Rate constant, k_{act}, for deactivation of the pyrimidine triplet, after diffusion effects have been removed, plotted as a function of the reciprocal of the absolute temperature.

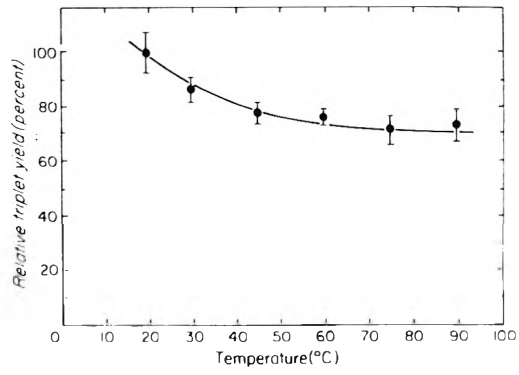

Figure 5. Plot of the relative triplet yield (expressed as a per cent) as a function of temperature for thymine. The yield is corrected for decay during the flash.

over a temperature range from 0 to 55° for diffusion of ^2H_2O in water (self-diffusion). Thus eq 4 probably applies quite well to the diffusion together of a triplet and ground-state pyrimidine suggesting in turn that eq 2 is valid for our situation. If this is so then the disagreement shown in Figure 3 must mean that once the two molecules have diffused together the reaction may still not take place due perhaps to incorrect orientation of the molecules. In addition the molecules may have to have sufficient kinetic energy to overcome an activation energy, E_a, before the reaction can take place.

Calculation of Activation Energy

The fact that diffusing molecules do not necessarily react at every collision has been included in a theoretical treatment, involving pair probability distribution and diffusion theory by Collins and Kimball,[21] Waite,[22,23] and Noyes.[24] Using these ideas we imagine the following mechanisms in the reaction

$$A + B \underset{k_{-diff}}{\overset{k_{diff}}{\rightleftharpoons}} (A:B) \xrightarrow{k_a} \text{products} \qquad (5)$$

where A and B can be considered the triplet and ground state molecule, respectively, and (A:B) a collision pair which can lead to products or diffuse apart with rate constant k_{diff}. The rate constant, k_a, leading to products, will contain steric hindrance factors, frequency of collision factor which may be lumped together as S, as well as a temperature-dependent term involving the activation energy E_a. In terms of temperature, k_a will be given by

$$k_a = S \exp(-E_a/RT) \qquad (6)$$

We would like to determine the bimolecular rate constant k_b for the disappearance of the triplet in terms of the rate constants of eq 5. Assuming the steady-state approximation for (A:B) we obtain

$$\frac{1}{k_b} = \frac{1}{k_{diff}} + \left(\frac{k_{-diff}}{k_{diff}}\right)\frac{1}{k_a} \qquad (7)$$

The quantity k_{-diff} is not known but should depend upon temperature in the same way as k_{diff}; hence their ratio will be temperature independent and may be represented by a constant C. Equation 7 reduces to

$$\frac{1}{k_b} = \frac{1}{k_{diff}} + \frac{C}{k_a} = \frac{1}{k_{diff}} + \frac{1}{k_{act}} \qquad (8)$$

and k_{act} is given by

$$k_{act} = \frac{S}{C}\exp(-E_a/RT) \qquad (9)$$

An equation similar to (8) was predicted by Waite.[23,24]

Using our measured values $(k_1 + k_1')$ for k_b and our calculated values for k_{diff} (eq 2) we obtain k_{act} from eq 8 and plot it against T^{-1} in Figure 4. This plot yields activation energies of 1.4 ± 0.2 and 1.2 ± 0.1 kcal/mol for thymine and orotic acid, respectively. From the intercepts, the preexponential factor is calculated to be 5.9 ± 0.9 × 10^{10} sec^{-1} for thymine and 1.7 ± 0.2 × 10^{10} sec^{-1} for orotic acid.

Interpretation of Results

The simplest interpretation of these data suggests that the molecules diffuse toward each other as predicted by simple diffusion theory which is about 5 times larger than the observed rate constant for the reaction. However, on contact the molecules do not necessarily react, and many collisions are probably required until the correct orientation is achieved. An energy barrier of about 1 kcal/mol must then be overcome for the reaction to take place. The fact that the activation energies for deactivation of the triplet state of thymine and orotic acid are equal within measurement error suggests that the same mechanism is involved in both pyrimidines. The fact that the preexponential factor for thymine is about 4 times as large as in orotic acid suggests that thymine has 4 times as many suitable steric configurations leading to a reaction. It may be a coincidence, but thymine[14] forms four dimers while orotic acid forms only one.

An alternative less attractive explanation is that the rate constant is determined only by diffusion and that this rate constant is smaller by a factor of 5 than that predicted by simple theory. This seems unlikely since a number of measurements for diffusion coefficients on molecules similar to pyrimidines give results close to that predicted by the simple theory.

Temperature Dependence of Triplet Yield

In these temperature studies, a marked decrease in the amplitude of the transient signal was observed as the temperature was increased, suggesting a decreased yield of triplet states. However, this conclusion is not valid since an increase in temperature increases the decay rate of the triplet so that a larger fraction decay during the

flash in the interval before useful observations can be made. When correction is made for the decay during the flash[16] most of the temperature dependence is removed as seen in Figure 5. We conclude that the yield of triplets is within 15% independent of temperature from 20 to 90°. Others have observed an increase of ϕ_{isc} with increase in temperature.[25,26] If this be so for pyrimidines then other deactivation pathways must show essentially the same temperature dependence.

We conclude from these findings that a study of the triplet yield as a function of temperature is not likely to be fruitful. To explain Fisher's[14] results one would require a measurement of the yield of triplets responsible for *each* of the dimers. In addition one would have to evaluate separately k_1 and k_1', which at the present time seems very difficult.

Acknowledgments. The authors take pleasure in acknowledging the financial assistance of the National Cancer Institute of Canada and the Medical Research Council of Canada. We are indebted to Drs. J. W. Hunt, M. J. Bronskill, J. P. Carver, and Mr. G. J. Fisher for many helpful discussions.

References and Notes

(1) H. E. Johns, "Methods in Enzymology," Vol. 16, K. Kustin, Ed., Academic Press, New York, N. Y., 1969, Chapter 8, pp 253–316.
(2) H. E. Johns, "Creation and Detection of the Excited State," Vol. 1, A. A. Lamola, Ed., 1971, pp 123–172.
(3) H. E. Johns, "XXIIIrd International Congress of Pure and Applied Chemistry," Vol. 8, Butterworths, London, 1971, pp 11–18.
(4) R. B. Setlow, *J. Cell. Comp. Physiol.*, **64**, (Suppl. 1), 51 (1964).
(5) K. C. Smith, "Photophysiology," A. C. Giese, Ed., Vol. 2, Academic Press, New York, N. Y., 1964, p 329.
(6) J. K. Setlow, "Current Topics in Radiation Research," M. Ebert and A. Howard, Ed., Vol. 2 North-Holland, Amsterdam, 1966, p 195.
(7) C. L. Greenstock, I. H. Brown, J. W. Hunt, and H. E. Johns, *Biochem. Biophys. Res. Commun.*, **27**, 431 (1967).
(8) I. H. Brown and H. E. Johns, *Photochem. Photobiol.*, **8**, 273 (1968).
(9) A. A. Lamola and J. Eisinger, *Biochim. Biophys. Acta*, **240**, 313 (1970).
(10) P. J. Wagner and D. J. Bucheck, *J. Amer. Chem. Soc.*, **92**, 181 (1970).
(11) J. C. LeBlanc, M. A. Herbert, D. W. Whillans, and H. E. Johns, *Rev. Sci. Instrum.*, **43**, 1814 (1972).
(12) W. B. Taylor, J. C. LeBlanc, D. W. Whillans, M. A. Herbert, and H. E. Johns, *Rev. Sci. Instrum.*, **43**, 1797 (1972).
(13) J. C. LeBlanc, A. Fenster, D. W. Whillans, M. A. Herbert, and H. E. Johns, *Rev. Sci. Instrum.*, **44**, 763 (1973).
(14) G. J. Fisher and H. E. Johns, *Photochem. Photobiol.*, **11**, 429 (1970).
(15) M. A. Herbert and H. E. Johns, *Photochem. Photobiol.*, **14**, 693 (1971).
(16) D. W. Whillans and H. E. Johns, *J. Amer. Chem. Soc.*, **93**, 1358 (1971).
(17) P. Debye, *Trans. Electrochem. Soc.*, **82**, 265 (1942).
(18) M. V. Smoluchowski, *Z. Phys. Chem.*, **92**, 129 (1917).
(19) J. H. Wang, *J. Amer. Chem. Soc.*, **73**, 510 (1951).
(20) J. H. Wang, *J. Amer. Chem. Soc.*, **73**, 4181 (1951).
(21) F. C. Collins and G. E. Kimball, *J. Colloid Sci.*, **4**, 425 (1949).
(22) T. R. Waite, *Phys. Rev.*, **107**, 463 (1957).
(23) T. R. Waite, *J. Chem. Phys.*, **28**, 103 (1958).
(24) S. M. Joyes, *J. Amer. Chem. Soc.*, **77**, 2042 (1955).
(25) E. R. Pantke and H. Labhart, *Chem. Phys. Lett.*, **16**, 255 (1972).
(26) J. B. Birks, "Photophysics of Aromatic Molecules," Wiley-Interscience, New York, N. Y., 1970.

Electron Paramagnetic Resonance Spectrum of the 1-Cyano-1-cyclopentyl Radical[1]

P. Smith,* D. W. House,[2] and L. B. Gilman

Paul M. Gross Chemical Laboratory, Department of Chemistry, Duke University, Durham, North Carolina 27706
(Received February 12, 1973)

Within a continuous-flow system, dilute oxygen-free solutions of 1,1′-azobis(1-cyanocyclopentane) in toluene have been irradiated with near-ultraviolet mercury radiation as the solution passed through the cavity of an X-band electron paramagnetic resonance, epr, spectrometer. By this method the epr spectrum of the 1-cyano-1-cyclopentyl radical, $\underline{CH_2(CH_2)_3}\dot{C}CN$, has been observed and characterized at *ca.* 26°. The spectrum is consistent with there being sufficiently rapid interconversion between the nonplanar forms of the radical that the four β-CH_2 protons appear equivalent, a conclusion in harmony with the epr data for analogous species.

Introduction

The ultraviolet irradiation of aliphatic azo compounds in the liquid phase affords an effective way of generating reactive radicals in sufficient concentration for successful electron paramagnetic resonance, epr, measurements.[3-8] In the present paper we have used this method to study the epr spectrum of the 1-cyano-1-cyclopentyl radical, $\underline{CH_2(CH_2)_3}\dot{C}CN$ or ·RCN, produced by the photolysis of 1,1′-azobis(1-cyanocyclopentane), NCRN:NRCN, in toluene within a continuous-flow system. The epr spectrum of ·RCN was found to be as expected, based, for example, on the liquid-phase epr spectra of analogous species such as the cyclopentyl radical,[9,10] ·RH, and simple acyclic 1-cyano radicals.[3-6,11]

Experimental Section

The experimental arrangement and procedures were essentially as described before, the sample cell being of internal path length 1.5 mm.[3] In place of polycrystalline 2,2′-diphenyl-1-picrylhydrazyl used previously,[3] the *g*

value standard was an aqueous solution of peroxylamine disulfonate within a thin-walled Pyrex capillary held to the face of the sample cell away from the mercury lamp.[12] Use of the latter standard was advantageous in that it allowed the field to be calibrated[3] and g value to be determined at the same time, the chief drawback being the instability of this standard when exposed to the photochemical radiation. Normally, the light filter combination was a right cylinder of internal path length 7.5 cm through which tap water flowed, the one plane face on the mercury-lamp side being of fused quartz and the other, of colored glass (Corning CS No. 7-51, 5.0 mm). However, for a few measurements where the highest signal intensities were desired, this filter was replaced by a similar one in which both plane faces were of fused quartz.[3]

1,1′-Azobis(1-cyanocyclopentane) was synthesized from cyclopentanone (2.0 mol) by a standard method[13] modified so that the final oxidation step was carried out by bubbling a small excess of chlorine gas into the solution of the hydrazo compound;[14] crude yield: 69% (47% lit.[13]). It was recrystallized from 95% ethanol freshly before use: mp 84–85°, uncor (83–84°, cor, lit.[13]); λ_{max} 344 and 344 mμ, ϵ_{max} 16.3 and 14.4 M^{-1} cm^{-1} (0.04 M in toluene and ethanol, respectively).

Epr measurements were taken with the use of oxygen-free 0.20 M solutions of NCRN:NRCN in toluene. The temperature of the reaction mixture on entering the irradiated zone of the sample cell was kept at 24°. With the use of the colored-glass filter combination, the flow rate was 0.04–0.07 ml sec^{-1}, corresponding to a temperature rise of 5–3° on passage through the irradiated zone. With the use of the other filter cell, the flow rate was 0.11–0.21 ml sec^{-1}, the temperature rise then being 6–4°. For comparison purposes, similar epr measurements were taken of the 1-cyano-1-methylethyl radical, $(CH_3)_2\dot{C}CN$, with the use of fresh samples of 2,2′-azobis(2-methylpropionitrile), $(CH_3)_2C(CN)N{:}NC(CN)(CH_3)_2$, in place of NCRN:NRCN and employing the colored-glass filter combination. The results obtained for this radical were essentially the same as previously reported[3] and will not be detailed here.

Results

The spectrum produced by the photolysis of NCRN:NRCN in toluene was intense, not significantly dependent with respect to intensity and structure on flow rate, and fully accountable in terms of one radical. By analogy with the liquid-phase epr spectra of related radicals[3-6,9-11] the probable form of the epr spectrum of ·RCN is a wide quintet (1:4:6:4:1) of narrow triplets (1:1:1) of very narrow quintets (1:4:6:4:1) arising from the four β-CH_2 protons, the CN nitrogen nucleus, and the four γ-CH_2 protons, respectively. The spectrum observed was largely as expected, *viz.*, five prominent, well-separated groups of lines centered 29 G from each other, each group being made up of three nonoverlapping, similarly sized subgroups of lines centered 3 G apart and each subgroup showing five lines 0.4 G apart. The fine structure of the subgroups within all but the two outermost wing groups gave evidence of more complexity beyond that expected for a simple (1:4:6:4:1) quintet. These effects were shown to arise from the second-order couplings, *viz.*, 0.51 and 0.25 G, which would be predicted[15] if the four β-CH_2 protons were equivalent, as found, for example, for the ·RH radical under similar conditions.[9]

TABLE I: Isotropic Hyperfine Coupling Constants and *g* Values for the 1-Cyano-1-cyclopentyl and 1-Cyano-1-methylethyl Radicals and Structurally Related Radicals

Radical[a]	Coupling constants, G α-H	β-H	γ-H	N	g value	Ref	F ratio[b]
·RH	21.48	35.16	0.53		*c*	9[d]	1.000
$\cdot RCH_3$		32.87	*c*	22.22[e]	2.0027	16[f]	0.935
·RCN		29.25	0.44	3.29	2.0030	*g*	0.832
·RNCO		28.8	*c*	4.2	2.0028	17[h]	0.819
·ROH		27.0	*c*		*c*	18[i]	0.768
$(CH_3)_2\dot{C}H$	22.11	24.68			*c*	9[j,k]	1.000
$(CH_3)_2\dot{C}CH_3$		22.72			*c*	9[k,l]	0.921
$(CH_3)_2\dot{C}CN$		20.54		3.33	2.0030	*m*	0.832
$(CH_3)_2\dot{C}NCO$		20.3		4.1	2.0028	17[h]	0.823
$(CH_3)_2\dot{C}OH$		19.90		0.48[n]	2.00315	19[o]	0.807

[a] ·R– = $\underline{CH_2(CH_2)_3\dot{C}}$-. The data were selected so that, as far as possible, radical pairs bearing the same –X group could be compared in similar, nonpolar media at a similar temperature close to 25°. With respect to the media, this goal was fairly well realized save for the alcohol radicals. The temperature criterion is considered adequately met in view of what is known about the temperature dependence of the $a_{\beta\text{-H}}$(CH) values compared in column 8. [b] For ·RX radicals, $[a_{\beta\text{-H}}(CH_2)\ [\cdot RX]/[a_{\beta\text{-H}}(CH_2)\ [\cdot RH]]$, denoted F_1(–X) in the text; for $(CH_3)_2CX$ radicals, $[a_{\beta\text{-H}}(CH_3)\ [(CH_3)_2\dot{C}X]]/[a_{\beta\text{-H}}(CH_3)\ [(CH_3)_2CH]]$, denoted F_2(–X) in the text. [c] Not reported. [d] In cyclopentane, −80°; see ref 10 for confirmatory data. [e] $a_{\beta\text{-H}}(CH_3)$. [f] In methylcyclopentane 10 v/v% in aliphatic ketone, −13°. [g] Present work; the maximum uncertainty in the *a* values is ca. 0.05 G save for $a_{\beta\text{-H}}(CH_2)$ where it is ca. 0.1 G; peak-to-peak line width ca. 0.21 G with no evidence for line-width alternation. The same $a_{\gamma\text{-H}}(CH_2)$ value was obtained at 51°. The *g* value is corrected for the second-order coupling, maximum uncertainty 0.0001. Of the two second-order β-CH_2 proton couplings, only the smaller (0.25 G) could be resolved as the larger (0.51 G) is too close to the size of $a_{\gamma\text{-H}}(CH_2)$. [h] In an adamantane matrix, room temperature. [i] In water, room temperature, pH 1; a coupling from the OH proton was not observed, probably because of the low pH.[19] [j] In propane, −85°. [k] See ref 10 and 16 for confirmatory data. [l] In neopentane, −13° and isobutane, −145°. [m] Present work, taken from the first-order spectrum; the maximum uncertainty in the *a* values is ca. 0.05 G and that for the *g* value, 0.0001. These results agree well with the comparable data of previous workers.[3,4] [n] $a_{\beta\text{-H}}$(OH). [o] In water, ca. 15°. The value of $a_{\beta\text{-H}}(CH_3)$ is noticeably solvent dependent[19,20] but that quoted agrees well with most others taken under comparable conditions.[21-25]

Table I compares the spectroscopic results we obtained for ·RCN and $(CH_3)_2\dot{C}CN$ with selected isotropic epr data available for related radicals.[9,16-19]

Discussion

Monosubstituted cyclopentanes exhibit conformational properties similar to those of cyclopentane,[26] hence we would expect monosubstituted cyclopentyl radicals to be like ·RH in conformational behavior.[9,10,27] The relatively limited epr data available on such radicals[16-18,28-32] seem to bear out this conclusion. The only 1-substituted 1-cyclopentyl radicals analogous to ·RCN[33] and for which isotropic epr spectra are available appear to be $\cdot RCH_3$,[16] ·RNCO,[17] and ·ROH.[18] For each, the four β-CH_2 protons are equivalent.[34]

The coupling constants for the radicals ·RH, $\cdot RCH_3$, ·RCN, ·RNCO, and ·ROH may be compared by way of the F_1(–X) and F_2(–X) ratios listed in Table I.[35] For a given –X, the F_1 and F_2 values are equal when –X is –H, $-CH_3$, –CN, and –NCO, for the case of –H this being necessarily so. These equalities suggest that a similar state of hybridization of the α-C obtains in these eight radicals and that the conformational properties of all four cyclic radicals are also alike. These conclusions seem reasonable as the cyclic radicals are unlikely to possess much ring strain[9,30] and so would be expected to adhere fairly closely to sp^2 hybridization[30,36-39] at the α carbon atom. However, the evidence available suggests that these β-CH cou-

plings might not be very sensitive to configurational changes at the α carbon site.[10,30]

The $F_1(-OH)$ and $F_2(-OH)$ ratios in Table I appear perhaps different by more than experimental error would allow.[40] If this difference is real and not, for example, a solvent effect, it may perhaps stem from the presence of the -OH substituent. The presence of the α-OH substituent in $(CH_3)\dot{C}OH$ is thought likely to cause the hybridization at the α-C to become of increased sp^3 character compared to those of the other $(CH_3)_2\dot{C}X$ radicals.[30,36,39] Accordingly, we may suppose that this sort of effect will tend to be also present in ·ROH, but not necessarily to the same extent, because the ring strain in this radical will tend to tip the energy balance so as to favor such an increase. Another way of showing this possible difference between the $F_1(-OH)$ and $F_2(-OH)$ ratios is by comparing the coupling-constant ratios $[a_{\beta\text{-H}}(CH_3)\ [(CH_3)_2\dot{C}X]]/[a_{\beta\text{-H}}(CH_2)\ [\cdot RX]]$, denoted $F_3(-X)$. These $F_3(-X)$ ratios are 0.702, 0.691, 0.702, 0.705, and 0.737, respectively, for -X equal to -H, $-CH_3$, -CN, -NCO, and -OH, the value of $F_3(-OH)$ being possibly larger than the rest.[40] If each radical is assumed to be essentially sp^2 hybridized at the α carbon, then we may further assume that an approximate equation of the form

$$a_{\beta\text{-H}}(CH) = B\rho^{\pi}_{\alpha\text{-C}} \cos^2 \theta \qquad (1)$$

holds,[41] where θ is the dihedral angle between the axis of the α carbon $2p_z$ orbital and the projection of the β-C-H bond in the plane passing through this axis and perpendicular to the α-C/β-C bond, $\rho^{\pi}_{\alpha\text{-C}}$ is the unpaired spin density in the $2p_z$ orbital, and B is a proportionality constant which is the same for all the radicals. In addition, we may assume that for $(CH_3)_2\dot{C}X$ radicals the average value of $\cos^2\theta$, $\langle\cos^2\theta\rangle$, is one half[9] and that $\rho^{\pi}_{\alpha\text{-C}}[(CH_3)_2\dot{C}X]$ approximately equals $\rho^{\pi}_{\alpha\text{-C}}[\cdot RX]$.[42] Hence

$$F_3(-X) = (2\ \langle\cos^2\theta\rangle)^{-1} \qquad (2)$$

where the θ refers to the ·RX radical. Substituting the arithmetic mean of the above $F_3(-X)$ ratios into eq 2 gives $\langle\cos^2\theta\rangle$ as 0.71, in rough agreement with estimates of this same quantity, *e.g.*, 0.625[18] and *ca.* 0.75,[28] based on the postulated conformational properties of ·RX-type radicals.

References and Notes

(1) This work was supported by National Science Foundation Grant No. GP-17579.
(2) Undergraduate Research Participant supported by National Science Foundation Grant No. GY-9902.
(3) P. Smith and R. D. Stevens, *J. Phys. Chem.*, **76**, 3141 (1972).
(4) P. Smith, L. B. Gilman, and R. A. DeLorenzo, *J. Magn. Resonance*, **10**, 179 (1973).
(5) S. Brumby, *Z. Naturforsch. A*, **25**, 12 (1970).
(6) S. A. Weiner and G. S. Hammond, *J. Amer. Chem. Soc.*, **91**, 986 (1969).
(7) A. Ohno, N. Kito, and Y. Ohnishi, *Bull. Chem. Soc. Jap.*, **44**, 470 (1971).
(8) P. Stilbs, G. Ahlgren, and B. Åkermark, *Tetrahedron Lett.*, 2387 (1972).
(9) R. W. Fessenden and R. H. Schuler, *J. Chem. Phys.*, **39**, 2147 (1963).
(10) H. Fischer, *J. Phys. Chem.*, **73**, 3834 (1969).
(11) *E.g.*, R. Livingston and H. Zeldes, *J. Magn. Resonance*, **1**, 169 (1969); H. Heftner and H. Fischer, *Ber. Bunsenges. Phys. Chem.*, **73**, 633 (1969).
(12) P. Smith and W. M. Fox, *Can. J. Chem.*, **47**, 2227 (1969).
(13) C. G. Overberger and M. B. Berenbaum, *J. Amer. Chem. Soc.*, **73**, 4883 (1951).
(14) M. J. Astle, "Industria Organic Nitrogen Compounds," Reinhold, New York, N. Y., 1961, p 235.
(15) R. W. Fessenden, *J. Chem. Phys.*, **37**, 747 (1962).
(16) H. Paul and H. Fischer, *J. Chem. Soc. D*, 1038 (1971).
(17) D. E. Wood, R. V. Lloyd, and W. A. Lathan, *J. Amer. Chem. Soc.*, **93**, 4145 (1971).
(18) C. Corvaja, M. Brustolon, and G. Giacometti, *Z. Phys. Chem. (Frankfurt am Main)*, **66**, 279 (1969).
(19) K. Eiben and R. W. Fessenden, *J. Phys. Chem.*, **75**, 1186 (1971).
(20) J. Q. Adams, *J. Amer. Chem. Soc.*, **90**, 5363 (1968).
(21) W. T. Dixon and R. O. C. Norman, *J. Chem. Soc.*, 3119 (1963).
(22) R. E. James and F. Sicilio, *J. Phys. Chem.*, **74**, 1166 (1970).
(23) R. Poupko and A. Loewenstein, *J. Chem. Soc. A*, 949 (1968).
(24) H. Zeldes and R. Livingston, *J. Chem. Phys.*, **45**, 1946 (1966).
(25) A. J. Dobbs, B. C. Gilbert, and R. O. C. Norman, *J. Chem. Soc., Perkin Trans. 2*, **68**, 786 (1972).
(26) M. Hanack, "Conformation Theory," Academic Press, New York, N. Y., 1965, Chapter 3; H. Booth, *Progr. NMR (Nucl. Magn. Resonance) Spectrosc.*, **5**, 149 (1969).
(27) *E.g.*, (a) C. Fauquenort, J. P. Dodelet, and P. Claes, *Bull. Soc. Chim. Belg.*, **80**, 315 (1971); (b) R. S. Drago and H. Peterson, Jr., *J. Amer. Chem. Soc.*, **89**, 5774 (1967); (c) B. Smaller, J. R. Remko, and E. C. Avery, *J. Chem. Phys.*, **48**, 5174 (1968).
(28) W. T. Dixon and R. O. C. Norman, *J. Chem. Soc.*, 4850 (1964).
(29) A. L. Buley, R. O. C. Norman, and R. J. Pritchett, *J. Chem. Soc. B*, 849 (1966).
(30) A. J. Dobbs, B. C. Gilbert, and R. O. C. Norman, *J. Chem. Soc. A*, 124 (1971); also see ref 25.
(31) J. W. Lown, *Can. J. Chem.*, **43**, 2571, 3294 (1965).
(32) *E.g.*, (a) Yu. D. Tsvetkov, J. R. Rowlands, and D. H. Whiffen, *J. Chem. Soc.*, 810 (1964); (b) J. E. Bennett, B. Mile, and A. Thomas, *J. Chem. Soc. A*, 298 (1968).
(33) The $\cdot RO^-$ radical anion appears to be the only 1-substituted 1-cyclopentyl radical ion for which an isotropic epr spectrum has been reported.[31] This spectrum showed all four β-CH_2 protons to be equivalent, $a_{\beta\text{-H}}(CH_2)$ equal to 13.8 ± 0.2 G (at room temperature, in aliphatic ether solution) which is very different from the $a_{\beta\text{-H}}(CH_2)$ [·ROH] value in Table I, 27.0 G. It might be argued that this difference stems partly from a medium effect for, in water at about room temperature, radicals such as $CH_3\dot{C}HOH$ and $(CH_3)_2\dot{C}OH$ and their corresponding conjugate bases have similarly sized $a_{\beta\text{-H}}(CH_3)$ values,[19,25] *e.g.*, $a_{\beta\text{-H}}(CH_3)$ equals 19.80 and 16.9 ± 0.1 G for $(CH_3)_2\dot{C}OH$ and $(CH_3)_2\dot{C}O^-$, respectively.[25] However, at a high enough temperature, 150°K, the epr spectrum of $\cdot RO^-$ in a cyclopentanone matrix has been shown[32b] to be essentially isotropic and to have all four β-CH_2 protons equivalent with $a_{\beta\text{-H}}(CH_2)$ equal to 27.8 ± 1.0 G; the analogous isotropic spectrum of $(CH_3)_2\dot{C}O^-$ in an acetone matrix at 120°K has $a_{\beta\text{-H}}(CH_3)$ equal to 16.4 ± 0.5 G.[32b]
(34) For two of these studies[17,18] the typical spectra shown suggest that the resolution attained was probably less than that in our work. Another index of the resolution in these earlier investigations[16-18] is that no γ-CH proton couplings were reported, although these might perhaps be expected, *e.g.*, see R. Livingston and H. Zeldes, *J. Chem. Phys.*, **44**, 1245 (1966), ref 9, ref 11, and Table I.
(35) For a given $(CH_3)_2\dot{C}X$ radical, the $F_2(-X)$ ratio is equal to $[1 - \Delta(-X)]$ where $\Delta(-X)$ is the Fischer $\Delta(-X)$ value, H. Fischer, *Z. Naturforsch. A*, **20**, 428 (1965).
(36) J. Cooper, A. Hudson, and R. A. Jackson, *Mol. Phys.*, **23**, 209 (1972).
(37) P. J. Krusic, P. Meakin, and J. P. Jesson, *J. Phys. Chem.*, **75**, 3438 (1971).
(38) M. C. R. Symons, *Nature (London)*, **222**, 1123 (1969).
(39) R. W. Fessenden, *J. Phys. Chem.*, **71**, 74 (1967); R. Livingston, J. K. Dohrmann, and H. Zeldes, *J. Chem. Phys.*, **53**, 2448 (1970); G. P. Laroff and R. W. Fessenden, *J. Chem. Phys.*, **55**, 5000 (1971); **57**, 5614 (1972).
(40) We tentatively estimate the maximum uncertainty in $F(-X)$ values to be 0.01, except of course for the $F_1(-H)$ and $F_2(-H)$ values.
(41) *E.g.*, ref 9, 18, and 28.
(42) The validity of this latter assumption is shown by the near equality fo $a_{\beta\text{-H}}(CH_3)[(CH_3)_3CCH_3]$ and $a_{\beta\text{-H}}(CH_2)[\cdot RCH_3]$, see Table I.

A Raman Spectroscopic Investigation of Molten Magnesium Nitrate–Sodium Nitrate and Magnesium Nitrate–Potassium Nitrate Mixtures

Mordechai Peleg

Department of Inorganic and Analytical Chemistry, The Hebrew University of Jerusalem, Jerusalem, Israel
(Received July 12, 1972; Revised Manuscript Received April 30, 1973)

A Raman spectroscopic study has been carried out on molten binary mixtures of magnesium nitrate with sodium nitrate and also potassium nitrate over a wide composition range. Doubling of the symmetric stretching mode of the nitrate ion (ν_1) as well as the multiplicity of other frequencies suggests that the nitrate is seeing two different environments. Two types of cavity potentials appear to fit the present results in preference to the possibilities of a perturbed lattice structure with dynamical coupling of the anion, or the presence of distinct complex ions. Comparison between the magnesium nitrate salts and a highly concentrated aqueous solution of magnesium nitrate suggests that the appearance of new vibrational frequencies is attributable to a new potential cavity being formed as the cation enters the cavity surrounding the nitrate ion and not to direct complex formation.

Introduction

Raman spectroscopic investigations on the magnesium nitrate–water system[1] revealed that the symmetric stretching mode ν_1 of the nitrate ion appears as a doublet at concentrations of $Mg(NO_3)_2 \cdot 2.4H_2O$ and $Mg(NO_3)_2 \cdot 2.0H_2O$. It was suggested that the above solutions may possess a perturbed lattice structure similar to the two-site model suggested by Irish, *et al.*[2] In order to further study the above-mentioned doubling of the ν_1 symmetric stretching mode, it was decided to investigate anhydrous molten magnesium nitrate by Raman spectroscopy. Due to decomposition of the magnesium nitrate salt at high temperatures it was necessary to employ molten binary mixtures of magnesium nitrate with either sodium nitrate or potassium nitrate at various concentrations.

Previous results have been reported for various divalent metal nitrate–alkali metal nitrate molten mixtures, both in Raman[3] and infrared spectroscopy.[4] Devlin, *et al.*,[5] noted for magnesium nitrate–alkali metal nitrate mixtures that the ν_1 mode for the nitrate ion appears at 1053 cm^{-1} in the Raman[3] and at 1038 cm^{-1} in the infrared[4] without producing corresponding Raman (1038 cm^{-1}) and infrared (1053 cm^{-1}) features. The observation was interpreted in terms of coupling of the vibrational modes of two or more nitrate ions associated with a common cation, or possibly a perturbated lattice structure. Hester and Krishnan[6] also reported the vibrational spectra of some alkali-metal nitrate-group IIa and IIb metal nitrate glasses, noting the splitting of the ν_1 mode into two components. The above authors postulated the existence in the glasses of definite magnesium nitrate complexes distributed in a matrix whose structure is eventually that of the simple alkali nitrate melts.

The present paper presents comprehensive results for magnesium nitrate–sodium nitrate and magnesium nitrate–potassium nitrate molten mixtures.

Experimental Section

The laser Raman apparatus employed in the present investigation is identical with that described previously.[1]

Baker Analyzed reagent grade $Mg(NO_3)_2 \cdot 6H_2O$, $NaNO_3$, and KNO_3 were used as the starting materials without further purification. The samples were prepared by mixing together the magnesium and alkali metal salts in the required proportions. The mixtures were heated under vacuum for several hours slowly increasing the temperature in order to remove the water present. Complete removal of water was ascertained by weighing. All samples were filtered under pressure through a glass frit directly into the Raman sample tube and then sealed off under vacuum. The mixtures were heated in a simple tube furnace to the desired temperature.

All the Raman bands were analyzed using a computer technique to separate overlapping or superimposed bands. The peaks were traced onto millimeter graph paper which enabled intensity *vs.* wavelength data to be recorded and transferred to the computer. The bands were analyzed for the best fit to the Gaussian function. As pointed out by Irish, *et al.*,[7] and observed in our results discretion and considerable physical knowledge of the system must be applied in such analyses lest nonexistent lines be invoked.

Results

The results for the Raman stretching modes of the nitrate ion in the magnesium nitrate–sodium nitrate and magnesium nitrate–potassium nitrate mixtures are recorded in Table I together with reexamined values for concentrated aqueous solutions of magnesium nitrate.[1] Also included in the table are the Raman modes for molten sodium[8] and potassium nitrates,[9] the crystalline tetra- and dihydrates of magnesium nitrate,[10,11] as well as the infrared data for a magnesium–potassium nitrate molten mixture.[4] Figure 1 shows the change in line shape for the ν_1 mode with varying amounts of alkali metal cation present, and Figure 2 shows the curve analysis for a ν_1 band.

Typical spectra of the 700–850 and 1300–1700-cm^{-1} regions are shown in Figures 3 and 4 which include also their curve analysis. The table shows the ν_4 mode as consisting of three bands and also the presence of a ν_2 mode which should be Raman inactive if the D_{3h} symmetry was

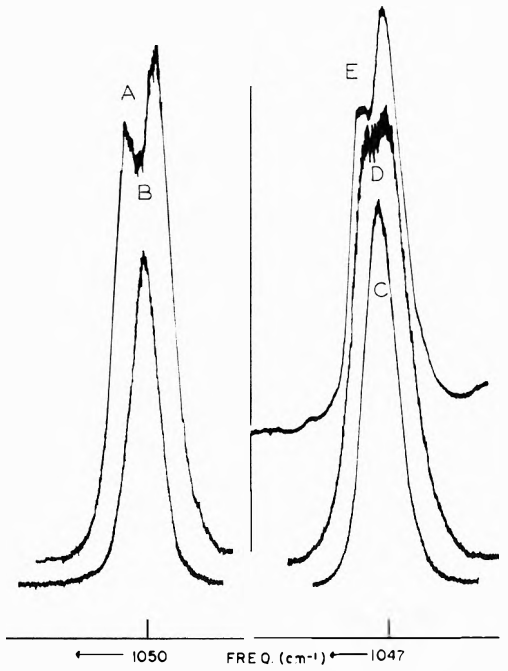

Figure 1. ν_1 frequency range for various melts: A, $Mg(NO_3)_2/NaNO_3$ (1/0.75); B, $Mg(NO_3)_2/NaNO_3$ (1/2.5); C, $Mg(NO_3)_2/KNO_3$ (1/2.0); D, $Mg(NO_3)_2/KNO_3$ (1/1.0); E, $Mg(NO_3)_2/KNO_3$ (1/0.67). (Spectra not run uncer identical conditions.)

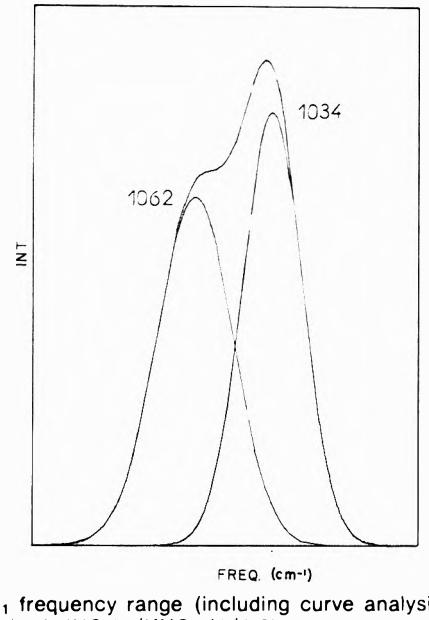

Figure 2. ν_1 frequency range (including curve analysis into two components): $Mg(NO_3)_2/KNO_3$ (1/1.0).

maintained. The ν_3 mode consists of four peaks and also the $2\nu_2$ band is split into two components. Both of the $2\nu_2$ bands were almost completely polarized proving that neither of these bands could be due to residual water which would give rise to only a partially polarized bending mode in this region.

The effect of temperature on the ν_1 peak position was found to be negligible. A comparison of results obtained for a magnesium nitrate–potassium nitrate mixture (ratio 1/1) at 250° and in the glassy state at room temperature showed only a decrease of two wave numbers in the ν_1 mode for a decrease in temperature of more than 200°. These results agree with those of Janz and James[9] that

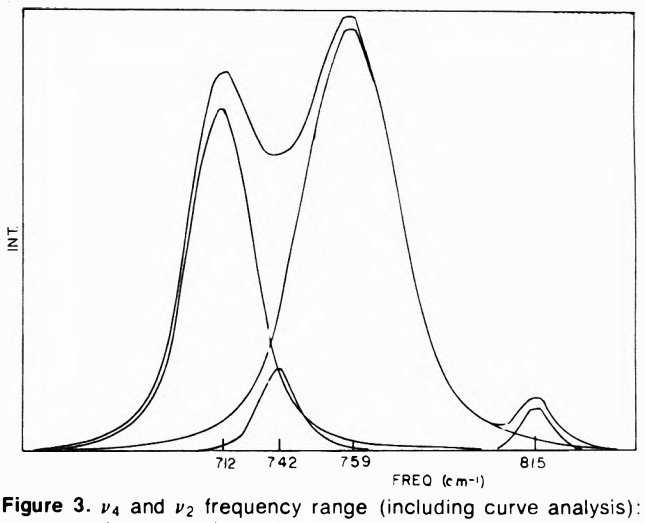

Figure 3. ν_4 and ν_2 frequency range (including curve analysis): $Mg(NO_3)_2/NaNO_3$ (1/0.75).

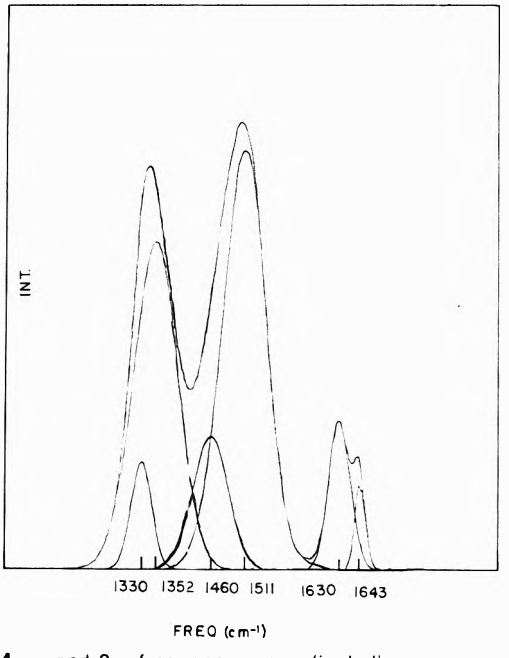

Figure 4. ν_3 and $2\nu_2$ frequency range (including curve analysis): $Mg(NO_3)_2/NaNO_3$ (1/1.7).

the symmetrical stretching frequency is temperature independent.

Discussion

Examination of Table I reveals a striking similarity between the spectra of the molten salt mixtures and the highly concentrated aqueous solution (aqueous melts) of magnesium nitrate. Further all the spectra show a continuous change of frequencies as the Mg^{2+} concentration is increased. This would suggest that the NO_3^- is experiencing a continuous environmental change that is predominantly affected by the presence of magnesium cations.

Except for the more dilute magnesium melts, the ν_1 symmetric mode consists of two frequencies, as in the case for the concentrated aqueous solution. For the melts, the intensities (peak areas) of the two bands in the ν_1 region are of the same order of magnitude. In the aqueous melts, the lower frequency intensity increases with respect to the other band as the water content decreases from 2.4 to 1.5.

TABLE I: Raman Frequencies (cm^{-1}) of Various Magnesium Nitrate Systems

Mol % Mg	Ratio	ν_4			ν_2			ν_1		ν_3					$2\nu_2$		Temp, °C	Ref
	$Mg(NO_3)_2/NaNO_3$																	
20	1/4.0	715	741	765	820			1050		1341	1350	1451	1510	1635		1652	250	
28	1/2.5	712	738	760	818		1050		1052	1337	1353	1455	1516	1629		1647	250	
37	1/1.7	716	739	764	821		1047		1056	1330	1352	1460	1511	1630		1643	200	
50	1/1.0	716	747	764	825		1046		1068	1324	1350	1470	1522	1620		1633	250	
57	1/0.75	712	742	759	815		1043		1068	1314	1358	1481	1520	1620		1630	340	
	$Mg(NO_3)_2/KNO_3$																	
20	1/4.0	714	727	758	820			1047		1346	1360	1463	1510	1635		1655	250	
33	1/2.0	712	730	754	818		1046		1051	1328	1375	1464	1514	1633		1640	225	
50	1/1.0	714	735	763	820		1034		1062	1322	1371	1480	1511	1626		1630	250	
60	1/0.67	712	727	762	815		1032		1062	1309	1355	1485	1509	1620		1626	325	
	$Mg(NO_3)_2/H_2O$																	
29	1/2.4	717		754			1034		1062	1320	1377	1469	1512		1634		120	1
33	1/2.0	717		755			1034		1062	1313	1370	1480	1520		1634		128	1
40	1/1.5						1034		1064								180	
	$NaNO_3$	719		732	828			1057			1365	1420			1656		336	8
												1383 (v broad)						9
	KNO_3		718					1048										
	$Mg(NO_3)_2/KNO_3$ (1/1 melt, ir)	708	750	760	805	820	1020		1050	1320	1405	1475					270	4
	$Mg(NO_3)_2 \cdot 2H_2O$ (crystal)		731	747	815			1067		1327	1374	1465			1630		Room temp	10
	$Mg(NO_3)_2 \cdot 4H_2O$ (crystal)		729	750	814			1045		1322	1340	1460		1632		1650	Room temp	11

The two frequencies, however, have approximately equal intensities once the water content falls below 2. Intensity changes with concentration for the aqueous melts might be due to structural changes that occur once the water content is reduced below the dihydrate concentration.

As previously stated, the two bands that appear in the ν_1 region are both attributable to the nitrate ion affected predominantly by the magnesium cation and not as suggested by Hester and Krishnan[6] that the higher frequency mode is due to an alkali metal nitrate matrix. The above authors also considered the lower frequency band as being due to a definite magnesium nitrate complex. However we would tend to rule out the existence of such a complex for a number of reasons. The lower frequency mode would be expected to have the same value in the three types of mixtures if this mode was attributable to a definite complex and also to have the same value at different concentrations. This is obviously not so; a value of 1046 cm^{-1} is noted for an equimolar mixture of magnesium and sodium nitrates, while for the potassium salt mixture the lower frequency mode is 1034 cm^{-1}. The bands are also strongly concentration dependent.

An alternative interpretation of the doubling of the ν_1 mode might be to consider a lattice-like structure for the melts as suggested by Wilmshurst and Senderoff[12] and further supported by Devlin, *et al.*,[13] from the observed effects for alkali metal and silver nitrate melts. However, Hester[14] has pointed out that it is surprising that a full factor-group analysis is needed to account for a melt spectrum when spectra even from low-temperature crystalline solids commonly can be accounted for with a site symmetry analysis instead of correlation splitting diagram. From work carried out on the dehydration of magnesium nitrate hexahydrate,[11] the ν_1 mode for the anhydrous magnesium salt was observed at 1098 cm^{-1} with a shoulder at 1106 cm^{-1}. Brooker, *et al.*,[15] have stated that the correlation field splitting in the symmetric stretch for the group II crystalline nitrates would be difficult to resolve at the high temperatures prevailing in the melt unless a significant decrease in the nitrate–nitrate distances accompanied fusion. Thus it appears unreasonable to assign the much larger splits (as compared to 8 cm^{-1} in the solid) of 25–30 cm^{-1} in the magnesium nitrate melts and solutions as being due to correlation field splitting in a melt that retained long-range lattice-like structure.

The present results would appear to indicate a structure for molten salts and aqueous melts based on a model less structured than the perturbed lattice model, but on the other hand retaining cages or cavities of one type of charged ion situated around the oppositly charged ion, similar to the model proposed by Brooker, *et al.*,[16] following the suggestion of Edgell, *et al.*[17] This would be a type of quasilattice model without the dynamical coupling or correlation field splitting associated with lattice structure. Instead a cation cage could be formed, for example, which would "trap" the anion inside. Thus, as stated by Brooker, *et al.*,[16] the selection rules for the nitrate group (if this were the anion inside the cage) would be determined by the symmetry of the field and not by the free ion selection rules. In the present investigation different types of cavities could be envisaged depending on whether the cage consisted of only alkali metal cations, or also magnesium cations. Further, due to the hindered rotation of the nitrate ion it would be expected that more than one type of cavity was possible for identical cage composition depending on where the magnesium ion was situated with respect to the nitrate ion. Due to the high polarization power of the magnesium ion with respect to the sodium and potassium ions it would be further expected that the replacement of an alkali metal cation by a magnesium ion should cause a strong asymmetry in the cage potential which would give rise to splitting of the degenerate modes (ν_3 and ν_4) and activation of the forbidden ν_2 mode.

Devlin and his coworker[18,19] have recently examined the vibrational spectra of molecular group I metal nitrate monomers, dimers, and aggregates in various inert matrices, as well as glassy thin films of the same nitrates. They noted that the monomer, dimer, trimer, etc. have respectively increasing ν_1 frequencies, while once the nitrate was in its most symmetrical environment, the undiluted glassy form, then the ν_1 mode had the highest frequency value. Devlin, *et al.*,[19] concurred with the model proposed by Brooker, *et al.*,[16] that the nitrate ion in a melt may assume two or more quite different environments (sites).

A general observation for the alkali metal nitrate melts is that the ν_1 frequency for the melt lies at about 10–20 cm^{-1} below that of the solid. Since for anhydrous solid magnesium nitrate the ν_1 value is 1098 cm^{-1} one might expect for the pure melt a value around 1080–1090 cm^{-1}. This value agrees well with Janz and Jame's[9] correlation diagrams between ν_1 and the cationic polarizing power. Certainly a value that would fall between the two ν_1 values for the mixed melts (1032–1064 cm^{-1}) appears difficult to reconcile with the previously suggested value (1080–1090 cm^{-1}). Thus it would appear that the two frequencies observed in the mixed melts (1034–1043 and 1062 cm^{-1}) might be due to lower symmetry environments caused by cages made up of different cations (*i.e.*, Mg^{2+} and Na^+ or Mg^{2+} and H_2O, etc.).

Janz and coworkers[20] have suggested four sites as being the most probable for a cation with respect to the nitrate ion in a melt. These sites are (1) above the plane of the ion and directly on the threefold axis or a "top" site; (2) along the N–O bond or a "corner" site; (3) bisecting the O–N–O angle or a "crook" site, and (4) a position intermediate to 1 and 3 or a "roll-on" site. Chang and Irish[21] on the basis of comparison with the spectra of solid hydrated magnesium nitrate[10] have suggested that for highly concentrated aqueous solutions of magnesium nitrate, the nitrate ion can assume both a monodentate (ν_1 = 1039 cm^{-1}) and bidentate (ν_1 = 1064 cm^{-1}) orientation. The strong similarity between the aqueous solution of magnesium nitrate and its binary melts suggests that different environments might be set up depending on where the Mg^{2+} are in the cage with respect to the nitrate. The lower frequency of the ν_1 region could be due to an environment with the magnesium in the "corner" site. The higher frequency would then be due to the magnesium in one of the other sites probably the "crook" site. Both the "corner" and "crook" sites would give rise to an asymmetrical field.

Although it is the magnesium ion that is primarily responsible for the potential field affecting the nitrate, the other cations also exert an influence as is readily observed by the different ν_1 values for the different binary melts. Since the asymmetry in the cavity is due to the fact that cations of nonequivalent polarizing power form the cavity, it would be expected that as the difference in polarizing power of the two types of cations forming the cavity increases thus the separation between the two ν_1 modes

TABLE II: Raman Frequencies (cm^{-1}) of the Two Types of Nitrate Ions in the Melts

	$Mg(NO_3)_2/NaNO_3$ (1/1)		$Mg(NO_3)_2/KNO_3$ (1/1)	
$\nu_3(A_1)$, ν_5 (B_1)	747	764	735	763
$\nu_6(B_2)$	825		820	
$\nu_2(A_1)$	1046	1068	1034	1062
$\nu_1(A_1)$	1324	1350	1322	1371
$\nu_4(B_1)$	1470	1522	1480	1511
$2\nu_6(A_1)$	1633	1620	1630	1626
	Site 1	Site 2	Site 1	Site 2

would also increase. This is in fact noted, the difference between the ν_1 peaks being 22 and 28 cm^{-1} for the sodium and potassium mixture, respectively. Hester's results[6] for magnesium nitrate–alkali metal nitrate glasses show ν_1 separation values of 13, 19, 20, and 28 as the alkali metal changes from sodium through potassium and rubidium to cesium nitrate.

The above picture of only two types of cavities in the molten mixtures may be an oversimplification. Brooker[16] noted an asymmetry in the ν_1 mode for pure molten $LiNO_3$ suggesting that even if only one cation is present in the melt, more than one type of potential cage may be formed. The difference in the cavities may be due to the number of cations forming the cage, *e.g.*, four or five. Thus in our present investigation more than two different cavities may exist. However, the accuracy of our studies indicates only the two main types.

The other vibrational modes can likewise be assigned to two different environments or sites. Table II shows the classification, following the designations used by Chang and Irish,[20] based on a C_{2v} perturbation of the NO_3^- ion.

In conclusion we believe that our results support Brooker's suggestion[16] that the multiplicity of frequencies observable in nitrate melts can adequately be described by considering each of the anions and cations as sitting in potential cages created by the near neighbor counter ions and not necessarily considering the melt as possessing long-range lattice-like structure. For highly concentrated aqueous solutions of nitrate salts the question therefore arises whether the appearance of new frequencies as the salt concentration increases should be attributed to definite complex formation through the direct interaction of the metal cation and an oxygen atom of the nitrate group. Instead the possibility exists that as the water content of an aqueous solution is lowered, the now unhydrated cation will form part of the cavity around the nitrate anion and thus give rise to new symmetry environments and hence to different vibrational frequencies.

Acknowledgment. The author wishes to thank Dr. D. E. Irish for helpful discussions.

References and Notes

(1) M. Peleg, *J. Phys. Chem.*, **76**, 1019 (1972).
(2) D. E. Irish, D. L. Nelson, and M. H. Brooker, *J. Chem. Phys.*, **54**, 654 (1971).
(3) G. J. Janz and T. R. Kozlowski, *J. Chem. Phys.*, **40**, 1699 (1964).
(4) R. E. Hester and K. Krishnan, *J. Chem. Phys.*, **47**, 1747 (1967).
(5) J. P. Devlin, P. C. Li, and R. P. J. Cooney in "Molten Salts—Characterisation and Analysis," G. Mamntov, Ed., Marcel Dekker, New York, N. Y., 1964, pp 220–223.
(6) R. E. Hester and K. Krishnan, *J. Chem. Soc. A*, 1955 (1968).
(7) D. E. Irish and H. Chen, *Appl. Spectrosc.*, **25**, 1 (1971).
(8) M. H. Brooker, A. S. Quist, and G. E. Boyd, *Chem. Phys. Lett.*, **5**, 357 (1970).
(9) G. J. Janz and D. W. James, *J. Chem. Phys.*, **35**, 739 (1961).
(10) T. G. Chang and D. E. Irish, *Can. J. Chem.*, **51**, 118 (1973).
(11) M. Peleg, *Isr. J. Chem.* in press.
(12) J. K. Wilmhurst and S. Senderoff, *J. Chem. Phys.*, **35**, 1078 (1961); J. K. Wilmhurst, *J. Chem. Phys.*, **39**, 1779 (1963).
(13) J. P. Devlin, K. Williamson, and G. Austin, *J. Chem. Phys.*, **44**, 2203 (1966); K. Williamson, P. Li, and J. P. Devlin, *J. Chem. Phys.*, **48**, 3891 (1968).
(14) R. E. Hester, "Advances in Molten Salt Chemistry," Vol. 1, J. Braunstein, G. Manantov, and G. P. Smith, Ed., Plenum Press, New York, N. Y., 1971, Chapter 1.
(15) M. H. Brooker, D. E. Irish, and G. E. Boyd, *J. Chem. Phys.*, **53**, 1083 (1970).
(16) M. H. Brooker, A. S. Quist, and G. E. Boyd, *Chem. Phys. Lett.*, **9**, 242 (1971).
(17) W. F. Edgell, J. Lyford, IV, R. Wright, W. Risen, Jr., and A. Watts, *J. Amer. Chem. Soc.*, **92**, 2240 (1970).
(18) D. Smith, D. W. James, and J. P. Devlin, *J. Chem. Phys.*, **54**, 4437 (1971).
(19) G. Pollard, N. Smyrl, and J. P. Devlin, *J. Phys. Chem.*, **76**, 1826 (1972).
(20) G. J. Janz and T. R. Kozlowski, *J. Chem. Phys.*, **40**, 1699 (1964); G. J. Janz and S. C. Wait, Jr., in Raman Spectroscopy., H. A. Szymanski, Ed., Plenum Press, New York, N. Y., 1967, pp 152, 153.
(21) T. G. Chang and D. E. Irish, *J. Phys. Chem.*, **77**, 52 (1973).

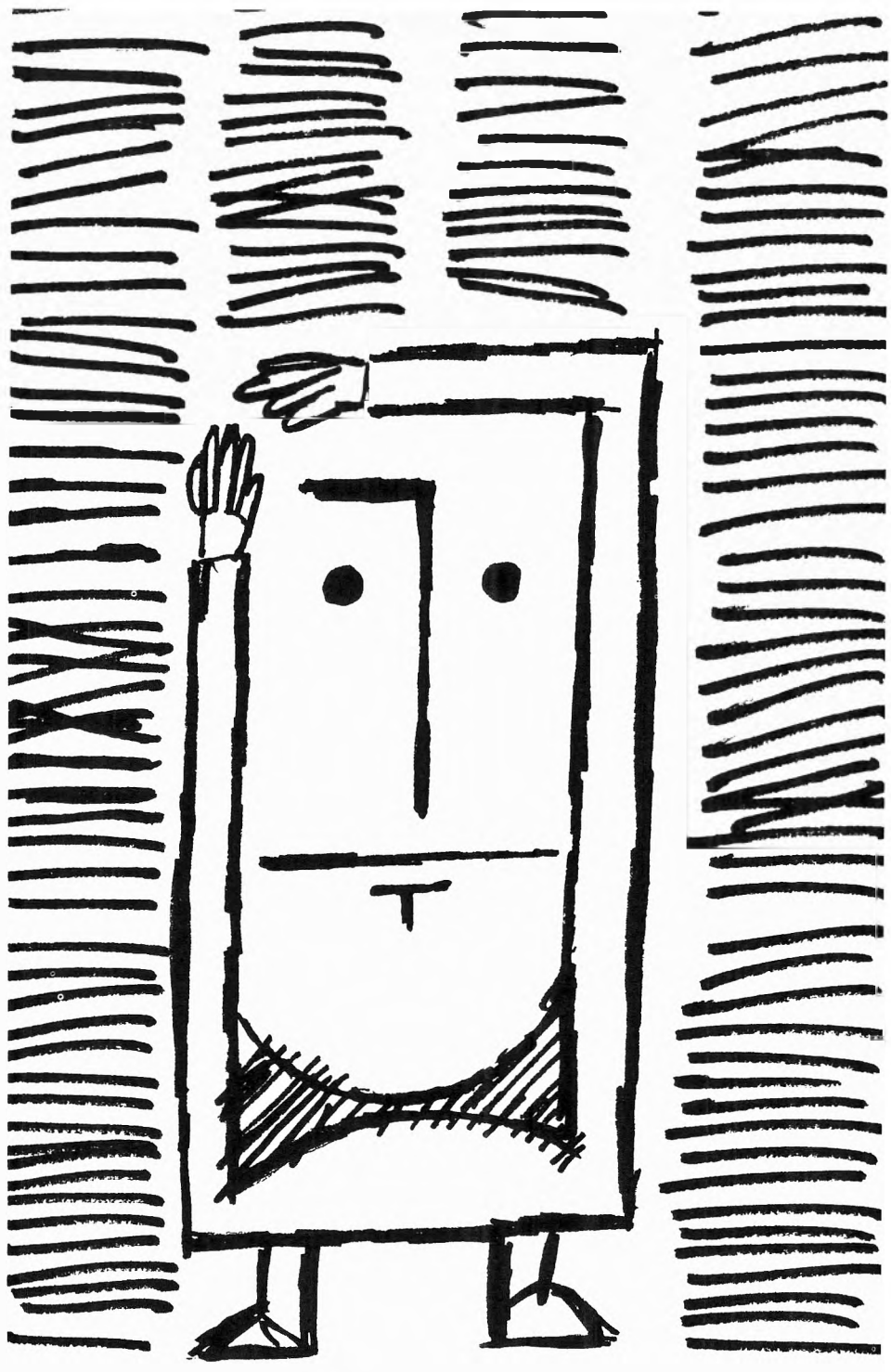

Caught In The Information Explosion? Then You Need Accounts Of Chemical Research!

ACCOUNTS gives you the information you need in all fields of chemical research. Its reviews are *short, concise* and *authoritative*. Most of the reviews are written by the investigators primarily responsible for the research described.

We know you'll profit from ACCOUNTS. According to SCIENCE 173, 471 (1972) ACCOUNTS is one of the *most important chemical journals in the world as measured by "impact factor"*

And it costs just a small amount of money a year!

Get an up-to-date perspective on what's taking place in chemical research. Just complete and return the order form. We'll take care of the rest.

. . . *another ACS service*

Accounts of Chemical Research
American Chemical Society
1155 Sixteenth Street, N.W.
Washington, D.C. 20036

Yes, I would like to subscribe to ACCOUNTS OF CHEMICAL RESEARCH at the rate checked below.

*ACS members	☐ U.S. $ 5.00	☐ **Canada, PUAS $ 9.00	☐ **Other Nations $10.00
Nonmembers	☐ U.S. $15.00	☐ **Canada, PUAS $19.00	☐ **Other Nations $20.00

☐ Payment enclosed *(payable to American Chemical Society)* ☐ Bill me ☐ Bill company.

Name _____ Position _____

Your Employer _____

Address ☐ Home ☐ Business _____

City _____ State _____ Zip _____

Employer's Business: ☐ Manufacturing ☐ Government ☐ Academic ☐ Other _____

If Manufacturer, Type of Products Produced _____

*NOTE: Subscriptions at ACS member rates are for personal use only. **Payment must be made in U.S. currency, by international money order, UNESCO coupons, U.S. bank draft, or order through your book dealer.

3-100

Tape Cassettes From The American Chemical Society

Famous Scientists

ENERGY

- ☐ **Energy: A Critique**
  Dr. Dean Abrahamson
  Puzzles of Air Pollution Arthur Levy
- ☐ **Fusion: Prospects & Pitfalls—I**
  Dr. H. Furth & Dr. H. Forsen
  Fusion: Prospects & Pitfalls—II
  Dr. H. Furth & Dr. H. Forsen
- ☐ **Antidote to the Energy Crisis**
  George Long
  Chemicals In the Environment
  Dr. Samuel Epstein
- ☐ **Fusion and Fission: An Appraisal**
  Dr. James L. Tuck
  The Prospects for Energy
  Dr. M. King Hubert

ENVIRONMENT

- ☐ **Man & Nature in South Florida**
  Rose McCluney
  The Slick Factor in Ocean Pollution
  Dr. Eugene Corcoran
- ☐ **The Damaged Air—I**
  The Damaged Air—II
- ☐ **How Smells Shape Up**
  Dr. John Amoore
  Urban Auto Design
- ☐ **Tough Filaments of Fragile Liquid**
  James Bacon
  Electricity from Rooftops
  Dr. Charles E. Backus
- ☐ **The Struggle for Clean Water—I**
  The Struggle for Clean Water—II
- ☐ **The Oil Mystery** Harold Bernard
  The Language of Odors
  Dr. Stanley Freeman
- ☐ **The Muskegon County Experiment**
  Dr. W. Bauer & Dr. J. Sheaffer
  The Sophisticated Dowser
  Dr. Richard Parizek
- ☐ **The Lonely Atom** Dr. Philip Skell
  How Green the Revolution
  Lester Brown
- ☐ **Mercury: Another Look, Part I**
  Dr. John Wood
  Mercury: Another Look, Part II
  Dr. John Wood & D. G. Langley
- ☐ **The Troubles with Water**
  Dr. Daniel Okun
  Pure Oxygen for Polluted Water
  Dr. Jack McWhirter
- ☐ **Bubble Machines & Pollution Finders**
  Dr. K. Patel & Dr. L. Kreuzer
  The Steam Engine: A Modern Approach Dr. W. Doerner & Dr. M. Bechtold
- ☐ **Insects: The Elements of Change—Parts I & II** Dr. Carroll M. Williams
- ☐ **New Weapons Against Insects**
  Dr. G. Staal & Dr. J. Siddall
  Moths, Drugs, & Pheromones
  Dr. Wendell Roelofs
- ☐ **The Lead Issue**
  H. Mayrsohn & M. H. Hyman
  Smog: An Environmental Dilemma
  Dr. James Pitts
- ☐ **The Fusion Torch**
  Dr. B. Eastlund & Dr. W. Gough
  The Impermanent Plastic
  Dr. James Guillet

CANCER RESEARCH

- ☐ **Chemicals Combating Cancer**
  Dr. David Grassetti
  Chemical Essence of Beer & Ale
  Dr. Rao Palamand
- ☐ **Cancer Research I—Perspective & Progress** Dr. Frank Rauscher
  Cancer Research II—Viruses
  Dr. R. Gallo & Dr. G. Todaro
- ☐ **Cancer Research III—Chemotherapy**
  Dr. C. Gordon Zubrod
  Cancer Research IV—Immunology
  Dr. Paul Levine
- ☐ **Cancer Research V—Environmental Agents** Dr. Umberto Saffiotti
  Cancer Research VI—NCI Roundtable

SCIENCE

- ☐ **Community Needs: New Emphasis in Research** Dr. H. Guyford Stever
  Aspirin vs. Prostaglandins
  Dr. John Vane
- ☐ **A Breakdown in Plastics—I**
  Drs. J. Guillet & G. Scott
  A Breakdown in Plastics—II
  Drs. J. Guillet & G. Scott
- ☐ **Protein: The Next Big Production?**
  Dr. Steven Tannenbaum
  Clean Energy: A One-Way Dream
  Dr. J. R. Eaton
- ☐ **Science, Scientists, & the Public Interest—I**
  Science, Scientists, & the Public Interest—II
- ☐ **Nitrosamines: A Reappraisal**
  Dr. Phillip Issenberg
  The Emperor of Ice Cream
  Dr. Wendell Arbuckle
- ☐ **Ethics and Genetics**
  Dr. Robert F. Murray
  The American Diet: A Critique
  Dr. Arnold Schaefer
- ☐ **Probing Creation** Dr. Myron A. Coler
  New Directions in U.S. Science
  Dr. William McElroy
- ☐ **Aspirins, Enzymes, & Fragrant Redheads** An Essay Report
  Vitamin D: A New Dimension
  Dr. Hector DeLuca
- ☐ **Pica** Dr. J. Julian Chisolm, Jr.
  Technology in the Nursery
  Dr. William J. Dorson
- ☐ **Engineering Microbes**
  Dr. Elmer Gaden
  Liquid Crystals: A Bright Promise
  Dr. George Heilmeier
- ☐ **Hot Brines in the Red Sea**
  Dr. David Ross
  Complete Corn Dr. Edwin T. Mertz
- ☐ **Lively Xenon** Dr. Neil Bartlett
  The Repressor Hunt
  Dr. Mark Ptashne
- ☐ **The New Prospectors**
  Dr. William Prinz
  A Sober Look at Alcoholism
  Dr. Jack Mendelsohn
- ☐ **Probing the Active Site**
  Dr. David Pressman
  The Puzzle of Diversity
  Dr. Oliver Smithies
- ☐ **Help for the Have Nots**
  Dr. Harrison Brown
  The Closing Circle Dr. Preston Cloud

BIO-MEDICAL

- ☐ **Insulin & Diabetes—I**
  Dr. George Cahill
  Insulin & Diabetes—II
  Dr. George Cahill
- ☐ **Stalking the Molecules of Memory**
  Dr. Leslie Iverson
  Immunotherapy
  Dr. Kenneth Bagshawe
- ☐ **Engineering Enzymes**
  Dr. Victor Edwards
  On Drugs, Plasticizers, & Mass Spec
  Dr. G. W. A. Milne
- ☐ **Body Metal** Dr. Thomas Clarkson
  Judging Technology Dr. E. G. Mesthene
- ☐ **Prospects for the Living Filter**
  Dr. Richard Parizek
  Coral Designs Dr. Eugene White
- ☐ **Bones, Teeth, & Ceramics**
  Thomas Driskell
  PCBs: The Accidental Pollutants
  Dr. Henry Enos
- ☐ **Birth Control: Problems & Prospects**
  Dr. Carl Djerassi
  Hormones, Terpenes, & the German Air Force Dr. A. J. Birch
- ☐ **Prospects for Implants**
  Dr. Donald Lyman
  New Dimensions for Polymers
  Dr. Alan Michaels
- ☐ **Fabricating Life** An Essay Report
  New Ways to Better Food
  Dr. R. W. F. Hardy
- ☐ **Chemistry of the Mind: Schizophrenia**
  Dr. Larry Stein
  Chemistry of the Mind: Depression
  Dr. Joel Elkes
- ☐ **The Molecules of Memory**
  Dr. W. L. Byrne & Dr. A. M. Golub
  The Matter with Memory
  Dr. J. McGaugh
- ☐ **Dissonant Harmony**
  Dr. Denham Harman
  Why We Grow Old Dr. Howard Curtis
- ☐ **New Materials for Spare Parts**
  Dr. V. Gott & Dr. A. Rubin
  Against Individuality
  Dr. R. Reisfeld & Dr. B. Kahan
- ☐ **A Richness of Lipids**
  Dr. Roscoe O. Brady
  Life: Origins to Quality
  Dr. Stanley Miller
- ☐ **The Nitrogen Fixer**
  Dr. Eugene van Tamelen
  Prostaglandins: A Potent Future
  Dr. E. J. Corey & Dr. S. Bergstrom
- ☐ **A Glass Revolution** Dr. S. D. Stookey
  A View of Genes Dr. Norman Davidson
- ☐ **Chemical Evolution**
  Dr. Russell Doolittle
  An Evolving Engine Dr. R. E. Dickerson

NOBEL PRIZE WINNERS

- ☐ **Dr. Linus Pauling**
  The Committed Scientist
  Dr. Jacob Bronowski
  Science and Man
- ☐ **Dr. Glenn Seaborg** The Atomic World of Glenn Seaborg
  Dr. George Wald Vision, Night Blindness, & Professor Wald
- ☐ **Dr. Melvin Calvin** The Search for Significance—Parts I & II

OUTER SPACE

- ☐ **Molecules in Space**
  Dr. D. Buhl & Dr. L. Snyder
  Chemistry Among the Stars
  Dr. Bertram Donn
- ☐ **Molecules Meeting Molecules**
  Dr. John Richards
  The Neutrinos of the Sun
  Dr. Raymond Davis

	ACS Members	Nonmembers
Single Cassette	$4.49	$5.49
Any Six Cassettes	$3.95/cassette	$4.95/cassette

Any 18 or more cassettes to one Address $3.75/cassette

Please add 75 cents handling charge for all orders in U.S.,
$1.00 for all orders outside U.S.

5% Discount if payment accompanies order

Order From: American Chemical Society, 1155 16th Street, N.W., Washington, D.C. 20036, ATTN: A. Poulos